THE STRUCTURE OF BPS SPECTRA

by

PIETRO LONGHI

A dissertation submitted to the

Graduate School - New Brunswick

Rutgers, The State University of New Jersey

In partial fulfillment of the requirements

For the degree of

Doctor of Philosophy

Graduate Program in Physics and Astronomy

Written under the direction of

Professor Gregory W. Moore

And approved by

_____

_____

_____

_____

_____

New Brunswick, New Jersey

OCTOBER, 2015

ABSTRACT OF THE DISSERTATION

The Structure of BPS Spectra

By Pietro Longhi

Dissertation Director:
Professor Gregory W. Moore

In this thesis we develop and apply novel techniques for analyzing BPS spectra of supersymmetric quantum field theories of class $\mathcal{S}$.

By a combination of wall-crossing, spectral networks and quiver methods we explore the BPS spectra of higher rank four-dimensional $\mathcal{N} = 2$ super Yang-Mills, uncovering surprising new phenomena. Focusing on the $SU(3)$ case, we prove the existence of wild BPS spectra in field theory, featuring BPS states of higher spin whose degeneracies grow exponentially with the energy. The occurrence of wild BPS states is surprising because it appears to be in tension with physical expectations on the behavior of the entropy as a function of the energy scale. The solution to this puzzle comes from realizing that the size of wild BPS states grows rapidly with their mass, and carefully analyzing the volume-dependence of the entropy of BPS states. We also find some interesting structures underlying wild BPS spectra, such as a Regge-like relation between the maximal spin of a BPS multiplet and the square of its mass, and the existence of a universal asymptotic distribution of spin-j irreps within a multiplet of given charge.

We also extend the spectral networks construction by introducing a refinement in the topological classification of 2d-4d BPS states, and identifying their spin with a topological invariant known as the "writhe of soliton paths". A careful analysis of the 2d-4d wall-crossing behavior of this refined data reveals that it is described by motivic Kontsevich-Soibelman transformations, controlled by the Protected Spin Character, a protected deformation of the BPS index encoding the spin of BPS

states. Our construction opens the way for the systematic study of refined BPS spectra in class $\mathcal{S}$ theories. We apply it to several examples, including ones featuring wild BPS spectra, where we find an interesting relation between spectral networks and certain functional equations.

For class $\mathcal{S}$ theories of A_1 type, we derive an alternative technique for computing generating functions of 2d-4d BPS spectra, based on the topological data of an ideal triangulation of the Riemann surface defining the theory. We provide a set of building blocks and corresponding rules, from which the 2d-4d spectra of a vast class of theories can be algorithmically recovered.

Finally, we present previously unpublished exact results on the BPS spectrum of the $SU(2)$ $\mathcal{N} = 2^*$ theory, and briefly comment on its wall crossing.

Acknowledgements

Completing this work surely required significant commitment and perseverance, these however would have been vain without the guidance, insight and support of many.

First and foremost I would like to thank my advisor, Greg Moore, for supporting and guiding me through graduate school. Thanks to him, I was lucky to work on unique and interesting projects, which would have been inaccessible otherwise. Working with Greg has been extremely stimulating, it taught me how important it is to keep looking well beyond one's current reach for the best approach to the most challenging problems – to the extent that mathematics' effectiveness in physics, albeit unreasonable, acquires the status of guiding principle.

I also had the privilege of collaborating with several excellent physicists on a number of projects, which are presented here only in part. I am deeply grateful to Nathaniel Craig, Dima Galakhov, Simon Knapen, Tom Mainiero, Andy Neitzke and Roberto Soldati for sharing their ideas and their energy, and for teaching me a lot through enjoyable and fruitful collaborations.

Over the past few years I have learned a tremendous amount from conversations with many postdocs and professors at various institutions. In particular, I would like to thank Costis Papageorgakis, Chan Y. Park, Daniel S. Park and Andy Royston for sharing their time and insights on several questions and ideas. I also wish to thank my peers Aria Basirnia and Daniel Egana for many interesting discussions, and for keeping me updated on the latest developments in the neighboring field of phenomenology, during these exciting years of discovery.

Finally, I thank my wife Giulia for her unconditional and constant support through daunting choices during the past few years, this thesis is dedicated to her.

Pietro Longhi

Rutgers University

May 2015

Dedication

A Giulia.

Table of Contents

List of Figures

Chapter 1

Introduction and Summary

In this thesis we develop and apply new tools for studying the non-perturbative dynamics of four-dimensional gauge theories with $\mathcal{N} = 2$ supersymmetry. The study of these theories has nowadays grown a long and rich history, punctuated by a number of crucial results, which fostered interest and led to more intensive investigation over the years. One feature that makes these models so attractive is the relatively high amount of supersymmetry, which severely constrains the dynamics, making the theories amenable to much exploration through purely field theoretic approaches. While highly constrained, the dynamics is nevertheless rich enough to mimic phenomena believed to occur in nature, providing tractable toy examples of poorly understood field theory phenomena, such as confinement and dynamical generation of mass scales. Another aspect responsible for much of the interest and progress on these theories is their relation to string theory and M theory. Like many other gauge theories, in various dimensions and with various amounts of supersymmetry, these models appear in low energy approximations to string/M theory, a viewpoint that shed much light, for example, on their non-perturbative dynamics and their duality webs. A third facet of this area of research, which came to prominence in recent years, is a rich interplay with active areas of mathematics. This proved both concrete and far-reaching, allowing to tackle difficult physics problems exploiting mathematical results, and vice versa. Much of the work presented in this thesis relies directly on these connections, which likely hold the potential for much further progress.

At very low energies, four-dimensional $\mathcal{N} = 2$ gauge theories exhibit a family of Coulomb phases, in which the effective dynamics is described by a supersymmetric abelian gauge theory. The Coulomb vacua are parametrized by a manifold $\mathcal{B}$ known as the *Coulomb branch*, in a generic vacuum $u \in \mathcal{B}$ the massless spectrum of the theory includes only abelian vector-multiplets, and the dynamics is

sensitive to u through the couplings in the effective action[1] $S_{eff}(u)$. An important consequence of the extended supersymmetry is the *BPS bound*, which states that any state carrying electromagnetic charge γ must be massive [112], with its mass bounded from below

$$M_\gamma(u) \geq |Z_\gamma(u)|\,, \tag{1.1}$$

where Z_γ is the central charge of that state. BPS states are the lightest charged states, those which saturate this bound, and will be our main subject of study. Another distinguished feature of BPS states is that they preserve only part of the super-Poincaré symmetry: while $|Z_\gamma| = M_\gamma$ is responsible for breaking translations and boosts to the little group, $\mathrm{Arg}(Z_\gamma)$ determines which *half* of the supercharges is preserved. Since BPS states are the lightest charged particles, the BPS spectrum is clearly a very important piece of information about the low energy dynamics of these theories, albeit an elusive one.

The elusive nature of BPS spectra is partially due to the fact that BPS states are non-perturbative soliton field configurations. Another complication is that they carry charge and mutually interact, as a consequence the spectrum may include their boundstates whenever stable ones exist. Since the couplings of the IR theory depend on the Coulomb moduli, a BPS boundstate may be stable within certain regions of the moduli space, while not in others. These phase transitions indeed occur, at special loci on $\mathcal{B}$. The central charge $Z_\gamma(u)$ depends linearly on the electromagnetic charge γ, hence the mass of a BPS boundstate is subject to the triangular inequality with respect to the masses of its constituents

$$|Z_{\gamma+\gamma'}(u)| \leq |Z_\gamma(u)| + |Z_{\gamma'}(u)|\,. \tag{1.2}$$

A boundstate is kinematically (un)stable as long as the strict inequality holds; however when it is saturated, a boundstate becomes only marginally stable and can undergo the transition from stable to unstable (or *vice versa*). The bound is saturated when $\mathrm{Arg}(Z_\gamma) = \mathrm{Arg}(Z_{\gamma'})$, conditions like this one define real-codimension one loci inside the Coulomb branch, known as *walls of marginal stability* (or MS walls[2]), which divide $\mathcal{B}$ into disjoint chambers. The BPS spectrum may jump discontinuously from one chamber to the next one: this is the *wall crossing phenomenon*, and plays a key role in the study of BPS spectra.

In fact, while wall-crossing may at first appear as a complication for studying the low-energy dynamics on the whole Coulomb branch, the jumps of the BPS spectrum across MS walls follow

[1] As well as through the u-dependent identification of the IR degrees of freedom with UV ones, although from the IR viewpoint, this relation becomes meaningful only once we consider the global picture over the Coulomb branch, considering e.g. varying u along nontrivial cycles of $\mathcal{B}$ [120].

[2] More precisely, another important condition is involved in the definition of MS walls. Namely that γ, γ' be charges of populated BPS states.

precise rules encoded by *wall crossing formulae* [14, 40, 60, 88]. These allow to determine the BPS spectrum on one side of an MS wall, based on knowledge of the spectrum on the other side. Wall crossing formulae are in fact a powerful tool to study the spectrum of a theory, allowing to probe the whole Coulomb branch while relying solely on knowledge of the spectrum in a single vacuum. Nevertheless, wall crossing alone does not provide a complete approach to finding the spectrum, falling short in one key aspect: one still needs to provide the input for the spectrum at *some* point on the Coulomb branch.

1.1 Class $\mathcal{S}$ theories and Spectral Networks

Recent years have witnessed tremendous progress in the study of BPS spectra, driven by the development of novel frameworks which opened the way for systematic spectroscopy within a large class of theories [11, 12, 61, 63–65]. Much of this thesis revolves around applications and extensions of the *spectral networks* technique of [63]. The relation of spectral networks to BPS states is rather involved, and begins with the low energy description of $4d$ $\mathcal{N}=2$ gauge theories in terms of families of Riemann surfaces, first uncovered by Seiberg and Witten [120, 121]. To a given theory corresponds a fibration of Riemann surfaces Σ_u over the Coulomb branch[3], together with a family of meromorphic differentials λ_u on Σ. The first homology group $H_1(\Sigma,\mathbb{Z})$ is identified with the lattice of gauge and flavor charges in the low energy abelian theory, and the central charge of a state with electromagnetic charge γ is

$$Z_\gamma(u) = \frac{1}{\pi}\oint_\gamma \lambda_u \,. \tag{1.3}$$

The periods of λ_u also determine the exact low energy effective action, including all perturbative and non-perturbative quantum corrections. The (Σ_u,λ_u) fibration over $\mathcal{B}$ includes monodromies around complex-codimension one singular loci of the Coulomb branch. These singularities correspond in fact to BPS particles becoming massless and the monodromies capture physical information on these states. The monodromy structure of the fibration furthermore provides a comprehensive conceptual picture for the rich web of dualities of the family of low energy theories.

Generalizations of Seiberg and Witten's solution to a large class of $4d$ $\mathcal{N}=2$ quiver gauge theories have been obtained soon thereafter, in several different ways. One approach is to consider certain decoupling limits of brane constructions in Type IIA string theory [83, 91, 92, 133]. In the decoupling limit, the 4d gauge theories describe the worldvolume dynamics of Dirichlet four-branes suspended between NS five-branes (possibly in presence of six-branes) arranged within configurations

[3] Away from singularities on $\mathcal{B}$

preserving eight supercharges. Quantum effects of the field theory are captured upon lifting the brane configurations to M-theory, where the system is described by a single *curved* fivebrane wrapping $\Sigma \times \mathbb{R}^{1,3}$. Another approach is based on establishing a connection between the gauge theories and certain integrable systems [46, 74, 101]. Here the role of the Σ is identified with the *spectral curve* of the integrable system, while the Coulomb branch is identified with the space of hamiltonian moduli. The periods of λ are parametrized by the fiber of the integrable system manifold above a fixed $u \in \mathcal{B}$.

A more recent approach, unifying aspects of both previous ones, is to view a 4d $\mathcal{N} = 2$ gauge theory as arising from the compactification of a stack of M5 branes wrapping a punctured Riemann surface C [64, 66, 83, 133]. The effective four dimensional theory, denoted by $S[\mathfrak{g}, C, D]$, is a twisted compactification of the six dimensional $(2, 0)$ theory, where a partial topological twist allows to preserve eight of the sixteen supercharges. The nomenclature refers to the data of the compactification, which includes a simply-laced Lie algebra $\mathfrak{g}$, a punctured Riemann surface C, and certain data D, specifying the behavior of worldvolume fields at the punctures. This category of theories has been named *class* $\mathcal{S}$ [64], after their defining property of originating from six-dimensions, which actually encodes a wealth of information about their dynamics. One striking insight originating from six dimensions is the identification of moduli spaces of marginal deformations with the Teichmüller moduli space of C [66], which provides a comprehensive conceptual picture of the intricate duality webs among different lagrangian descriptions. Another key feature tied to six dimensions involves the finite-radius compactification of these theories on $S^1 \times \mathbb{R}^3$, whose quantum dynamics has been related to Hitchin systems on C [64]. The relation of class $\mathcal{S}$ theories to Hitchin systems plays a central role in the study of their BPS spectra. The S^1 compactification admits an effective description as an $\mathcal{N} = 4$ sigma model with hyper-kähler target space $\mathcal{M}$, having a natural fibration over $\mathcal{B}$ with fibers parametrized by 't Hooft-Wilson lines wrapping the S^1 [122]. BPS states of the 4d theory contribute quantum corrections to the metric on $\mathcal{M}$, since they now wrap the compactification circle and contribute finite-size corrections to the path integral, weighted by factors of $e^{-R|Z_\gamma|}$ (R is the compactification radius).

The effective metric on $\mathcal{M}$ thus contains information about the BPS spectrum of the corresponding class $\mathcal{S}$ theory, but a puzzle readily arises in this picture: thinking of $\mathcal{M}$ as a fibration over $\mathcal{B}$, how is smoothness of the metric compatible with the fact that it depends on the BPS spectrum, since the latter jumps discontinuously across walls of marginal stability? This question was first explored by the authors of [60] who approached the problem by studying in detail how BPS states correct the metric, introducing the *twistor-TBA construction* construction of hyperkähler metrics. A central piece of data of the standard twistor construction are certain holomorphic functions –

Darboux coordinates– $\mathcal{X}_\gamma(u,\theta;\zeta)$ on the twistor space $\mathcal{M}\times\mathbb{C}^\times$ (here $u\in\mathcal{B}$, θ is a coordinate on the fiber above u, and ζ is a coordinate on the twistor sphere of complex structures of $\mathcal{M}$), BPS states enter in their construction with contributions weighted by the *BPS index*[4] $\Omega(\gamma;u)$. The $\mathcal{X}_\gamma$ are only piecewise holomorphic in ζ, and exhibit a Stokes phenomenon involving jumps across meridians on the twistor sphere, located at phases of (central charges of) populated BPS states. These jumps correspond precisely to *Kontsevich-Soibelman symplectomorphisms* and are controlled by the BPS index

$$\mathcal{X}_\gamma(u,\theta;\zeta') \;=\; \mathcal{K}_{\gamma'}^{\Omega(\gamma';u)}\mathcal{X}_\gamma(u,\theta;\zeta)\,, \tag{1.4}$$

in particular, $\Omega(\gamma,u)$ can be computed by comparing $\mathcal{X}_\gamma(u,\theta;\zeta')$ and $\mathcal{X}_\gamma(u,\theta;\zeta)$. At any given $u\in\mathcal{B}$ the Stokes jumps of these functions thus "detect" BPS states, and the whole spectrum can be encoded into the *spectrum generator*, defined as the phase ordered product of the corresponding symplectomorphisms

$$\mathbb{S} \;=:\prod_\gamma \mathcal{K}_\gamma^{\Omega(\gamma;u)}:\,. \tag{1.5}$$

Rather than a mere definition, this operator holds the key to the solution to the puzzle: in [60] it was shown that smoothness of the quantum corrected metric of $\mathcal{M}$ (argued on field theoretic grounds) implies that the jumps of the BPS spectrum across MS walls must be such to compensate for jumps of the phase ordering of $\mathcal{K}_\gamma$ operators, leaving the spectrum generator invariant

$$:\prod_\gamma \mathcal{K}_\gamma^{\Omega(\gamma;u)}: \;=\; :\prod_\gamma \mathcal{K}_\gamma^{\Omega(\gamma;u')}:\,. \tag{1.6}$$

In other words, the spectrum generator is an *invariant of wall crossing*, this is the content of the *Konstevich-Soibelman wall crossing formula* [88].

In the specific case of class $\mathcal{S}$ theories, $\mathcal{M}$ is identified with the moduli space of solutions to Hitchin's equations on C,

$$\begin{aligned} F + R^2[\varphi,\overline{\varphi}] &= 0 \\ \partial_{\bar z}\varphi + [A_{\bar z},\varphi] &= 0 \\ \partial_z\overline{\varphi} + [A_z,\overline{\varphi}] &= 0 \end{aligned} \tag{1.7}$$

supplemented with the boundary data D. More properly $\mathcal{M}$ is identified with the corresponding *Hitchin system*, this comes with a lagrangian fibration $\mathcal{M}\to\mathcal{B}$ over the parameter space of hamiltonians, which is identified with the Coulomb branch of the four dimensional theory. The spectral curve of the Hitchin system

$$\Sigma:\,\{\lambda\,|\,\det(\lambda-\varphi)=0\} \quad\subset T^*C \tag{1.8}$$

[4] An integer-valued supersymmetric index, roughly counting the dimensionality of the BPS Hilbert space of states with charge γ, up to a sign. We will review its definition in detail in Section 3.1.

is identified with the Seiberg-Witten curve of the theory, while the restriction of the tautological 1-form λ on T^*C corresponds to the Seiberg-Witten differential.

The definition of the spectral curve implies that it has a natural presentation as a ramified covering of C. This means that there is a projection map $\pi : \Sigma \to C$, with the roots of the characteristic polynomial (1.8) corresponding to sheets of the cover. Let γ be a closed path on Σ, whose homology class (by a small abuse of notation) we also denote by $\gamma \in H_1(\Sigma, \mathbb{Z})$, running on sheets[5] λ_i, λ_j as depicted in figure 1.1. Defining $\lambda_{ij} := \lambda_j - \lambda_i$, we may consider the following refinement[6] of the BPS bound:

$$|Z_\gamma| = \frac{1}{\pi}\left|\oint_\gamma \lambda\right| = \frac{1}{\pi}\left|\int_{\pi(\gamma)} \lambda_{ij}\right| \leq \frac{1}{\pi}\int_{\pi(\gamma)} |\lambda_{ij}| = M_\gamma\,, \tag{1.9}$$

where M_γ at this point just denotes the area of the shaded disc embedded inside T^*C and bounded by γ. In fact, as we will momentarily argue following [64], M_γ really is the mass of a particle state

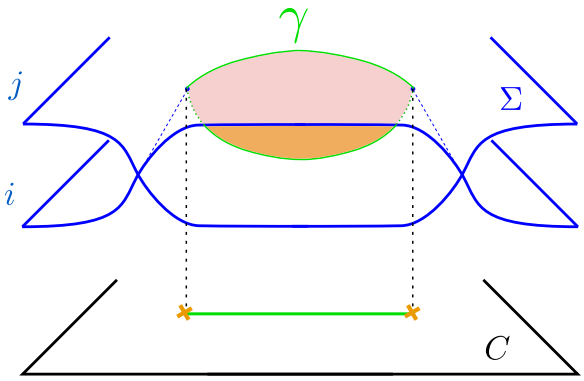

Figure 1.1: A BPS cycle bounding an M2 brane

with electromagnetic charge γ. Recalling the M theory interpretation of T^*C as the neighborhood of the fivebrane worldvolume, one may consider membranes ending on the fivebrane: in the limit of small separation of the fivebranes, the M2 transverse worldvolume would stretch precisely within T^*C. In particular, a membrane whose boundary wraps a one-cycle γ on Σ, while extending along a timelike curve in $\mathbb{R}^{1,3}$, will appear in the effective four dimensional theory as a charged massive soliton. The charge of this particle is precisely the homology class γ, since the membrane couples to the fivebrane two-form field, whose periods on Σ give rise to the four dimensional abelian gauge fields. The central charge of the particle state is given by the period $\frac{1}{\pi}\oint_\gamma \lambda$. The mass on the other

[5]The definition of sheets of the covering is subordinate to a choice of branch cuts and to a choice of trivialization.

[6]In general there is no reason why the pieces of a path $\gamma \subset \Sigma$ running on sheets λ_i, λ_j should project to the same image on C. On the other hand, due to holomorphicity of λ the value of the integral is invariant under homological deformations of γ, and we will assume that suitable deformation of this type always exist. As will be presently clarified, the paths of interest to us enjoy this property by construction.

hand depends on both the area and tension of the membrane worldvolume: when the membrane is a disc bounded by γ as depicted in figure 1.1, the mass is precisely $\frac{1}{\pi}\int_{\pi(\gamma)}|\lambda_{ij}|$ [64].

Therefore (1.9) should be viewed as a *geometric* version of the BPS bound [83, 102, 103]. Such bound is saturated by *actual geometric cycles* on Σ which project to *paths on* C along which

$$\frac{\lambda_{ij}(z)}{|\lambda_{ij}(z)|} = \frac{Z_\gamma}{|Z_\gamma|} =: \zeta \tag{1.10}$$

is a constant phase. Conversely, given a path on C with this type of geometry, it will lift to a *BPS cycle* on Σ only if it begins and ends at branch points. In some cases this kind of constraint has a discrete set of solutions, while in other cases there might be continuous families of solutions. Only M2 branes with such a compatible profile along Σ are BPS: in general the existence of a BPS state of charge γ in the spectrum of the four dimensional effective theory will depend on the existence of a BPS cycle in the corresponding homology class. As the Coulomb branch moduli are varied, so is $\lambda_{ij}(u,z)$, and solutions to these constraints may appear or disappear: this is a geometric perspective on the wall crossing phenomenon.

The systematic study of BPS spectra can in fact be translated into the geometric problem of finding all BPS paths on C – i.e. paths that can be lifted to closed cycles γ on Σ and satisfy the geometric BPS constraint (1.9), with phase $\zeta = Z_\gamma/|Z_\gamma|$ dictated by the corresponding homology class γ. However, while the existence of a finite BPS path does imply the possible presence of BPS states, more structure needs to be considered in order to determine relevant physical information, such as the number of BPS states, or their spin. As will be reviewed in Chapter 3, spectral networks [63] accomplish precisely this. $\mathcal{W}_\zeta$ is a one-parameter family of networks whose "streets" are BPS paths on C, sourcing from branch points, or from "joints" (intersections of two streets). The ζ-dependence of the family $\mathcal{W}_\zeta$ allows to probe the whole BPS spectrum by scanning over all phases $\mathrm{Arg}(\zeta) \in \mathbb{R}/2\pi\mathbb{Z}$. Attached to each "street" of the network is certain combinatorial data associated

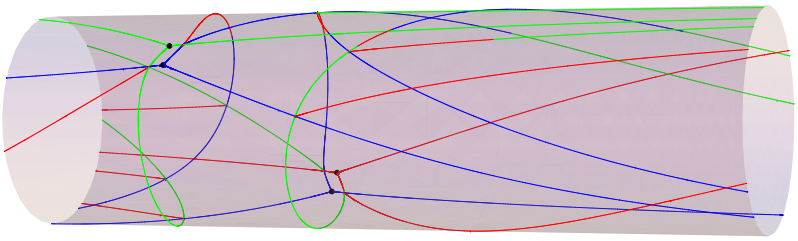

Figure 1.2: A spectral network on a cylinder C. Different colors denote streets of different types.

with *2d-4d BPS states*, a kind of BPS states of the four dimensional theory in presence of a BPS

surface defect. Surface defects and the corresponding 2d-4d BPS states play a key role in the definition of spectral networks. In the UV, such defects can be described in terms of a two dimensional $\mathcal{N} = (2,2)$ quantum field theory living on $\mathbb{R}^{1,1} \subset \mathbb{R}^{1,3}$, coupled to the four dimensional ambient theory through the gauging of global symmetries of the 2d theory by four dimensional gauge fields [9, 65, 68, 69, 76–79]. In the IR, the bulk degrees of freedom generally reduce to abelian gauge fields, with an effective action parametrized by the Coulomb branch of vacua. The two dimensional theory develops a superpotential with a discrete set of (genecally) non-degenerate massive vacua $\{i\}_{i=1}^{k}$, leaving no massless 2d degrees of freedom in the IR. From the bulk viewpoint, an IR surface defect in a given vacuum appears as a source of monodromy for the abelian fields, much like a generalized version of a solenoid. The lightest states on the defect are in fact 2d solitons, which interpolate between two vacua (i, j) from one spatial boundary to the other. A 2d soliton appears from the bulk viewpoint as a space-dependent monodromy of the abelian gauge fields, with a profile of variation determined by the 2d field configuration.

As a consequence of the coupling of the 2d and the 4d systems, any amount of flavor charge carried by a 2d soliton corresponds to some gauge charge of the 4d theory. In fact, one may consider (ij) solitons a and b, interpolating between the same vacua i and j, but differing by a net flavor charge. Schematically, let us indicate this for now as $a - b = \gamma$, meant to indicate that the a-soliton carries a net flavor charge of γ as compared to the b soliton. From the bulk viewpoint, the monodromy profile generated by a differs from the profile of b by a net flux of charge γ, much as if soliton a were a boundstate of soliton b with a 4d soliton of charge γ. Indeed, in this sense 4d solitons may "bind" to 2d solitons, forming a class of states known as *2d-4d BPS states* [65].

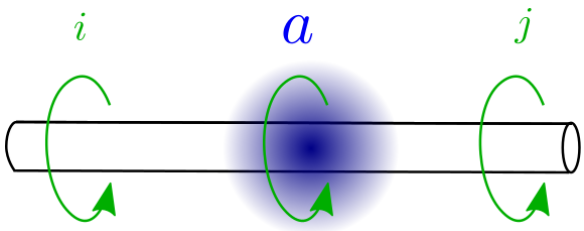

Figure 1.3: A soliton a supported on a surface defect, as it would appear in physical space. The soliton interpolates between vacua i and j, corresponding to different values of the monodromy of the bulk abelian gauge fields.

In addition to familiar 2d solitons interpolating between different vacua, surface defects in 2d-4d coupled systems exhibit a new type of solitons interpolating between a vacuum and itself. These are particularly interesting, as they are key in establishing the connection between 2d BPS spectra and

4d BPS spectra which allows to compute the latter from the former through the spectral networks technique. A soliton of this type generally carries nontrivial flavor charge from the 2d viewpoint, corresponding to a 4d electromagnetic charge. In fact, from the bulk viewpoint such 2d solitons appear as a change in the monodromy corresponding to a net flux carried by the abelian gauge fields, a configuration that is indistinguishable (from the bulk IR viewpoint) from having a charged 4d soliton on the defect in the given vacuum.

Class $\mathcal{S}$ theories admit a particular family of defects, known as *canonical surface defects* and denoted by $\mathbb{S}_z$. They are labeled by points $z \in C$, since in the M-theoretic construction they result from the presence of a semi-infinite membrane ending on the fivebranes along $\mathbb{R}^{1,1} \times \{z\} \subset \mathbb{R}^{1,3} \times C$ [65]. One peculiar aspect of canonical defects is that their vacua coincide with pre-images $\{z^{(i)}\}_i$ of z on Σ [65, 69], and therefore a 2d-4d soliton is labeled by a pair of sheets[7] (λ_i, λ_j) on Σ. As in the case of generic defects, two solitons interpolating between the same vacua $(z^{(i)}, z^{(j)})$ may differ by a net flavor charge in the 2d theory, corresponding to a gauge charge from the bulk viewpoint. Since the lattice of gauge charges is identified with $H_1(\Sigma, \mathbb{Z})$, the topological charge of a 2d soliton interpolating between a given pair of vacua is naturally classified by the relative homology class of an open path γ_{ij} on Σ, stretching from $z^{(i)}$ to $z^{(j)}$. The central charge and mass of a 2d soliton on $\mathbb{S}_z$ are given by

$$Z_{\gamma_{ij}} = \frac{1}{\pi} \int_{\pi(\gamma_{ij})} \lambda_{ij} \qquad\qquad M_{\gamma_{ij}} = \frac{1}{\pi} \int_{\pi(\gamma_{ij})} \left|\lambda_{ij}\right|, \tag{1.11}$$

it follows that the BPS condition $M_{\gamma_{ij}} = |Z_{\gamma_{ij}}|$ for 2d solitons coincides precisely with the geometric BPS bound encountered above. Indeed each point on a street p of a spectral network $\mathcal{W}_\zeta$ labels a canonical surface defect $\mathbb{S}_z$, carrying 2d-4d BPS solitons with central charges of phase ζ. As anticipated, to each street of the network is associated certain combinatorial data of 2d-4d BPS states: this is precisely the BPS spectrum of 2d solitons, expressed as a set of relative homology classes on Σ and integers:

$$\left\{ a \in H_1^{rel}((z^{(i)}, z^{(j)}); \Sigma, \mathbb{Z}) \,;\; \mu(a) \in \mathbb{Z} \right\} \tag{1.12}$$

the former correspond to topological charges of 2d solitons, and the latter to a supersymmetric index [27] counting solitons of the given charge.

Just like 4d "vanilla" BPS states, 2d-4d BPS states also exhibit a wall crossing behavior [25, 26, 65], whereby two solitons may bind together into a single one. More precisely, a $(z^{(i)}, z^{(j)})$ soliton may bind with a $(z^{(j)}, z^{(k)})$ soliton for certain values of the 2d couplings, forming a $(z^{(i)}, z^{(k)})$ soliton

[7] To have a global labeling of sheets of Σ, one must first choose branch cuts and trivialize the cover.

boundstate. For solitons of canonical defects, these "2d walls of marginal stability" are loci where a street of ij type of $\mathcal{W}_\zeta$ has some point in common with a street of jk type from the same network. On the one hand, if $i \neq k$ the resulting boundstate is a new 2d-4d BPS state, whose topological charge is simply the relative homology class obtained by natural composition (concatenation of open paths on Σ) of the topological charges of the two constituents. This is what happens in correspondence of joints of $\mathcal{W}_\zeta$, depicted on the left of Figure 1.4. On the other hand when $i = k$ the boundstate carries a purely four-dimensional topological charge[8] $\gamma = cl(\gamma_{ij} \circ \gamma_{ji})$, and appears from the bulk viewpoint as a 4d BPS soliton stuck on the IR defect in vacuum i. In other words, 2d BPS solitons

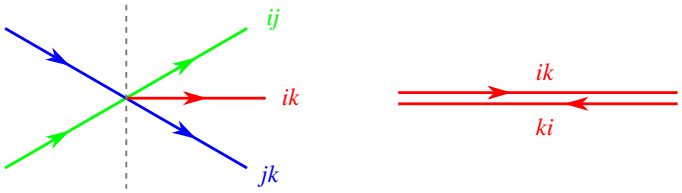

Figure 1.4: Wall crossing of 2d-4d BPS states as manifest in spectral networks on C. Left: only 2d-4d BPS solitons of ij and jk types exist for $\mathbb{S}_z$ supported on the left of the dashed line, while ik solitons may also exist on the right. Right: ik solitons may concatenate with ki solitons for certain values of u, boundstates are ii-type solitons carrying pure flavor charge of the 2d theory, corresponding to a gauge charge from the bulk viewpoint.

living on the surface defect can bind together into a 4d BPS soliton of the bulk theory: this is the mechanism underlying the *2d-4d wall crossing phenomenon*, first elucidated in [65]. Through 2d-4d wall-crossing, the 2d BPS spectrum is sensitive to the bulk "vanilla" BPS states, hence allowing to probe the latter by studying the former: this mechanism is key to computing 4d BPS spectra through spectral networks. In keeping with the previous logic, this phenomenon may also be seen at the level of spectral networks, although it is somewhat more special than regular joints. In fact, if $\mathbb{S}_z$ simultaneously supports 2d BPS states of charges γ_{ik}, γ_{ki} with the same phase ζ, it follows that $\mathcal{W}_\zeta$ must contain two BPS paths (streets of the network) running through z: one parametrized by λ_{ik} and the other by λ_{ki}, having opposite orientations as displayed on the right in Figure 1.4.

The appearance of "two-way" streets generally corresponds to values of ζ for which $\mathcal{W}_\zeta$ has a degenerate topology. A sub-network of two-way streets is of course a generalization of the "finite BPS geodesics" that were previously associated with 4d BPS states as a consequence of their M theory interpretation. However, from the viewpoint of spectral networks, rather than being merely a finite BPS geodesic, a two-way street carries the additional data of 2d degeneracies. By exploiting the 2d-4d wall-crossing picture, where boundstates of 2d BPS solitons produce 4d BPS solitons,

[8] Here $\circ$ denotes concatenation of paths, and cl is the closure map, turning an open path with matching endpoints into a closed one.

the degeneracies of the latter can in fact be obtained from careful combinatorics of the data of the former. More specifically, perturbing the critical phase ζ in either direction gives two resolved

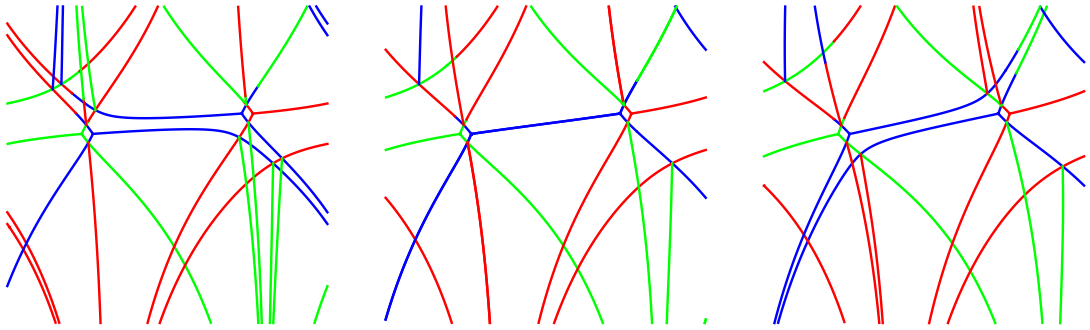

Figure 1.5: Center: a network with degenerate topology occurs when streets of "opposite" types collide head-on. The blue segment in the middle consists of two such streets. (Here C is a cylinder, obtained by identification of the left and right edges of the picture.) Left and right: networks from the same family $\mathcal{W}_\zeta$ at slightly different phases have a non-degenerate topology, exhibiting two different resolutions of the two degenerate streets.

inequivalent networks $\mathcal{W}_{\zeta^\pm}$ (see Figure 1.5), encoding the spectrum of 2d-4d BPS states before and after the jump. Then the data of these two spectra, when packaged into a certain physically- and mathematically-motivated generating function $F(\wp)$ (its definition and interpretation will be reviewed in detail in Section 3.1), are related precisely by a Kontsevich-Soibelman transformation (1.4). Conversely, comparing the 2d soliton content of $\mathcal{W}_{\zeta^\pm}$ it is possible to *compute* the 4d BPS degeneracies $\Omega(\gamma; u)$ of those states responsible for the jump of $\mathcal{W}_\zeta$. This is how BPS degeneracies are captured by spectral networks: as ζ is continuously varied one focuses on the topological jumps of $\mathcal{W}_\zeta$, the 4d BPS spectrum is then extracted from a detailed study of the combinatorics of 2d-4d soliton spectra in correspondence of the jumps. A detailed review of these techniques and their applications is provided in Section 3.1.

We turn next to introducing the main content of this thesis, based on the papers [72, 73, 95] as well as unpublished joint work [96]. Sections 1.2-1.5 present the main results, while each of the corresponding chapters 2-5 gives the corresponding in-depth exposition and discussion. Chapter 6 concludes with a look to the future, we collect the most interesting questions raised by our work, and promising directions.

1.2 The Spectrum Generator of 2d-4d BPS States for $S[A_1, C, D]$ theories

Chapter 2 focuses on A_1-type theories of class $\mathcal{S}$. These are special in a number of ways: for one thing their BPS spectrum contains only hypermultiplets and vectormultiplets; another special feature is

that their spectral networks are dual to ideal triangulations of C. A third distinguishing feature of A_1 theories is that a *single* triangulation actually encodes the whole BPS spectrum, bypassing the need to study the jumps that occur varying ζ [64] – a potentially challenging task [63, 64, 73]. More precisely, from the topology of an ideal triangulation it is possible to extract the spectrum generator $\mathbb{S}$ of 4d BPS states, from which the full spectrum can be deduced. Then a natural question to ask is whether there exists an analog of the spectrum generator of 4d BPS states, which captures all 2d-4d BPS states. In fact, upon introducing suitable generalizations of the $\mathcal{X}_\gamma$ coordinates, associated with topological charges of 2d-4d BPS states and denoted by $\mathcal{Y}_{\gamma_{ij}}$ [65], the 2d-4d BPS degeneracies ω, μ are actually encoded into a product of Poisson morphisms acting on these new functions[9]

$$\begin{aligned} \mathcal{Y}'_{\gamma_{ij}} &= \mathbb{S}\, \mathcal{Y}_{\gamma_{ij}} \\ \mathbb{S} &=: \prod_{\gamma} \mathcal{K}_\gamma^{\omega} \prod_{\gamma_{ij}} \mathcal{S}_{\gamma_{ij}}^{\mu} : \end{aligned} \tag{1.13}$$

In some explicit examples, detailed formulae for the transformation $\mathbb{S}$ are provided by equations (2.61), (2.64), (2.77), (2.98) and (2.111) below, and by the equations right above them. The main goal of this Chapter is to find an algorithm to compute the transformed $\mathcal{Y}'_{\gamma_{ij}}$ directly in terms of the original $\mathcal{Y}_{\gamma_{ij}}$, based on knowledge of a *single* triangulation. Our result is a set of formulae for the $\mathcal{Y}'_{\gamma_{ij}}$, expressing them in terms of the original coordinates and the given ideal triangulation. The expressions we derive encode the action of the most general $\mathbb{S}$ on the $\mathcal{Y}_{\gamma_{ij}}$, and they can be easily applied to any specific situation. Just like in the pure 4d case, once adapted to the specific situation under study, our formulae encode the 2d-4d BPS degeneracies. Our formulae provide therefore a systematic approach to the study of 2d-4d spectra of A_1-type theories: as we show through examples, it is fairly easy to recover the simplest finite spectra from our general expressions, while more complicated theories will probably require some sort of algorithm to extract the degeneracies.

1.3 Wild Wall Crossing

In Chapter 3 we turn our attention to higher rank gauge theories, and investigate their BPS spectra by means of spectral networks and wall-crossing techniques. As noted by various authors, theories of class $S[A_{K-1}]$ for $K > 2$ could have higher spin BPS states, beyond the familiar hypermultiplets and vectormultiplets which occur in theories of class $S[A_1]$. One result of this chapter is that this

[9] here $\mathcal{K}_\gamma, \mathcal{S}_{\gamma_{ij}}$ correspond respectively to morphisms induced by 4d and 2d-4d BPS states, and : : denotes an ordering by phases of central charges of the product.

expectation is indeed correct: higher spin BPS multiplets do occur at some points of the Coulomb branch in one explicit theory of class $S[A_2]$, namely the pure $d = 4$, $\mathcal{N} = 2$, $SU(3)$ theory.

In addition, we find a much more surprising phenomenon: theories of class S can have *wild BPS spectra*, i.e. at some points of the Coulomb branch, the number of BPS states with mass $\leq M$ grows *exponentially* with M. The main result of this chapter is two independent demonstrations, in Sections 3.2 and 3.3, that wild spectra appear in the pure $d = 4, \mathcal{N} = 2, SU(3)$ theory. The possibility that there could be such exponential growth in BPS degeneracies in field theory was suggested some time ago in [84].

As explained in Section 3.6 below, this exponential growth is physically a bit surprising. Indeed, the existence of a conformal fixed point defining the 4d theory, plus dimensional analysis, implies that the degeneracy of BPS states at energy E in finite volume V cannot grow faster than $\exp[\text{const} \times V^{1/4}E^{3/4}]$. On the other hand, here we are finding that the spectrum of BPS 1-particle states grows like $\exp[\text{const} \times E]$. The resolution of this puzzle must lie in the difference between BPS 1-particle states and states in the finite volume Hilbert space; we propose that the size of the objects represented by the BPS 1-particle states grows with E, so that for any fixed V, most of the BPS 1-particle states simply do not fit into the finite-volume Hilbert space. Indeed, in Section 3.6, using Denef's picture of BPS bound states, we demonstrate directly that their size does indeed grow with E. The invalid exchange of large E and large V limits when accounting for field theory entropy should perhaps serve as a cautionary tale.

Here is the fundamental idea which we use to find wild BPS degeneracies. Suppose we have an $\mathcal{N} = 2$ theory and a point of the Coulomb branch in which the spectrum contains two BPS hypermultiplets, of charges γ and γ', and no bound states thereof — i.e. we have the BPS degeneracies $\Omega(\gamma) = 1$, $\Omega(\gamma') = 1$, $\Omega(a\gamma + b\gamma') = 0$ for all other $a, b \geq 0$. Then suppose we move on the Coulomb branch to a point where the central charges Z_γ and $Z_{\gamma'}$ have the same phase. Such a point lies on a wall of marginal stability. On the other side of the wall, the spectrum includes bound states with charge $a\gamma + b\gamma'$ for various a, b. Their precise degeneracies can be determined by the Kontsevich-Soibelman wall-crossing formula, and indeed depend *only* on the integer $m = \langle \gamma, \gamma' \rangle$. For this reason we call the collection of BPS states thus generated an "m-cohort."

The cases $m = 1$ and $m = 2$ occur already in the theories of class $S[A_1]$. For $m = 1$ an m-cohort contains only a single bound state; for $m = 2$ an m-cohort contains an infinite set of hypermultiplets plus a single vector multiplet. In either case, at any rate, one does not get wild degeneracies. In contrast, for $m > 2$ the wall-crossing formula shows that an m-cohort does contain wild degeneracies. Indeed, even if one restricts attention to charges of the form $n(\gamma + \gamma')$, one already has exponential

growth. This is explained and made precise in Proposition 3.2.4, Section 3.4.3, and Section 3.5.3 below. With this in mind, for any $m > 2$, we will say that a theory contains "m-wild degeneracies" if its BPS spectrum contains an m-cohort.

The BPS degeneracies arising in m-cohorts have been studied at some length in the mathematics literature because they arise as Donaldson-Thomas invariants attached to the m-Kronecker quiver in one region of its stability parameter space. The latter have been intensively studied in [115–118, 127, 128]. One interesting feature noted there is that for $m > 2$, the phases of the central charges of BPS states in an m-cohort are *dense* in some arc of the circle.

This discussion motivates two approaches to the problem of exhibiting wild degeneracies in a physical theory. Our first approach goes via the "spectral networks" of [63, 70]: rather than studying the wall-crossing directly, we make a guess about the kind of spectral networks which *could* arise from wall-crossing involving two hypermultiplets with arbitrary $m = \langle \gamma, \gamma' \rangle$. For $m = 1$ the network we draw looks like a saddle, which motivates an equine terminology: our networks are built from constituents we call "horses" (defined in Section. 4.4, Figure 3.3, and detailed in Appendix C), glued together to form "m-herds." See Figure 3.4 for some examples. We show moreover that m-herds indeed occur in physical spectral networks at some particular points of the Coulomb branch of the $SU(3)$ theory: see Figure 3.5 for the evidence. The general rules of spectral networks, combined with Proposition 3.1 and Proposition 3.2 below, lead to the following formula for the BPS spectrum for charges of the form $n(\gamma + \gamma') := n\gamma_c$ in the wild region. We first form a generating function $P_m(z)$ related to the BPS spectrum by

$$P_m(z) = \prod_{n=1}^{\infty} (1 - (-1)^{mn} z^n)^{n\Omega(n\gamma_c)/m}. \tag{1.14}$$

Then, Proposition 3.1 states that $P_m(z)$ is a solution of the algebraic equation (4.111), which we reproduce here:

$$P_m = 1 + z \left(P_m\right)^{(m-1)^2}. \tag{1.15}$$

This equation had been identified previously by Kontsevich and Soibelman [88] and by Gross and Pandharipande [75], as the one governing the generating function of BPS degeneracies of an m-cohort, for charges of the form $n(\gamma + \gamma')$. It follows that if we have an m-herd ($m > 2$) somewhere in our theory, then our theory does contain at least the part of an m-cohort corresponding to charges of the form $n(\gamma + \gamma')$. In particular, if the theory contains an m-herd, then it does contain wild degeneracies. Since we have found m-herds at some points of the Coulomb branch in the pure $SU(3)$ theory, we conclude that we indeed have wild degeneracies in that theory.

The algebraic equation (1.15) is apparently an instance of a more general phenomenon. It has been observed by Kontsevich that the generating functions of Donaldson-Thomas invariants are often solutions of algebraic equations. For the Kronecker quiver and some other special cases Kontsevich has proved that these equations exist [86]. Our analysis via spectral networks produces the algebraic equation (1.15) in a direct way. Moreover, we expect that this will happen more generally, as we explain in Appendix F. Thus spectral networks seem to be a natural framework for understanding Kontsevich's observation.

Our second method of demonstrating the existence of wild spectra uses wall-crossing more directly. Namely, in Section 3.3.2 we exhibit a path on the Coulomb branch which begins in a strong coupling chamber with a finite set of BPS states, and leads to a wall-crossing between two hypermultiplet charges γ, γ' with $\langle \gamma, \gamma' \rangle = 3$. As we have discussed above, the existence of such a path directly implies the existence of wild spectra. In fact this gives more than we got from the spectral network: it shows that there is a whole 3-cohort in the spectrum. In Section 3.4.2 we perform some nontrivial checks of this statement by factorizing the spectrum generator derived from the known finite spectrum in a strong coupling chamber. In Section 3.4.3 we also check numerically the exponential growth of the BPS degeneracies for sequences of charges of the form $n(a\gamma + b\gamma')$, $n \to \infty$, for various values of a, b.

In Section 3.5 we discuss the behavior of the "BPS quivers" of the $SU(3)$ theory along the path found in Section 3.3.2. It turns out that the Kronecker 3-quiver is in fact a subquiver of the BPS quiver, after one has performed suitable mutations and made a suitable choice of half-plane to define simple roots. We similarly argue that for *all* $m \geq 3$ (not only $m = 3$) there are Kronecker m-subquivers and corresponding m-wild spectra on the Coulomb branch of the $SU(3)$ theory.

In the course of our investigations we also studied the protected spin characters (a.k.a. "refined BPS degeneracies") for the m-Kronecker quiver in the wild region. Our main tool was the "motivic" Kontsevich-Soibelman formula [88, 90]. While investigating these spin degeneracies we discovered some beautiful but strange systematics. Some of these were previously discovered by Weist and Reineke in [128] and [118], respectively, but some are new. We collect them in Section 3.7. Perhaps the most notable new observation is that the spin degeneracies appear, (on the basis of numerical data), to obey a universal scaling law. See equations (3.106) and (3.107).

1.4 Protected Spin Characters from Spectral Networks

In Chapter 4 we describe a refinement of the Spectral Networks method for computing BPS degeneracies. We propose an algorithm to compute the spin content, or more properly, the protected spin character, of the space of BPS states at a given charge. One motivation for such an algorithm is that, while the range of applicability of the spectral networks technique is rather large, the information it provides about BPS states is, in a sense, somewhat limited. On the one hand, as already anticipated, the only information about BPS states of the 4d gauge theory which can be extracted from spectral networks is the BPS index. On the other hand, the results of chapter 3 (in particular, of section 3.7) emphasize that BPS spectra can exhibit a rather rich structure, which is missed by the BPS index alone, but is captured by the protected spin character (PSC). The PSC provides a refined description of BPS states, in particular by encoding their spin, thereby capturing the rich structures of wild spectra uncovered in [73]. Given its importance, and the questions raised by the occurrence of wild spectra, it would be desirable to develop a framework for a systematic study of the PSC. The main result of this Chapter is a proposal for extracting PSC data from a certain *refined* version of spectral networks, thus generalizing the BPS index formula of [63]. Specifically, we propose a method for computing the spin of both *framed* and *vanilla* BPS states. (The terminology comes from [61, 63, 65].)

We will argue below that spectral networks actually contain much more information than hitherto utilized. In section 4.1 we formulate precise conjectures explaining where such extra information sits within the network data, and how it encodes spin degeneracies. A key ingredient is the refinement of the classification of soliton paths induced by *regular homotopy*. After introducing a suitable formal algebra associated with this refinement, in section 4.2 we provide the related generalization of the formal parallel transport of [63]. This involves establishing a refined version of the *detour rules*, whose physical interpretation explains the wall-crossing of framed BPS states. The refinement by regular homotopy allows one to associate to each path $\mathfrak{a}$ an integer known as the *writhe* $\mathrm{wr}(\mathfrak{a})$, consisting of a certain signed sum over self-intersections. We identify the writhe with the spin of a framed BPS state, while its charge is given by the canonical projection to relative homology. In the same way as framed degeneracies are good probes to study vanilla BPS indices, the framed PSCs obtained in this way serve the same purpose for computing vanilla PSCs.

Important consistency checks come from the halo picture of framed wall-crossing [14, 61], which was crucial in linking jumps of PSCs at walls of marginal stability and the motivic Kontsevich-Soibelman wall-crossing formula [88, 90]. The main idea here is to associate a path $\wp$ on the ultraviolet

curve C with a supersymmetric interface between surface defect theories [65]. We find that the halo picture easily emerges within our proposal if we restrict to a certain type of susy interface. We provide a criterion that distinguishes this special class and call them *halo-saturated interfaces*. Physically, their crucial feature is that their wall-crossing behavior mimics that of line defects [61]. The wall-crossing behavior of more generic interfaces is one issue which remains only partially understood, in particular it would be desirable to shed light on the halo interpretation of the framed wall crossing of generic interfaces. In section 4.3.4 we study a particular example and find some apparent tension with the halo picture. However, by taking into account a refinement of the homology on Σ induced by the presence of the interface, we eventually find a reconciliation with the halo interpretation. A systematic understanding of how the halo picture fits with our conjectures for generic interfaces is left as an interesting and important open problem for the future.

We would like to mention another curious conjecture, even though it is not central to the main development of the paper. Only certain states in a vanilla multiplet will bind to a generic interface [63, 65, 95]. This suggests that each state within the vanilla multiplet can be associated with a *subnetwork* of the critical network $\mathcal{W}_c$, and that the halos forming around the interface depend on how the latter[10] intersects the various subnetworks. Towards the end of section 4.3.4 we mention this hypothesis when discussing contributions from "phantom" halos to the $\mathcal{K}$-wall jumps of framed PSCs, while we defer a more detailed study to appendix H, where supporting evidence is also offered.

We leave a proof of our conjectures to future work. We concentrate instead on how they are realized in various examples, and on their consequences. The results are in perfect agreement with other approaches, such as results derived from motivic wall-crossing (see for example [73]) or from quiver techniques. In particular, we consider the rich playground provided by the wild BPS states investigated in [73]. These wild BPS states typically furnish high-dimensional and highly reducible representations of the group of spatial rotations. In a wild chamber of the Coulomb branch one finds BPS multiplets of arbitrarily high spin. In this phase of the IR theory the number of BPS states grows exponentially with the mass, a surprising fact for a gauge theory [73, 84, 85]. We will apply our techniques both to the *herd networks*, which describe a particular type of wild state, as well as to a new type of wild critical network which is a close cousin of the herds. Wild spectral networks have been associated with algebraic equations for generating functions of BPS indices [73, 75, 88, 90]. For instance, it was found (see [73, eq.(1.1)]) that herd networks encode an algebraic equation familiar in the context of the tropical vertex group. By exploiting our construction of the formal

[10] More properly, the relative homology class associated to it.

parallel transport, we derive a deformation of that equation

$$P(z,y) = 1 + z \prod_{s=-(m-2)}^{m-2} P(zy^{2s}, y)^{m-1-|s|}\,, \tag{1.16}$$

which is of a *functional* nature. We check that (1.16) correctly describes the generating function of PSCs, and discuss its consistency with quiver representation theory (in particular with Kac's theorem [73, 116] and Poincaré polynomial stabilization [118]).

Finally, since the use of formal variables and the introduction of the writhe might seem artificial to some readers, in §4.5.2 we propose a framework in which all these crucial ingredients arise naturally. A quantization of the moduli space of flat abelian connections on the Seiberg-Witten curve naturally yields an operator algebra resembling that of our formal variables. From a slightly different viewpoint, our formal variables may be thought of as Wilson operators of a certain abelian Chern-Simons theory. From this perspective both the refined classification of paths (which are singular knots in our case) by regular homotopy and the role of the writhe are no surprise at all (see e.g. [50]). We do not develop the relation of our story to Chern-Simons theory in detail, rather we limit ourselves to some preliminary remarks. However we do expect an interpretation of our refined construction of the formal parallel transport as a *map between observables* of two distinguished Chern-Simons theories.

1.5 The BPS spectrum of the $SU(2)$ $\mathcal{N} = 2^*$ theory

Despite the great deal of progress in finding the BPS spectrum of many $\mathcal{N} = 2$ theories in recent years [11, 12, 63, 64], finding that of a rather simple and beautiful theory, the $SU(2)$ $\mathcal{N} = 2^*$ theory, has proven somewhat recalcitrant to the existing techniques. In chapter 5 we give a solution to the problem by combining an analysis of the weak coupling spectrum using the method of the spectrum generator introduced in [64]. The content of this chapter is based on unpublished work in collaboration with Greg Moore [96].

Let us summarize the main result here. There is a one-dimensional Coulomb branch, the u-plane, with a rank three local system Γ of charges with three singularities with monodromy conjugate to T^2. Locally we may choose a trivialization with generators γ_i, $i \in \mathbb{Z} \mod 3$ satisfying $\langle \gamma_i, \gamma_{i+1} \rangle = 2$. The sum $\gamma_f = \gamma_1 + \gamma_2 + \gamma_3$ is a monodromy-invariant flavor charge and has a fixed central charge $Z(\gamma_f; u) = m$ throughout the u-plane. Assuming that the $Z(\gamma_i, u)$ lie within the same half complex plane, there is then an exceptional locus

$$\mathcal{E} = \bigcup_{i=1}^{3} \mathcal{E}_i\,, \qquad \mathcal{E}_i = \{u | Z(\gamma_i; u)/m > 0,\, \mathrm{Arg}\, Z(\gamma_{i+1}; u) < \mathrm{Arg}\, Z(\gamma_{i-1}; u)\} \tag{1.17}$$

where the BPS spectrum is exceptionally simple. A pedantic reader will certainly find this statement a bit disturbing, since $\mathcal{E}_i$ correspond to walls of marignal stability, where the spectrum is ill-defined. An *astute* reader, however, will further note that no wall crossing may happen at such wall, due to the vanishing of $\langle \gamma, \gamma' \rangle$ for any two charges whose central charges align here[11]. Therefore, it makes perfect sense to speak of the spectrum at these loci.

Let us focus on the case $u \in \mathcal{E}_3$, where $\operatorname{Arg} Z(\gamma_2) > \operatorname{Arg} Z(\gamma_1)$. Then we claim that[12]

$$\begin{aligned} \Omega(n\gamma_1 + (n+1)\gamma_2, u; y) &= 1 \qquad n \geq 0 \\ \Omega(\gamma_3, u; y) &= 1 \\ \Omega(\gamma_1 + \gamma_2; u; y) &= y + y^{-1} \\ \Omega(2\gamma_1 + 2\gamma_2 + \gamma_3, u; y) &= 1 \\ \Omega((n+1)\gamma_1 + n\gamma_2, u; y) &= 1 \qquad n \geq 0 \end{aligned} \tag{1.18}$$

and $\Omega(\gamma, u; y) = 0$ for all other charges (except for charges whose negative is a member of the above list, since of course $\Omega(-\gamma, u; y) = \Omega(\gamma, u; y)$)[13]. Analogous results hold on the other loci $\mathcal{E}_i$.

Equation (1.18) may be described simply in words. There is a region of $\mathcal{E}_3$ in which we can discuss the spectrum in semiclassical terms. In a suitable duality frame we expect a massive vector multiplet from the spontaneous breaking of $SU(2) \to U(1)$. This accounts for states of charge $\gamma_1 + \gamma_2$. In addition the field-theoretic hypermultiplet provides states with charges $\gamma_f \pm (\gamma_1 + \gamma_2)$. Finally, there are 't Hooft-Polyakov magnetic monopoles that form dyonic boundstates with the massive W-bosons of charges $\pm(\gamma_1 + \gamma_2)$. These account for the remaining charges in the list (1.18).

In general such a semiclassical analysis *cannot* determine the full spectrum because it is hard to analyze the relevant supersymmetric quantum mechanics on monopole moduli spaces with higher magnetic charge. It is precisely at this point that the spectrum generator of [64] comes to the rescue. We recall that the spectrum generator is defined as the product of KS transformations associated to occupied BPS rays in a halfplane $\mathbb{H}_\vartheta$:

$$\mathbb{S} = \prod_{\gamma : \vartheta < \operatorname{Arg} -Z_\gamma(u) < \vartheta + \pi}^{\curvearrowleft} \mathcal{K}_\gamma^{\Omega(\gamma;u)}. \tag{1.19}$$

A key result of [64] is a straightforward algorithm for computing $\mathbb{S}$ *exactly*, in closed form, as a symplectic transformation, from a spectral network [63] (equivalently, a WKB triangulation) of

[11] More precisely, no wall crossing that could be detected by the Kontsevich Soibelman formula. It is however true that there will be marginally stable boundstates of mutually local states, their (in)stability must be determined by other means.

[12] The $\Omega(\gamma, u; y)$ employed here is precisely the protected spin character introduced previously.

[13] An important exception are *pure flavor* BPS states, i.e. those which do not carry any net gauge charge (this notion is invariant of the choice of e.m. duality frame). These are not captured by Kontsevich-Soibelman wall crossing, and contribute trivial factors to $\mathbb{S}$; they can be studied, however, by means of spectral networks.

phase ϑ. In a word, our main computation in this chapter is to show that the spectrum (1.18) completely accounts for the spectrum generator of the $SU(2)$ $\mathcal{N} = 2^*$ theory computed from the algorithm of [64]. This computation is carried out in §5.3.2

Using the Kontsevich-Soibelman wall-crossing formula [88, 90] we can now in principle determine the spectrum in any other region of the Coulomb branch. We give some illustrative results in section 5.4. The general pattern is that the factorization of $\mathbb{S}$ involves an *infinite* number of vectormultiplets, each with its corresponding "cohort" of dyonic boundsates. Indeed, the loci $\mathcal{E}_i$ are extremely special in that they have a single vectormultiplet. We also argue that all the wall-crossing events are copies of the basic SU(2) wall-crossing, involving creation/annihilation of $2-$cohorts, implying the absence of wild walls.

Chapter 2

The Spectrum Generator in Coupled 2d-4d Systems

2.1 Spectrum generating functions in 2d-4d systems

2.1.1 A short account of the GMN construction

Let us begin by recalling some fundamental ingredients from papers [61, 64, 65]. At generic u on the Coulomb branch $\mathcal{B}$ of $\mathcal{N} = 2$ four-dimensional SYM, there is a family of WKB triangulations T^{ϑ}_{WKB} of C, defined as the isotopy class of the flow

$$\langle \partial_t, \lambda \rangle \in e^{i\vartheta}\mathbb{R}^{\times} \tag{2.1}$$

where λ is the Seiberg-Witten differential. These triangulations are piecewise independent of ϑ and the BPS spectrum manifests itself through jumps of T^{ϑ}_{WKB} at values of ϑ coinciding with $Arg\, Z_{\gamma_{BPS}}$. The Hitchin system arises by considering a different kind of compactification, namely taking the the 6d theory on a circle, which leads to 5d super Yang-Mills, then considering the "4d BPS instantons" on the space-like directions, finally reducing the corresponding self-duality equations on C. The M-theory engineering of these theories provides the data that is necessary to specify the corresponding Hitchin system, in particular the behavior of the Higgs field φ and of the connection A at singular points, in correspondence of M5-brane intersections [32, 59]. The solutions of the Hitchin system that satisfy the boundary conditions, modulo gauge, are parameterized by a hyperkahler manifold $\mathcal{M}$ which is also the moduli space of flat $sl(2, \mathbb{C})$ connections defined by

$$\mathcal{A} = \frac{R}{\zeta}\varphi + A + R\zeta\bar{\varphi}, \qquad \zeta \in \mathbb{C}^{\times}. \tag{2.2}$$

At each singularity there is a monodromy matrix M_i associated with this connection, which depends on the boundary data as well as on ζ, R. Each of the M_i has two eigen-sections s_i, $\tilde{s}_i$, with respective eigenvalues μ_i, μ_i^{-1}. The *small flat section* at a singularity is defined to be the $\mathcal{A}$-flat eigen-section s_i , chosen between the two such that its norm decreases when evaluated along WKB lines that flow into the singularity. The choice of small flat section at each singularity is a "decoration" of T_{WKB}.

Each edge of the triangulation corresponds to a homology cycle of the spectral curve of the Hitchin system. Let Γ denote the lattice generated by such cycles, to each $\gamma \in \Gamma$ one associates a corresponding Fock-Goncharov coordinate $\mathcal{X}_\gamma$ defined by

$$\mathcal{X}_\gamma = -\frac{(s_i \wedge s_j)(s_k \wedge s_\ell)}{(s_j \wedge s_k)(s_\ell \wedge s_i)} \tag{2.3}$$

where i, j, k, ℓ denote the four singularities -ordered counterclockwise- at the corners of a quadrilateral with E_γ stretching between singularities i, k. Here the cycles γ belong to Γ, the homology sublattice of gauge charges. The jumps of T^ϑ_{WKB} are quantitatively described by Poisson transformations $\mathcal{K}_{\gamma'}$ acting on the $\mathcal{X}_\gamma$, there are two main types of jumps: one due to a BPS hypermultiplet and one due to a vectormultiplet. Naively, keeping track of the jumps as ϑ varies is one way to recover the BPS spectrum, however typical spectra are infinite and in practice cannot be obtained with this method. The BPS spectrum divides evenly into *particles* and their CPT conjugates, by adopting an appropriate definition of particle , the central charges can be taken to lie within a half of the complex plane; therefore varying ϑ over an angle of π captures all the states of interest. The full BPS spectrum is then encoded into the transformations $\mathcal{X}^\vartheta_{\gamma_i} \mapsto \mathcal{X}^{\vartheta+\pi}_{\gamma_i}$ (γ_i runs over a basis of Γ), these determine[1] an operator $\mathbb{S}$ having a *unique* factorization

$$\mathbb{S} = \prod_\gamma \mathcal{K}_\gamma^{\Omega(\gamma,u)} \tag{2.5}$$

where $\Omega(\gamma, u)$ are the BPS degeneracies for states of charge γ.

At this point, this method might appear quite inconvenient, because of the difficulties involved in constructing explicitly Fock-Goncharov coordinates. As a matter of fact, however, there are simple expressions for the $\mathcal{X}^{\vartheta+\pi}_{\gamma_i}$ in terms of the initial FG coordinates. In [64] a fairly easy recipe for writing them down was provided, which applies to all A_1 theories of class $\mathcal{S}$. For later convenience we briefly recall the key idea behind it. The crucial step is to notice that $T^{\vartheta+\pi}_{WKB}$ has the same topology as T^ϑ_{WKB}, but inverted flow direction, the overall effect of this is to switch the definition

[1]The Fock-Goncharov coordinates obey the multiplication rules

$$\mathcal{X}_\gamma \mathcal{X}_{\gamma'} = \mathcal{X}_{\gamma+\gamma'} \tag{2.4}$$

thus, the transformations of *basis coordinates* (those associated to a basis of Γ) determine that of any $\mathcal{X}_\gamma$.

of small flat section at each singularity, this amounts to a change in the *decoration* of T_{WKB} also known as the *omnipop*. One can then write down the *spectrum generating functions* S_i, defined by

$$\mathcal{X}_{\gamma_i}^{\vartheta+\pi} = \mathbb{S}\,\mathcal{X}_{\gamma_i}^{\vartheta} \;=\; S_i\,\mathcal{X}_{\gamma_i}^{\vartheta} \tag{2.6}$$

by noting that, in the ratio $\mathcal{X}_{\gamma_i}^{\vartheta+\pi}/\mathcal{X}_{\gamma_i}^{\vartheta}$, terms containing the new small flat sections cancel out. As a side note, we stress that the spectrum generating functions only implicitly encode the BPS spectrum, while the factorization of the spectrum generator $\mathbb{S}$ into $\mathcal{K}$ operators ultimately encodes the spectrum in an explicit fashion.

The aim of this paper is to extend this technique to the case of coupled $2d-4d$ systems. In fact, just like gauge charges of the 4d IR theory have a nice geometric interpretation as representatives of $H_1(\Sigma,\mathbb{Z})$, correspondingly charges of $2d$ solitons are described by introducing a set of Γ-torsors Γ_{ij}, $i,j\in\mathcal{V}$ the set of vacua of the defect.[2] An element of Γ_{ij} corresponds then to a representative of the relative homology class of oriented open paths on Σ, running from z_i to z_j, two of the lifts of $z\in C$ to Σ, where z is the position of the defect. This interpretation, together with the natural notion of composition of oriented paths, determines whether two charges can be "added together". The $2d-4d$ BPS spectrum is studied by introducing an enlarged set of Fock-Goncharov variables $\mathcal{Y}_a$[3], where a is any charge belonging to Γ,Γ_{ij}.

The construction of the $\mathcal{Y}$ is analogous to that of the $\mathcal{X}$ for the pure gauge charges, while we review it below for the other types of charges. Two distinct sets of degeneracies are employed to describe the full 2d-4d spectrum: the $\omega:\Gamma\times\coprod_{i,j}\Gamma_{ij}\to\mathbb{Z}$, satisfying $\omega(\gamma,a+b)=\omega(\gamma,a)+\omega(\gamma,b)$ and the $\mu:\Gamma_{ij}\to\mathbb{Z}$ defined for each $\gamma_{ij},\ i\neq j$. The picture is closely analogous to the 4d one: the spectrum manifests itself through an ordered product of transformations acting on the $\mathcal{Y}$, this time however there are two different types of transformations.

$$\mathbb{S} =: \prod_{\gamma}\mathcal{K}_{\gamma}^{\omega}\prod_{\gamma_{ij}}\mathcal{S}_{\gamma_{ij}}^{\mu}: \tag{2.8}$$

where the : : indicate that the product is ordered according to the phases of the central charges of the BPS states involved.

[2] Physically, the rationale is that an element γ_{ij} of one of these torsors represents a $2d$ soliton state carrying some $4d$ gauge charge.

[3] The $\mathcal{Y}$ obey a *twisted* multiplication rule

$$\mathcal{Y}_a\mathcal{Y}_b = \begin{cases} \sigma(a,b)\mathcal{Y}_{a+b} & \text{if } a+b \text{ is defined} \\ 0 & \text{otherwise} \end{cases} \tag{2.7}$$

the definition of the twisting function $\sigma(a,b)$ can be found in §7 of [65]

2.1.2 The conjugate section at a singularity

For later convenience, we now determine explicitly the "large" flat section $\tilde{s}_P$ at a singular point $P \in C$, written in terms of s_a and of the $\mathcal{X}_a$ in the star-shaped neighborhood of P.

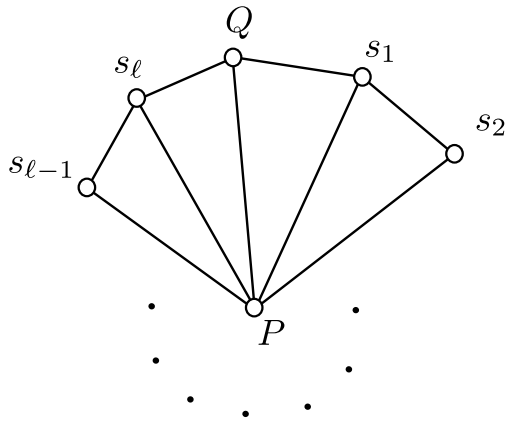

Figure 2.1: The triangulation of C around a generic regular singularity.

Let us begin with the case, shown in fig.2.1, in which P is a regular singular point, and every point in its neighborhood is a regular singular point. Define

$$\Sigma(P; Q \to Q) = 1 + \mathcal{X}_{P,\ell} + \mathcal{X}_{P,\ell}\mathcal{X}_{P,\ell-1} + \cdots + (\mathcal{X}_{P,\ell} \cdots \mathcal{X}_{P,1}) \tag{2.9}$$

this can be expressed [64] in terms of flat sections as

$$\Sigma(P; Q \to Q) = (1 - \mu_P^2) \frac{(s_P \wedge s_\ell)(s_Q \wedge \tilde{s}_P)}{(s_Q \wedge s_\ell)(s_P \wedge \tilde{s}_P)}. \tag{2.10}$$

solving for $\tilde{s}_P$ we have[4]

$$\tilde{s}_P = \xi_P \left[(\Sigma(P; Q \to Q)(s_Q, s_\ell) s_P - (1 - \mu_P^2)(s_P, s_\ell) s_Q \right] \tag{2.11}$$

where ξ_P is a constant depending on the normalization convention we choose. Both $\Sigma(P; Q \to Q)$ and μ_P have explicit expressions in terms of the $\mathcal{X}_a$, so this is the form of $\tilde{s}_P$ we were after. This has a straightforward extension to the case in which any of P and its neighbors are irregular punctures, we deal with it below.

2.1.3 The omnipop for solitonic FG coordinates

We focus on the *shortest* representatives of each relative homology class. The spectrum generator for more general ones can be obtained by employing the twisted product law of the $\mathcal{Y}$: writing $\mathcal{Y}_{\gamma_{ij}^0 + \gamma}$

[4] To lighten notation, we use $(s_a, s_b) \equiv (s_a \wedge s_b)$ from here on.

as a twisted product of coordinates corresponding to the "simplest" solitonic charges $\mathcal{Y}_{\gamma_{ij}^0}$ together with purely gauge $\mathcal{Y}_\gamma$.

Any WKB triangulation of C carries a corresponding decomposition into quadrilateral *cells* C_{ab} bounded by four *separating* WKB lines [64], i.e. with vertices consisting of two turning points and two singularities a and b, subject to the constraint that there aren't any singularities, nor turning points within the cell. As a first example, let us consider a single surface defect located at $z \in C_{ab}$, within a quadrilateral which vertices are all regular punctures, our goal is to compute the omnipop for the $\mathcal{Y}$ corresponding to a BPS ij-soliton. This type of situation was examined in §7.5.2 of [65], $T^\vartheta_{\mathrm{WKB}}$ is shown in Fig.2.2.

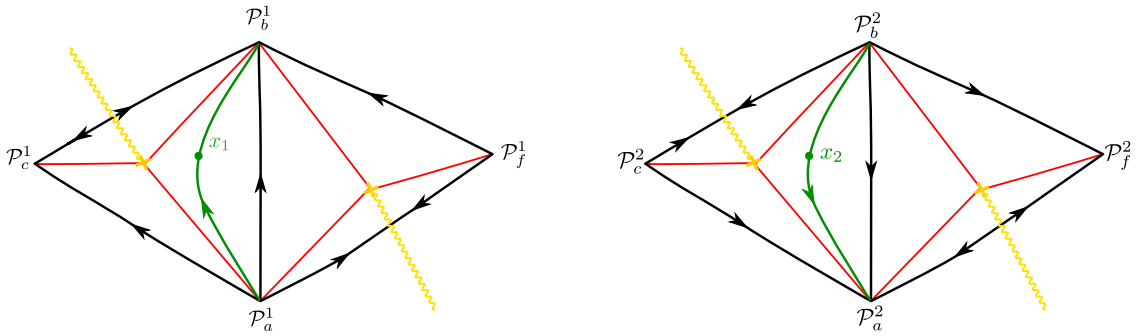

Figure 2.2: A quadrilateral containing z, at an angle ϑ: sheet 1 on the left, sheet 2 on the right. The path γ_{12} runs from x_1 (the lift of z in sheet 1) straight to the turning point inside triangle abc on sheet 1, then back from the turning point to x_2 on sheet 2.

According to eq.(7.36) of [65]

$$\mathcal{Y}_{\gamma_{12}} = \frac{(s_a, s_c)}{(s_b, s_a)(s_b, s_c)} s_b(z) \otimes s_b(z) \tag{2.12}$$

We briefly review the rules leading to this result.

2.1.3.1 Defining the $\mathcal{Y}_{\gamma_{ij}}$

There are two equivalent definitions of the $\mathcal{Y}$, we quickly review how these coordinates are obtained and set our conventions for the rest of this work. For clarity, we report the pictures of the two sheets of Σ in a neighborhood of cell C_{ab}, indicating the direction (as given by the sign of $\langle \lambda, \partial_t \rangle \mathrm{e}^{-i\vartheta}$) of WKB lines on each sheet. We use $\mathcal{P}_\alpha^{1,2}$ for the lifts of singular points on sheets $1, 2$ respectively. Adopting the conventions of [65]: γ_{12} is the simplest path from z to the turning point in triangle abc, when lifted, it flows from sheet 1 to sheet 2.

First method

We begin by applying the methods described in section 7.5.2 of [65]. We first identify a homotopy equivalent to γ_{12}, made from edges of the WKB triangulation, on Σ: we choose the path

$$x_1 \to \mathcal{P}_b^1 \to \mathcal{P}_c^2 \to \mathcal{P}_a^2 \to \mathcal{P}_b^2 \to x_2 \tag{2.13}$$

we must pass through $\mathcal{P}_b^1$ at the beginning because of the direction of the WKB line through x_1 and similarly for $\mathcal{P}_b^2$ at the end because of the direction of the WKB line through x_2. We have the equivalence

$$\gamma_{12} \sim \hat{E}_{b,x_1} - \hat{E}_{b,c} + \hat{E}_{c,a} - \hat{E}_{a,b} + \hat{E}_{b,x_2} \tag{2.14}$$

where the signs are dictated by comparison of the direction of the path of our choice with that of the WKB edges employed. The $\hat{E}$ are oriented lifts of the edges on C and they are understood to be taken on the sheet on which we are working, that is actually specified by eq. (2.13). Equation (7.27) of [65] defines

$$\mathcal{X}^{\vartheta}_{n,b,b}(z,z) = \prod_{\alpha,\beta} (s_\alpha, s_\beta)^{n_{\alpha\beta}} \; s_b^{\vartheta}(z) \otimes s_b^{\vartheta}(z) \tag{2.15}$$

where $n_{\alpha\beta}$ is a matrix such that $\gamma_{12} = \sum n_{\alpha\beta}\hat{E}_{\alpha\beta}$, therefore in our case (2.14) yields

$$\mathcal{X}^{\vartheta}_{n,b,b}(z,z) = s_b(z) \otimes s_b(z) \; \frac{(s_c, s_a)}{(s_a, s_b)(s_b, s_c)}. \tag{2.16}$$

There is a sign for passing from the untwisted $\mathcal{X}$ to the twisted $\mathcal{Y}$, which is positive according to the rules outlined in appendix F.1 of [65]. So (2.16) gives $\mathcal{Y}_{\gamma_{12}}$.

Second method

As discussed in appendix F in [65], the proper definition of the $\mathcal{Y}_a$ is slightly more involved, we now recall it and then use it to re-derive the result (2.16). This method has two advantages: signs are fixed unambiguously, and the procedure is somewhat faster. We will use this second type of construction throughout the rest of this work.

As we mentioned above, to each WKB triangulation corresponds a cell decomposition into quadrilaterals. Considering the union of the edges from T_{WKB} and those from the cell decomposition yields a finer decomposition into "sectors". For example, in fig.2.2 the sector containing z is the triangle whose vertices are a, b and the branch point on the left, and whose edges are the the generic path (in black) from a to b, together with the two separating WKB paths running between the branch point and a, b respectively.

More generally, denote by S the sector containing the surface defect. Also, let z_i, z_j be two of the

lifts of z. Consider a path in C from z to the turning point on the boundary of S, and denote by $\gamma_{ij,S}$ the odd sum of its lifts, namely an oriented open path in Σ running from z_i to z_j. Let a be the vertex of T_{WKB} reached by flowing along a lifted WKB path from z_i, and let (abc) be the vertices of the triangle in counterclockwise order, then define $s_{i,S} := s_a(s_b, s_c)$ and similarly define $s_{j,S}$. Finally, $\mathcal{Y}_{\gamma_{ij},S}$ is defined to be the fiber endomorphism of the rank-2 bundle over the point z that maps

$$s_{i,S} \mapsto 0\,, \qquad s_{j,S} \mapsto \nu_{i,S} s_{i,S} \tag{2.17}$$

with $\nu_{i,S} = +1$ (respectively -1) if the lifted generic WKB path through z_i runs counterclockwise (clockwise) around the triangle. Letting $\gamma_{ii,0}$ be the element of Γ_{ii} corresponding to $0 \in \Gamma$, define $\mathcal{Y}_{\gamma_{ii,0}}$ to be the fiber endomorphism

$$s_i \mapsto s_i\,, \qquad s_j \mapsto 0. \tag{2.18}$$

Variables $\mathcal{Y}_{\gamma_{ij}+\gamma}$ and $\mathcal{Y}_{\gamma_{ii,0}+\gamma}, \gamma \in \Gamma$, corresponding to more general elements of the Γ-torsors are obtained via the twisted multiplication laws. In our specific case, we have

$$s_{1,S} = s_b(s_c, s_a) \qquad s_{2,S} = s_a(s_b, s_c), \tag{2.19}$$

and the fiber endomorphisms

$$\begin{aligned} \mathcal{Y}_{\gamma_{ii}} &= \frac{s_{j,S}(z) \otimes s_{i,S}(z)}{(s_{i,S}, s_{j,S})} \\ \mathcal{Y}_{\gamma_{ij}} &= \nu_{i,S} \frac{s_{i,S}(z) \otimes s_{i,S}(z)}{(s_{j,S}, s_{i,S})} \end{aligned} \tag{2.20}$$

where $\nu_1 = 1 = -\nu_2$. Therefore, we have explicitly

$$\begin{aligned} \mathcal{Y}_{\gamma_{11},0} &= \frac{s_a(z) \otimes s_b(z)}{(s_b, s_a)} \qquad & \mathcal{Y}_{\gamma_{22},0} &= \frac{s_b(z) \otimes s_a(z)}{(s_a, s_b)} \\ \mathcal{Y}_{\gamma_{12}} &= s_b(z) \otimes s_b(z) \frac{(s_c, s_a)}{(s_a, s_b)(s_b, s_c)} \qquad & \mathcal{Y}_{\gamma_{21}} &= s_a(z) \otimes s_a(z) \frac{(s_b, s_c)}{(s_a, s_b)(s_c, s_a)} \end{aligned} \tag{2.21}$$

Although the definition of Fock-Goncharov coordinates might appear somewhat unmotivated, this in fact generalizes the $\mathcal{X}_\gamma, \gamma \in \Gamma$ in agreement both with the twisted multiplication laws of the $\mathcal{Y}_a$, and with the morphisms induced by crossing $\mathcal{S}$ or $\mathcal{K}$ walls, details can be found in appendix F of [65].

2.1.3.2 The case of regular punctures

We now set about deriving the expression for $\tilde{\mathcal{Y}}_{\gamma_{12}} := \mathcal{Y}_{\gamma_{12}}^{\vartheta+\pi}$ in terms of the $\mathcal{Y}_a := \mathcal{Y}_a^{\vartheta}$. To begin with, recall that sending $\vartheta \to \vartheta + \pi$ inverts the direction of the WKB flow, as well as switching decorations

at the punctures. The inversion of the WKB flow has different effects on gauge and solitonic charges. Sending $\vartheta \to \vartheta + \pi$ yields $\gamma^{\vartheta+\pi} = -\gamma^{\vartheta}$ since, for 4d gauge charges, the orientation of cycles γ is defined by the intersection with WKB lines. In contrast, for soliton charges a path γ_{ij} is specified to go from sheet i to sheet j, within a certain relative homology class, thus its orientation will remain unchanged under an omnipop. As a consequence, the procedure for obtaining the spectrum generator will be slightly different from the one for the pure 4d case. More precisely, for gauge charges one can derive $\mathbb{S}$ by evaluating the transformation [64]

$$\mathcal{X}_{\gamma}^{\vartheta+\pi} = \mathcal{X}_{\gamma}^{\vartheta} \cdot \left(\mathcal{X}_{E}^{T_{\mathrm{WKB}(\vartheta,\lambda^2)}}\, \tilde{\mathcal{X}}_{E}^{T_{\mathrm{WKB}(\vartheta,\lambda^2)}}\right)^{-1}. \tag{2.22}$$

This result relies on the fact that, under the omnipop,

$$\mathcal{X}_{\gamma_E^{\vartheta}} \mapsto \mathcal{X}_{\gamma_E^{\vartheta+\pi}} = \mathcal{X}_{-\gamma_E^{\vartheta}} = \mathcal{X}_{\gamma_E^{\vartheta}}^{-1}$$

As we mentioned, this is not the case with solitonic charges: after sending $\vartheta \mapsto \vartheta + \pi$ a charge γ_{ij} still runs from sheet i to sheet j. Since we can no longer employ this trick, we will instead directly inspect $\tilde{\mathcal{Y}}_a$.

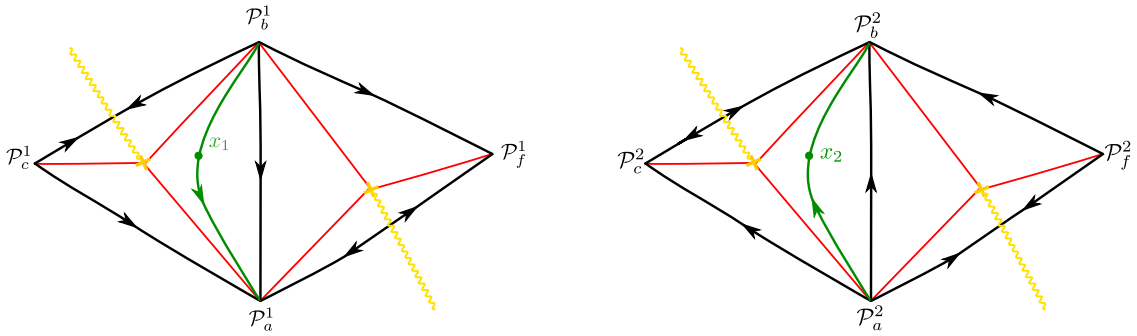

Figure 2.3: A quadrilateral containing z, at an angle $\vartheta + \pi$: sheet 1 on the left, sheet 2 on the right. The path γ_{12} runs from x_1 straight to the turning point in triangle abc, on sheet 1, then back from the turning point to x_2 on sheet 2.

We begin by applying again the rules in (2.20) to write down $\mathcal{Y}_{\gamma_{12}}^{\vartheta+\pi}$ in terms of the new sections: we now have

$$\tilde{s}_1(z) = \tilde{s}_a(z)(\tilde{s}_b, \tilde{s}_c) \qquad \tilde{s}_2(z) = \tilde{s}_b(z)(\tilde{s}_c, \tilde{s}_a) \qquad \tilde{\nu}_1 = -\tilde{\nu}_2 = - \tag{2.23}$$

therefore, applying (2.20) gives

$$\tilde{\mathcal{Y}}_{\gamma_{12}} = \tilde{s}_a(z) \otimes \tilde{s}_a(z)\, \frac{(\tilde{s}_b, \tilde{s}_c)}{(\tilde{s}_a, \tilde{s}_b)(\tilde{s}_c, \tilde{s}_a)} \tag{2.24}$$

The next step is finding an expression for $\tilde{\mathcal{Y}}_{\gamma_{12}}$ in terms of $\mathcal{Y}_a$. In order to do so, let us consider a neighborhood of triangle abc, as shown in Fig.2.4, we can employ eq.(2.11) to get the conjugate flat

sections:

$$\begin{aligned} &P \to a, \quad Q \to b, \quad \ell \to c \\ &\tilde{s}_a \;=\; \xi_a \left[\Sigma_a^{b\to b}(b,c)s_a + (1-\mu_a^2)(c,a)s_b\right] \end{aligned} \tag{2.25}$$

where we understand the shorthands $\Sigma_\alpha^{\beta\to\beta} := \Sigma(\alpha;\beta\to\beta)$ and $(\alpha,\beta) := (s_\alpha, s_\beta)$. Similarly, we have the other sections by cyclic permutation of the indices

$$\begin{aligned} &P \to b, \quad Q \to c, \quad \ell \to a \\ &\tilde{s}_b \;=\; \xi_b \left[\Sigma_b^{c\to c}(c,a)s_b + (1-\mu_b^2)(a,b)s_c\right] \end{aligned} \tag{2.26}$$

$$\begin{aligned} &P \to c, \quad Q \to a, \quad \ell \to b \\ &\tilde{s}_c \;=\; \xi_c \left[\Sigma_c^{a\to a}(a,b)s_c + (1-\mu_c^2)(b,c)s_a\right] \end{aligned}$$

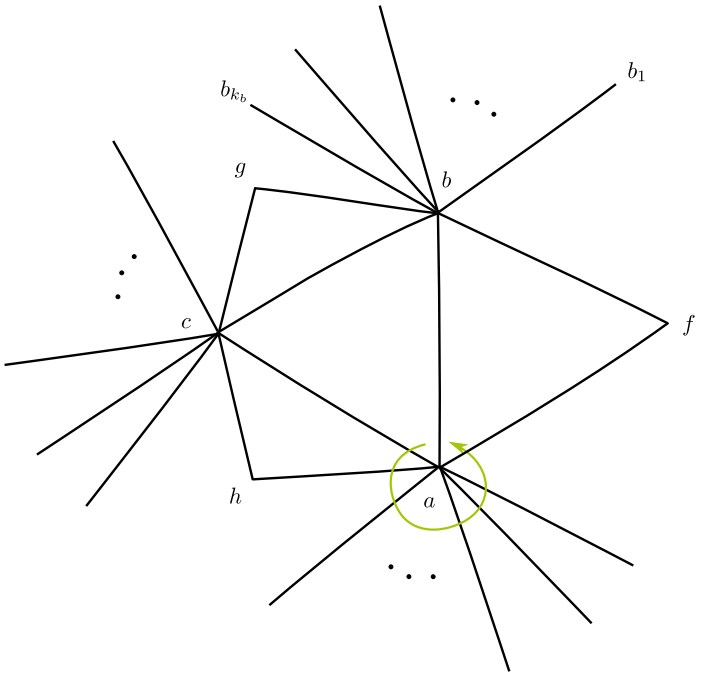

Figure 2.4: Punctures a, b, c are regular, indicated is the path for computing $\Sigma(a; b \to b)$

We first compute

$$\begin{aligned} \tilde{s}_a(z) \otimes \tilde{s}_a(z) = \xi_a^2 \big\{ &\left[\Sigma_a^{b\to b}(b,c)\right]^2 s_a \otimes s_a + (1-\mu_a^2)^2 (a,c)^2 s_b \otimes s_b \\ &+ \Sigma_a^{b\to b}(1-\mu_a^2)(b,c)(c,a)[s_a \otimes s_b + s_b \otimes s_a] \big\}\,, \end{aligned} \tag{2.27}$$

from now on, we'll drop the normalization factors ξ_α, since they cancel out in eq.(2.24). In order to compute the other piece of eq.(2.24) we first evaluate

$$\begin{aligned}(\tilde{s}_a, \tilde{s}_b) = &\left[\Sigma_a^{b\to b}\Sigma_b^{c\to c} - \Sigma_a^{b\to b}(1-\mu_b^2) + (1-\mu_a^2)(1-\mu_b^2)\right] \\ &\times (a,b)(b,c)(c,a),\end{aligned} \tag{2.28}$$

together with cyclic permutations of the three indices. For later convenience, we define the quantities

$$\begin{aligned}\Xi(X,Y;x,y) &:= [XY - X(1-y^2) + (1-x^2)(1-y^2)] \\ \omega_{a,b,c} &:= (s_a,s_b)(s_b,s_c)(s_c,s_a),\end{aligned} \tag{2.29}$$

for each triple of vertices a, b, c of a triangle, labeled counter-clockwise.

Equations (2.28) can be summarized as

$$(\tilde{s}_a, \tilde{s}_b) = \Xi(\Sigma_a^{b\to b}, \Sigma_b^{c\to c}; \mu_a, \mu_b)\, \omega_{a,b,c} \tag{2.30}$$

In order to avoid confusion below, let us stress here that some care is needed, when using this notation: the Σ's appearing into Ξ must be those related to the triangle abc, thus e.g. for fig.2.8, one *cannot* write $(\tilde{s}_c, \tilde{s}_b) = \Xi(\Sigma_c^{b\to b}, \Sigma_b^{c\to c}; \mu_c, \mu_b)\, \omega_{a,b,c}$, because the clockwise labeling would impose to work in triangle c, b, g. One can, of course, use $(\tilde{s}_c, \tilde{s}_b) = -(\tilde{s}_b, \tilde{s}_c)$ and work on triangle a, b, c instead.

Notice that, since $\omega_{a,b,c}$ is antisymmetric under odd permutations of the indices, in particular a, b, then we must have $\Xi(A, B; x, y) = \Xi(B, A; y, x)$ which is *not* trivial from the definition of Ξ, but must be justified by studying the properties of the Σ's.

From (2.28) follows

$$\begin{aligned}\frac{(\tilde{s}_b, \tilde{s}_c)}{(\tilde{s}_a, \tilde{s}_b)(\tilde{s}_c, \tilde{s}_a)} = &\frac{1}{\omega_{a,b,c}}\ \Xi(\Sigma_b^{c\to c}, \Sigma_c^{a\to a}; \mu_b, \mu_c) \\ &\times \left[\Xi(\Sigma_a^{b\to b}, \Sigma_b^{c\to c}; \mu_a, \mu_b)\, \Xi(\Sigma_c^{a\to a}, \Sigma_a^{b\to b}; \mu_c, \mu_a)\right]^{-1}\end{aligned} \tag{2.31}$$

The factors Ξ have well defined expressions in terms of $\mathcal{Y}_\gamma$: see eq.(11.9) of [64]. Eventually, we come to the explicit expression for $\tilde{\mathcal{Y}}_{\gamma_{12}}$

$$\begin{aligned}\tilde{\mathcal{Y}}_{\gamma_{12}} = &\frac{1}{\omega_{a,b,c}}\ \Xi(\Sigma_b^{c\to c}, \Sigma_c^{a\to a}; \mu_b, \mu_c) \\ &\times \left[\Xi(\Sigma_a^{b\to b}, \Sigma_b^{c\to c}; \mu_a, \mu_b)\, \Xi(\Sigma_c^{a\to a}, \Sigma_a^{b\to b}; \mu_c, \mu_a)\right]^{-1} \\ &\times \left\{\left[\Sigma_a^{b\to b}(b,c)\right]^2 s_a \otimes s_a + (1-\mu_a^2)^2 (a,c)^2 s_b \otimes s_b\right. \\ &\left.+\Sigma_a^{b\to b}(1-\mu_a^2)(b,c)(c,a)[s_a \otimes s_b + s_b \otimes s_a]\right\} \\ &= \Xi(\Sigma_b^{c\to c}, \Sigma_c^{a\to a}; \mu_b, \mu_c) \\ &\times \left[\Xi(\Sigma_a^{b\to b}, \Sigma_b^{c\to c}; \mu_a, \mu_b)\, \Xi(\Sigma_c^{a\to a}, \Sigma_a^{b\to b}; \mu_c, \mu_a)\right]^{-1} \\ &\times \left\{(\Sigma_a^{b\to b})^2 \mathcal{Y}_{\gamma_{21}} + (1-\mu_a^2)^2 \mathcal{Y}_{\gamma_{12}} + \Sigma_a^{b\to b}(1-\mu_a^2)\left[\mathcal{Y}_{\gamma_{22}=0} - \mathcal{Y}_{\gamma_{11}=0}\right]\right\}\end{aligned} \tag{2.32}$$

Similar, tedious but straightforward, calculations give

$$\begin{aligned}
\tilde{\mathcal{Y}}_{\gamma_{11}=0} &= \frac{\tilde{s}_b(z)\otimes\tilde{s}_a(z)}{(\tilde{s}_a,\tilde{s}_b)} \\
&= \left[\Xi(\Sigma_a^{b\to b},\Sigma_b^{c\to c};\mu_a,\mu_b)\right]^{-1} \\
&\times\left\{\Sigma_a^{b\to b}\Sigma_b^{c\to c}\mathcal{Y}_{\gamma_{22}=0}+\Sigma_b^{c\to c}(1-\mu_a^2)\mathcal{Y}_{\gamma_{12}}\right. \\
&\left.-\Sigma_a^{b\to b}(1-\mu_b^2)\left[\mathcal{Y}_{\gamma_{22}=0}+\mathcal{Y}_{\gamma_{21}}\right]-(1-\mu_a^2)(1-\mu_b^2)\left[\mathcal{Y}_{\gamma_{12}}-\mathcal{Y}_{\gamma_{11}=0}\right]\right\} \\
\tilde{\mathcal{Y}}_{\gamma_{22}=0} &= \frac{\tilde{s}_a(z)\otimes\tilde{s}_b(z)}{(\tilde{s}_b,\tilde{s}_a)} \\
&= -\left[\Xi(\Sigma_a^{b\to b},\Sigma_b^{c\to c};\mu_a,\mu_b)\right]^{-1} \\
&\times\left\{-\Sigma_a^{b\to b}\Sigma_b^{c\to c}\mathcal{Y}_{\gamma_{11}=0}+\Sigma_b^{c\to c}(1-\mu_a^2)\mathcal{Y}_{\gamma_{12}}\right. \\
&\left.-\Sigma_a^{b\to b}(1-\mu_b^2)\left[\mathcal{Y}_{\gamma_{21}}-\mathcal{Y}_{\gamma_{11}=0}\right]-(1-\mu_a^2)(1-\mu_b^2)\left[\mathcal{Y}_{\gamma_{12}}+\mathcal{Y}_{\gamma_{22}=0}\right]\right\} \\
\tilde{\mathcal{Y}}_{\gamma_{21}} &= \tilde{s}_b(z)\otimes\tilde{s}_b(z)\frac{(\tilde{s}_c,\tilde{s}_a)}{(\tilde{s}_a,\tilde{s}_b)(\tilde{s}_b,\tilde{s}_c)} \\
&= \Xi(\Sigma_c^{a\to a},\Sigma_a^{b\to b};\mu_c,\mu_a) \\
&\times\left[\Xi(\Sigma_a^{b\to b},\Sigma_b^{c\to c};\mu_a,\mu_b)\,\Xi(\Sigma_b^{c\to c},\Sigma_c^{a\to a};\mu_b,\mu_c)\right]^{-1} \\
&\times\left\{(\Sigma_b^{c\to c})^2\mathcal{Y}_{\gamma_{12}}-\Sigma_b^{c\to c}(1-\mu_b^2)\left[2\mathcal{Y}_{\gamma_{12}}+\mathcal{Y}_{\gamma_{22}=0}-\mathcal{Y}_{\gamma_{11}=0}\right]\right. \\
&\left.+(1-\mu_b^2)^2\left[\mathcal{Y}_{\gamma_{12}}+\mathcal{Y}_{\gamma_{21}}+\mathcal{Y}_{\gamma_{22}=0}-\mathcal{Y}_{\gamma_{11}=0}\right]\right\}
\end{aligned}$$

2.1.3.3 Extension to irregular punctures: one irregular puncture

Suppose b, c are regular punctures and a is now irregular. A pop acts in two combined ways on the decorated triangulation at the irregular puncture, as explained in §8 of [64]:

- on the decoration – a pop can be regarded as the action by 1 on the $\mathbb{Z}$ torsor of decorations at the irregular puncture: labeling vertices $\ldots Q_j, Q_{j+1}\ldots$ clockwise with corresponding decorations $\ldots s_n, s_{n+1}\ldots$, then after sending $\vartheta\to\vartheta+\pi$ the decorations associated to vertices will be $\ldots s_{n-1}, s_n\ldots$.

- on the vertices – a pop acts as a cyclic permutation of the vertices associated with an irregular puncture, this is easy to see e.g. in AD theories, where the irregular puncture is at infinity: here we can actually follow the evolution of the triangulation as $\vartheta\mapsto\vartheta+\pi$, we see the WKB rays rotating counterclockwise by an angle $2\pi/(N+2)$

The overall effect is a combination of these two, they don't add up, rather, they describe the same behavior.

Therefore, referring to fig.2.5, equation (2.24) still holds. The rules for expressing $\tilde{s}_b, \tilde{s}_c$ don't change, while we have $\tilde{s}_a = s_{\tilde{a}}$.

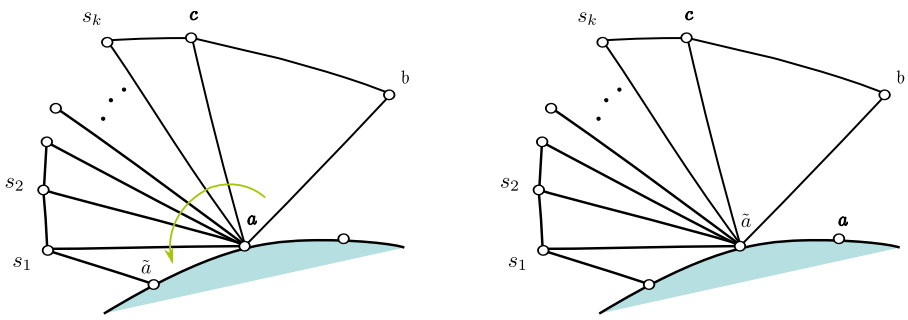

Figure 2.5: The defect's parameter z sits in cell C_{ab}, within a triangle whose vertex a is an irregular puncture. Indicated in yellow is the path for parallel transport, employed in constructing $\Sigma_a^{b\to\tilde{a}}$

The suitable generalization of (2.10) is (see [64])

$$\Sigma_a^{b\to\tilde{a}} = \frac{(s_{\tilde{a}}, s_b)(s_a, s_c)}{(s_b, s_c)(s_{\tilde{a}}, s_a)} \tag{2.33}$$

from which we derive[5]

$$s_{\tilde{a}} = \xi_{\tilde{a}}[\Sigma_a^{b\to\tilde{a}}\,(b,c)\,s_a \;+\; (c,a)\,s_b] \tag{2.34}$$

Notice that this corresponds to making the replacements $\Sigma_a^{b\to b} \to \Sigma_a^{b\to\tilde{a}},\ \mu_a^2 \to 0$ into eq (2.25). Therefore, we can immediately write down the outer products of sections at popped vertices, in a way that is analogous to (2.30)

$$\begin{aligned}(\tilde{s}_a, \tilde{s}_b) &= \Xi(\Sigma_a^{b\to\tilde{a}}, \Sigma_b^{c\to c}; 0, \mu_b)\,\omega_{a,b,c}\\ (\tilde{s}_c, \tilde{s}_a) &= \Xi(\Sigma_c^{a\to a}, \Sigma_a^{b\to\tilde{a}}; \mu_c, 0)\,\omega_{a,b,c}\end{aligned} \tag{2.35}$$

similarly, computing again $s_{\tilde{a}} \otimes s_{\tilde{a}}$ just involves making the above-mentioned replacements. Eventually, we have the new expression for $\tilde{\mathcal{Y}}_{\gamma_{12}}$

$$\begin{aligned}\tilde{\mathcal{Y}}_{\gamma_{12}} &= \Xi(\Sigma_b^{c\to c}, \Sigma_c^{a\to a}; \mu_b, \mu_c)\\ &\times \left[\Xi(\Sigma_a^{b\to\tilde{a}}, \Sigma_b^{c\to c}; 0, \mu_b)\,\Xi(\Sigma_c^{a\to a}, \Sigma_a^{b\to\tilde{a}}; \mu_c, 0)\right]^{-1}\\ &\times \left\{(\Sigma_a^{b\to\tilde{a}})^2\mathcal{Y}_{\gamma_{21}} + \mathcal{Y}_{\gamma_{12}} + \Sigma_a^{b\to\tilde{a}}\,[\mathcal{Y}_{\gamma_{22}=0} - \mathcal{Y}_{\gamma_{11}=0}]\right\}\end{aligned} \tag{2.36}$$

Similar expressions for $\tilde{\mathcal{Y}}_{\gamma_{21}}$, $\tilde{\mathcal{Y}}_{\gamma_{11}=0}$, $\tilde{\mathcal{Y}}_{\gamma_{22}=0}$ are obtained after applying the proper substitutions.

2.1.3.4 Extension to irregular punctures: general case

It is straightforward to extend the above reasoning to the case in which any combination of a, b, c are regular or irregular. If a vertex α is irregular, one must apply the corresponding replacements:

[5] In the case of N=1 AD theory, this result together with identity (2.44) gives the expected $\tilde{s}_a = s_c$.

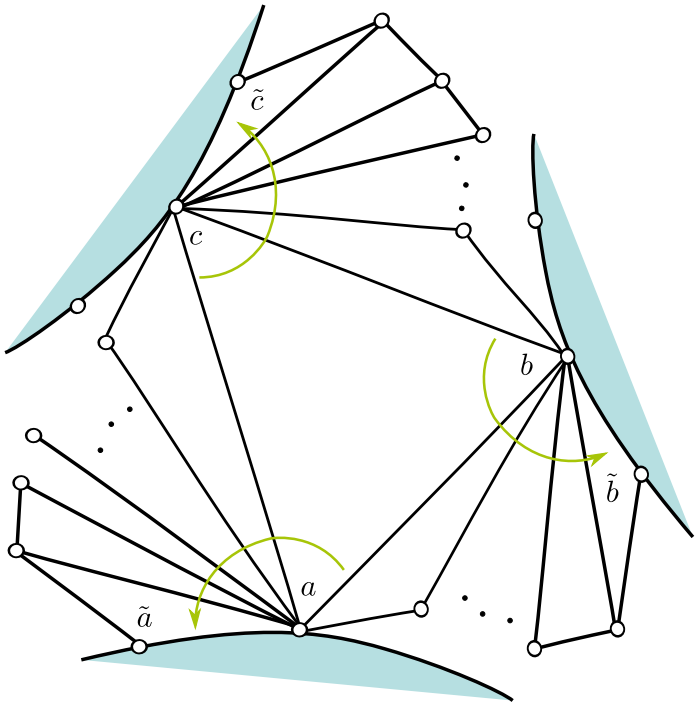

Figure 2.6: The defect's parameter z sits in cell C_{ab}, within a triangle whose vertices are all irregular punctures

$\Sigma_\alpha^{\beta\to\beta} \to \Sigma_\alpha^{\beta\to\tilde{\beta}}$ and $\mu_\alpha^2 \to 0$, into expression (2.32), where α, β, γ is an ordered triple valued in $\{a, b, c\}$.

2.1.4 Including line defects

We now want to derive the spectrum generator in presence of line defects. The simplest case of a single line defect will be considered.

2.1.4.1 Defects in the same cell, different sectors

Let's start with the situation of fig.2.7: both z, z' lie within cell C_{ab}. We first assume all punctures to be regular, and later generalize.

In analogy with what we have seen so far, we define the WKB coordinates corresponding to framed BPS states as follows. Let S, S' be the sectors[6] in which z, z' lie respectively. On sheet i we define $s_{i,S}(z) = s_1(z)\,(s_2, s_3)$ $(s_{i',S'}(z') = s_1(z')\,(s_2, s_3))$ where $s_1(z)$ $(s_1(z'))$ is the small flat section of the vertex into which the WKB line through z (z') flows, evaluated at z (z'). The triple 123 indicates a counterclockwise labeling of the vertices of the triangles containing z, z'.

[6] a sector is a subset of C bounded by a WKB edge and two separatrices

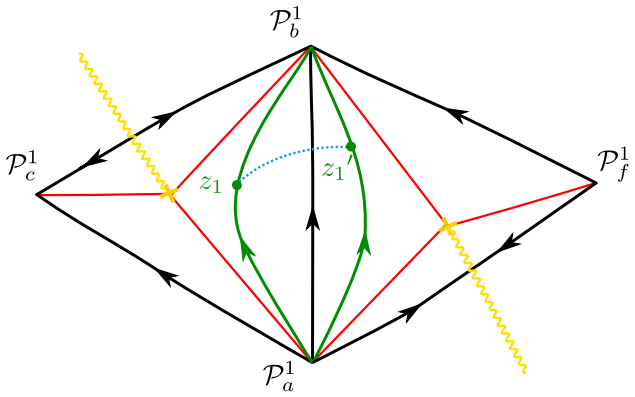

Figure 2.7: Sheet 1, at angle ϑ

We define the bundle morphisms (understanding $i = i' \neq j = j'$)

$$\begin{aligned} \mathcal{Y}_{ii'} &: \begin{cases} s_i(z) \to s_{i'}(z') \\ s_j \to 0 \end{cases} && = \frac{s_j(z) \otimes s_{i'}(z')}{(s_{i'}, s_j)} \\ \mathcal{Y}_{ij'} &: \begin{cases} s_i(z) \to 0 \\ s_j(z) \to \nu_i \, s_{i'}(z') \end{cases} && = \nu_i \, \frac{s_i(z) \otimes s_{i'}(z')}{(s_j, s_{i'})} \end{aligned} \tag{2.37}$$

in close analogy to the reasoning in appendix F of [65]; we omitted the subscripts indicating the cells, since such information is specified by whether we evaluate at z or z'. The sign $\nu_{i,S}$ is positive if the WKB line through $s_i(z)$ flows counterclockwise within the triangle containing z, negative otherwise: it really depends on the sector, not just on the cell, of z.

A remark is in order here: this definition is not explicitly stated in [65], but it follows naturally by extending what is defined in appendix F of that reference for the fiber endomorphisms (see eq (2.20)), along with enforcing normalization invariance. However, in eq. (8.11) of [65], in order to get $\mathcal{Y}_{-+'}$, the second line of (2.37) must be changed to

$$\mathcal{Y}_{ij'} = \nu_j \, \frac{s_j(z) \otimes s_{j'}(z')}{(s_i, s_{j'})} \tag{2.38}$$

leaving the first line unchanged. Eventually, all the spectra we will derive in the rest of this work will match with those of cases analyzed in [65], provided we make the proper identifications.

Therefore in our case we identify

$$\begin{aligned} s_1(z) &= s_b(z)\,(s_c, s_a) & s_{1'}(z') &= s_b(z')\,(s_a, s_f) \\ s_2(z) &= s_a(z)\,(s_b, s_c) & s_{2'}(z') &= s_a(z')\,(s_f, s_b) \end{aligned} \tag{2.39}$$

together with the signs $\nu_1 = -\nu_{1'} = -\nu_2 = \nu_{2'} = +$.

Consider the two "simplest paths" (not crossing any separatrices) between z and z', lying entirely on sheets 1 and 2, to them associate respectively: $\mathcal{Y}^{\vartheta}_{11'} \equiv \mathcal{Y}_{11'}$, $\mathcal{Y}^{\vartheta}_{22'} \equiv \mathcal{Y}_{22'}$; similarly, the "simplest" paths from sheet 1 to 2, and vice versa, are $\mathcal{Y}^{\vartheta}_{12'} \equiv \mathcal{Y}_{12'}$, $\mathcal{Y}^{\vartheta}_{21'} \equiv \mathcal{Y}_{21'}$. They read

$$\begin{aligned} \mathcal{Y}_{11'} &= \frac{s_a(z) \otimes s_b(z')}{(s_b, s_a)} \qquad \mathcal{Y}_{22'} = \frac{s_b(z) \otimes s_a(z')}{(s_a, s_b)}, \\ \mathcal{Y}_{12'} &= s_b(z) \otimes s_b(z') \, \frac{(s_c, s_a)}{(s_a, s_b)(s_b, s_c)} \qquad \mathcal{Y}_{21'} = s_a(z) \otimes s_a(z') \, \frac{(s_b, s_c)}{(s_a, s_b)(s_c, s_a)}. \end{aligned} \tag{2.40}$$

After sending $\vartheta \to \vartheta + \pi$, we have the new quantities

$$\begin{aligned} \tilde{s}_1(z) &= \tilde{s}_a(z) \, (\tilde{s}_b, \tilde{s}_c) \qquad \tilde{s}_{1'}(z') = \tilde{s}_a(z') \, (\tilde{s}_f, \tilde{s}_b) \\ \tilde{s}_2(z) &= \tilde{s}_b(z) \, (\tilde{s}_c, \tilde{s}_a) \qquad \tilde{s}_{2'}(z') = \tilde{s}_b(z') \, (\tilde{s}_a, \tilde{s}_f) \end{aligned} \tag{2.41}$$

together with the new signs $\tilde{\nu}_1 = -\tilde{\nu}_{1'} = -\tilde{\nu}_2 = \tilde{\nu}_{2'} = -$.

Applying again definitions (2.37), the new coordinates read

$$\begin{aligned} \mathcal{Y}^{\vartheta+\pi}_{11'} &=: \tilde{\mathcal{Y}}_{11'} = \frac{\tilde{s}_b(z) \otimes \tilde{s}_a(z')}{(\tilde{s}_a, \tilde{s}_b)}, \\ \mathcal{Y}^{\vartheta+\pi}_{22'} &=: \tilde{\mathcal{Y}}_{22'} = \frac{\tilde{s}_a(z) \otimes \tilde{s}_b(z')}{(\tilde{s}_b, \tilde{s}_a)} \\ \mathcal{Y}^{\vartheta+\pi}_{12'} &=: \tilde{\mathcal{Y}}_{12'} = \tilde{s}_a(z) \otimes \tilde{s}_a(z') \, \frac{(\tilde{s}_b, \tilde{s}_c)}{(\tilde{s}_a, \tilde{s}_b)(\tilde{s}_c, \tilde{s}_a)}, \\ \mathcal{Y}^{\vartheta+\pi}_{21'} &=: \tilde{\mathcal{Y}}_{21'} = \tilde{s}_b(z) \otimes \tilde{s}_b(z') \, \frac{(\tilde{s}_c, \tilde{s}_a)}{(\tilde{s}_a, \tilde{s}_b)(\tilde{s}_b, \tilde{s}_c)}. \end{aligned} \tag{2.42}$$

Employing eq.s (2.25)(2.26) and (2.30) we obtain

$$\begin{aligned} \tilde{\mathcal{Y}}_{11'} = & \left[\Xi(\Sigma_a^{b\to b}, \Sigma_b^{c\to c}; \mu_a, \mu_b)\right]^{-1} \\ & \times \Big\{ \Sigma_a^{b\to b}\Sigma_b^{c\to c} \, \mathcal{Y}^{\vartheta}_{22'} \, + \, \Sigma_b^{c\to c}(1-\mu_a^2) \, \mathcal{Y}^{\vartheta}_{12'} \\ & + (1-\mu_a^2)(1-\mu_b^2) \, \frac{s_c(z) \otimes s_b(z')}{(s_b, s_c)} \, + \, \Sigma_a^{b\to b}(1-\mu_b^2) \, \frac{s_c(z) \otimes s_a(z')}{(s_c, s_a)} \Big\} \end{aligned} \tag{2.43}$$

In order to fix the second row, *i.e.* to eliminate $s_c(z)$, we employ the identity

$$s_a(z) \, (s_b, s_c) \, + \, s_b(z) \, (s_c, s_a) \, + \, s_c(z) \, (s_a, s_b) \, = \, 0 \tag{2.44}$$

and get

$$\begin{aligned} \tilde{\mathcal{Y}}_{11'} = & \left[\Xi(\Sigma_a^{b\to b}, \Sigma_b^{c\to c}; \mu_a, \mu_b)\right]^{-1} \\ & \times \big\{ \Sigma_a^{b\to b}\Sigma_b^{c\to c} \, \mathcal{Y}_{22'} \, + \, \Sigma_b^{c\to c}(1-\mu_a^2) \, \mathcal{Y}_{12'} \\ & - (1-\mu_a^2)(1-\mu_b^2) \, [\mathcal{Y}_{12'} - \mathcal{Y}_{11'}] \\ & - \, \Sigma_a^{b\to b}(1-\mu_b^2) \, [\mathcal{Y}_{21'} + \mathcal{Y}_{22'}] \big\} \end{aligned} \tag{2.45}$$

Similar, tedious but straightforward, calculations show that

$$\begin{aligned}\tilde{\mathcal{Y}}_{22'} = &- \left[\Xi(\Sigma_a^{b\to b}, \Sigma_b^{c\to c}; \mu_a, \mu_b)\right]^{-1} \\ &\times \left\{-\Sigma_a^{b\to b}\Sigma_b^{c\to c}\,\mathcal{Y}_{11'} \,+\, \Sigma_b^{c\to c}(1-\mu_a^2)\,\mathcal{Y}_{12'}\right. \\ &- (1-\mu_a^2)(1-\mu_b^2)\,\left[\mathcal{Y}_{12'} + \mathcal{Y}_{22'}\right] \\ &\left. - \,\Sigma_a^{b\to b}(1-\mu_b^2)\,\left[\mathcal{Y}_{21'} - \mathcal{Y}_{11'}\right]\right\}\end{aligned} \tag{2.46}$$

$$\begin{aligned}\tilde{\mathcal{Y}}_{12'} = &\,\Xi(\Sigma_b^{c\to c}, \Sigma_c^{a\to a}; \mu_b, \mu_c) \\ &\times \left[\Xi(\Sigma_a^{b\to b}, \Sigma_b^{c\to c}; \mu_a, \mu_b)\,\Xi(\Sigma_c^{a\to a}, \Sigma_a^{b\to b}; \mu_c, \mu_a)\right]^{-1} \\ &\times \left\{(\Sigma_a^{b\to b})^2\mathcal{Y}_{21'} + (1-\mu_a^2)^2\mathcal{Y}_{12'} + \Sigma_a^{b\to b}(1-\mu_a^2)\,\left[\mathcal{Y}_{22'} - \mathcal{Y}_{11'}\right]\right\}\end{aligned}$$

$$\begin{aligned}\tilde{\mathcal{Y}}_{21'} = &\,\Xi(\Sigma_c^{a\to a}, \Sigma_a^{b\to b}; \mu_c, \mu_a) \\ &\times \left[\Xi(\Sigma_a^{b\to b}, \Sigma_b^{c\to c}; \mu_a, \mu_b)\,\Xi(\Sigma_b^{c\to c}, \Sigma_c^{a\to a}; \mu_b, \mu_c)\right]^{-1} \\ &\times \left\{(\Sigma_b^{c\to c})^2\mathcal{Y}_{12'} - \Sigma_b^{c\to c}(1-\mu_b^2)\,\left[2\mathcal{Y}_{12'} + \mathcal{Y}_{22'} - \mathcal{Y}_{11'}\right]\right. \\ &\left. +(1-\mu_b^2)^2\,\left[\mathcal{Y}_{12'} + \mathcal{Y}_{21'} + \mathcal{Y}_{22'} - \mathcal{Y}_{11'}\right]\right\}\end{aligned}$$

Extension to irregular punctures

If one or more of the vertices a, b, c, f belong to an *irregular puncture*, we obtain the new spectrum generator by using the analogue of eq.(2.34) in place of (2.25), (2.26), ultimately this amounts to performing the substitutions mentioned in subsection 2.1.3.4.

2.1.4.2 Defects in same sector

Suppose z, z' are in the same sector of cell C_{ab}, mark a point z'' in the *other* sector of cell C_{ab}: then use the twisted product law of the $\mathcal{Y}_a$, to glue together paths $z \to z''$ and $z'' \to z'$.

For future convenience, we point out a few features here. Looking back at last section, one might notice that the only changes come from substituting $s_{1'} = s_b(z')(s_c, s_a)$, $s_{2'} = s_a(z')(s_b, s_c)$ in eq.(2.39) and $\tilde{s}_{1'} = \tilde{s}_a(z')(\tilde{s}_b, \tilde{s}_c)$, $\tilde{s}_{2'} = \tilde{s}_b(z')(\tilde{s}_c, \tilde{s}_a)$ in eq.(2.41), together with flipping the signs $\nu_{i'}$, $\tilde{\nu}_{i'}$.

The point is that none of what we change comes into play in the expressions of the $\mathcal{Y}$, $\tilde{\mathcal{Y}}$ (s_f never appears, indeed, due to cancellations). Henceforth if we move z' across the ab edge nothing changes, as long as it keeps lying in the same cell.

2.1.4.3 Defects in neighboring cells

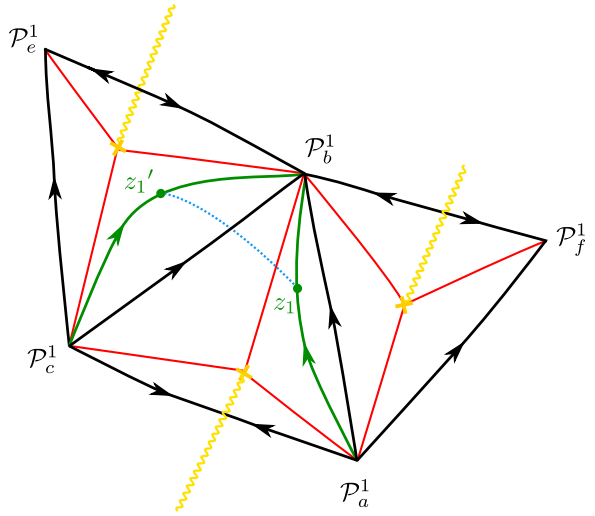

Figure 2.8: Line defect connecting neighboring cells

Referring to fig.2.8 we consider the case where z, z' are in neighboring cells with the choice of sectors shown in the picture. Other choices of sectors can be achieved by using the twisted multiplication rule of the $\mathcal{Y}$ to attach to z or z' the paths described in the previous subsection.

Following the rules sketched above, we have now

$$\begin{aligned} s_1(z) &= s_b(z)\,(s_c, s_a) \qquad s_{1'}(z') = s_b(z')\,(s_e, s_c) \\ s_2(z) &= s_a(z)\,(s_b, s_c) \qquad s_{2'}(z') = s_c(z')\,(s_b, s_e) \end{aligned} \tag{2.47}$$

$$\nu_1 = \nu_{1'} = -\nu_2 = -\,\nu_{2'} = +$$

yielding

$$\begin{aligned} \mathcal{Y}_{11'}^{\vartheta} &= \frac{s_2(z) \otimes s_{1'}(z')}{(s_{1'}, s_2)} = \frac{s_a(z) \otimes s_b(z')}{(s_b, s_a)}, \\ \mathcal{Y}_{22'}^{\vartheta} &= \frac{s_1(z) \otimes s_{2'}(z')}{(s_{2'}, s_1)} = \frac{s_b(z) \otimes s_c(z')}{(s_c, s_b)}, \\ \mathcal{Y}_{12'}^{\vartheta} &= \nu_1 \frac{s_1(z) \otimes s_{1'}(z')}{(s_2, s_{1'})} = s_b(z) \otimes s_b(z')\, \frac{(s_c, s_a)}{(s_a, s_b)(s_b, s_c)}, \\ \mathcal{Y}_{21'}^{\vartheta} &= \nu_2 \frac{s_2(z) \otimes s_{2'}(z')}{(s_1, s_{2'})} = -\frac{s_a(z) \otimes s_c(z')}{(s_c, s_a)}. \end{aligned} \tag{2.48}$$

After sending $\vartheta \to \vartheta + \pi$ we have

$$\begin{aligned} \tilde{s}_1(z) &= \tilde{s}_a(z)\,(\tilde{s}_b, \tilde{s}_c) \qquad \tilde{s}_{1'}(z') = \tilde{s}_c(z')\,(\tilde{s}_b, \tilde{s}_e) \\ \tilde{s}_2(z) &= \tilde{s}_b(z)\,(\tilde{s}_c, \tilde{s}_a) \qquad \tilde{s}_{2'}(z') = \tilde{s}_b(z')\,(\tilde{s}_e, \tilde{s}_c) \end{aligned} \tag{2.49}$$

$$\tilde{\nu}_1 = \tilde{\nu}_{1'} = -\tilde{\nu}_2 = -\,\tilde{\nu}_{2'} = -$$

therefore, applying the definitions gives

$$\begin{aligned}\tilde{\mathcal{Y}}_{11'} &= \frac{\tilde{s}_b(z)\otimes\tilde{s}_c(z')}{(\tilde{s}_c,\tilde{s}_b)} \qquad \tilde{\mathcal{Y}}_{22'} = \frac{\tilde{s}_a(z)\otimes\tilde{s}_b(z')}{(\tilde{s}_b,\tilde{s}_a)} \\ \tilde{\mathcal{Y}}_{12'} &= -\frac{\tilde{s}_a(z)\otimes\tilde{s}_c(z')}{(\tilde{s}_c,\tilde{s}_a)} \qquad \tilde{\mathcal{Y}}_{21'} = \tilde{s}_b(z)\otimes\tilde{s}_b(z')\,\frac{(\tilde{s}_c,\tilde{s}_a)}{(\tilde{s}_a,\tilde{s}_b)(\tilde{s}_b,\tilde{s}_c)}.\end{aligned} \tag{2.50}$$

We start working on $\mathcal{Y}_{11'}^{\vartheta+\pi} \equiv \tilde{\mathcal{Y}}_{11'}$, at the denominator we have $(\tilde{s}_c,\tilde{s}_b)$, in employing (2.30)[7] we choose to work within triangle abc. Thus we refer to eq.s (2.26), and have

$$\begin{aligned}\tilde{\mathcal{Y}}_{11'} &= [-\Xi(\Sigma_b^{c\to c},\Sigma_c^{a\to a};\mu_b,\mu_c)\omega_{a,b,c}]^{-1} \\ &\times\{\Sigma_b^{c\to c}\Sigma_c^{a\to a}\,(c,a)(a,b)\,s_c(z)\otimes s_c(z') \\ &+\Sigma_b^{c\to c}\,(c,a)(b,c)(1-\mu_c^2)\,s_b(z)\otimes s_a(z') \\ &+\Sigma_c^{a\to a}\,(a,b)^2(1-\mu_b^2)\,s_c(z)\otimes s_c(z') \\ &+(1-\mu_b^2)(1-\mu_c^2)\,(a,b)(b,c)\,s_c(z)\otimes s_c(z')\big\}\end{aligned} \tag{2.51}$$

in order to have proper asymptotics, one must use the analogue of (2.44) to substitute both $s_a(z')$ and $s_c(z)$, notice that since we are "working in triangle abc" it is convenient to apply such identities among these vertices, in order to benefit from proper cancellations. The resulting expression reads

$$\begin{aligned}\tilde{\mathcal{Y}}_{11'} &= [\Xi(\Sigma_b^{c\to c},\Sigma_c^{a\to a};\mu_b,\mu_c)]^{-1} \\ &\times\big\{\Sigma_b^{c\to c}\Sigma_c^{a\to a}\mathcal{Y}_{22'}+\Sigma_b^{c\to c}\,(1-\mu_c^2)(\mathcal{Y}_{12'}-\mathcal{Y}_{22'}) \\ &-(\Sigma_c^{a\to a}+\mu_c^2-1)(1-\mu_b^2)(\mathcal{Y}_{21'}+\mathcal{Y}_{22'}) \\ &+(1-\mu_b^2)(1-\mu_c^2)(\mathcal{Y}_{11'}-\mathcal{Y}_{12'})\big\}\end{aligned} \tag{2.52}$$

[7] As we stressed in defining Ξ, it would be a mistake to write e.g.

$$(\tilde{s}_c,\tilde{s}_b) = \Xi(\Sigma_c^{b\to b},\Sigma_b^{c\to c};\mu_c,\mu_b)\omega_{a,b,c}.$$

There are two possibilities here:

$$(\tilde{s}_c,\tilde{s}_b) = -(\tilde{s}_b,\tilde{s}_c) = -\Xi(\Sigma_b^{c\to c},\Sigma_c^{a\to a};\mu_b,\mu_c) = +\Xi(\Sigma_c^{b\to b},\Sigma_b^{e\to e};\mu_c,\mu_b)\omega_{c,b,e}$$

A similar procedure leads to

$$\tilde{\mathcal{Y}}_{22'} = [\Xi(\Sigma_a^{b\to b}, \Sigma_b^{c\to c}; \mu_a, \mu_b)]^{-1} \left\{\Sigma_a^{b\to b}\Sigma_b^{c\to c}\mathcal{Y}_{11'} + \Sigma_a^{b\to b}(1-\mu_b^2)\mathcal{Y}_{21'} \right.$$
$$\left. -\Sigma_b^{c\to c}(1-\mu_a^2)\mathcal{Y}_{12'} + (1-\mu_a^2)(1-\mu_b^2)\mathcal{Y}_{22'}\right\}$$

$$\tilde{\mathcal{Y}}_{12'} = [\Xi(\Sigma_c^{a\to a}, \Sigma_a^{b\to b}; \mu_c, \mu_a)]^{-1} \left\{\Sigma_a^{b\to b}\Sigma_c^{a\to a}\mathcal{Y}_{21'} + \Sigma_c^{a\to a}(1-\mu_a^2)\mathcal{Y}_{22'} \right.$$
$$\left. -\Sigma_a^{b\to b}(1-\mu_c^2)(\mathcal{Y}_{11'} + \mathcal{Y}_{21'}) + (1-\mu_a^2)(1-\mu_c^2)(\mathcal{Y}_{12'} - \mathcal{Y}_{22'})\right\} \tag{2.53}$$

$$\tilde{\mathcal{Y}}_{21'} = \frac{\Xi(\Sigma_c^{a\to a}, \Sigma_a^{b\to b}; \mu_c, \mu_a)}{\Xi(\Sigma_a^{b\to b}, \Sigma_b^{c\to c}; \mu_a, \mu_b)\Xi(\Sigma_b^{c\to c}, \Sigma_c^{a\to a}; \mu_b, \mu_c)}$$
$$\times \left\{(\Sigma_b^{c\to c})^2\mathcal{Y}_{12'} - \Sigma_b^{c\to c}(1-\mu_b^2)(\mathcal{Y}_{22'} + \mathcal{Y}_{12'} + \mathcal{Y}_{11'})\right.$$
$$\left. +(1-\mu_b^2)^2(\mathcal{Y}_{21'} + \mathcal{Y}_{22'})\right\}$$

2.1.4.4 Variation on the case of neighboring cells

Here we briefly repeat the above calculation, but the path from z to z' now goes clockwise around the turning point. For simplicity we take the case in which both z, z' belong to the same triangle. This will be useful when considering $N = 1$ AD theory with a line defect.

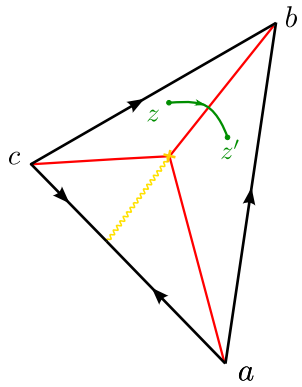

Figure 2.9: A variation on the case of neighboring cells

We refer to fig.2.9.

$$s_1(z) = s_b(z)\,(s_c, s_a) \qquad s_2(z) = s_c(z)\,(s_a, s_b)$$
$$s_{1'}(z') = s_b(z')\,(s_c, s_a) \qquad s_{2'}(z') = s_a(z')\,(s_b, s_c) \tag{2.54}$$
$$\nu_1 = -\nu_2 = -$$

From the definitions (2.37) follow

$$\begin{aligned}
\mathcal{Y}_{11'} &= \frac{s_2(z)\otimes s_{1'}(z')}{(s_{1'},s_2)} = \frac{s_c(z)\otimes s_b(z')}{(s_b,s_c)} \\
\mathcal{Y}_{22'} &= \frac{s_1(z)\otimes s_{2'}(z')}{(s_{2'},s_1)} = \frac{s_b(z)\otimes s_a(z')}{(s_a,s_b)} \\
\mathcal{Y}_{12'} &= \nu_1\,\frac{s_1(z)\otimes s_{1'}(z')}{(s_2,s_{1'})} = s_b(z)\otimes s_b(z')\frac{(s_c,s_a)}{(s_a,s_b)(s_b,s_c)} \\
\mathcal{Y}_{21'} &= \nu_2\,\frac{s_2(z)\otimes s_{2'}(z')}{(s_1,s_{2'})} = \frac{s_c(z)\otimes s_a(z')}{(s_a,s_c)}
\end{aligned} \tag{2.55}$$

After sending $\vartheta \to \vartheta + \pi$ we have instead

$$\begin{gathered}
\tilde{s}_1(z) = \tilde{s}_c(z)\,(\tilde{s}_a,\tilde{s}_b) \qquad \tilde{s}_2(z) = \tilde{s}_b(z)\,(\tilde{s}_c,\tilde{s}_a) \\
\tilde{s}_{1'}(z') = \tilde{s}_a(z')\,(\tilde{s}_b,\tilde{s}_c) \qquad \tilde{s}_{2'}(z') = \tilde{s}_b(z')\,(\tilde{s}_c,\tilde{s}_a) \\
\tilde{\nu}_1 = -\tilde{\nu}_2 = +
\end{gathered} \tag{2.56}$$

From the definitions (2.37), and employing eq.s (2.25), (2.26), (2.30) follow

$$\begin{aligned}
\tilde{\mathcal{Y}}_{11'} &= [\Xi(\Sigma_a^{b\to b},\Sigma_b^{c\to c};\mu_a,\mu_b)]^{-1}\,\big\{\Sigma_a^{b\to b}\Sigma_b^{c\to c}\mathcal{Y}_{22'} + \Sigma_b^{c\to c}(1-\mu_a^2)\mathcal{Y}_{12'} \\
&\quad -\Sigma_a^{b\to b}(1-\mu_b^2)\mathcal{Y}_{21'} + (1-\mu_a^2)(1-\mu_b^2)\mathcal{Y}_{11'}\big\} \\
\\
\tilde{\mathcal{Y}}_{22'} &= [\Xi(\Sigma_b^{c\to c},\Sigma_c^{a\to a};\mu_b,\mu_c)]^{-1}\,\big\{\Sigma_b^{c\to c}\Sigma_c^{a\to a}\mathcal{Y}_{11'} - \Sigma_c^{a\to a}(1-\mu_b^2)[\mathcal{Y}_{11'}-\mathcal{Y}_{21'}] \\
&\quad -\Sigma_b^{c\to c}(1-\mu_c^2)[\mathcal{Y}_{12'}+\mathcal{Y}_{11'}] + (1-\mu_b^2)(1-\mu_c^2)[\mathcal{Y}_{11'}+\mathcal{Y}_{22'}+\mathcal{Y}_{12'}-\mathcal{Y}_{21'}]\big\} \\
\\
\tilde{\mathcal{Y}}_{12'} &= [\Xi(\Sigma_c^{a\to a},\Sigma_a^{b\to b};\mu_c,\mu_a)]^{-1}\,\big\{\Sigma_c^{a\to a}\Sigma_a^{b\to b}\mathcal{Y}_{21'} - \Sigma_c^{a\to a}(1-\mu_a^2)\mathcal{Y}_{11'} \\
&\quad +\Sigma_a^{b\to b}(1-\mu_c^2)[\mathcal{Y}_{22'}-\mathcal{Y}_{21'}] + (1-\mu_c^2)(1-\mu_a^2)[\mathcal{Y}_{12'}+\mathcal{Y}_{11'}]\big\} \\
\\
\tilde{\mathcal{Y}}_{21'} &= \Xi(\Sigma_c^{a\to a},\Sigma_a^{b\to a};\mu_c,\mu_a)[\Xi(\Sigma_b^{c\to c},\Sigma_c^{a\to a};\mu_b,\mu_c)\Xi(\Sigma_a^{b\to b},\Sigma_b^{c\to c};\mu_a,\mu_b)]^{-1} \\
&\quad \times\big\{(\Sigma_b^{c\to c})^2\mathcal{Y}_{12'} + (1-\mu_b^2)^2[\mathcal{Y}_{21'}-\mathcal{Y}_{11'}] \\
&\quad +\Sigma_b^{c\to c}(1-\mu_b^2)[\mathcal{Y}_{11'}-\mathcal{Y}_{22'}-\mathcal{Y}_{12'}]\big\}
\end{aligned} \tag{2.57}$$

2.2 Extracting the spectrum using $\mathbb{S}$

We now provide some examples of how to apply the results of §2.1. In the cases reviewed below, using $\mathbb{S}$ to extrapolate the spectrum is quick and easy. As we will see, it essentially amounts to

matching pictures, which is achieved by matching vertex labels and sheet labels. According to this picture, we expect to have wall crossing for solitonic charges whenever labels jump: this occurs when z crosses a separating line or a branch cut[8], in agreement with the results of [65].

2.2.1 $N = 1$ AD theory without line defects

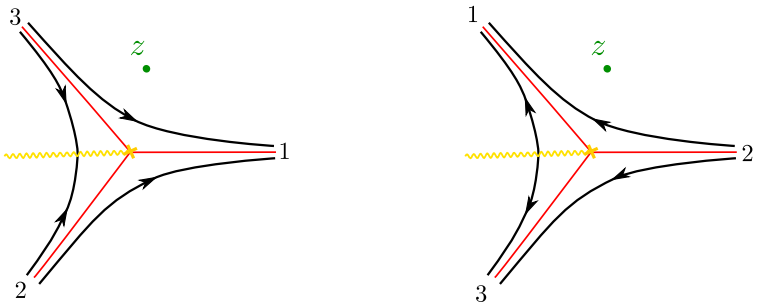

Figure 2.10: The + sheet, on the left at angle $\vartheta = 0$, on the right at angle $\vartheta = \pi$.

For the $N = 1$ Argyres-Douglas theory we have $\phi_2(z) = -z\,dz^2$, on $C = \mathbb{C}P^1$, meaning that there is one irregular singularity at infinity, a turning point in $z = 0$, and Σ is a two-sheeted cover of C. We consider the theory in presence of a single surface defect sitting at z, with $Arg(z) \in [0, 2\pi/3]$, as in fig.2.10. Notice that vertices are labeled clockwise (counter-clockwise as seen from a neighborhood of the irregular puncture at infinity).

We now want to apply the results obtained in section 2.1.3 to derive the spectrum. Compare figures 2.2 and 2.10: matching the flow of WKB lines through z in both pictures entails the identifications for the vertices $a \leftrightarrow 1,\ b \leftrightarrow 3,\ c \leftrightarrow 2$ together with the identification of sheets

$$\text{sheet } 2 \leftrightarrow \text{sheet } + \tag{2.58}$$

and similarly for sheets 1 and $-$.

Indeed, *identifying the sheets properly is all we need*: this entails

$$\begin{aligned} &\mathcal{Y}_{11} \leftrightarrow \mathcal{Y}_{--}, \qquad \mathcal{Y}_{12} \leftrightarrow \mathcal{Y}_{-+}, \qquad \dots \\ &\tilde{\mathcal{Y}}_{11} \leftrightarrow \tilde{\mathcal{Y}}_{--}, \qquad \tilde{\mathcal{Y}}_{12} \leftrightarrow \tilde{\mathcal{Y}}_{-+}, \qquad \dots \end{aligned} \tag{2.59}$$

thus, employing expressions (2.32) and (2.33), and making the replacements explained in §§2.1.3.3, 2.1.3.4 should give the transformation generated by $\mathbb{S}$. As a matter of fact, in this particularly simple example, we have only degenerate edges, thus we replace all $\mu_\alpha^2 = 0$, and all $\Sigma = \Xi = 1$.

[8] A branch cut is not physically meaningful, so the reader may be puzzled by its relevance in jumps of the spectrum. In this context if z crosses the cut, this amounts to a deck transformation, or to exchanging the lifts of z to Σ. In other words, when z crosses a cut we switch $\gamma_{ij} \leftrightarrow \gamma_{ji}$ which explains why we see a "jump" in the spectrum: we are really just switching notation, accordingly the jump must reflect such exchange of charges.

With these rules, eq.s (2.32) and (2.33) give the transformation

$$\begin{cases} \tilde{\mathcal{Y}}_{12} = \mathcal{Y}_{12} + \mathcal{Y}_{21} + \mathcal{Y}_{22} - \mathcal{Y}_{11} \\ \tilde{\mathcal{Y}}_{21} = \mathcal{Y}_{21} \\ \tilde{\mathcal{Y}}_{11} = \mathcal{Y}_{11} - \mathcal{Y}_{21} \\ \tilde{\mathcal{Y}}_{22} = \mathcal{Y}_{22} + \mathcal{Y}_{21} \end{cases} \leftrightarrow \begin{cases} \tilde{\mathcal{Y}}_{-+} = \mathcal{Y}_{-+} + \mathcal{Y}_{+-} + \mathcal{Y}_{++} - \mathcal{Y}_{--} \\ \tilde{\mathcal{Y}}_{+-} = \mathcal{Y}_{+-} \\ \tilde{\mathcal{Y}}_{--} = \mathcal{Y}_{--} - \mathcal{Y}_{+-} \\ \tilde{\mathcal{Y}}_{++} = \mathcal{Y}_{++} + \mathcal{Y}_{+-} \end{cases} \tag{2.60}$$

This corresponds to the transformation

$$\mathcal{S}^{\mu}_{+-} : \mathcal{Y}_{++} \mapsto (1 - \mu_{+-}\mathcal{Y}_{+-})\, \mathcal{Y}_{++}\, (1 + \mu_{+-}\mathcal{Y}_{+-}) \tag{2.61}$$

with $\mu_{+-} = +1$, and similarly for the other $\mathcal{Y}$'s. This means that the BPS spectrum contains only one soliton γ_{+-}: $\mathbb{S} = \mathcal{S}^{\mu}_{+-}$ (together with its antiparticle), consequently there can't be any marginal stability wall, nor wall crossing.

2.2.2 $N = 1$ AD theory: framed wall crossing

2.2.2.1 Small angular separation

We now consider what happens in presence of a line defect [61, 82], namely an interface between two surface defects [65]. Let the two surface defects sit at points z, z' on C, we consider $\mathcal{Y}^{\vartheta=0}_{++'}$, associated to the path shown in fig.2.11.

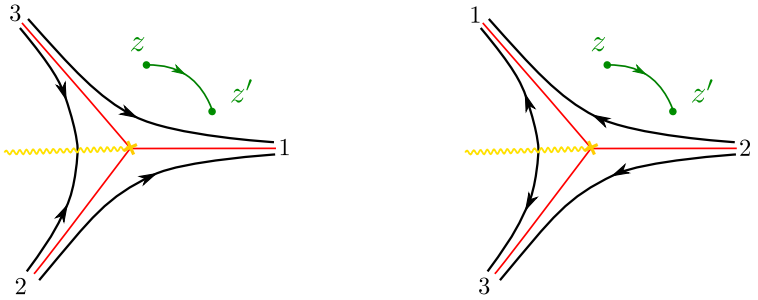

Figure 2.11: The + sheet, on the left at angle $\vartheta = 0$, on the right at angle $\vartheta = \pi$.

We can then apply the machinery of sections 2.1.4.1 and 2.1.4.2 and quickly obtain the spectrum generator.

Comparing figures 2.7 and 2.11 we immediately see that to adapt the general discussion to our case we must identify

$$\text{sheet2} \leftrightarrow \text{sheet+} \tag{2.62}$$

and accordingly identify sheets 1 and $-$. Having to deal with an irregular puncture, we must make the replacements mentioned at the end of section 2.1.4.1. Since all edges involved are boundary edges we just have to replace all $\mu^2 = 0$, $\Sigma = 1 = \Xi$ into equations (2.45), (2.46).

Doing so, gives immediately the *omnipop* transformation

$$\begin{cases} \tilde{\mathcal{Y}}_{12'} = \mathcal{Y}_{12'} + \mathcal{Y}_{21'} + \mathcal{Y}_{22'} - \mathcal{Y}_{11'} \\ \tilde{\mathcal{Y}}_{21'} = \mathcal{Y}_{21'} \\ \tilde{\mathcal{Y}}_{11'} = \mathcal{Y}_{11'} - \mathcal{Y}_{21'} \\ \tilde{\mathcal{Y}}_{22'} = \mathcal{Y}_{22'} + \mathcal{Y}_{21'} \end{cases} \leftrightarrow \begin{cases} \tilde{\mathcal{Y}}_{-+'} = \mathcal{Y}_{-+'} + \mathcal{Y}_{+-'} + \mathcal{Y}_{++'} - \mathcal{Y}_{--'} \\ \tilde{\mathcal{Y}}_{+-'} = \mathcal{Y}_{+-'} \\ \tilde{\mathcal{Y}}_{--'} = \mathcal{Y}_{--'} - \mathcal{Y}_{+-'} \\ \tilde{\mathcal{Y}}_{++'} = \mathcal{Y}_{++'} + \mathcal{Y}_{+-'} \end{cases} \tag{2.63}$$

All these transformations can be traced back to the action of

$$\mathbb{S} = \mathcal{S}_{+'-'}\mathcal{S}_{+-}, \tag{2.64}$$

with $\mu(+'-') = \mu(+-) = +1$, as one could naively expect from the discussion of the previous section: the spectrum contains two BPS solitons, one for each surface defect, and each of them undergoes exactly the same wall crossing as that of eq. (2.61), since both defects will get crossed by the same WKB ray as in that case.

Notice that, in order to match our result with the example analyzed in [65] section 8.1.1, one needs to apply the label exchange $ij \leftrightarrow ji$ as described in remark (2.38). After doing this, one recovers the transformations of eq.s (8.9), (8.10) in the reference.

As a check, we give a full derivation of the spectrum generator, this will also be useful in analyzing line defects below. According to the rules sketched above

$$\begin{gathered} s_+(z) = s_1(z)\,(s_3, s_2) \qquad s_{+'}(z') = s_1(z')\,(s_3, s_2) \\ s_-(z) = s_3(z)\,(s_2, s_1) \qquad s_{-'}(z') = s_3(z')\,(s_2, s_1) \\ \nu_+ = -\nu_- = - = \nu_{+'} = -\nu_{-'} \end{gathered} \tag{2.65}$$

therefore, from (2.37) we have

$$\begin{aligned} \mathcal{Y}^{\vartheta}_{++'} &= \frac{s_3(z) \otimes s_1(z')}{(s_1, s_3)} \qquad & \mathcal{Y}^{\vartheta}_{--'} &= \frac{s_1(z) \otimes s_3(z')}{(s_3, s_1)} \\ \mathcal{Y}^{\vartheta}_{+-'} &= s_1(z) \otimes s_1(z')\,\frac{(s_3, s_2)}{(s_1, s_3)(s_2, s_1)} \qquad & \mathcal{Y}^{\vartheta}_{-+'} &= s_3(z) \otimes s_3(z')\,\frac{(s_2, s_1)}{(s_1, s_3)(s_3, s_2)}, \end{aligned} \tag{2.66}$$

setting $\vartheta = \pi$ gives the situation of fig.2.11.

$$\begin{gathered} \tilde{s}_+(z) = s_1(z)\,(s_3, s_2) \qquad \tilde{s}_{+'}(z') = s_1(z')\,(s_3, s_2) \\ \tilde{s}_-(z) = s_2(z)\,(s_1, s_3) \qquad \tilde{s}_{-'}(z') = s_2(z')\,(s_1, s_3) \\ \tilde{\nu}_+ = -\tilde{\nu}_- = + = \tilde{\nu}_{+'} = -\tilde{\nu}_{-'} \end{gathered} \tag{2.67}$$

Therefore, rules (2.37) now give

$$\begin{aligned} \tilde{\mathcal{Y}}_{++'} &= \frac{s_2(z)\otimes s_1(z')}{(s_1,s_2)} \qquad \tilde{\mathcal{Y}}_{--'} = \frac{s_1(z)\otimes s_2(z')}{(s_2,s_1)} \\ \tilde{\mathcal{Y}}_{+-'} &= s_1(z)\otimes s_1(z')\frac{(s_3,s_2)}{(s_2,s_1)(s_1,s_3)} \qquad \tilde{\mathcal{Y}}_{-+'} = s_2(z)\otimes s_2(z')\frac{(s_1,s_3)}{(s_3,s_2)(s_2,s_1)}. \end{aligned} \tag{2.68}$$

We can now employ eq. (2.44), and get e.g.

$$\tilde{\mathcal{Y}}_{++'} = \mathcal{Y}_{++'} + \mathcal{Y}_{+-'} \tag{2.69}$$

similarly, repeating the machinery one finds

$$\begin{aligned} \tilde{\mathcal{Y}}_{--'} &= \mathcal{Y}_{--'} - \mathcal{Y}_{+-'} \\ \tilde{\mathcal{Y}}_{-+'} &= \mathcal{Y}_{-+'} + \mathcal{Y}_{+-'} + \mathcal{Y}_{++'} - \mathcal{Y}_{--'} \\ \tilde{\mathcal{Y}}_{+-'} &= \mathcal{Y}_{+-'} \end{aligned} \tag{2.70}$$

in agreement with the above result.

Now, having a line defect, we can consider its expectation value at some angle ϑ: before the omnipop

$$\langle L_{\wp,\zeta}\rangle = \mathcal{Y}_{++'} + \mathcal{Y}_{--'}. \tag{2.71}$$

Since $\langle L_{\wp,\zeta}\rangle$ must not jump as ϑ varies, we can rewrite it at $\vartheta+\pi$ by inverting eq.s(2.69), (2.70) and plugging into (2.71). This gives

$$\langle L_{\wp,\zeta}\rangle = \tilde{\mathcal{Y}}_{++'} + \tilde{\mathcal{Y}}_{--'}. \tag{2.72}$$

We see no framed wall crossing. Comparing with §8.1.1 of [65] the explanation is the following one: as is shown in the reference, referring to fig.19 therein, framed wall crossing occurs when we compare between situations such as (A) and (B) (if e.g. in situation (A) $\vartheta=\vartheta_0$, situation (C) has $\vartheta=\vartheta_0+\pi$, and (B) is some particular intermediate situation), but no difference exists between situations (A) and (C). This agrees with eq.(8.10) of [65].

2.2.2.2 Large angular separation

Let us now consider the case when z, z' are separated by an angle between $2\pi/3$ and π, as shown in fig.2.12. In [65] the *clockwise* transformation for $\vartheta\mapsto\vartheta-\pi$ is considered (see end of section 8.1.1 there), our methods are suitable for studying an omnipop, i.e. an increase of ϑ by π, nonetheless once we obtain the transformation for this, we can match with [65] by recalling that in the sector $[\vartheta,\vartheta-\pi]$ the spectrum consists of the corresponding *antiparticles*.

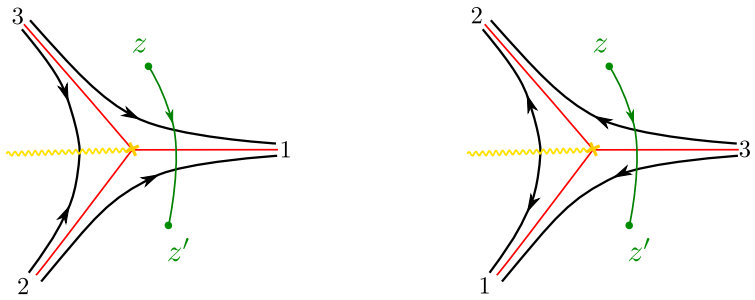

Figure 2.12: The + sheet, on the left at angle $\vartheta = 0$, on the right at angle $\vartheta = -\pi$.

Let us therefore study the regular omnipop first. This case matches with the analysis carried out in section 2.1.4.4: comparing figures 2.9 and 2.12 entails the identification

$$\text{sheet1} \leftrightarrow \text{sheet+} \tag{2.73}$$

therefore, we can employ eq.s (2.57): setting all $\mu^2 \mapsto 0$, $\Sigma \mapsto 1$, $\Xi \mapsto 1$, they read

$$\begin{cases} \tilde{\mathcal{Y}}_{11'} = \mathcal{Y}_{11'} + \mathcal{Y}_{22'} + \mathcal{Y}_{12'} - \mathcal{Y}_{21'} \\ \tilde{\mathcal{Y}}_{22'} = \mathcal{Y}_{22'} \\ \tilde{\mathcal{Y}}_{12'} = \mathcal{Y}_{12'} + \mathcal{Y}_{22'} \\ \tilde{\mathcal{Y}}_{21'} = \mathcal{Y}_{21'} - \mathcal{Y}_{22'} \end{cases} \leftrightarrow \begin{cases} \tilde{\mathcal{Y}}_{++'} = \mathcal{Y}_{++'} + \mathcal{Y}_{--'} + \mathcal{Y}_{+-'} - \mathcal{Y}_{-+'} \\ \tilde{\mathcal{Y}}_{--'} = \mathcal{Y}_{--'} \\ \tilde{\mathcal{Y}}_{+-'} = \mathcal{Y}_{+-'} + \mathcal{Y}_{--'} \\ \tilde{\mathcal{Y}}_{-+'} = \mathcal{Y}_{-+'} - \mathcal{Y}_{--'} \end{cases} \tag{2.74}$$

these are generated by[9]

$$\mathbb{S}(\vartheta + \pi, \vartheta) \;=\; \mathcal{S}_{-+}\mathcal{S}_{+'-'} \tag{2.76}$$

meaning that $\mu(-+) = +1 = \mu(+'-')$.

We therefore conclude that the spectrum generator in the other half-plane will be

$$\mathbb{S}(\vartheta, \vartheta - \pi) \;=\; \mathcal{S}_{+-}\mathcal{S}_{-'+'} \tag{2.77}$$

Now, to match with the example in [65], we need to make the following consideration: inverting eq.s (2.74) amounts to switching the tildes and all $ij \to ji$ as well as $i'j' \to j'i'$ namely, we get

$$\begin{cases} \mathcal{Y}_{++'} = \tilde{\mathcal{Y}}_{++'} + \tilde{\mathcal{Y}}_{--'} - \tilde{\mathcal{Y}}_{+-'} + \tilde{\mathcal{Y}}_{-+'} \\ \mathcal{Y}_{--'} = \tilde{\mathcal{Y}}_{--'} \\ \mathcal{Y}_{+-'} = \tilde{\mathcal{Y}}_{+-'} - \tilde{\mathcal{Y}}_{--'} \\ \mathcal{Y}_{-+'} = \tilde{\mathcal{Y}}_{-+'} + \tilde{\mathcal{Y}}_{--'} \end{cases} \tag{2.78}$$

[9]Here we are using the following set of twisting functions:

$$\sigma(-+, ++') = \sigma(+'-', ++') = 1 = -\sigma(+'-', -+') = -\sigma(-+, +-') \tag{2.75}$$

this would be the action of $\mathbb{S}(\vartheta, \vartheta+\pi) = \mathbb{S}(\vartheta+\pi, \vartheta)^{-1}$, describing the *clockwise* transformation from $\vartheta = \pi$ to $\vartheta = 0$. What we found is that, in this example switching $ij \leftrightarrow ji$ in the $\mathcal{Y}$'s labels corresponds precisely to switching the *clockwise*$\leftrightarrow$*counterclockwise* jumps of ϑ by angles of π. We claim that this also holds for the spectrum generator in the other half plane, we prove this in the following subsection.

Now, according to remark (2.38) this switching of labels is just what we must employ to match our conventions with those of [65]. Therefore, we arrive at the conclusion that our $\mathbb{S}(\vartheta, \vartheta-\pi)$ is precisely the transformation they find in going *clockwise* from $\vartheta = 0$ to $\vartheta = -\pi$. Indeed they match, see eq.s (8.12) therein: $\mathcal{E}_C = \mathcal{S}_{+-}\mathcal{S}_{-'+'}\mathcal{E}_A$.

The above derivation of the spectrum was straightforward, although the matching with [65] might appear a bit artificial. Let us prove that this is actually correct: we now give a full derivation of the spectrum generator when $\vartheta \mapsto \vartheta - \pi$ (i.e. following the direction taken by the reference).

We start with $\vartheta = 0$, our building blocks are now

$$\begin{aligned} s_+(z) &= s_1(z)\,(s_3, s_2) \qquad s_{+'}(z') = s_1(z')\,(s_3, s_2) \\ s_-(z) &= s_3(z)\,(s_2, s_1) \qquad s_{-'}(z') = s_2(z')\,(s_1, s_3) \\ \nu_+ &= -\nu_- = - = -\nu_{+'} = \nu_{-'} \end{aligned} \tag{2.79}$$

therefore, from (2.37) we have

$$\begin{aligned} \mathcal{Y}^{\vartheta}_{++'} &= \frac{s_3(z)\otimes s_1(z')}{(s_1, s_3)} \qquad \mathcal{Y}^{\vartheta}_{--'} = \frac{s_1(z)\otimes s_2(z')}{(s_2, s_1)} \\ \mathcal{Y}^{\vartheta}_{+-'} &= s_1(z)\otimes s_1(z')\,\frac{(s_3, s_2)}{(s_1, s_3)(s_2, s_1)} \qquad \mathcal{Y}^{\vartheta}_{-+'} = \frac{s_3(z)\otimes s_2(z')}{(s_2, s_3)}, \end{aligned} \tag{2.80}$$

setting $\vartheta = -\pi$ gives the situation of fig.2.12.

$$\begin{aligned} \tilde{s}_+(z) &= s_2(z)\,(s_1, s_3) \qquad \tilde{s}_{+'}(z') = s_1(z')\,(s_3, s_2) \\ \tilde{s}_-(z) &= s_3(z)\,(s_2, s_1) \qquad \tilde{s}_{-'}(z') = s_3(z')\,(s_2, s_1) \\ \tilde{\nu}_+ &= -\tilde{\nu}_- = + = -\tilde{\nu}_{+'} = \tilde{\nu}_{-'} \end{aligned} \tag{2.81}$$

where we now understand $\tilde{\mathcal{Y}} := \mathcal{Y}^{-\pi}$. Therefore, rules (2.37) now give

$$\begin{aligned} \tilde{\mathcal{Y}}_{++'} &= \frac{s_3(z)\otimes s_1(z')}{(s_1, s_3)} \qquad \tilde{\mathcal{Y}}_{--'} = \frac{s_2(z)\otimes s_3(z')}{(s_3, s_2)} \\ \tilde{\mathcal{Y}}_{+-'} &= \frac{s_2(z)\otimes s_1(z')}{(s_1, s_2)} \qquad \tilde{\mathcal{Y}}_{-+'} = s_3(z)\otimes s_3(z')\frac{(s_2, s_1)}{(s_1, s_3)(s_3, s_2)}. \end{aligned} \tag{2.82}$$

We can employ eq. (2.44), and get directly

$$\begin{aligned}
\tilde{\mathcal{Y}}_{++'} &= \mathcal{Y}_{++'} \\
\tilde{\mathcal{Y}}_{--'} &= \mathcal{Y}_{--'} + \mathcal{Y}_{++'} + \mathcal{Y}_{+-'} - \mathcal{Y}_{-+'} \\
\tilde{\mathcal{Y}}_{-+'} &= \mathcal{Y}_{-+'} - \mathcal{Y}_{++'} \\
\tilde{\mathcal{Y}}_{+-'} &= \mathcal{Y}_{+-'} + \mathcal{Y}_{++'}
\end{aligned} \tag{2.83}$$

These transformations correspond to going *clockwise* from $\vartheta = 0$ to $\vartheta = -\pi$, they are the inverse of the *counterclockwise* $\vartheta = -\pi \mapsto \vartheta = 0$ which reads

$$\begin{aligned}
\mathcal{Y}_{++'} &= \tilde{\mathcal{Y}}_{++'} \\
\mathcal{Y}_{--'} &= \tilde{\mathcal{Y}}_{--'} + \tilde{\mathcal{Y}}_{++'} - \tilde{\mathcal{Y}}_{+-'} + \tilde{\mathcal{Y}}_{-+'} \\
\mathcal{Y}_{-+'} &= \tilde{\mathcal{Y}}_{-+'} + \tilde{\mathcal{Y}}_{++'} \\
\mathcal{Y}_{+-'} &= \tilde{\mathcal{Y}}_{+-'} - \tilde{\mathcal{Y}}_{++'}
\end{aligned} \tag{2.84}$$

these result precisely from the action of

$$\mathbb{S}(\vartheta, \vartheta - \pi) = \mathcal{S}_{+-}\mathcal{S}_{-'+'} \tag{2.85}$$

in agreement with our previous derivation.

With a line defect at hand, we can examine the associated expectation value at some angle ϑ: before the omnipop (cf. eq.(8.11) in [65])[10]:

$$\langle L_{\wp,\zeta} \rangle \;=\; \mathcal{Y}_{++'} + \mathcal{Y}_{+-'} + \mathcal{Y}_{--'}. \tag{2.86}$$

Since $\langle L_{\wp,\zeta} \rangle$ must not jump as ϑ varies, we can rewrite it at $\vartheta = -\pi$ by inverting eq.s(2.83) and plugging into (2.86). This gives

$$\langle L_{\wp,\zeta} \rangle \;=\; \tilde{\mathcal{Y}}_{++'} + \tilde{\mathcal{Y}}_{-+'} + \tilde{\mathcal{Y}}_{--'}. \tag{2.87}$$

this corresponds to acting on $\langle L_{\wp,\zeta} \rangle$ with

$$\begin{aligned}
&(1 - \mathcal{Y}_{-'+'})(1 - \mathcal{Y}_{+-})\langle L_{\wp,\zeta} \rangle (1 + \mathcal{Y}_{+-})(1 + \mathcal{Y}_{-'+'}) \\
&\equiv\; (1 - \mathcal{Y}_{+-})\langle L_{\wp,\zeta} \rangle (1 + \mathcal{Y}_{-'+'})
\end{aligned} \tag{2.88}$$

that means $\mathbb{S}(\vartheta, \vartheta - \pi) = \mathcal{S}_{\gamma_{-'+'}}\mathcal{S}_{\gamma_{+-}}$, together with $\mu(\gamma_{-'+'}) = 1 = \mu(\gamma_{+-})$.[11]

[10] Note: as remarked in eq.(2.38) for us $\mathcal{Y}_{ij'}$ have i and j switched, as compared to [65], so here our $\mathcal{Y}_{+-'}$ corresponds to their $\mathcal{Y}_{-+'}$, and vice versa

[11] Note on twisting functions: we are using

$$\begin{aligned}
\sigma(+-, -+') &= +1 \qquad \sigma(+-, --') = -1 \\
\sigma(--', -'+') &= -1 \qquad \sigma(+-', -'+') = +1
\end{aligned} \tag{2.89}$$

The first row is explicitly employed in [65], see footnote at p.114; the first sign of the second row is implicitly used in eq. (8.10) in that reference; the last sign is derivable by means of the cocycle condition for twisting functions (2.24).

2.2.3 $N = 2$ AD theory

We now turn to the case of $N = 2$ AD theory, label-matching is slightly more delicate here, hence we first give a derivation of $\mathbb{S}$ by carrying out a complete analysis of how T_{WKB} evolves with ϑ, later we obtain $\mathbb{S}$ relying only on the results of 2.1.3, this will be much faster and agree exactly with the former derivation, as well as with the analysis of [65].

2.2.3.1 Full derivation of the spectrum generator

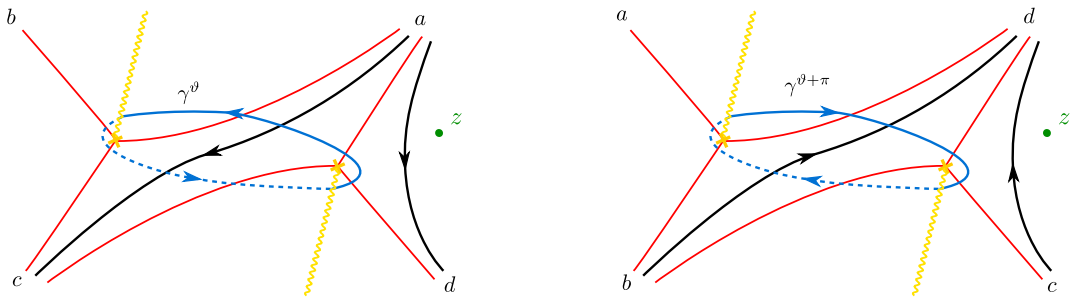

Figure 2.13: The WKB triangulation on sheet 2 as seen from the *north pole* of $\mathbb{CP}^1$: on the left at ϑ and on the right at $\vartheta + \pi$. The topology remains the same, while the flow of WKB lines switches direction, moreover there is a cyclic permutation of the vertices, since they all belong to the same irregular puncture at the south pole.

In this theory the Seiberg-Witten differential is given by $P_2(z) = z^2+2m$. The only deformation is log-normalizable (see [64]), hence the Coulomb branch is a single point. Let us adopt the conventions of section 8.1.2 in [65], in particular we will choose the same conventions for the orientation of paths on C. Figure 2.13 shows how the WKB triangulation evolves in passing from ϑ to $\vartheta + \pi$ on sheet 2. This is justified as follows: on the one hand, the topology of the triangulation must be the same, with the orientation of WKB lines inverted; on the other hand one can follow how the triangulation evolves step by step, as shown in fig.2.14[12] (also see fig. 45 in [64]), which explains manifestly the nature of the spectrum: we must have an $\mathcal{S}$ factor due to the fact that a separatrix crosses z, and then a $\mathcal{K}$ factor because of the flip; this interpretation is confirmed by equation (8.14) in the reference, moreover by placing z, say, in the upper region, one sees that there will be 2 $\mathcal{S}$ factors instead of 1, because two separatrices cross z, as confirmed by eq. (8.15) in the reference, and so on. To begin our analysis of the spectrum in the region on the right, we first identify, as usual

$$s_2 = s_d(s_a, s_c) \quad s_1 = s_a(s_c, s_d) \quad \nu_1 = + = -\nu_2 \tag{2.90}$$

[12]Since we have an irregular singularity at infinity, the WKB rays will rotate as ϑ increases, for $N = 4$ we have a rotation by $\pi/2$ for $\vartheta \mapsto \vartheta + \pi$ as the labels show

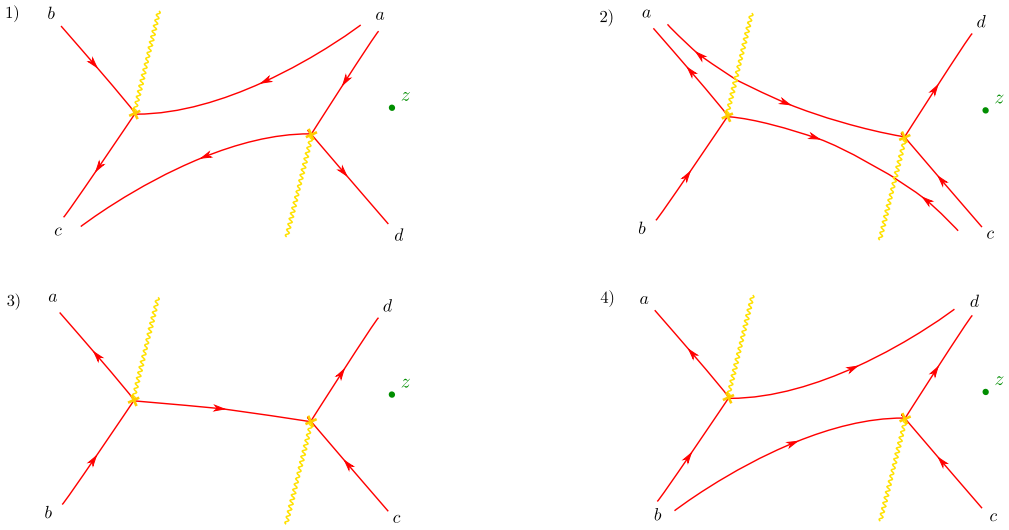

Figure 2.14: Evolution of the WKB triangulation as $\vartheta \mapsto \vartheta + \pi$. Between stages 1 and 2 an $\mathcal{S}$ factor occurs, since the separating line at d crosses z, at stage 3 we have a jump from the hypermultiplet as indicated by the flip, hence the spectrum will contain a $\mathcal{K}$ factor as well.

After the omnipop, we'll have

$$\tilde{s}_2 = s_d(s_b, s_c) \quad \tilde{s}_1 = s_c(s_d, s_b) \quad \tilde{\nu}_1 = - = -\tilde{\nu}_2 \tag{2.91}$$

Following rules (2.20) we have immediately

$$\begin{aligned} \mathcal{Y}_{12} = s_a \otimes s_a \frac{(s_c, s_d)}{(s_d, s_a)(s_a, s_c)} \qquad & \mathcal{Y}_{21} = s_d \otimes s_d \frac{(s_a, s_c)}{(s_d, s_a)(s_c, s_d)} \\ \mathcal{Y}_{11} = \frac{s_d \otimes s_a}{(s_a, s_d)} \qquad & \mathcal{Y}_{22} = \frac{s_a \otimes s_d}{(s_d, s_a)} \end{aligned} \tag{2.92}$$

together with

$$\mathcal{Y}_\gamma = \frac{(s_a, s_b)(s_c, s_d)}{(s_b, s_c)(s_d, s_a)} = (\mathcal{Y}_{-\gamma})^{-1}. \tag{2.93}$$

After sending $\vartheta \mapsto \vartheta + \pi$ we have instead

$$\begin{aligned} \tilde{\mathcal{Y}}_{12} &= -s_c \otimes s_c \frac{(s_d, s_b)}{(s_d, s_c)(s_b, s_c)} \\ &= \frac{(s_a, s_c)(s_d, s_b)}{(s_b, s_c)(s_d, s_a)} \left[\mathcal{Y}_{12} + \mathcal{Y}_{21} + \mathcal{Y}_{11} - \mathcal{Y}_{22}\right] \end{aligned} \tag{2.94}$$

extrapolating s_b in terms of s_a, s_c from the analogue of (2.44) we get

$$(s_a, s_c)(s_d, s_b) = (s_b, s_c)(s_d, s_a) - (s_a, s_b)(s_c, s_d) \tag{2.95}$$

hence,

$$\begin{aligned} \tilde{\mathcal{Y}}_{12} &= (1 - \mathcal{Y}_\gamma) \left[\mathcal{Y}_{12} + \mathcal{Y}_{21} + \mathcal{Y}_{22} - \mathcal{Y}_{11}\right] \\ &= (1 - \mathcal{Y}_\gamma)\,(1 - \mathcal{Y}_{21})\,\mathcal{Y}_{12}\,(1 + \mathcal{Y}_{21}) \end{aligned} \tag{2.96}$$

It's straightforward to follow the rules and obtain the other coordinates: by employing (2.44) we find

$$\begin{aligned}\tilde{\mathcal{Y}}_{21} &= \tilde{\nu}_2 \frac{\tilde{s}_2 \otimes \tilde{s}_2}{(\tilde{s}_1, \tilde{s}_2)} = (1 - \mathcal{Y}_\gamma)^{-1} \mathcal{Y}_{21} \\ \tilde{\mathcal{Y}}_{11} &= \frac{\tilde{s}_2 \otimes \tilde{s}_1}{(\tilde{s}_1, \tilde{s}_2)} = \mathcal{Y}_{11} - \mathcal{Y}_{21} \\ \tilde{\mathcal{Y}}_{22} &= \frac{\tilde{s}_1 \otimes \tilde{s}_2}{(\tilde{s}_2, \tilde{s}_1)} = \mathcal{Y}_{22} + \mathcal{Y}_{21}\end{aligned} \tag{2.97}$$

recalling that $\langle \gamma_{ii}, \gamma \rangle = 0$, we recognize the spectrum generator

$$\mathbb{S} = \mathcal{S}_{21}\, \mathcal{K}_\gamma \tag{2.98}$$

in agreement with eq.(8.14) of [65].

2.2.3.2 Adapting the general spectrum generator

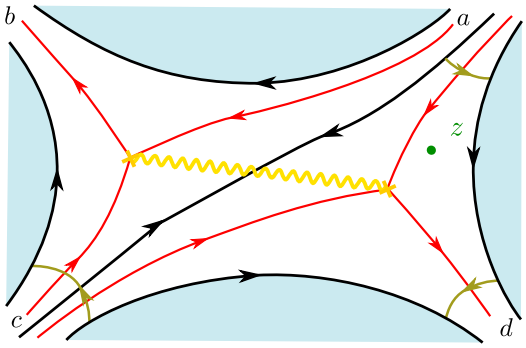

Figure 2.15: The WKB triangulation at angle ϑ, on sheet 2. Indicated are the paths for computing $\Sigma_a^{c\to d}$, $\Sigma_c^{d\to b}$, $\Sigma_d^{a\to c}$ around vertices a, c, d respectively

We now apply the results of section 2.1.3 to derive $\mathbb{S}$. As usual this just requires matching labels correctly, this is slightly more delicate than in previous examples, therefore we will explain it in some detail.

In order to match the two situations, comparing figures 2.2 and 2.15, it is straightforward to identify

$$\text{sheet } 2 \leftrightarrow \text{sheet } 2 \tag{2.99}$$

in order to read the $\tilde{\mathcal{Y}}$'s from those in eq.s (2.32), (2.33) we must take two steps

1. replace labels according to

$$a \to d \qquad b \to a \qquad c \to c \tag{2.100}$$

2. perform the replacements suitable to irregular punctures, as explained in section 2.1.3.4. For this example we have simply (by definition, or by combining (2.34) with (2.44))

$$\tilde{s}_a = s_d, \quad \tilde{s}_b = s_a, \quad \tilde{s}_c = s_b, \quad \tilde{s}_d = s_c$$

Labels only occur within Ξ's and Σ's, therefore we only need to replace

$$\begin{aligned}
&\Sigma_a^{b\to b} \overset{(1)}{\mapsto} \Sigma_d^{a\to a} \overset{(2)}{\mapsto} \Sigma_d^{a\to c} = 1 \\
&\Sigma_b^{c\to c} \overset{(1)}{\mapsto} \Sigma_a^{c\to c} \overset{(2)}{\mapsto} \Sigma_a^{c\to d} = 1 \\
&\Sigma_c^{a\to a} \overset{(1)}{\mapsto} \Sigma_c^{d\to d} \overset{(2)}{\mapsto} \Sigma_c^{d\to b} = 1 + \mathcal{X}_\gamma = 1 - \mathcal{Y}_\gamma
\end{aligned} \tag{2.101}$$

Where, in the last column we used the definition of Σ (11.9) of [64]. Notice that, since a, b, c, d all belong to an irregular puncture, all μ^2 must be set to zero, as explained in section 2.1.3.3. Employing the definition of the Ξ's (2.29), we can perform the following replacement for the Ξ's:

$$\begin{aligned}
&\Xi(\Sigma_a^{b\to b}, \Sigma_b^{c\to c}; \mu_a, \mu_b) \mapsto 1 \\
&\Xi(\Sigma_b^{c\to c}, \Sigma_c^{a\to a}; \mu_b, \mu_c) \mapsto 1 - \mathcal{Y}_\gamma \\
&\Xi(\Sigma_c^{a\to a}, \Sigma_a^{b\to b}; \mu_c, \mu_a) \mapsto 1
\end{aligned} \tag{2.102}$$

Given these, we can now directly read off the omnipop transformation from (2.32), (2.33)

$$\begin{aligned}
\tilde{\mathcal{Y}}_{12} &= (1 - \mathcal{Y}_\gamma)\,[\mathcal{Y}_{12} + \mathcal{Y}_{21} + \mathcal{Y}_{22} - \mathcal{Y}_{11}] \\
\tilde{\mathcal{Y}}_{21} &= (1 - \mathcal{Y}_\gamma)^{-1}\,\mathcal{Y}_{21} \\
\tilde{\mathcal{Y}}_{11} &= \mathcal{Y}_{11} - \mathcal{Y}_{21} \\
\tilde{\mathcal{Y}}_{22} &= \mathcal{Y}_{22} + \mathcal{Y}_{21}
\end{aligned} \tag{2.103}$$

in agreement with our full derivation.

Wall crossing formulae: by repeating the above reasoning, one can determine the spectra for various deformations of the surface defect. According to our derivation, there will be a jump whenever the labeling changes: this occurs precisely when we move from one cell to another (the vertex labels change), or when we cross a branch cut (the sheet labels change). Therefore we expect precisely 6 different regions with their own spectra. This is exactly what [65] found.

2.2.4 The $\mathbb{C}P^1$ sigma model

The next example we consider is that of the $\mathbb{C}P^1$ sigma model presented in [65]. As pointed out there, the 4d dynamics is trivial (no wall crossing), while we do have some 2d phenomena.

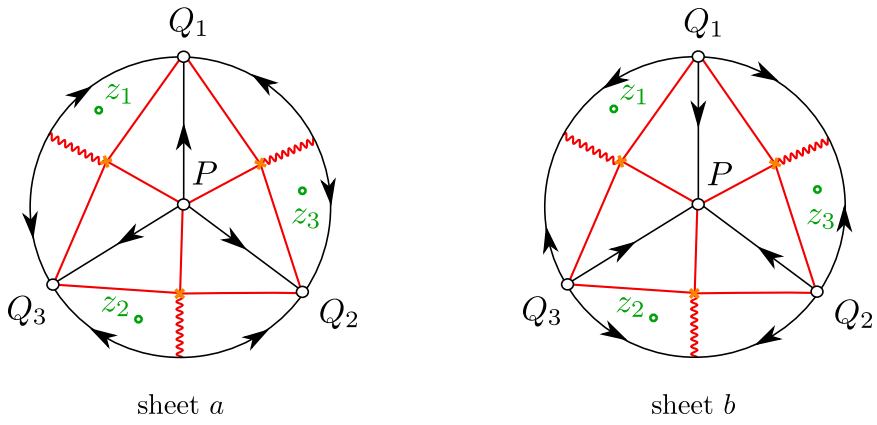

Figure 2.16: The six-fold cover at angle ϑ, the surface defect sitting at strong coupling. For convenience points at infinity have been mapped at finite distance.

The Seiberg-Witten curve is described by

$$\lambda^2 = \left(\frac{\Lambda^2}{z} + \frac{m^2}{z^2}\right) dz^2 \tag{2.104}$$

which encodes a turning point at $z = -m^2/\Lambda^2$, as well as a regular singularity in $z = 0$ and an irregular singularity at infinity with one Stokes sector. The triangulation consists therefore of one degenerate triangle on each of the two sheets. In order to build the coordinates, we must locally pass to a three-fold covering on each of the two sheets, as pointed out in [64].

After doing so, we end up with the six-fold cover illustrated in fig.2.16. Let us start with the so-called strong coupling regime, and choose to work within the triangle denoted by vertices Q_1, P, Q_3. We will understand z to stand for z_1. Let M be the monodromy matrix for parallel transport around P, then $M \cdot s_3 = s_1 = M^{-1} \cdot s_2$, and we denote $\mathcal{Y}_\gamma = \mathcal{Y}_{\gamma_{i,P}}$, $\forall i = 1, 2, 3$. The vertices Q_i belong to an irregular vertex, while P is regular, therefore we must employ the rules of §2.1.3.4 in order to match the spectrum generator correctly. Taking a look at fig. 2.2, we have the following identifications:

$$\begin{gathered} Q_1 \to \mathcal{P}_a \qquad Q_3 \to \mathcal{P}_b \qquad P \to \mathcal{P}_c \\ \text{sheet } a \;\to\; \text{sheet } 2 \end{gathered} \tag{2.105}$$

since Q_1, Q_3 are irregular we set $\mu_a, \mu_b \to 0$. Notice that, since we have an irregular singularity at infinity

$$\tilde{s}_1 = s_2 \qquad \tilde{s}_2 = s_3 \qquad \tilde{s}_3 = s_1 \tag{2.106}$$

therefore we evaluate the modified Σ's according to our prescriptions[13]

$$\begin{aligned}
&\Sigma_a^{b\to\tilde{a}} = \Sigma_1^{3\to 2} \ = 1 - \mathcal{Y}_{\gamma_{1P}} \ = 1 - \mathcal{Y}_\gamma \\
&\Sigma_b^{c\to\tilde{b}} = \Sigma_3^{P\to 1} \ = 1 \\
&\Sigma_c^{a\to a} = \Sigma_P^{1\to 1} \ = 1 - \mathcal{Y}_{\gamma_{3P}} + \mathcal{Y}_{\gamma_{3P}}\mathcal{Y}_{\gamma_{2P}} \ = 1 - \mathcal{Y}_\gamma + \mathcal{Y}_\gamma^2
\end{aligned} \tag{2.107}$$

entailing the explicit expressions

$$\begin{aligned}
\Xi(\Sigma_a^{b\to\tilde{a}}, \Sigma_b^{c\to\tilde{b}}; \mu_a, \mu_b) \ &= \ 1 \\
\Xi(\Sigma_b^{c\to\tilde{b}}, \Sigma_c^{a\to a}; \mu_b, \mu_c) \ &= \ 1 - \mathcal{Y}_\gamma + \mathcal{Y}_\gamma^2 \\
\Xi(\Sigma_c^{a\to a}, \Sigma_a^{b\to\tilde{a}}; \mu_c, \mu_a) \ &= \ 1 - \mathcal{Y}_\gamma + \mathcal{Y}_\gamma^2
\end{aligned} \tag{2.108}$$

We are now ready to read the omnipop transformation from eqs. (2.32), (2.33): they read

$$\begin{aligned}
\tilde{\mathcal{Y}}_{aa} &= \mathcal{Y}_{aa} + (1 - \mathcal{Y}_\gamma)\mathcal{Y}_{ab} \\
\tilde{\mathcal{Y}}_{bb} &= \mathcal{Y}_{bb} - (1 - \mathcal{Y}_\gamma)\mathcal{Y}_{ab} \\
\tilde{\mathcal{Y}}_{ab} &= \mathcal{Y}_{ab} \\
\tilde{\mathcal{Y}}_{ba} &= \mathcal{Y}_{ba} + (1 - \mathcal{Y}_\gamma)^2\mathcal{Y}_{ab} + (1 - \mathcal{Y}_\gamma)(\mathcal{Y}_{aa} - \mathcal{Y}_{bb})
\end{aligned} \tag{2.109}$$

by direct inspection[14], these correspond to the spectrum generator[15]

$$\mathbb{S} \ = \ \mathcal{S}_{\gamma_{ab}+\gamma}\,\mathcal{S}_{\gamma_{ab}} \tag{2.111}$$

we find two 2d solitons whose charges differ by the flavor charge γ. This is consistent with what is found in §8.2 of [65], where they find a soliton with charge $\tilde{\gamma}_{12}$ and one with charge $\gamma_{12} = \gamma_f - \tilde{\gamma}_{21} = \gamma_f + \tilde{\gamma}_{12}$.

Let us now investigate the weak coupling regime. Suppose that z lies in the sector indicated in fig. 2.17. Then, looking at fig.2.2 we identify

$$\begin{gathered}
Q_1 \to \mathcal{P}_b \qquad Q_3 \to \mathcal{P}_c \qquad P \to \mathcal{P}_a \\
\text{sheet } a \ \to \ \text{sheet } 1
\end{gathered} \tag{2.112}$$

since Q_1, Q_3 are irregular we set $\mu_b, \mu_c \to 0$, while $\mu_a^2 = \mu^2 = -\mathcal{Y}_\gamma$[16]. We evaluate the modified Σ's

[13] we use eq. (11.9) of [64] together with the fact that $\mathcal{Y}_\gamma = -\mathcal{X}_\gamma$, as pointed out in appendix F of [65].

[14] we use $\sigma(\gamma, \gamma_{\alpha\beta}) = 1, \ \forall \alpha, \beta \in \{a, b\}$

[15] we employ the following twisting functions:

$$\begin{aligned}
\sigma(aa, ab) = \sigma(bb, ab) = \sigma(aa + \gamma, ab + \gamma) &= \ + \\
\sigma(aa, ab + \gamma) = \sigma(bb, ab + \gamma) = \sigma(ba, ab) = \sigma(ba, ab + \gamma) &= \ -
\end{aligned} \tag{2.110}$$

[16] cf. eq.(7.6) in [64]

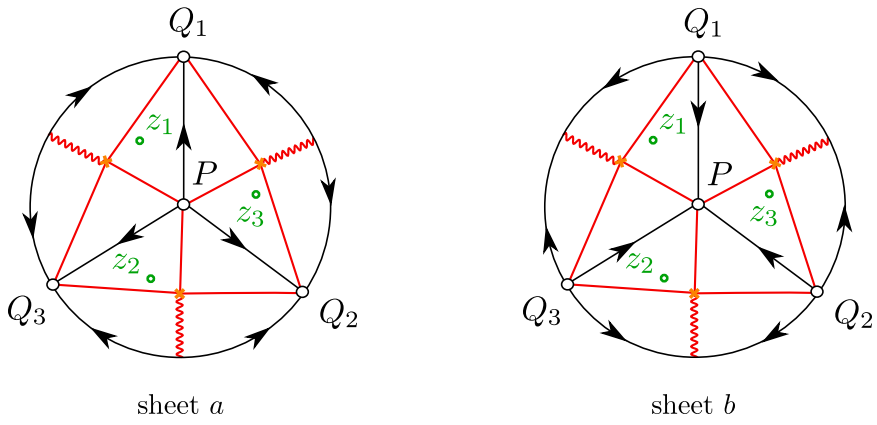

Figure 2.17: The six-fold cover at angle ϑ with the surface defect in the weak coupling region

according to our prescriptions

$$\begin{aligned}\Sigma_a^{b\to b} = \Sigma_P^{1\to 1} &= 1 - \mathcal{Y}_\gamma + \mathcal{Y}_\gamma^2 \\ \Sigma_b^{c\to \tilde{b}} = \Sigma_1^{3\to 2} &= 1 - \mathcal{Y}_\gamma \\ \Sigma_c^{a\to \tilde{c}} = \Sigma_3^{P\to 1} &= 1\end{aligned} \tag{2.113}$$

entailing the explicit expressions

$$\begin{aligned}\Xi(\Sigma_a^{b\to b}, \Sigma_b^{c\to \tilde{b}}; \mu_a, \mu_b) &= 1 + \mathcal{Y}_\gamma^2 - \mathcal{Y}_\gamma^3 \\ \Xi(\Sigma_b^{c\to \tilde{b}}, \Sigma_c^{a\to \tilde{c}}; \mu_b, \mu_c) &= 1 \\ \Xi(\Sigma_c^{a\to \tilde{c}}, \Sigma_a^{b\to b}; \mu_c, \mu_a) &= 1 - \mathcal{Y}_\gamma + \mathcal{Y}_\gamma^2\end{aligned} \tag{2.114}$$

therefore, from eqs. (2.32), (2.33) we read off the omnipop transformation

$$\begin{aligned}\tilde{\mathcal{Y}}_{aa} &= (1 + \mathcal{Y}_\gamma^2 - \mathcal{Y}_\gamma^3)^{-1} \\ &\quad \times \left[(1 + \mathcal{Y}_\gamma)\mathcal{Y}_{aa} - (\mathcal{Y}_\gamma - \mathcal{Y}_\gamma^2 + \mathcal{Y}_\gamma^3)\mathcal{Y}_{bb} - (\mathcal{Y}_\gamma + \mathcal{Y}_\gamma^2)\mathcal{Y}_{ab} - (1 - \mathcal{Y}_\gamma + \mathcal{Y}_\gamma^2)\mathcal{Y}_{ba}\right] \\ \tilde{\mathcal{Y}}_{bb} &= (1 + \mathcal{Y}_\gamma^2 - \mathcal{Y}_\gamma^3)^{-1} \\ &\quad \times \left[(1 + \mathcal{Y}_\gamma)\mathcal{Y}_{bb} - (\mathcal{Y}_\gamma - \mathcal{Y}_\gamma^2 + \mathcal{Y}_\gamma^3)\mathcal{Y}_{aa} - (\mathcal{Y}_\gamma + \mathcal{Y}_\gamma^2)\mathcal{Y}_{ab} + (1 - \mathcal{Y}_\gamma + \mathcal{Y}_\gamma^2)\mathcal{Y}_{ba}\right] \\ \tilde{\mathcal{Y}}_{ab} &= \left[(1 + \mathcal{Y}_\gamma^2 - \mathcal{Y}_\gamma^3)(1 - \mathcal{Y}_\gamma + \mathcal{Y}_\gamma^2)\right]^{-1} \\ &\quad \times \left[(1 + \mathcal{Y}_\gamma)^2\mathcal{Y}_{ab} + (1 - \mathcal{Y}_\gamma + \mathcal{Y}_\gamma^2)^2\mathcal{Y}_{ba} + (1 + \mathcal{Y}_\gamma^2 - \mathcal{Y}_\gamma^3)(1 + \mathcal{Y}_\gamma)(\mathcal{Y}_{bb} - \mathcal{Y}_{aa})\right] \\ \tilde{\mathcal{Y}}_{ba} &= \left[(1 + \mathcal{Y}_\gamma^2 - \mathcal{Y}_\gamma^3)(1 - \mathcal{Y}_\gamma + \mathcal{Y}_\gamma^2)\right]^{-1} \\ &\quad \times \left[\mathcal{Y}_{ba} + \mathcal{Y}_\gamma^2\mathcal{Y}_{ab} + \mathcal{Y}_\gamma(\mathcal{Y}_{bb} - \mathcal{Y}_{aa})\right]\end{aligned} \tag{2.115}$$

It is not easy to read the spectrum generator off these transformations. As pointed out in [65], there should be two solitons with charges $\gamma + \gamma_{aa}$, $\gamma + \gamma_{bb}$, as well as two towers of states with charges $\gamma_{ab} + n\gamma$, $\gamma_{ba} + n\gamma$.

Chapter 3

Wild Wall Crossing and BPS Giants

3.1 Brief Review of Spectral Networks

In this section we give a brief review of the spectral network machinery and its use for computing BPS spectra in $\mathcal{N} = 2$, $d = 4$ theories of class S. For a more complete discussion we refer the reader to [63]. For a more informal (but incomplete) review see [106].

3.1.1 The Setting

Recall that the $\mathcal{N} = 2$, $d = 4$ theories of class S are specified by three pieces of data [59, 64]:

1. A Lie algebra $\mathfrak{g}$ of ADE type (as in [63] the following discussion assumes $\mathfrak{g} = A_{K-1}$),
2. a compact Riemann surface C with punctures at points $\mathfrak{s}_1, \cdots, \mathfrak{s}_n \in C$,
3. a collection of defect operators D located at the punctures.

To shed some light on this collection of data, we note that such theories can be constructed via a partial twist (preserving eight supercharges) of the $\mathcal{N} = (2, 0)$, $d = 6$ theory $S[\mathfrak{g}]$ defined on $\mathbb{R}^{3,1} \times C$. The defect operators D are codimension-2 defects located at $\mathbb{R}^{3,1} \times \{\mathfrak{s}_1\}$, $\cdots$, $\mathbb{R}^{3,1} \times \{\mathfrak{s}_n\}$. A four-dimensional $\mathcal{N} = 2$ field theory is produced after integrating out the degrees of freedom along C and is labeled $S[\mathfrak{g}, C, D]$.

We now present some useful definitions.

Definitions

1. The *Coulomb branch* $\mathcal{B}$ of $S[\mathfrak{g}, C, D]$ is the set of tuples $(\phi_2, \cdots, \phi_K)$ of holomorphic r-differentials ϕ_r with singularities at $\mathfrak{s}_1, \cdots, \mathfrak{s}_n \in C$ prescribed by the defect operators D.

2. Let $u = (\phi_2, \cdots, \phi_K) \in \mathcal{B}$ and denote the holomorphic cotangent bundle of C as $\mathcal{T}^*C$. Then the *spectral cover* is a K-sheeted branched cover $\pi_u : \Sigma_u \to C$, where Σ_u is the subvariety[1]

$$\Sigma_u := \{\lambda \in \mathcal{T}^*C : \lambda^K + \sum_{r=2}^{K} \phi_r \lambda^{K-r} = 0\} \subset \mathcal{T}^*C, \tag{3.1}$$

and the projection π_u is the restriction of the standard projection $\mathcal{T}^*C \to C$.

3. As $\Sigma_u \subset \mathcal{T}^*C$ it carries a natural holomorphic 1-form which is just the restriction of the tautological (Liouville) 1-form. In the spirit of its tautological nature we abuse notation and denote this 1-form λ_u.

Often we will work over a fixed $u \in \mathcal{B}$; so eventually the index u will be dropped where there is no ambiguity.

3.1.1.1 Spectral Cover Crash Course

Let us make some observations about the spectral cover. First, the fibers are given by

$$\pi_u^{-1}(z) = \{\lambda(z) \in \mathcal{T}_z^*C : \lambda(z)^K + \sum_{r=2}^{K} \phi_r(z) \lambda^{K-r}(z) = 0\},$$

i.e. the roots of the defining polynomial of Σ_u at the point z. Generically, $\pi_u^{-1}(z)$ consists of K distinct roots, although at particular values of z (branch points) two or more roots may coincide. In fact, letting $C' = C - \{\text{branch points}\}$, $\pi_u|_{C'}$ is a K-fold (unramified) cover of C'.

If $\pi_u|_{C'}$ is a non-trivial cover, the roots do not fit together into global holomorphic 1-forms on C as they undergo monodromy around branch points. However, restricted to the complement of a choice of branch cuts on C, the cover is trivializable: a projection of K distinct sheets onto the complement. Each sheet is the graph traced out by a root of the defining polynomial; such roots are distinct holomorphic differential forms. A choice of trivialization of the restricted cover is a bijective map between the set of K sheets and the set $\{1, 2, \ldots, K\}$, or equivalently, a labeling of the roots of the defining polynomial from 1 to K.

Definitions

1. Make a suitable choice of branch cuts for the branched cover $\pi_u : \Sigma_u \to C$. The complement of these branch cuts in C will be denoted by C^c.

2. A choice of trivialization of $\pi^{-1}(C^c) \to C^c$ will be denoted by a labeling of the roots of the defining polynomial for Σ, i.e. a labeling $\lambda_i \, (i = 1, \ldots, K)$, where each λ_i (a holomorphic

[1] Σ_u is also called the Seiberg-Witten curve.

1-form on C^c) is a distinct root of the defining polynomial for Σ. Note that this gives us a labeling of sheets: the ith sheet is the graph of λ_i in $\mathcal{T}^*C$. If we wish, we can extend the $\lambda_i(z)$ to branch points z to speak of "collisions" of sheets.

3. For later convenience, we define

$$\lambda_{ij} := \lambda_i - \lambda_j.$$

As in [63] we will assume that all branch points are simple, i.e. at most two sheets of Σ collide at any z.

Definition A branch point of type ij $(i, j \in 1, \cdots, K)$ is a point $z \in C$ where the ith and jth sheets of Σ_u collide, i.e, $\lambda_i(z) = \lambda_j(z)$.

The data of the full spectral cover can be recovered after trivializing by specifying the monodromy around all branch points, and all closed cycles of C. In this paper, we assume *simple ramification*: in a neighborhood around each branch point, the spectral cover looks like the branched cover $z \mapsto z^2$ of the disk. Thus, for a simple closed curve surrounding a branch point of type ij, there is a $\mathbb{Z}/2\mathbb{Z}$ monodromy

$$\lambda_i \leftrightarrow \lambda_j.$$

Monodromy around an arbitrary closed cycle of C may permute the sheets in a more complicated fashion.

3.1.1.2 BPS objects in $S[A_{K-1}, C, D]$

Theories of class S admit a zoo rich in BPS species, each of which has a different classical description from the point of view of the six-dimensional geometry of $\mathbb{R}^{3,1} \times C$. Our ultimate interest in this paper is in the 4D (vanilla) BPS states, but the power behind the spectral network machine draws heavily on the symbiosis between these different species; so we take a moment to project each of them into the spotlight.

BPS Strings and "vanilla" 4D BPS states

4D BPS states in the four-dimensional $\mathcal{N} = 2$ theory arise from extended objects in the 6D description: BPS strings. In the effective IR description, at a point $u \in \mathcal{B}$, BPS strings wrap closed paths p on the branched cover $\Sigma_u \subset \mathcal{T}^*C \to C$. The resulting states are classified by their homology classes

$\gamma = [p] \in H_1(\Sigma_u; \mathbb{Z})$ in the sense that there is a natural grading of the Hilbert space of BPS strings as

$$\mathcal{H}^{\mathrm{BPS}}(u) = \bigoplus_{\gamma \in H_1(\Sigma_u;\mathbb{Z})} \mathcal{H}(\gamma; u),$$

commuting with the action of the super-Poincaré group.

Definition The *charge lattice* of 4D BPS states at a point $u \in \mathcal{B}$ is $\Gamma_u = H_1(\Sigma_u; \mathbb{Z})$. It is equipped with an antisymmetric pairing $\langle \cdot, \cdot \rangle : \Gamma_u \times \Gamma_u \to \mathbb{Z}$ given by the intersection form on $H_1(\Sigma_u; \mathbb{Z})$.

To count the number of BPS states of a particular charge γ we recall a major celebrity of this paper: the second helicity supertrace (a.k.a. the "BPS degeneracy" or "BPS index")

$$\Omega(\gamma; u) = -\frac{1}{2} \mathrm{Tr}_{\mathcal{H}(\gamma;u)} (2J_3)^2 (-1)^{2J_3},$$

where J_3 is any generator of the rotation subgroup of the massive little group. This index is piecewise constant on $\mathcal{B}$, jumping across real codimension-1 walls of marginal stability on $\mathcal{B}$ where two BPS states with linearly independent charges $\gamma, \gamma' \in \Gamma_u$ have central charges of the same phase: $\mathrm{Arg}\,(Z_\gamma) = \mathrm{Arg}\,(Z_{\gamma'})$. To compute this index we will not rely on its definition as a supertrace, but instead utilize the geometric methods of the spectral network machine.

Remarks

1. On $\mathcal{B}$ there may be (complex) codimension-1 loci where a cycle of Σ_u degenerates. Let $\mathcal{B}^* = \mathcal{B} - \{\text{degeneration loci}\}$. Then the collection $\widehat{\Gamma} = \{\Gamma_u\}_{u \in \mathcal{B}^*}$ forms a local system of lattices $\widehat{\Gamma} \to \mathcal{B}^*$. This local system is often equipped with a non-trivial monodromy action.

2. As mentioned previously, we will often drop the subscript $u \in \mathcal{B}$ as we will often be working over a single point on the Coulomb branch, or choosing a local trivialization of the local system of lattices on some open set.

3. Strictly speaking, the lattice of charges Γ_u is not quite $H_1(\Sigma_u; \mathbb{Z})$ [64]; in the theory we consider in this paper, though, Γ_u is just a sublattice of $H_1(\Sigma_u; \mathbb{Z})$, and for our considerations there is no harm in replacing Γ_u by $H_1(\Sigma_u; \mathbb{Z})$. (If we considered the theory with $\mathfrak{g} = \mathfrak{gl}(K)$ instead of $\mathfrak{g} = \mathfrak{sl}(K)$ then the charge lattice would be literally $H_1(\Sigma_u; \mathbb{Z})$.)

4. From the four-dimensional point of view, Γ_u is the lattice of electric/magnetic and flavor charges in the IR effective abelian gauge theory defined at u.

Fix $u \in \mathcal{B}$. The central charge and mass of a string $p : S^1 \to \Sigma$ are[2]

$$Z_p = \frac{1}{\pi}\int_p \lambda,$$
$$M_p = \frac{1}{\pi}\int_p |\lambda|.$$

With this, the BPS condition $|Z_p| = M_p$ is given by

$$\int_p \lambda = e^{i\vartheta}\int_p |\lambda| \tag{3.2}$$

for some $\vartheta = \mathrm{Arg}(Z_p) \in \mathbb{R}/2\pi\mathbb{Z}$. The value of ϑ specifies which four-dimensional BPS subalgebra is preserved. We can rewrite this condition in more useful form; indeed, let v_p denote a vector field along the path p, then (3.2) is true iff

$$\mathrm{Im}\left[e^{-i\vartheta}\langle\lambda, v_p\rangle\right] = 0. \tag{3.3}$$

Solitons

The theory $S[\mathfrak{g}, C, D]$ is equipped with a special set of BPS surface defect operators $\{\mathbb{S}_z\}_{z\in C}$ parameterized (in the UV[3]) by points on C. In the IR, for fixed $u \in \mathcal{B}$, the operator $\mathbb{S}_z$ possesses finitely many massive vacua labeled by the set $\pi^{-1}(z)$ (with $\pi = \pi_u$). Letting $z \in C'$, then *solitons* are BPS states[4] bound to the defect $\mathbb{S}_z$, which interpolate between two different vacua. Classically, they are given by oriented paths $s : [0, 1] \to \Sigma$ with endpoints $s(0)$, $s(1) \in \pi^{-1}(z)$; furthermore, each such path satisfies a BPS condition that we will now describe.

Consider a soliton path s such that, after choosing a trivialization, s only runs along sheets i and j and such that the projection $s_C := \pi \circ s$ is a connected open path on C. Let v_{s_C} be a vector field along the path s_C. Then, the BPS condition is the differential equation

$$\mathrm{Im}\left[e^{-i\vartheta}\langle\lambda_{ij}, v_{s_C}\rangle\right] = 0 \tag{3.4}$$

for some fixed angle ϑ. For more complicated solitons that travel along more than two sheets, we can break the soliton up into a concatenation of partial solitons running along various pairs of sheets; each partial soliton involved in the concatenation must satisfy (3.4) where ij is replaced by the relevant pair of sheets, and ϑ is the same for each partial soliton. Hence, the BPS condition for solitons leads to a system of $\binom{K}{2}$ differential equations on C' (one for each disjoint pair of sheets).

[2]The integral $\int_p \lambda$ is only a function of the class $[p] \in H_1(\Sigma; \mathbb{Z})$; hence, the central charge reduces to a function $\Gamma \to \mathbb{C}$.

[3]In the six-dimensional UV description, the operator $\mathbb{S}_z$ attached to a point $z \in C$ is a surface defect which intersects C at a single point.

[4]After insertion of $\mathbb{S}_z$ there are four remaining supercharges. A BPS soliton preserves two supercharges.

For such a soliton s, broken into partial solitons $\{s^r\}_{r=1}^L$ as decribed above, its central charge and mass are

$$\begin{aligned} Z_s &= \sum_{r=1}^{L} \frac{1}{\pi} \int_{s_C^r} \lambda_{ij} \\ M_s &= \sum_{r=1}^{L} \frac{1}{\pi} \int_{s_C^r} |\lambda_{ij}|. \end{aligned} \tag{3.5}$$

We can now identify the angle as the phase of the central charge, $\vartheta = \mathrm{Arg}(Z_s)$, and indeed the BPS condition is equivalent to $M_s = |Z_s|$.

As with 4D BPS states, solitons also carry a charge, but now given by a relative homology class as they are open paths.

Let $z \in C'$; choose a labeling of the K points in $\pi^{-1}(z) \in C'$.

Definition

1. Let $z_l \in \pi^{-1}(z)$ denote the pre-image of $z \in C'$ on the lth sheet. Then a soliton is of type ij if it is given by a path that begins on z_i and ends on z_j. We also refer to such solitons as *ij-solitons.*

2. $\Gamma_{ij}(z,z)$ is the set of charges of ij-solitons, i.e.

$$\Gamma_{ij}(z,z) := \{[a] \in H_1(\Sigma, \{z_i\} \cup \{z_j\}; \mathbb{Z}) : a \text{ is a 1-chain with } \partial a = z_j - z_i\}.$$

3. The total set of soliton charges is

$$\Gamma(z,z) := \bigsqcup_{i,j=1}^{K} \Gamma_{ij}(z,z).$$

Remarks

1. A soliton s can be extended by "parallel transporting" its endpoints. Indeed, let s be a soliton of type ij with $s(0)$, $s(1) \in \pi^{-1}(z)$. Now, given a path $q : [0,1] \to C'$ from z to z', let $q\{n\}$ denote the lift of q to the nth sheet of Σ defined by lifting the initial point $q(0)$ to sheet n; then one can define the transported path,

$$\mathbb{P}_q s = q\{j\} \star s \star q^-\{i\} \tag{3.6}$$

where $\star$ denotes concatenation of paths, and $q^-\{i\}$ is $q\{i\}$ with reversed orientation. The resulting path on Σ has endpoints in $\pi^{-1}(z')$. If s is an ij soliton, then the path $\mathbb{P}_q s$ is a soliton iff q satisfies (3.4) for the same pair of sheets ij.

2. $\bigcup_{z\in C'}\Gamma(z,z)\to C'$ is a local system over C': for any path $q:[0,1]\to C$ there is a parallel transport map $P_q:\Gamma(q(0),q(0))\to\Gamma(q(1),q(1))$, induced by the map $\mathbb{P}_q$ defined above, and only depending on the homotopy class of q relative to the endpoints. (Henceforth we abbreviate this as "rel endpoints.")

3. If there is an extension of an ij-soliton through a branch cut emanating from an ij branch point, it becomes a ji-soliton. More generally, if a soliton passes through any branch cut, its type is permuted according to the permutation of sheets across the branch cut.

Just as with 4D vanilla BPS states, for each $a_z\in\Gamma(z,z)$, there is an index $\mu(a_z)\in\mathbb{Z}$ that counts BPS solitons of charge a_z. Again, this can be defined as a supertrace over an appropriate BPS subspace, however, we will compute it via geometric methods. Using the parallel transport map described in the remarks above, this BPS index is also stable along extensions of solitons at generic $z\in C'$; [5] it jumps only at points $z\in C'$ where solitons of different types exist and interact. This motivates the following (notation-simplifying) definitions.

Definitions

1. A soliton $s:[0,1]\to\Sigma$ is said to be of *phase* θ if it satisfies the BPS condition[6] (3.4) for $\vartheta=\theta$.

2. A point $z\in C$ is said to *support* a soliton of phase ϑ if there exists a soliton s with $[s]\in\Gamma(z,z)$ and $\mu([s])\neq 0$. A path p on C supports a family of solitons of phase ϑ if each point on p supports a soliton fitting into a 1-parameter family of solitons of phase ϑ. When the phase ϑ is clear from context, occasionally we will just say that p supports a family of solitons.

3. Let $p\subset C$ be a path on C supporting a family of solitons of phase ϑ extending a soliton s_0 with charge $a_z=[s_0]\in\Gamma(z,z)$. With an abuse of notation, occasionally a will denote any one of the parallel transports of a_z along the path p.

4. Let $z\in p$ and $a_z\in\Gamma(z,z)$. If the index $\mu(a_z)$ is constant for any soliton in the family generated by parallel transports of $a_z\in\Gamma(z,z)$ along $p\subset C$, then we will denote the index by $\mu(a,p)\in\mathbb{Z}$.

Framed 2D-4D States

We consider one final BPS construction: the framed 2D-4D states. Given $\vartheta\in\mathbb{R}/(2\pi\mathbb{Z})$, z_1, $z_2\in C$, and $\wp$ a path on C from z_1 to z_2, one can associate two surface defects $\mathbb{S}_{z_1}$ and $\mathbb{S}_{z_2}$, along with a

[5] In the sense that if s is an ij soliton, and q is a sufficiently small path on Σ satisfying (3.4), then $\mu([s])=\mu(P_q[s])$

[6] Thought of as a system of equations on each "partial soliton" as described above.

supersymmetric interface $L_{\wp,\vartheta}$ between these two surface defects.[7] The interface is supersymmetric in the sense that it preserves two out of the four supercharges preserved by the surface defects; the parameter ϑ controls which two are preserved. Framed 2D-4D states are the vacua of the theory after insertion of this defect.

Geometrically, such a state is represented by a path $f : [0,1] \to \Sigma$ such that there exists a finite subdivision of times

$$[0,1] = [0,t_1] \cup [t_1,t_2] \cup \cdots \cup [t_{N-1},1]$$

and, with respect to this subdivision:

- $f|_{[0,t_1]}$ and $f|_{[t_{N-1},1]}$ have images in $\pi^{-1}(\wp)$ (in particular, the path begins on a lift of z_1 and ends on a lift of z_2).
- If $1 < i < N-2$, then $f_{[t_i,t_{i+1}]}$ is either a soliton of phase ϑ, or has image in $\pi^{-1}(\wp)$.

When f is projected to C the resulting path looks like $\wp$ with finitely many diversions to solitons (and back) along the way. In [61], such a path f is referred to as a *millipede with body $\wp$ and phase ϑ*.

Similar to solitons, we can classify framed 2D-4D states by their values in a set of charges given by relative homology classes $[f]$, for f a millipede; as the geometric description above suggests, now the relative cycles can have boundaries on pre-images of two different points on C.

Definition Let $\wp : [0,1] \to C$ with $\wp(0) = z$ and $\wp(1) = w$; with a choice of labeling of sheets above $\pi^{-1}(z)$ and $\pi^{-1}(w)$, let z_i (resp. w_i) be a point on the ith sheet in $\pi^{-1}(z)$ (resp. $\pi^{-1}(w)$). Then, the set of charges of framed 2D-4D states corresponding to $\wp$ is

$$\Gamma(z,w) := \bigsqcup_{i,j=1}^{K} \{[a] \in H_1(\Sigma, \{z_i\} \cup \{z_j\}; \mathbb{Z}) : a \text{ is a 1-chain with } \partial a = w_j - z_i \} .$$

Furthermore, for each $a \in \Gamma(z,w)$ we define the counting index $\overline{\Omega}(L_{\wp,\vartheta}, a)$ that, once again, can be defined via a supertrace over an appropriate Hilbert space, but we will only utilize its interpretation from a geometric perspective.

Remark It is believed that the theory obtained after insertion of the defect $L_{\wp,\vartheta}$ only depends on the homotopy class (rel boundary) of $\wp$. This homotopy invariance is the key ingredient that ties the story of spectral networks together.

[7] From the four-dimensional perspective, $L_{\wp,\vartheta}$ is a line defect extended along $\mathbb{R}^{0,1}$ and living on the interface between $\mathbb{S}_{z_1}$ and $\mathbb{S}_{z_2}$.

3.1.1.3 Adding a Little Twist

Before proceeding to the definition of the $\mathcal{W}_\vartheta$ networks, we make an important technical detour. As discussed in [63], the indices $\mu(a)$ and $\overline{\Omega}(L_{\wp,\vartheta}, a)$ are only well-defined up to a sign, due to potential integer shift ambiguities in the fermion number operators that enter their definitions. To correct these ambiguities globally over all regions of parameter space, it suffices to construct (geometrically motivated) $\mathbb{Z}/2\mathbb{Z}$ extensions of Γ and $\Gamma(z,w)$. First, a bit of notation that will be used throughout this section and part of Appendix C.

Definition Let S be a real surface, then $\xi^S : \widetilde{S} \to S$ is the unit tangent bundle projection to S.

The map $\xi^S_* : H_1(\widetilde{S};\mathbb{Z}) \to H_1(S;\mathbb{Z})$ has a kernel generated by the homology class that has a representative winding once around some fiber.

Definition Let $H \in H_1(\widetilde{\Sigma};\mathbb{Z})$ denote the homology class represented by a 1-chain that winds once around a fiber of $\widetilde{\Sigma} \to \Sigma$, then

$$\widetilde{\Gamma} := H_1(\widetilde{\Sigma};\mathbb{Z})/\left(2H\right).$$

We abuse notation and denote the image of H in $\widetilde{\Gamma}$ by H again.

It follows that $\widetilde{\Gamma}$ is a $\mathbb{Z}/2\mathbb{Z}$ extension of Γ, i.e there is an exact sequence of abelian groups,

$$0 \to \mathbb{Z}/2\mathbb{Z} \to \widetilde{\Gamma} \to \Gamma \to 0.$$

Similarly, for framed states and solitons we define extended charge sets. First we pass through an intermediate construction.

Definition Let $\widetilde{\pi} : \widetilde{\Sigma} \to \widetilde{C}$ be the restriction of $d\pi : T\Sigma \to TC$ to the unit tangent bundle. For fixed $\widetilde{z}$, $\widetilde{w} \in \widetilde{C}$, choose a labeling of sheets above $\pi^{-1}(z)$ and $\pi^{-1}(w)$; let z_i (resp. w_i) be a point on the ith sheet in $\pi^{-1}(z)$ (resp. $\pi^{-1}(w)$), then define

$$\begin{aligned} G_{ij}(\widetilde{z},\widetilde{w}) &:= \left\{ [a] \in H_1(\widetilde{\Sigma}, \{\widetilde{z}_i\} \cup \{\widetilde{w}_j\};\mathbb{Z}) : a \text{ is a 1-chain with } \partial a = \widetilde{w}_j - \widetilde{z}_i \right\}, \\ G(\widetilde{z},\widetilde{w}) &:= \bigsqcup_{i,j=1}^{K} G_{ij}(\widetilde{z},\widetilde{w}). \end{aligned} \tag{3.7}$$

Remark $G(\widetilde{z},\widetilde{w})$ is equipped with an $H_1(\widetilde{\Sigma};\mathbb{Z})$ action given by the addition of a closed cycle (at the level of chains).

This allows us to make the following definition,

Definition

$$\widetilde{\Gamma}(\widetilde{z},\widetilde{w}) := G(\widetilde{z},\widetilde{w})/\langle 2H\rangle. \tag{3.8}$$

Sometimes it is useful to view $\widetilde{\Gamma}(\widetilde{z},\widetilde{w})$ as a disjoint union of quotients of G_{ij}:

Definition

$$\widetilde{\Gamma}_{ij}(\widetilde{z},\widetilde{w}) := G_{ij}(\widetilde{z},\widetilde{w})/\langle 2H\rangle.$$

So we may write,

$$\widetilde{\Gamma}(\widetilde{z},\widetilde{w}) := \bigsqcup_{i,j=1}^{K} \widetilde{\Gamma}_{ij}(\widetilde{z},\widetilde{w}).$$

Remark

$\widetilde{\Gamma}(\widetilde{z},\widetilde{w})$ is equipped with a $\widetilde{\Gamma}$ action, descending from addition of a closed cycle with a relative cycle. For $\gamma \in \widetilde{\Gamma}$ and $a \in \widetilde{\Gamma}(\widetilde{z},\widetilde{w})$ we will denote this action by $\gamma : a \mapsto a+\gamma = \gamma + a$. In fact, for any ordered pair ij, $\widetilde{\Gamma}_{ij}(\widetilde{z},\widetilde{w})$ is a torsor for $\widetilde{\Gamma}$.

$\widetilde{\Gamma}(\widetilde{z},\widetilde{w})$ carries an extra $\mathbb{Z}/2\mathbb{Z}$'s worth of "winding" information in the sense that $\widetilde{\Gamma}(\widetilde{z},\widetilde{w}) \overset{\text{proj}}{\to} \Gamma(z,w)$ is a principal $\mathbb{Z}/2\mathbb{Z}$ bundle, with proj given by forgetting lifts[8], and the $\mathbb{Z}/2\mathbb{Z}$ action given by adding H.

Now, a soliton is a smooth curve on Σ; furthermore, the tangent vectors at the endpoints (which lie on disjoint sheets) of a soliton are oppositely oriented in the sense that their pushforwards to C are oppositely oriented.

Definition Let $\widetilde{z} \in \widetilde{C}$, then $-\widetilde{z} \in \widetilde{C}$ is the unit tangent vector pointing in the opposite direction to $\widetilde{z}$.

Remark To every soliton (represented by a smooth path) there is a natural lifted charge in $\widetilde{\Gamma}(\widetilde{z},-\widetilde{z})$ that descends from the relative homology class of the soliton's tangent framing lift.

We introduce one final piece of technology. First, note that for each $\widetilde{z} \in \widetilde{C'}$ there is a disjoint union of K lattices inside of the set $\widetilde{\Gamma}(\widetilde{z},\widetilde{z})$:

$$\bigsqcup_{i=1}^{K} \widetilde{\Gamma}_{ii}(\widetilde{z},\widetilde{z}) \subset \widetilde{\Gamma}(\widetilde{z},\widetilde{z}).$$

[8]More precisely, proj is the map descending from the induced map on relative homology $(\xi^{\Sigma})_* : H_1\left(\widetilde{\Sigma}, \pi^{-1}(\widetilde{z}) \cup \pi^{-1}(\widetilde{w}); \mathbb{Z}\right) \to H_1\left(\Sigma, \pi^{-1}(z) \cup \pi^{-1}(w); \mathbb{Z}\right)$ where $z = \left(\pi \circ \xi^{\Sigma}\right)(\widetilde{z})$ and $w = \left(\pi \circ \xi^{\Sigma}\right)(\widetilde{w})$.

Any representative of an element in $\widetilde{\Gamma}_{ii}(\widetilde{z},\widetilde{z})$ has zero boundary, hence, is actually a cycle. Indeed,there is a canonical "basepoint forgetting" isomorphism of lattices $\widetilde{\Gamma}_{ii}(\widetilde{z},\widetilde{z}) \cong \widetilde{\Gamma}$ for each $i = 1, \cdots, K$, descending from the identity map at the level of chain representatives. This allows us to define the *closure* map.

Definition

$$\mathrm{cl} : \bigcup_{i=1}^{K} \widetilde{\Gamma}_{ii}(\widetilde{z},\widetilde{z}) \to \widetilde{\Gamma}$$

is the map which acts on each component by the "basepoint-forgetting" map described above.

Now, due to the sign ambiguity in μ and $\underline{\Omega}$ then, naïvely, only their absolute values are well-defined: i.e. we have functions,

$$\begin{aligned} \mu_{\geq 0} &: \bigcup_{z\in C'} \Gamma(z,z) \to \mathbb{Z}_{\geq 0} \\ \overline{\underline{\Omega}}_{\geq 0}(\wp,\cdot) &: \bigcup_{(z,w)\in C'\times C'} \Gamma(z,w) \to \mathbb{Z}_{\geq 0}. \end{aligned}$$

However, with our "lifted charge" definitions, we can lift $\mu_{\geq 0}$ to a function $\mu : \bigcup_{\widetilde{z}\in\widetilde{C'}} \widetilde{\Gamma}(\widetilde{z},-\widetilde{z}) \to \mathbb{Z}$ such that $\forall a \in \bigcup_{\widetilde{z}\in\widetilde{C'}} \widetilde{\Gamma}(\widetilde{z},-\widetilde{z})$,

$$\begin{aligned} |\mu(a)| &= \mu_{\geq 0}(\xi_*^{\Sigma} a) \\ \mu(a+H) &= -\mu(a). \end{aligned} \tag{3.9}$$

Similarly, fixing a path $\wp$ on C, the framed BPS degeneracies lift to well-defined functions $\overline{\underline{\Omega}}(L_{\wp,\vartheta},\cdot) : \bigcup_{(\widetilde{z},\widetilde{w})\in\widetilde{C'}\times\widetilde{C'}} \widetilde{\Gamma}(\widetilde{z},\widetilde{w}) \to \mathbb{Z}$ such that $\forall a \in \bigcup_{(\widetilde{z},\widetilde{w})\in\widetilde{C'}\times\widetilde{C'}} \widetilde{\Gamma}(\widetilde{z},\widetilde{w})$,

$$\begin{aligned} \left|\overline{\underline{\Omega}}\left(L_{\wp,\vartheta},a\right)\right| &= \overline{\underline{\Omega}}_{\geq 0}\left(L_{\wp,\vartheta},\xi_*^{\Sigma} a\right) \\ \overline{\underline{\Omega}}\left(L_{\wp,\vartheta},a+H\right) &= -\overline{\underline{\Omega}}\left(L_{\wp,\vartheta},a\right). \end{aligned} \tag{3.10}$$

3.1.2 The $\mathcal{W}_\vartheta$ Networks

Using (3.4), we can produce a concrete picture of (the projections to C of) ij-solitons on the curve C. This motivates the following definitions.

Definition Fix $\vartheta \in \mathbb{R}/2\pi\mathbb{Z}$, for each (ordered) pair of sheets ij we define a (real) oriented line field $l_{ij}(\vartheta)$ on C^c given at every $z \in C^c$ by

$$l_{ij,z}(\vartheta) := \left\{ v \in T_z C : \mathrm{Im}\left[e^{-i\vartheta}\langle \lambda_{ij}, v\rangle\right] = 0 \right\},$$

with v positively oriented if $\mathrm{Re}\left[e^{-i\vartheta}\langle \lambda_{ij}, v\rangle\right] > 0$.

Given an integral curve p of $l_{ij}(\vartheta)$, the orientation of $l_{ij}(\vartheta)$ tells us how to lift the curve back to a curve p_Σ on Σ.

Definition Any integral curve p (on C') of $l_{ij}(\vartheta)$ has a lift to a curve p_Σ on Σ defined as the union of $p\{i\}$ (the lift of p to the ith sheet), and $p^-\{j\}$ (the lift of p to the jth sheet, reversing orientation).

Remarks

- Fix $z_* \in C^c$ and take a neighborhood U of z_* that does not contain any branch cuts of type ij. Then for each ordered pair ij we can define local coordinates $w_{ij} : U \to \mathbb{C}$ by

$$w_{ij}(z) = \int_{z_*}^{z} (\lambda_i - \lambda_j)\,. \tag{3.11}$$

  In these coordinates, the integral curves of $l_{ij}(\vartheta)$ are precisely the straight lines of inclination ϑ.

- Note that the line field $l_{ji}(\vartheta)$ is just $l_{ij}(\vartheta)$ with reversed orientation.

- On a cycle surrounding a branch point of type ij, the monodromy action induces $\lambda_{ij} \mapsto \lambda_{ji} = -\lambda_{ij}$; hence, $l_{ij}(\vartheta) \mapsto l_{ji}(\vartheta)$ (i.e., the line field orientation reverses when passing through a branch cut extending from a branch point.)

We can finally define the (real) codimension-1 networks of interest.

Definition

$$\mathcal{W}_\vartheta = \bigcup_{\text{ordered pairs } ij} \{p : p \text{ is an integral curve of } l_{ij}(\vartheta) \text{ and } p \text{ supports a soliton of phase } \vartheta\} \subset C'.$$

The network $\mathcal{W}_\vartheta$ is composed of individual integral curve segments, which may interact and join each other at vertices on C'.

Definitions

1. An individual integral curve segment on $\mathcal{W}_\vartheta$ is called a *street*.[9] A *street of type* ij is a street that is an integral curve of $l_{ij}(\vartheta)$.

2. A joint is a point on C' where two or more streets of different types meet.

[9] In [63] these were also referred to as S-walls.

The upshot of all these constructions is that now we have a solidified picture of solitons via a network on C'. Indeed, we can lift $\mathcal{W}_\vartheta$ to a graph on $\mathrm{Lift}(\mathcal{W}_\vartheta) \subset \Sigma$ by taking the union of the lifts (as defined above) p_Σ of each street p. Then an ij soliton of phase ϑ traces out a path supported on $\mathrm{Lift}(\mathcal{W}_\vartheta)$, and begins and ends on points z_i, z_j that are lifts to the ith and jth streets (respectively) of a point z on a street of type ij. In particular, an ij street of $\mathcal{W}_\vartheta$ represents the endpoints of a set of solitons of type ij.

From a constructive viewpoint, however, the reader may feel unsatisfied as we have not yet defined how to determine the condition that $p \subset \mathcal{W}_\vartheta$ actually *supports* a soliton of phase ϑ, i.e. $\mu(a,p) \neq 0$, for some a the charge of a soliton of phase ϑ. To fill this void we remark that there are exactly three integral curves of $l_{ij}(\vartheta) \cup l_{ji}(\vartheta)$ emerging from each ij-branch point. On each such integral curve p there is a family of solitons represented by "small" paths: for $z \subset p$ and $z_i, z_j \in \pi^{-1}(z)$ lifts of z to sheet i and sheet j (respectively), there is a soliton supported on p_Σ traveling from $z_i \in \Sigma$, through the ramification point on Σ, to $z_j \in \Sigma$. Such solitons become arbitrarily light as z approaches the branch point. Furthermore, as argued in [63], letting a be the (lifted) charge of any soliton in this family, we assign

$$\mu(a,p) = +1. \tag{3.12}$$

Terminology The "light" solitons described in the previous paragraph will be called *simpletons*.

We defer the problem of determining the soliton indices μ on all other streets until the appropriate definitions are developed in the next section; for now it will suffice to say that, with this condition, the soliton indices on all other streets can be determined via a set of algebraic equations.

3.1.2.1 $\mathcal{K}$-walls and Degenerate Networks

Of particular interest in this paper will be $\mathcal{W}_\vartheta$ networks of a very special type.

Definition A street $p \subset \mathcal{W}_\vartheta$ is *two-way* if it consists of a coincident ij-street and a ji-street. Equivalently, p supports ij-solitons and ji-solitons. A street that is not two-way is called *one-way*. A network that contains a two-way street is said to be *degenerate*.

We adopt the following convention in order to keep track of the individual directions of the constituent one-way streets of a two-way street.

Convention Let p be a two-way street consisting of coincident ij and ji-streets, then we will say p is of type ij and assign it the orientation of its constituent ij-street. (Or, equivalently, we will say p is of type ji and assign it the orientation of its constituent ji-street.)

As described in [63], sec. 6.2, for generic values of ϑ, the network $\mathcal{W}_\vartheta$ will only contain one-way streets due to a bifurcation behavior of integral curves near branch points. However, at critical values $\vartheta_c \in \mathbb{R}/\mathbb{Z}$, an ij street will collide with a ji street and the network $\mathcal{W}_{\vartheta_c}$ will contain two-way streets. Now we make an important claim:

$\mathcal{W}_\vartheta$ contains a two-way street $\Rightarrow \exists$ a homologically non-trivial closed loop on Σ satisfying (3.3) for some phase $\vartheta \in \mathbb{R}/2\mathbb{Z}$.

To see this, fix a point $z \in p \subset C$ on any two-way street p; without loss of generality we will say p is of type ij. Then z supports a soliton of type ij and a soliton of type ji, both of the same phase ϑ; the concatenation of these two paths yields a closed loop l satisfying (3.3) for the phase ϑ. Moreover, this loop is homologically non-trivial. Indeed, the period of l is just the sum of the periods of the two solitons forming it. However, both have periods (central charges) of the same phase; so the sum must be nonzero.

Thus, via the claim, a degenerate network automatically leads to a possible 4D BPS state of charge $[l] \in \Gamma$; in fact, there are possible BPS states of charges $n[l]$, $n \in \mathbb{Z}_{>0}$. All that remains is to determine the BPS indices $\Omega(n[l])$ which, as expressed more explicitly below, are computable from the soliton data supported on $\mathcal{W}_\vartheta$.

In practice, degenerate networks can be found by looking for discontinuous changes in the topology of $\mathcal{W}_\vartheta$ as ϑ is varied. Indeed, if a region $R \subset \mathbb{R}/\mathbb{Z}$ does not contain any degenerate networks then, as ϑ is varied continuously in R, the network $\mathcal{W}_\vartheta$ also varies continuously (in the sense described in [63]). However, if the region R contains a single critical angle ϑ_c, the bifurcation of integral curves near a branch point induces a discontinuous change in the topology of $\mathcal{W}_\vartheta$ as ϑ is varied[10] past ϑ_c. (If we consider the parameter space of ϑ and the Coulomb branch then the locus where degenerate networks appear defines $\mathcal{K}$-*walls*.)

3.1.2.2 Formal Variables

In order to construct the generating functions that keep track of various BPS degeneracy indices, it is helpful to construct spaces of formal variables with some algebraic structure.

[10] However, there may be an accumulation point of critical angles as in the picture of the vector multiplet when $K = 2$ (see [63]). Around such an accumulation point the topology of $\mathcal{W}_\vartheta$ rapidly changes, and there is no open region containing the accumulation point where the topology smoothly varies. Even "worse," as we will see, the critical angles can densely fill an open interval.

Definition $\mathbb{Z}[\![\widetilde{\Gamma}]\!]$ is the commutative ring of formal series generated by formal variables X_γ, $\gamma \in \widetilde{\Gamma}$ such that

$$X_0 = 1,$$
$$X_H = -1,$$
$$X_\gamma X_{\gamma'} = X_{\gamma+\gamma'}.$$

To define an algebraic structure for formal variables in 2D-4D/soliton charges, we note that there is a partially defined "addition" operation.

Definitions

1. Let $a \in \widetilde{\Gamma}(\widetilde{z}_1, \widetilde{z}_2)$, then
$$\text{end}(a) = \widetilde{z}_2$$
$$\text{start}(a) = \widetilde{z}_1.$$

2. Let $a, b \in \bigcup_{\widetilde{z},\widetilde{w}\in\widetilde{C}} \widetilde{\Gamma}(\widetilde{z},\widetilde{w})$, then if $\text{end}(a) = \text{start}(b)$ there is a well-defined operation (concatenation of paths) $a + b \in \bigcup_{\widetilde{z},\widetilde{w}\in\widetilde{C}} \widetilde{\Gamma}(\widetilde{z},\widetilde{w})$ descending from the usual addition of relative homology cycles.

With this we can define the space of interest.

Definition The *homology path algebra* $\mathcal{A}$ is the non-commutative $\mathbb{Z}[\![\widetilde{\Gamma}]\!]$-algebra of formal series generated by formal variables X_a, for every $a \in \bigcup_{\widetilde{z},\widetilde{w}\in\widetilde{C}} \widetilde{\Gamma}(\widetilde{z},\widetilde{w})$; such that

1. For $\gamma \in \widetilde{\Gamma}$,
$$X_\gamma X_a = X_{a+\gamma} = X_{\gamma+a},$$

2. for any a, $b \in \bigcup_{\widetilde{z},\widetilde{w}\in\widetilde{\Sigma}} \widetilde{\Gamma}(\widetilde{z},\widetilde{w})$
$$X_a X_b = \begin{cases} X_{a+b}, & \text{if } \text{end}(a) = \text{start}(b) \\ 0, & \text{otherwise} \end{cases}.$$

There are two important $\mathbb{Z}[\![\widetilde{\Gamma}]\!]$-subalgebras of $\mathcal{A}$.

Definition

1. $\mathcal{A}_S$ is the $\mathbb{Z}[\![\widetilde{\Gamma}]\!]$-subalgebra generated by formal variables in soliton charges $a \in \bigcup_{\widetilde{z}\in\widetilde{C}} \widetilde{\Gamma}(\widetilde{z}, -\widetilde{z})$.

2. $\mathcal{A}_C$ is the (commutative) $\mathbb{Z}[\![\widetilde{\Gamma}]\!]$-subalgebra generated by formal variables in $a \in \bigcup_{\widetilde{z}\in\widetilde{C}} \bigsqcup_{i=1}^{K} \widetilde{\Gamma_{ii}}(\widetilde{z}, \widetilde{z})$.

The closure map can be easily extended to $\mathcal{A}_C$.

Definition

$$\mathrm{cl} : \mathcal{A}_C \to \mathbb{Z}[\![\widetilde{\Gamma}]\!]$$

is the linear extension of the map

$$\mathrm{cl}(X_a) = X_{\mathrm{cl}(a)}.$$

We now define generating functions for BPS indices.

Definition For each path $\wp$ from $z \in C$ to $w \in C$ that represents an interface $L_{\wp,\vartheta}$, we associate the framed generating function

$$F(\wp, \vartheta) := \sum_{a_* \in \Gamma(z,w)} \overline{\Omega}(L_{\wp,\vartheta}, a) X_a \in \mathcal{A},$$

where $a \in \widetilde{\Gamma}(\widetilde{z}, \widetilde{w})$ is a lift of the charge $a_* \in \Gamma(z, w)$ such that $\widetilde{z}$ and $\widetilde{w}$ are the unit tangent vectors at the ends of $\wp$.

For each street p of type ij, we associate two *soliton generating functions*: $\Upsilon(p)$, that encodes the indices of solitons of type ij, and $\Delta(p)$, that encodes the indices of solitons of type ji.

Definition Let $z \in p \subset C$, then we define

$$\Upsilon_z(p) := \sum_{a_* \in \Gamma_{ij}(z,z)} \mu(a) X_a \in \mathcal{A}_S \tag{3.13}$$

$$\Delta_z(p) := \sum_{b_* \in \Gamma_{ji}(z,z)} \mu(b) X_b \in \mathcal{A}_S, \tag{3.14}$$

where $a \in \widetilde{\Gamma}_{ij}(\widetilde{z}, -\widetilde{z})$, $b \in \widetilde{\Gamma}_{ji}(-\widetilde{z}, \widetilde{z})$ denote respective lifts of $a_* \in \Gamma_{ij}(z, z)$ and $b_* \in \Gamma_{ji}(z, z)$, for $\widetilde{z} \in \widetilde{C}$ the unit tangent vector agreeing with the orientation of p at the point $z \in C$.[11]

[11] As $\widetilde{\Gamma}(\widetilde{z}, -\widetilde{z})$ is a principal $\mathbb{Z}/2\mathbb{Z}$ bundle over $\Gamma(z, z)$, there are two possible lifts of a_* related by addition of H. Via $X_H = -1$ along with (3.9) and (3.10), the definition of $\Upsilon_z(p)$ is independent of the choice of lift. This argument also applies to $\Delta_z(p)$.

Definition From the soliton generating functions on a street p, we can define the *street factor*,

$$\begin{aligned} Q(p) &:= \mathrm{cl}\left[1 + \Upsilon_z(p)\Delta_z(p)\right] \\ &= 1 + \sum_{a_* \in \Gamma_{ij}(z,z), b_* \in \Gamma_{ji}(z,z)} \mu(a)\mu(b) X_{\mathrm{cl}(a+b)} \in \mathbb{Z}[\![\widetilde{\Gamma}]\!]. \end{aligned}$$

where $z \in C$ is any point on p.

Remark As the notation suggests, $Q(p)$ is independent of the choice of point z. This follows as the index $\mu(a)$ is constant as any charge a is parallel transported along any path supported on $p \subset C$. By the same reasoning, for any $z, z' \in p$, $\Upsilon_z(p)$ and $\Upsilon_{z'}(p)$ are related by applying an appropriate parallel transport map [12] (similarly for $\Delta_z(p)$ and $\Delta_{z'}(p)$).

And now for the punchline.

3.1.2.3 Computing $\Omega(n\gamma_c)$

The power of the spectral network machine can be summarized with the following squiggly arrows:

Jumping of Framed 2D-4D Spectrum + Homotopy Invariance of $L_{\wp,\vartheta}$ $\overset{(A)}{\rightsquigarrow}$ Soliton Spectrum $\overset{(B)}{\rightsquigarrow}$ (Vanilla) 4D spectrum.

To understand (A): the framed generating function $F(\wp, \vartheta)$ is piecewise constant in the sense that as the endpoints of $\wp$ are varied on $C - \mathcal{W}_\vartheta$, then $F(\wp, \vartheta)$ does not vary in $\mathcal{A}$; however, if an endpoint of $\wp$ is varied across a street of $\mathcal{W}_\vartheta$, then $F(\wp, \vartheta)$ will jump in a manner depending on the spectrum of solitons located on that street. Indeed, $F(\wp, \vartheta)$ is the sum of the charges of "millipedes," and as the "body" $\wp$ of each such millipede crosses the street p, then the millipede can gain an extra leg by detouring along a soliton supported along p; hence, the spectrum of 2D-4D states (represented by millipedes) will jump. To reproduce the soliton spectrum we utilize the homotopy invariance of the operator $L_{\wp,\vartheta}$ to equate the different jumps of $F(\wp, \vartheta)$ across different, but homotopic (rel endpoints), paths $\wp$. The resulting equations are equivalent to conditions on the soliton generating functions. These conditions, combined with the simpleton input data (3.12), allow us to completely determine the soliton generating functions, which encapsulate the soliton spectrum.

To describe (B), let $\Gamma_c \subset \Gamma$ be the lattice of charges γ with $e^{-i\vartheta_c} Z_\gamma \in \mathbb{R}_-$; then the degenerate network $\mathcal{W}_{\vartheta_c}$ captures all of the 4D BPS states carrying charges $\gamma \in \Gamma_c$. Their spectrum can be extracted from the generating functions $Q(p)$. But, first we have to deal with a technical point.

[12] For this reason, the point z in soliton generating functions is often dropped as in the calculations of Appendix C.

Definitions

1. For every curve q on a surface S, there is a canonical "lift" $\widehat{q}$ to a curve on $\widetilde{S}$, given by the tangent framing.

2. For each $\gamma \in \Gamma$, we define another lift $\widetilde{\gamma} \in \tilde{\Gamma}$ by the following rule. First, represent γ as a union of smooth closed curves β_m on Σ. Then $\widetilde{\gamma}$ is the sum of $\widehat{\beta}_m$, shifted by $\left(\sum_{m\leq n} \delta_{mn} + \#(\beta_m \cap \beta_n)\right) H$ (of course, because we work modulo $2H$, all that matters here is whether this sum is odd or even.)

One can check directly (see Appendix E) that $\tilde{\gamma}$ so defined is independent of the choice of how we represent γ as a union of β_m; this requirement is what forced us to add the tricky-looking shift.

Then, for each street p, we factorize $Q(p)$ as a product:

Definition

$$Q(p) = \prod_{\gamma\in\Gamma_c} (1 - X_{\widetilde{\gamma}})^{\alpha_\gamma(p)}. \tag{3.15}$$

This representation determines the coefficients $\alpha_\gamma(p)$.

Definition Let $\mathbf{m}p_\Sigma \in C_1(\Sigma;\mathbb{Z})$ be the one-chain corresponding to the lift p_Σ, then we define[13]

$$L(\gamma) := \sum_{\text{streets p}} \alpha_\gamma(p)\mathbf{m}p_\Sigma \in C_1(\Sigma;\mathbb{Z}). \tag{3.16}$$

Now, as shown in [63], the magic of this definition is that $L(\gamma)$ is actually a 1-cycle satisfying the BPS condition (3.2) for $\vartheta = \vartheta_c$. [14] Let us make the further assumption that Γ_c is a rank-1 lattice, which holds automatically off of the walls of marginal stability on $\mathcal{B}$, then it follows that both γ and $[L(\gamma)]$ are multiples of a choice of generator $\gamma_c \in \Gamma_c$. With this in mind, the journey to the end of the squiggly arrow (B) follows by analyzing the jumping of $F(\wp,\vartheta)$, but now as ϑ is varied across the critical angle ϑ_c (fixing $\wp$). The resulting analysis (see [63], sec. 6) leads us to the desired result:

$$[L(\gamma)] = \Omega(\gamma)\gamma, \qquad \gamma \in \Gamma_c, \tag{3.17}$$

from which all BPS indices of 4D BPS states with central charge phase ϑ_c can be computed.

[13] Note that the sum over streets in (3.16) reduces to a sum over two-way streets; indeed, $Q(p) \neq 1$ iff p is two-way.
[14] This last comment follows from the fact that $\int_{p_\Sigma} \lambda = \int_p \lambda_{ij} \in e^{i\vartheta_c}\mathbb{R}_{<0}$ for any street p of type ij.

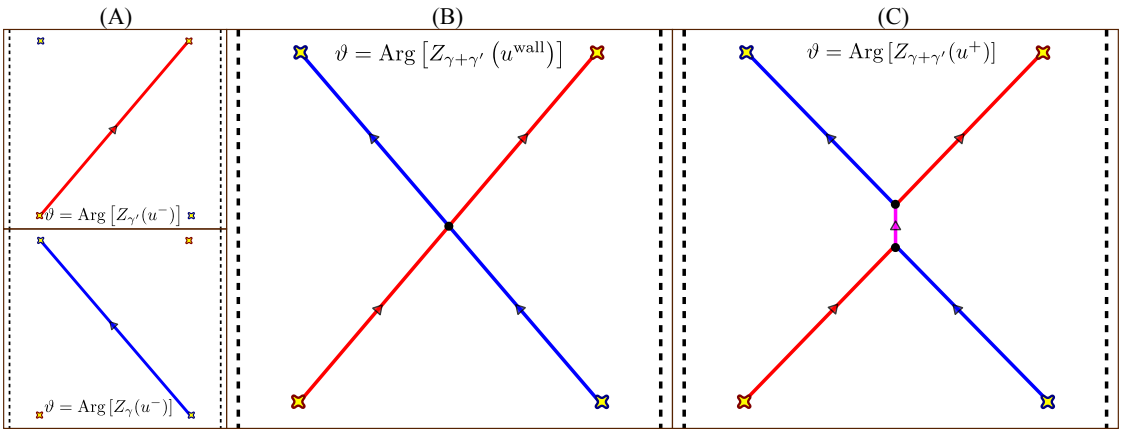

Figure 3.1: A hypothetical wall-crossing of two hypermultiplets with charges γ, γ' such that $\langle\gamma,\gamma'\rangle = 1$. Streets of type 12 are shown in red, 23 in blue, and 13 in fuchsia; only two-way streets are depicted. Arrows denote street orientations according to the convention described in Section 3.1.2.1. Yellow crosses denote branch points. Arrows denote the direction of solitons of type 12, 23, or 13 (according to the street). The black dotted lines are identified to form the cylinder. (A): The two hypermultiplet networks at a point u^- just "before" the wall of marginal stability. (B): The hypermultiplet networks at a point u^{wall} on the wall of marginal stability and at phase $\vartheta = \mathrm{Arg}\left[Z_\gamma(u^{\mathrm{wall}})\right] = \mathrm{Arg}\left[Z_{\gamma'}(u^{\mathrm{wall}})\right] = \mathrm{Arg}\left[Z_{\gamma+\gamma'}(u^{\mathrm{wall}})\right]$. (C): Slightly "after" the wall at a point u^+, a BPS bound state of charge $\gamma+\gamma'$ is born and a two-way street of type 13 "grows" as one proceeds away from the wall.

Abstract Spectral Networks

It is possible to abstract the properties of the $\mathcal{W}_\vartheta$ networks in order to draw networks on C that do not necessarily come from integral curves of (3.4). It is not necessary to give a precise list of the properties here, and we instead refer the interested reader to Section 9 of [63]. There, the abstracted networks are particularly useful for defining the "non-abelianization map" between moduli spaces of flat $GL(1)$-bundles on Σ, and flat $GL(K)$-bundles on C. In this paper, however, our interest in abstract spectral networks will be in constructions of *potential* $\mathcal{W}_\vartheta$ networks. Indeed, the m-herds mentioned in the introduction, and introduced in Section 4.4, are examples of abstract networks on an arbitrary curve C. By searching the parameter space of the pure $SU(3)$ theory, where $C = S^1\times\mathbb{R}$ and $K = 3$, it turns out that a large subset of m-herds actually arise as $\mathcal{W}_\vartheta$ networks at various points on the Coulomb branch.

3.2 Spectral network analysis of a wild point on the Coulomb branch

3.2.1 Horses and Herds

We begin by describing a sequence of spectral networks that may arise in the hypothetical wall-crossing between two BPS hypermultiplets of charges γ, $\gamma' \in \Gamma$ such that $\langle\gamma,\gamma'\rangle = m$. Indeed,

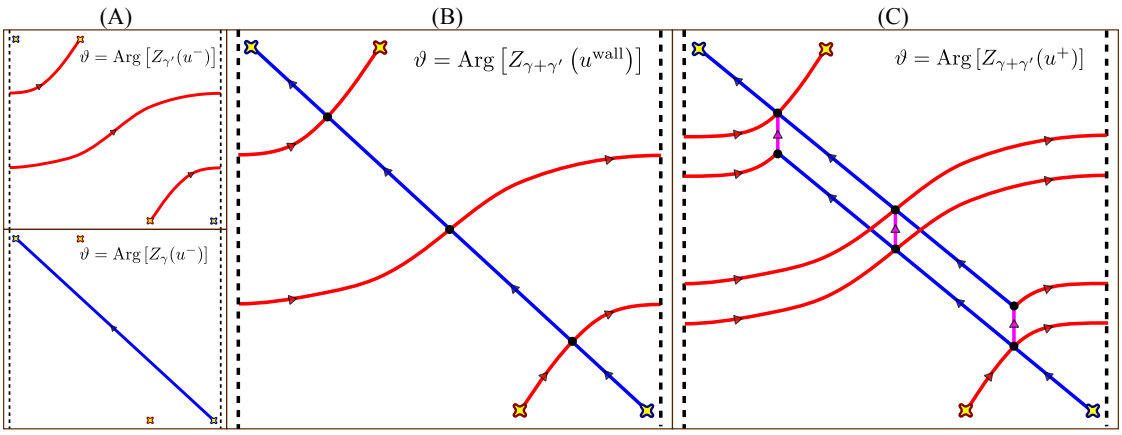

Figure 3.2: A hypothetical wall-crossing of two hypermultiplets with charges γ, γ' such that $\langle\gamma, \gamma'\rangle = 3$. The story is similar to that described in the caption of Fig. 3.1.

assume at some point on the Coulomb branch there are two BPS states (occurring at different phases) such that the degenerate network associated to each state has a single two-way street given by a simple curve passing through two branch points of the same type (frame (A) of Figs. 3.1-3.2); such spectral networks are associated to BPS hypermultiplets. Now, assume that there exists a marginal stability wall on the Coulomb branch associated to the (central charge phase) crossing of these two hypermultiplets (and no other BPS states). On the other side of the wall, a possible bound state of charge $\gamma + \gamma'$ may be formed (where γ, γ' are the charges of the original hypermultiplets). Figs. 3.1-3.2 depict three hypothetical snapshots along a path passing through the wall of marginal stability for the cases $m = 1, 3$; frame (C) depicts a guess at the appearance of the degenerate network associated to the bound state of charge $\gamma+\gamma'$. After drawing such pictures for progressively higher m, and given a sufficient dose of mildly-confused staring, one will begin to notice that the (two-way streets of) networks associated to the bound state of charge $\gamma+\gamma'$ can be decomposed into m-components that look like "extended" saddles; as they are the generalization of saddles we have no choice but to call each such component a "horse."

Definitions

1. A *horse street* $p \in \{a_1, a_2, a_3, b_1, b_2, b_3, c, \overline{a_1}, \overline{a_2}, \overline{a_3}, \overline{b_1}, \overline{b_2}, \overline{b_3}\}$ is one of the streets of Fig. 3.3 (left frame).

2. Let N be a spectral network (subordinate to some branched cover $\Sigma \to C$) and $U \subset C'$ be an open disk region. Then $U \cap N$ is a *horse* if a subset of its streets can be identified with Fig. 3.3 in a way such that:

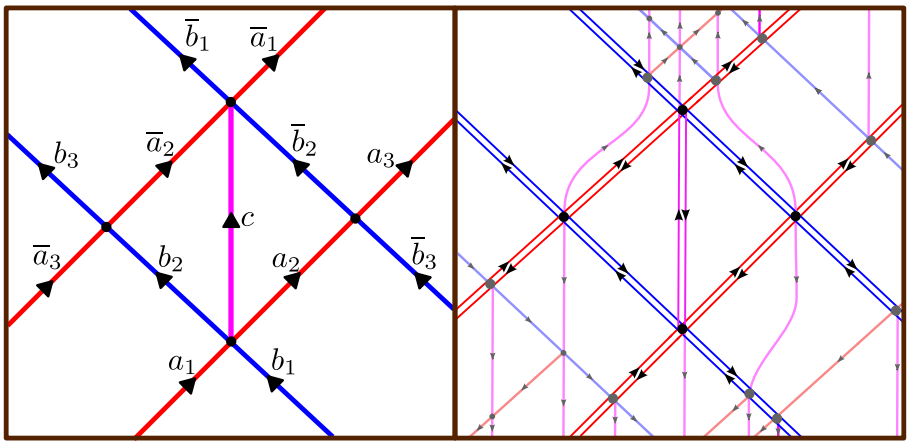

Figure 3.3: *Left Frame*: Two-way streets of a horse on some open disk U; the solid streets depicted are capable of being two-way; one-way streets are not shown. The sheets of the cover $\Sigma \to C$ are (locally) labeled from 1 to $K \geq 3$. Red streets are of type 12, blue streets are of type 23, and fuchsia streets are of type 13. We choose an orientation for this diagram such that all streets "flow up." *Right Frame*: A relatively simple example of a horse with one-way streets shown as partially transparent and two-way streets resolved (using the "British resolution", cf. Appendix B or [63]). One can imagine horses with increasingly intricate "backgrounds" of one-way streets.

a) every two-way street is a horse street,

b) there is always a two-way street identified with the street labeled c.

We can reconstruct the two-way streets of the full spectral network by gluing m horses back together. This leads us to the following working definition (a more complete definition is provided in Appendix C), which we extend to any curve C.

Working Definition Given a collection of m horses, let $p^{(l)}$ denote a horse street on the lth horse ($l = 1, \cdots, m$). A spectral network on a curve C is an m-herd if its two-way streets are generated by gluing together m horses using the following relations:

$$\begin{aligned} a_1^{(l)} &= a_3^{(l-1)} \\ b_1^{(l)} &= b_3^{(l-1)} \\ \overline{a_1}^{(l)} &= \overline{a_3}^{(l+1)} \\ \overline{b_1}^{(l)} &= \overline{b_3}^{(l+1)}, \end{aligned} \tag{3.18}$$

and such that $a_1^{(1)}$, $b_1^{(1)}$, $\overline{a_1}^{(m)}$, and $\overline{b_1}^{(m)}$ are connected to four distinct branch points.

Remark It can be shown from our definition that a 1-herd (which consists of a single horse) is just a saddle. Indeed, a small computation will show that $Q(p)$ is nontrivial ($Q(p) \neq 1$) only for

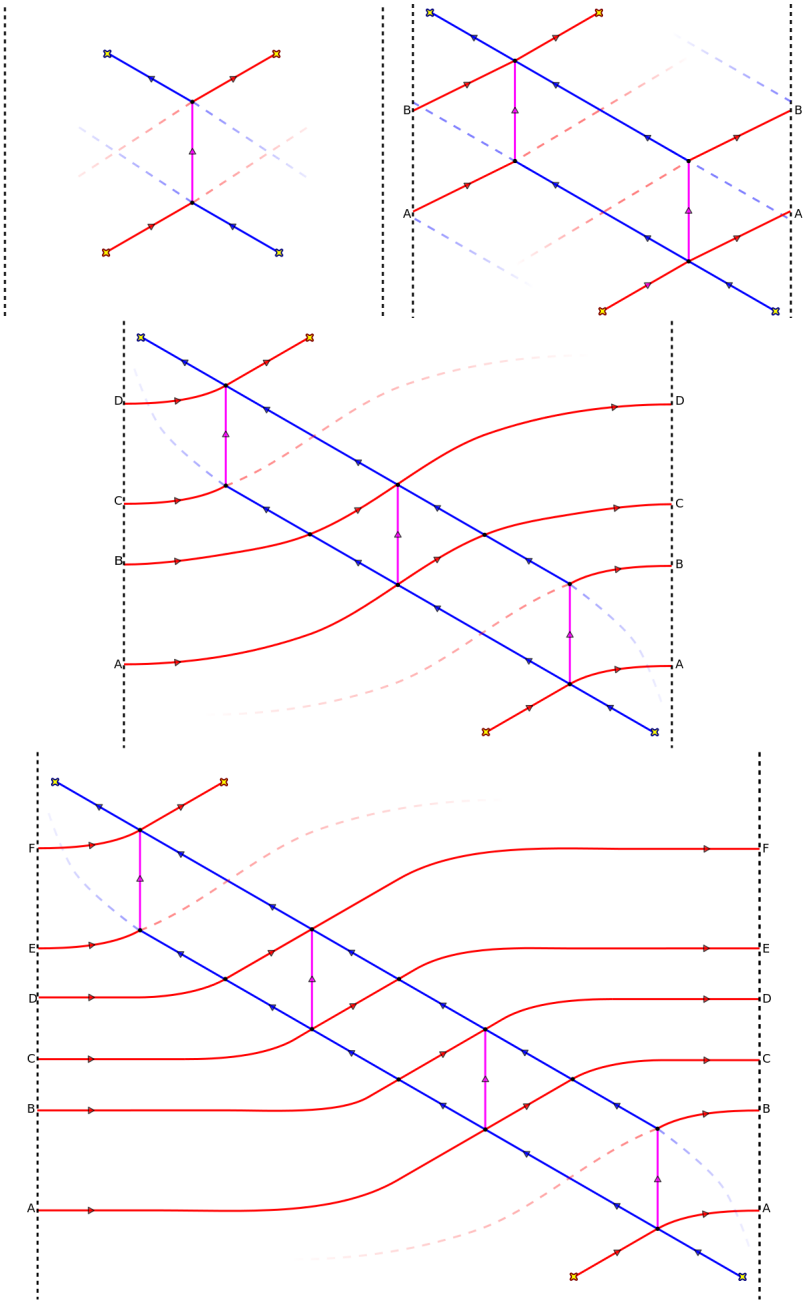

Figure 3.4: The first four herds on the cylinder. Solid streets are two-way; dotted, transparent streets are streets of Fig. 3.3 that happen to be only one-way as indicated by Prop. 3.2.1. The black dotted lines are identified to form the cylinder and capital Latin letters are placed on either side to aid in the identification of streets. Top row (from left to right): The 1-herd (saddle) and 2-herd. The middle row shows a 3-herd and the bottom row shows a 4-herd.

$p = a_1, \overline{a_1}, b_1, \overline{b_1},$ and c; this leads us to the picture of a saddle extending from four branch points (pictured in the top left corner of Fig. 3.4).

An advantage of the decomposition into horses is computability: a horse should be thought of as a scattering machine which takes inflowing solitons, and regurgitates outgoing solitons as well as all spectral data "bound" to the horse.[15] The combinatorial problem of computing the BPS degeneracies $\Omega(n\gamma_c)$, $n \geq 1$, using spectral network machinery, is then greatly simplified and explicit results can be obtained for all $m \geq 1$. In fact, we have the following.

Proposition 3.2.1. *Let N be an m-herd, then $Q(p)$ for all two-way streets p on N are given in terms of powers of a single generating function P_m satisfying the algebraic equation*

$$P_m = 1 + z\,(P_m)^{(m-1)^2}, \tag{3.19}$$

where $z = (-1)^m X_{\widetilde{\gamma}+\widetilde{\gamma}'}$ for some $\gamma, \gamma' \in H_1(\Sigma;\mathbb{Z})$ such that $\langle \gamma, \gamma' \rangle = m$. In particular, adopting the notation $Q(p,l) := Q(p^{(l)})$,

$$\begin{aligned}
P_m &= Q(c,l) \\
(P_m)^{m-l} &= Q(a_2,l) = Q(b_2,l) = Q(a_3,l) = Q(b_3,l) \\
(P_m)^{l-1} &= Q(\overline{a_2},l) = Q(\overline{b_2},l) = Q(\overline{a_3},l) = Q(\overline{b_3},l) \\
(P_m)^{m-l+1} &= Q(a_1,l) = Q(b_1,l) \\
(P_m)^{l} &= Q(\overline{a_1},l) = Q(\overline{b_1},l).
\end{aligned} \tag{3.20}$$

for $l = 1, \cdots, m$.

Proof. See Appendix C.6 for the full calculational proof. □

The precise cycle $\gamma_c = \gamma + \gamma'$ that appears depends on the embedding of N in C as a graph. Further, as shown at the end of Appendix C.6, there are cycles representing γ and γ' that look like the charges of simple "saddle-connection" hypermultiplets. Indeed, the cycle representing either γ or γ' projects down to a path on C that runs between two distinct branch points of the same type. These are precisely the (hypothetical) hypermultiplets whose wall-crossing motivated the construction of m-herds.[16]

[15] See Appendix C.3 for a the precise and explicit description of the horse as a scattering machine.

[16] The representative cycles discussed here, however, do not live entirely on $\mathrm{Lift}(N) \subset \Sigma$. Roughly speaking representatives of γ, γ' are given by the lifts of paths running along the $a_i, \overline{a_i}$ and b_i, $\overline{b_i}$ respectively, but these do not define closed paths on Σ without running through at least one street of type 13.

Remarks

- A street p is two-way iff $Q(p) \neq 1$. Thus, (3.20) states that on the first ($l = 1$) and last ($l = m$) horses, some streets depicted in Fig. 3.3 are only one-way.

- When $m = 1, 2$, (4.111) has easily derivable solutions:

$$P_1 = 1 + z, \tag{3.21}$$

$$P_2 = (1 - z)^{-1}. \tag{3.22}$$

  For a saddle ($m = 1$), this result, combined with (3.20), states that there are five two-way streets; each such two-way street p is equipped with a generating function $Q(p) = 1 + z$, as originally derived in [63].

3.2.2 Connection with Kontsevich-Soibelman, Gross-Pandharipande

The algebraic equation (4.111) and relevant solutions appear in a conjecture by Kontsevich and Soibelman (KS) [88], later proven by Reineke [115] and generalized by Gross-Pandharipande (GP) [75]. A series solution of (4.111) can be obtained using the Lagrange formula for reversion of series and the result for $m > 1$ is [88]:

$$\begin{aligned} P_m &= \sum_{n=0}^{\infty} \frac{1}{1 + (m^2 - 2m)n} \binom{(m-1)^2 n}{n} z^n, \\ &= \exp\left[\sum_{n=1}^{\infty} \frac{1}{(m-1)^2 n} \binom{(m-1)^2 n}{n} z^n \right]. \end{aligned} \tag{3.23}$$

To describe the connection between our result and that of KS and GP, we review the generalized conjecture of GP, briefly adopting their notation in [75].

The algebraic equation (4.111) appears in [75]. [17] There, the object of study is a group of (formal 1-parameter familes of) automorphisms of the torus $\mathbb{C}^* \times \mathbb{C}^*$ generated by $\theta_{(a,b),f}$ that are defined by

$$\theta_{(a,b),f}(x) = f^{-b} \cdot x, \quad \theta_{(a,b),f}(y) = f^a \cdot y$$

where x and y are coordinate functions on the two factors of $\mathbb{C}^* \times \mathbb{C}^*$, $(a, b) \in \mathbb{Z}^2$, and f is a formal series of the form

$$f = 1 + x^a y^b \left[t f_1(x^a y^b) + t^2 f_2(x^a y^b) + \cdots \right], \; f_i(z) \in \mathbb{C}[z].$$

[17] A different, but related, algebraic equation on the quantity $(P_m)^m$ was originally stated by Kontsevich and Soibelman in [88].

Alternatively we may say $f \in \mathbb{C}[x, x^{-1}, y, y^{-1}][[t]]$ (i.e. f is a formal power series in t with coefficients Laurent polynomials in x and y). Such automorphisms preserve the holomorphic symplectic form

$$\omega = (xy)^{-1} dx \wedge dy.$$

Now, letting

$$S_q = \theta_{(1,0),(1+tx)^q}, \quad T_r = \theta_{(0,1),(1+ty)^r},$$

we consider the commutator

$$T_r^{-1} \circ S_q \circ T_r \circ S_q^{-1} = \prod^{\rightarrow} \theta_{(a,b),f_{(a,b)}} \tag{3.24}$$

where the product on the right hand side is over primitive vectors $(a, b) \in \mathbb{Z}^2$ (i.e. $\gcd(a, b) = 1$) such that $a, b > 0$, and the order of the product is taken with increasing slope a/b from left to right. The conjecture of Gross-Pandharipande involves the slope 1 term of (3.24).

Conjecture (Gross-Pandharipande)

For arbitrary (q, r), the slope 1 term $\theta_{(1,1),f_{(1,1)}}$ in (3.24) is specified by

$$f_{1,1} = \left(\sum_{n=0}^{\infty} \frac{1}{(qr - q - r)n + 1} \binom{(q-1)(r-1)n}{n} t^{2n} x^n y^n \right)^{qr}.$$

The case $q = r$ was first conjectured by KS, and later proven by Reineke. Now, letting

$$\mathcal{P}_{q,r} = \sum_{n=0}^{\infty} \frac{1}{(qr - q - r)n + 1} \binom{(q-1)(r-1)n}{n} t^{2n} x^n y^n, \tag{3.25}$$

For general q, r, Gross and Pandharipande noted that $\mathcal{P}_{q,r}$ satisfies the equation

$$t^2 xy \left(\mathcal{P}_{q,r}\right)^{(q-1)(r-1)} - \mathcal{P}_{q,r} + 1 = 0; \tag{3.26}$$

so that $f_{1,1}$ is an algebraic function (over $\mathbb{Q}(t, x, y)$).

In the case $q = r = m$, the equation (3.26) and solution (3.25) bear striking similarity to (4.111) and (3.23), which motivates identifying $t^2 xy = z$ in hopes of identifying $\mathcal{P}_{m,m}$ with P_m.

To motivate the identification $t^2 xy = z$, we turn our attention back to the original motivation for our definition of m-herds: they are expected to arise after two hypermultiplets of charges γ, γ', with $\langle \gamma, \gamma' \rangle = m$, cross a wall of marginal stability. If m-herds do arise in this manner, then in the resulting wall-crossing formula we should expect the P_m to be related to the generating function for the KS transformations attached to the charges $n(\gamma + \gamma')$, $n > 0$. We now go about unpacking the identification of such a wall crossing formula with (3.24).

Assume on one side of the wall $\mathrm{Arg}(Z_\gamma) < \mathrm{Arg}(Z_{\gamma'})$, then the wall crossing formula reads (see Section 3.4.1)

$$\mathcal{K}_\gamma \mathcal{K}_{\gamma'} = \mathcal{K}_{\gamma'} \left[\prod_{(a,b)\in\mathbb{Z}^2} (\mathcal{K}_{a\gamma+b\gamma'})^{\Omega(a\gamma+b\gamma')} \right] \mathcal{K}_\gamma \tag{3.27}$$

where all products are taken in order of increasing central charge phase (when read from left to right) and the $\mathcal{K}_\alpha$ are transformations on a twisted Poisson algebra of functions on the torus $T = \Gamma \otimes_{\mathbb{Z}} \mathbb{C}^\times$, i.e. the space of functions generated by polynomials in formal variables $Y_\alpha, \alpha \in \Gamma$ equipped with twisted product given by

$$Y_\alpha Y_\beta = (-1)^{\langle\alpha,\beta\rangle} Y_{\alpha+\beta}. \tag{3.28}$$

T is equipped with a holomorphic symplectic form induced by the symplectic pairing on Γ; it is equivalently given by the holomorphic Poisson bracket

$$\{Y_\alpha, Y_\beta\} = \langle\alpha,\beta\rangle Y_\alpha Y_\beta. \tag{3.29}$$

Now, the $\mathcal{K}_\alpha$ are symplectomorphisms that act as

$$\mathcal{K}_\alpha : Y_\beta \mapsto (1 - Y_\alpha)^{\langle\alpha,\beta\rangle} Y_\beta. \tag{3.30}$$

For $\langle\gamma,\gamma'\rangle = m$, it follows that

$$\begin{aligned} &\mathcal{K}_\gamma : Y_\gamma \mapsto Y_\gamma, && \mathcal{K}_{\gamma'} : Y_\gamma \mapsto (1 - Y_{\gamma'})^{-m} Y_\gamma, \\ &\mathcal{K}_\gamma : Y_{\gamma'} \mapsto (1 - Y_\gamma)^m Y_{\gamma'}, && \mathcal{K}_{\gamma'} : Y_{\gamma'} \mapsto Y_{\gamma'}. \end{aligned} \tag{3.31}$$

We identify the torus $\mathbb{C}^\times \times \mathbb{C}^\times$ of Gross-Pandharipande by the subtorus of T generated by

$$x := Y_\gamma$$

$$y := Y_{\gamma'};$$

then by (3.31) we have[18]

$$\mathcal{K}_\gamma = \theta_{(1,0),(1-x)^m} = S_m$$

$$\mathcal{K}_{\gamma'} = \theta_{(0,1),(1-y)^m} = T_m.$$

Furthermore, noting that

$$x^a y^b = (-1)^{\langle a\gamma, b\gamma'\rangle} Y_{a\gamma+b\gamma'} = (-1)^{mab} Y_{a\gamma+b\gamma'}, \tag{3.32}$$

then

$$\begin{aligned} \mathcal{K}_{a\gamma+b\gamma'} : x = Y_\gamma &\mapsto (1 - Y_{a\gamma+b\gamma'})^{-mb} Y_\gamma = (1 - (-1)^{mab} x^a y^b)^{mb} x \\ : y = Y_{\gamma'} &\mapsto (1 - Y_{a\gamma+b\gamma'})^{-ma} Y_{\gamma'}^{ma} = (1 - (-1)^{mab} x^a y^b)^{-ma} y; \end{aligned}$$

[18] To make the identification with S_m and T_m we evaluate the formal (time) parameter at $t = -1$. Alternatively, we could set $-tx = Y_\gamma$ and $-ty = Y_{\gamma'}$.

giving the identification

$$\mathcal{K}_{a\gamma+b\gamma'} = \theta_{(a,b),(1-(-1)^{mab}x^a y^b)^m}.$$

On the right hand side of (3.27) $\text{Arg}(Z_\gamma) > \text{Arg}(Z_{\gamma'})$ and so the phase ordered product is equivalent to ordering by increasing slope a/b from left to right. This completes the identification of (3.27) with (3.24). Matching the slope 1 terms in both equations,

$$\theta_{(1,1),f_{1,1}} = \prod_{n\geq 1} \left(\mathcal{K}_{n\gamma_c}\right)^{\Omega(n\gamma_c)},$$

where $\gamma_c := \gamma + \gamma'$; in terms of generating functions, this is equivalent to the statement[19]

$$f_{1,1} = \prod_{n\geq 1} \left[(1-(-1)^{mn}z^n)^m\right]^{n\Omega(n\gamma_c)}.$$

Equivalently, as $f_{1,1} = (\mathcal{P}_{m,m})^{m^2}$,

$$(\mathcal{P}_{m,m})^m = \prod_{n\geq 1}(1-(-1)^{mn}z^n)^{n\Omega(n\gamma_c)}. \tag{3.33}$$

Now assume that the generating function P_m, derived in the context of spectral networks, *is* the generating function $\mathcal{P}_{m,m}$, derived in the context of wall crossing; then, given the exponents $\{\alpha_n\}_{n\geq 1}$ of the factorization of P_m (see (3.35)), (3.33) predicts spectral network techniques will show $\Omega(n\gamma_c) = m\alpha_n/n$. As we will see, this prediction is confirmed with Prop. 3.2.2.

3.2.3 Herds of horses are wild (for $m \geq 3$)

Definition For each two-way street p, define the sequence of exponents $\{\alpha_n(p,l)\}_{n\geq 1} \subset \mathbb{Z}$ via

$$Q(p,l) = \prod_{n=1}^{\infty}(1-(-1)^{mn}z^n)^{\alpha_n(p,l)}. \tag{3.34}$$

We also define the sequence of integers $\{\alpha_n\}_{n\geq 1}$ via

$$P_m = \prod_{n=1}^{\infty}(1-(-1)^{mn}z^n)^{\alpha_n}. \tag{3.35}$$

By Prop. 3.2.1, we can express all $\alpha_n(p,l)$ as multiples of α_n. [20]

Remark The choice of signs $(-1)^{mn}$ follows from our convention of factorization, defined by (3.15), in terms of formal variables in the image of $Y_\gamma \mapsto X_{\widetilde{\gamma}}$ (which forms an embedding of the twisted algebra of Y_γ, $\gamma \in \Gamma$, as subalgebra of $\mathbb{Z}[\![\widetilde{\Gamma}]\!]$ as detailed in Appendix E). By Prop. 3.2.1, $z^n = (-1)^{mn}X_{n\widetilde{\gamma}_c}$ for some $\gamma_c \in \Gamma$, leading to the choice of signs in (3.34).

[19] To see this, let $g_n = (1-(-1)^{mn}(xy)^n)^m$, then $\mathcal{K}_{n\gamma_c} = \theta_{(n,n),g_n} = \theta_{(1,1),(g_n)^n}$; furthermore, as $\theta_{(1,1),(g_n)^n}$ fixes the product xy: $\theta_{(1,1),(g_n)^n} \circ \theta_{(1,1),(g_l)^l} = \theta_{(1,1),(g_n)^n(g_l)^l}$.

[20] The radius of convergence R of the series in equation (4.111) is $\log R = -c_m$, where c_m is given in equation (3.40); in particular $R < 1$. Therefore, the product expansion is only a formal expansion and is not absolutely convergent; otherwise, it would predict that all the singularities of $d\log P$ sit on the unit circle.

Proposition 3.2.2.

$$[L(n\gamma_c)] = m\alpha_n\gamma_c \in H_1(\Sigma;\mathbb{Z}).$$

Proof (sketch). A rough argument goes as follows. Note that, using Prop. 3.2.1 and the definition of $L(n\gamma_c)$ in (3.16), we have

$$\begin{aligned} L(n\gamma_c) &= \sum_{l=1}^{m}\sum_{p^{(l)}} \alpha_n(p,l)\mathbf{m}p^{(l)} \\ &= \alpha_n \sum_{l=1}^{m} \Big\{ \mathbf{m}c^{(l)} + (m-l)\left(\mathbf{m}a_2{}^{(l)} + \mathbf{m}a_3{}^{(l)} + \mathbf{m}b_2{}^{(l)} + \mathbf{m}b_3{}^{(l)}\right) \\ &+ (l-1)\left(\mathbf{m}\overline{a_2}^{(l)} + \mathbf{m}\overline{a_3}^{(l)} + \mathbf{m}\overline{b_2}^{(l)} + \mathbf{m}\overline{b_3}^{(l)}\right) + \\ &+ (m-l+1)\left(\mathbf{m}a_1{}^{(l)} + \mathbf{m}b_1{}^{(l)}\right) + l\left(\mathbf{m}\overline{a_1}^{(l)} + \mathbf{m}\overline{b_1}^{(l)}\right)\Big\}. \end{aligned} \tag{3.36}$$

Each term in this sum can be split up into a sum of words of the form

$$\mathbf{m}a_1^{(1)} + \mathbf{m}b_1^{(1)} + (\cdots) + \mathbf{m}\overline{a}_1^{(m)} + \mathbf{m}\overline{b}_1^{(m)},$$

Each such word represents a closed cycle on the lift of the m-herd to a graph on Σ, and is homologous[21] to γ_c. As $\mathbf{m}a_1^{(1)}$, $\mathbf{m}b_1^{(1)}$, $\mathbf{m}\overline{a}_1^{(m)}$, $\mathbf{m}\overline{b}_1^{(m)}$ all come with multiplicity m in (3.36), then there are m such words and the proposition follows. A full proof, using brute-force homology calculations, can be found in Appendix C.8. □

Via (3.17), the immediate result of Prop. 3.2.2 is that

$$\Omega(n\gamma_c) = \frac{m\alpha_n}{n};$$

so all that remains is to compute α_n. For the cases $m = 1, 2$: using (3.21) and (3.22) we immediately have[22]

$$\alpha_n = \begin{cases} \delta_{n,1}, & \text{if } m = 1 \\ -\delta_{n,1}, & \text{if } m = 2 \end{cases} \Rightarrow \Omega(n\gamma_c) = \begin{cases} \delta_{n,1}, & \text{if } m = 1 \\ -2\delta_{n,1}, & \text{if } m = 2 \end{cases}. \tag{3.37}$$

More generally, we can find an explicit form for α_n by taking the log of both sides of (3.35), matching powers of z, and applying Möbius inversion to derive

$$\alpha_n = \frac{1}{n}\sum_{d|n}(-1)^{md+1}\mu\left(\frac{n}{d}\right)\frac{1}{(d-1)!}\left[\frac{d^d}{dz^d}\log(P_m)\right]_{z=0},$$

where μ is the Möbius mu function. Using (3.23),

$$\alpha_n = \frac{1}{(m-1)^2 n}\sum_{d|n}(-1)^{md+1}\mu\left(\frac{n}{d}\right)\binom{(m-1)^2 d}{d},\ m \geq 2.$$

[21] This homological equivalence can be shown using explicit calculations of the form shown in Appendix C.8. For the reader that wishes to avoid excruciating detail: sufficient staring at some simple examples will suffice.

[22] The case $m = 1$ (i.e. the saddle) was also computed in [63].

Corollary 3.2.3. *For $m \geq 2$,*

$$\Omega(n\gamma_c) = \frac{m}{(m-1)^2 n^2} \sum_{d|n} (-1)^{md+1} \mu\left(\frac{n}{d}\right) \binom{(m-1)^2 d}{d}. \tag{3.38}$$

This agrees with the result of Reineke[23] in the last section of [115]. A table of the values of $\Omega(n\gamma_c)$ is provided in Appendix C.9 for $1 \leq n, m \leq 7$. From this explicit result, we can deduce the large n asymptotics for the non-trivial[24] case $m \geq 3$.

Proposition 3.2.4. *Let $m \geq 3$, then as $n \to \infty$,*

$$\Omega(n\gamma_c) \sim (-1)^{mn+1} \left(\frac{1}{m-1}\sqrt{\frac{m}{2\pi(m-2)}}\right) n^{-5/2} e^{c_m n}, \tag{3.39}$$

where c_m is the constant

$$c_m = (m-1)^2 \log\left[(m-1)^2\right] - m(m-2)\log\left[m(m-2)\right]. \tag{3.40}$$

Proof. Restricting n to be an element of an infinite subsequence of primes, the sum over divisors simplifies and the claimed asymptotics (restricted to this subsequence) follow immediately using Stirling's asymptotics and (3.38). See Appendix D for a full proof. □

3.2.4 Herds in the pure $SU(3)$ theory

Now, finally, let us exhibit some points of the Coulomb branch of the pure $SU(3)$ theory where m-herds actually occur in spectral networks $\mathcal{W}_\vartheta$.

In the pure $SU(3)$ theory, the curve C is $\mathbb{CP}^1$ with two defects. It is natural to view it topologically as the cylinder $\mathbb{R} \times S^1$. Moreover, the spectral curve (3.42) has 4 branch points. Thus, the pictures of actual spectral networks in this theory look much like the "hypothetical" spectral networks we considered in Figures 3.1, 3.2.

In particular, consider the parameters

$$u_2 = -3, \quad u_3 = \frac{95}{10} \tag{3.41}$$

(in the notation of (3.42).) At this point, in accordance with the discussion of Section 4.4, we consider two charges γ, γ' supporting BPS hypermultiplets, represented simply by paths connecting pairs of branch points across the cylinder, as in the left side of Figure 3.2. In particular they have

[23] Reineke showed (in our notation) $\Omega(n\gamma_c) = \frac{1}{(m-2)n^2} \sum_{d|n} (-1)^{md+1} \mu(n/d) \binom{(m-1)^2 d - 1}{d}$. To translate between results, we use the observation that $\binom{(m-1)^2 d}{d} = \frac{(m-1)^2}{m(m-2)} \binom{(m-1)^2 d - 1}{d}$.

[24] In the case $m = 2$, using the identity $\sum_{d|n} \mu(d) = \delta_{n,1}$ in (3.38) reproduces the result $\Omega(n\gamma_c) = -2\delta_{n,1}$ of (3.37).

$\langle \gamma, \gamma' \rangle = 3$. By numerically computing the appropriate contour integrals we find that these charges have $Z_\gamma = 7.244 - 9.083i$, $Z_{\gamma'} = 20.980 - 40.148i$.

Now, our proposal in Section 4.4 was that when we have two such hypermultiplets, there will be a wall of marginal stability in the Coulomb branch when Z_γ and $Z_{\gamma'}$ become aligned, and on one side of that wall, the spectral network at the phase $\vartheta = \operatorname{Arg} Z_{\gamma+\gamma'}$ will contain a 3-herd. So, we plot the spectral network at phase $\vartheta = \operatorname{Arg} Z_{\gamma+\gamma'}$, and find Figure 3.5. Comparing with Figure 3.4, we see that the two-way streets in this network make up a 3-herd as desired.[25]

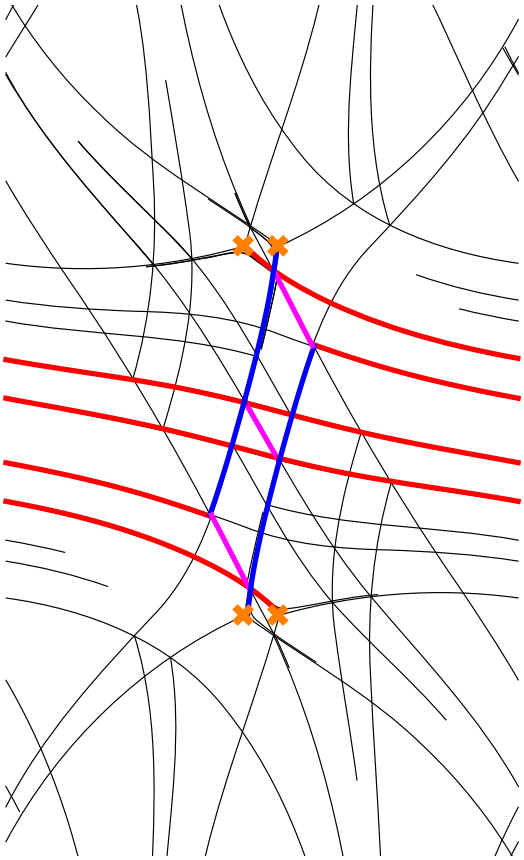

Figure 3.5: The spectral network $\mathcal{W}_\vartheta$ which occurs in the pure $SU(3)$ theory at the point (3.41) of the Coulomb branch. The phase ϑ has been chosen very close to the critical phase $\vartheta = \operatorname{Arg} Z_{\gamma+\gamma'}$. Here we represent the cylinder C as the periodically identified plane, i.e., the left and right sides of the figure should be identified. Streets which become two-way at $\vartheta = \operatorname{Arg} Z_{\gamma+\gamma'}$ are shown in thick red, blue and fuchsia. We do not show the whole network but only a cutoff version of it, as described in [63].

Moving u_3 in the positive real direction, we have similarly found a 4-herd, a 5-herd and a 6-herd. It is natural to conjecture that one can similarly obtain m-herds for any m in this way. Of course, at a fixed point in the Coulomb branch it is in general possible that there could be m-herds for many

[25] In particular, our point (3.41) is on the side of the wall where the 3-herd exists. The wall of marginal stability where the 3-herd disappears can be reached by moving u_3 in the negative real direction.

different values of m at different values of ϑ.

In any case, the existence of 3-herds in the pure $SU(3)$ theory is already enough to show that the analysis of the last few sections is not only a theoretical exercise: the wild BPS degeneracies we found there indeed occur in the $\mathcal{N} = 2$ supersymmetric pure $SU(3)$ Yang-Mills theory!

3.3 Wild regions for pure $SU(3)$ theory from wall-crossing

In the previous section we exhibited an example of a class of spectral networks that lead to the m-wild degeneracies of slope $(1, 1)$. An explicit point on the Coulomb branch of the pure $SU(3)$ theory which produces such a spectral network for $m = 3$ was given in equation (3.41) above.

In the present section we start anew, and use wall crossing and quiver techniques to give an alternative demonstration that wild degeneracies exist on the Coulomb branch of the pure $SU(3)$ theory.

3.3.1 Strong Coupling Regime of the Pure $SU(3)$ Theory

The spectral curve Σ of pure $SU(3)$ SYM theory is

$$\lambda^3 - \frac{u_2}{z^2}\,\lambda\,(dz)^2 + \left(\frac{1}{z^2} + \frac{u_3}{z^3} + \frac{1}{z^4}\right)(dz)^3 = 0. \tag{3.42}$$

It is a branched three-sheeted covering of the cylinder C, with six ramification points. There are four branch points corresponding to two-cycles of S_3, and there are also ramifications at the irregular singularities at $0, \infty$, with associated permutations of the sheets given by three-cycles.

In the strong coupling region, i.e. at small values of the moduli u_2, u_3, the BPS spectrum is finite; so the spectral network evolves in a rather simple fashion. As a concrete example we choose $u_2 = 0.7$, $u_3 = 0.4i$; then varying ϑ from 0 to π we encounter six degenerate networks containing finite webs, which are depicted in Figure 3.6.

We assign to these cycles the charges γ_1, γ_2, $\gamma_2 + \gamma_4$, $\gamma_1 + \gamma_3$, γ_3, γ_4, Figure 3.7 shows the charge assignments with the basis cycles resolved.

The mutual intersections of cycles can be read off Figure 3.7, and are summarized by the following pairing matrix $P_{ij} = \langle \gamma_i, \gamma_j \rangle$

$$P = \begin{pmatrix} 0 & -2 & 1 & 0 \\ 2 & 0 & -2 & 1 \\ -1 & 2 & 0 & -2 \\ 0 & -1 & 2 & 0 \end{pmatrix}. \tag{3.43}$$

For a video showing the evolution of the spectral network through an angle of π, see [1].

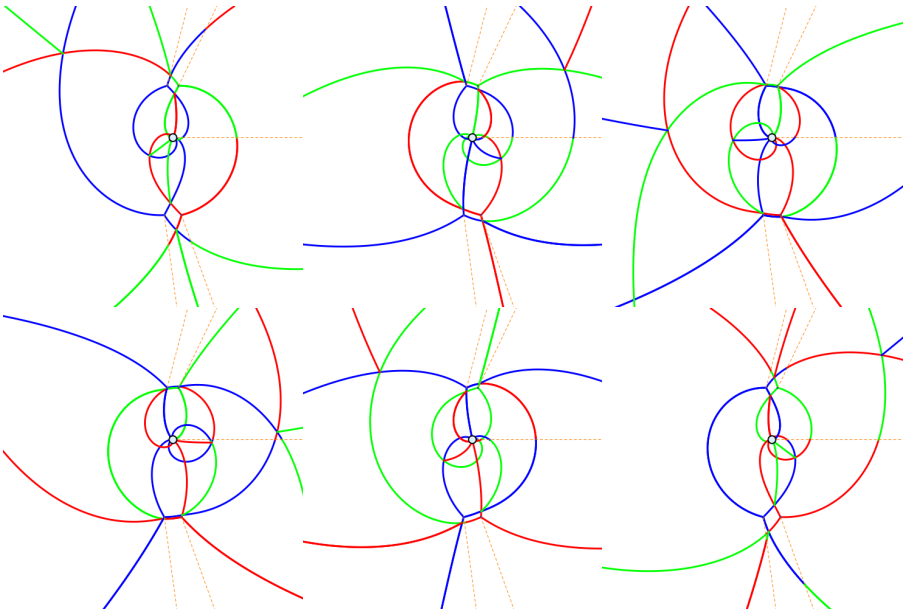

Figure 3.6: The six hypermultiplets in the strong coupling chamber: from the top left, the flips corresponding to $\gamma_1, \gamma_2, \gamma_1+\gamma_3, \gamma_2+\gamma_4, \gamma_3, \gamma_4$. $Arg\, Z_{\gamma_1} < Arg\, Z_{\gamma_2} < Arg\, Z_{\gamma_3} < Arg\, Z_{\gamma_4}$. Here we represent the cylinder C as the punctured plane.

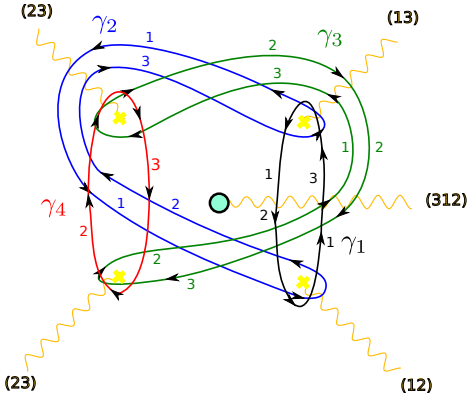

Figure 3.7: The labeling of finite networks. We only show the four basis hypermultiplets $\gamma_1, \ldots, \gamma_4$. The trivialization is indicated by the branch cuts (wavy lines, the associated permutations of sheets are also specified), the sheets on which the cycles run are indicated explicitly. Here we represent the cylinder C as the punctured plane.

3.3.2 A path on the Coulomb branch

We now consider a straight path on the Coulomb branch of the pure $SU(3)$ theory, parameterized by

$$\begin{aligned} u_2(t) &= (u_2^{(f)} - u_2^{(i)})t + u_2^{(i)}, \\ u_3(t) &= (u_3^{(f)} - u_3^{(i)})t + u_3^{(i)}, \end{aligned} \tag{3.44}$$

with $t \in [0,1]$ and

$$\begin{aligned} u_2^{(i)} = 0.7, \quad u_3^{(i)} = 0.4i \quad \text{(strong coupling chamber)} \\ u_2^{(f)} = 0.56 - 0.75i, \quad u_3^{(f)} = 2 + 1.52i \quad \text{(wild chamber)} \end{aligned} \tag{3.45}$$

As discussed above, the spectrum in the strong coupling chamber is known (see for example [63]) to consist of six hypermultiplets. As we move along our path we cross several walls of marginal stability, with consequent jumps of the BPS spectrum. In order to study the evolution of the BPS spectrum, we must track explicitly the evolution of central charges. Variation of the moduli also induces changes in the geometry of the Seiberg-Witten curve Σ, therefore in computing the central charges at different points one must take care of deforming the cycles in a way compatible with the flat parallel transport of the local system $\widehat{\Gamma} \to \mathcal{B}^*$. Starting from the point studied in Section 3.3.1, the evolution of branch points can be tracked on C, as shown in Figure 3.8.

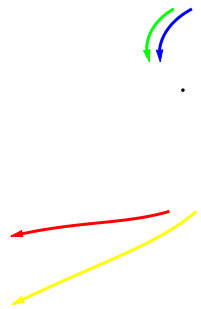

Figure 3.8: The picture shows the projection of the Seiberg-Witten curve on C. The four arrows show the progression of the four branch points as we vary $u_{2,3}$ along the path of equation (3.44). The black dot is the singularity at $z = 0$. The central charges have been computed numerically using Mathematica and, as a check, they evolve smoothly along the path (see [2]).

3.3.3 Cohorts in pure $SU(3)$

As the moduli cross walls of marginal stability, the BPS spectrum jumps according to a regular pattern. At a wall MS(γ, γ') for two populated hypermultiplets, with $\langle \gamma, \gamma' \rangle = m > 0$, the KS wall

crossing formula predicts

$$\mathcal{K}_{\gamma'}\mathcal{K}_{\gamma} =: \prod_{a,b\geq 0} \mathcal{K}_{a\gamma+b\gamma'}^{\Omega(a\gamma+b\gamma')} : \tag{3.46}$$

where the normal ordering symbols : : on the right hand side indicate that factors are ordered according to the phases of central charges, phase-ordering on the right hand side is the opposite of that on the left-hand side. We refer to the spectrum on the right hand side as the *cohort* generated by γ, γ', and will occasionally denote it by $\mathcal{C}_m(\gamma, \gamma')$. An important fact to note about cohorts, following from the linearity of the central charge homomorphism, is that

$$\text{Arg}\, Z_{\gamma'} < \text{Arg}\, Z_{a\gamma+b\gamma'} < \text{Arg}\, Z_{\gamma}, \qquad \forall a, b \geq 0 \tag{3.47}$$

for moduli corresponding to the right hand side of (3.46).

Quite generally, the wall-crossing of two hypermultiplet states with pairing m can be analyzed in terms of the corresponding m-Kronecker quiver (see [12, 39]), from this perspective the degeneracies of an m-cohort correspond to Euler characteristics of moduli spaces of (semi)stable quiver representations.

Cohort structures $\mathcal{C}_m$ with $m = 1, 2$ are known exactly. Examples of such cohorts have been encountered a number of times in the literature [60, 61, 64, 75, 87], and are common in A_1 theories of class $\mathcal{S}$. For later convenience, we recall the structure of the $m = 2$ cohort in figure 3.9.

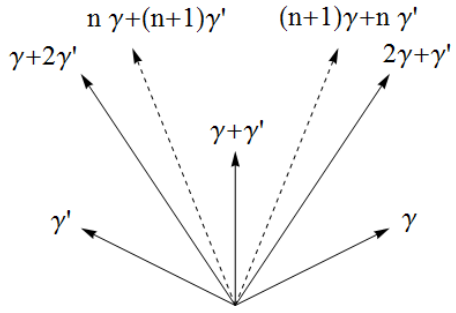

Figure 3.9: The populated BPS rays of the $m = 2$ cohort (a schematic depiction of central charges in the complex plane). The state with charge $\gamma + \gamma'$ is a BPS vectormultiplet ($\Omega = -2$), surrounded by two infinite towers of hypermultiplets ($\Omega = 1$), represented by dashed arrows.

As we start moving along our path on the Coulomb branch, from $t = 0$ to $t = 1$, several cohorts are created. The first wall of marginal stability is $\text{MS}(\gamma_1 + \gamma_3, \gamma_2 + \gamma_4)$, with $\langle \gamma_1 + \gamma_3, \gamma_2 + \gamma_4 \rangle = 2$, thus a $\mathcal{C}_2$ cohort is generated. As we proceed along the path, other BPS states undergo wall-crossing, generating other $\mathcal{C}_2$ cohorts. As shown in Fig. 3.10, first γ_1 generates a cohort with γ_2, then γ_3, γ_4 generate a similar cohort, finally another $m = 2$ cohort is generated by wall crossing of γ_1 and

$\gamma_2+\gamma_4$. At this point, *i.e.* within a chamber around $t = 0.95$, the spectrum can be schematically summarized as the union of four $\mathcal{C}_2$ cohorts

$$\mathcal{C}_2(\gamma_2+\gamma_4,\gamma_1+\gamma_3)\cup\mathcal{C}_2(\gamma_2,\gamma_1)\cup\mathcal{C}_2(\gamma_4,\gamma_3)\cup\mathcal{C}_2(\gamma_1,\gamma_2+\gamma_4) \tag{3.48}$$

consisting of four vectormultiplets, and infinite towers of hypermultiplets.

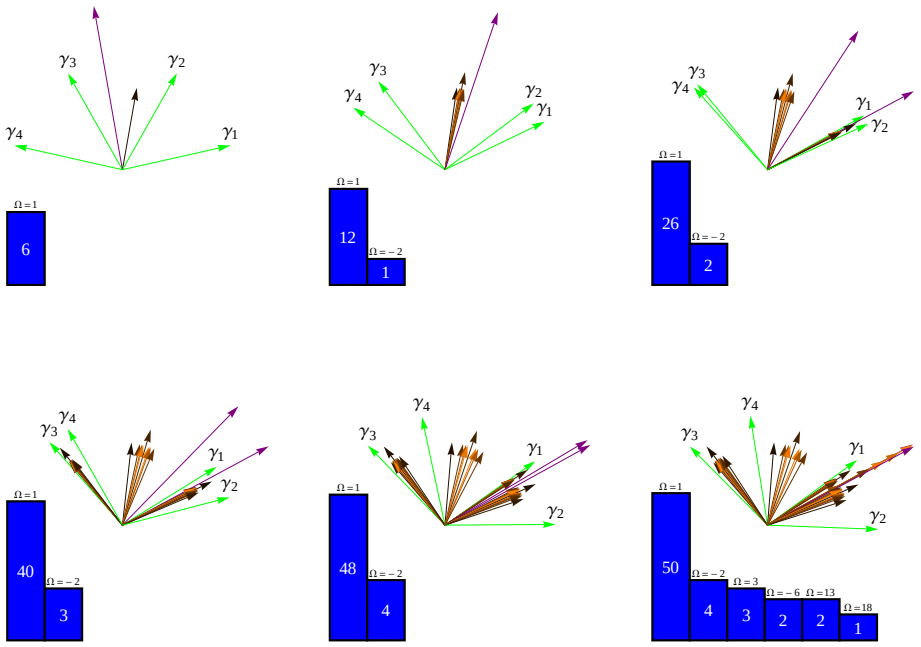

Figure 3.10: The evolution of the spectrum is illustrated. Green arrows represent the basis hypermultiplets, the purple arrows are $\gamma_2+\gamma_4$ and $2\gamma_1+\gamma_2$, the two states that generate the $m = 3$ cohort. For other charges, increasing length denotes higher $|\Omega|$ and lighter shades denote larger charges. First picture: the strong coupling chamber. Second picture: the states $\gamma_1+\gamma_3$ and $\gamma_2+\gamma_4$ have crossed and created a $\mathcal{C}_2$ cohort. Third picture: γ_2 and γ_1 cross and create another cohort. Fourth picture: the cohort generated by γ_3,γ_4. Fifth picture: $\gamma_2+\gamma_4$ and γ_1 have crossed and created a cohort. In the sixth picture $\gamma_2+\gamma_4$ and $2\gamma_1+\gamma_2$ have crossed, generating wild degeneracies.. For a video showing the full evolution of the spectrum along our path, see [3].

Proceeding further along our path, we encounter another wall of marginal stability: $\gamma_2+\gamma_4$ undergoes wall-crossing with $2\gamma_1+\gamma_2$ generating a new cohort with $m = 3$. This phenomenon has not been studied before, and deserves a detailed analysis. We anticipate here that this cohort contains distinctive new features, such as a wealth of higher spin states and a cone of densely populated BPS rays.

It is worth stressing that merely finding a point on the Coulomb branch where $Z_{\gamma_2+\gamma_4}$ approaches $Z_{2\gamma_1+\gamma_2}$ is hardly sufficient to claim that such wall-crossing happens. In addition one must make sure that such rays are populated. This is certainly the case in our example. Another important

requirement is the absence of populated rays between $Z_{\gamma_2+\gamma_4}$ and $Z_{2\gamma_1+\gamma_2}$, as we approach their mutual wall of marginal stability. We claim that there aren't any, based on two independent facts. First, at values of the moduli just before $MS(\gamma_2+\gamma_4, 2\gamma_1+\gamma_2)$, the spectral network shows simple, smooth evolution for $\operatorname{Arg} Z_{2\gamma_1+\gamma_2} < \vartheta < \operatorname{Arg} Z_{\gamma_2+\gamma_4}$, see [4]. Second, our explicit path on the Coulomb branch – together with property (3.47) of cohorts – guarantees that all boundstates created so far fall outside of the cone bounded by the central charges of $2\gamma_1+\gamma_2$, $\gamma_2+\gamma_4$: indeed if a populated boundstate were between $\gamma_2+\gamma_4$ and $2\gamma_1+\gamma_2$, it would have to be one of the following

- a boundstate of $2\gamma_1+\gamma_2$ with a charge counterclockwise of $\gamma_2+\gamma_4$
- a boundstate of $\gamma_2+\gamma_4$ with a charge clockwise of $2\gamma_1+\gamma_2$
- a boundstate of two charges lying respectively counterclockwise of $\gamma_2+\gamma_4$ and clockwise of $2\gamma_1+\gamma_2$
- a boundstate due to one of the antiparticles

All these possibilities are clearly ruled out by our explicit choice of path. Our analysis relies on the numerical evaluation of central charges at several points on the Coulomb branch, video [2] shows the smooth evolution of central charges of basis hypermultiplets along the path, ensuring that integration contours have been adapted suitably. Another important check is the following: at fixed u_2, u_3 we tune the spectral network to the phase of central charges (as predicted numerically), and we check that there are indeed degenerate networks.

3.3.4 Wall-crossings with intersections $m > 3$

So far we have encountered an MS wall of two hypermultiplets with intersection pairing 3, but there is nothing special about $m = 3$. The path proposed in (3.44) can be extended through walls of marginal stability with $m = 4, 5$, and higher. The strategy is simply to look for a direction on the Coulomb branch, along which the ray $\gamma_2+\gamma_4$ sweeps across the infinite tower of hypermultiplets with charges $(n+1)\gamma_1+n\gamma_2$.

For example, moving along a straight line from $(u_2^{(f)}, u_3^{(f)})$ to

$$u_2^{(4)} = 0.56 - 0.75i, \qquad u_3^{(4)} = 2.00 + 1.99i \tag{3.49}$$

induces wall-crossing of $\gamma_2+\gamma_4$ with $3\gamma_1+2\gamma_2$, with intersection $\langle \gamma_2+\gamma_4, 3\gamma_1+2\gamma_2\rangle = 4$. In this chamber the spectrum gains a new $m = 4$ cohort, described by the 4-Kronecker quiver.

Proceeding further, along a straight segment, to

$$u_2^{(5)} = 0.56 - 0.75i, \qquad u_3^{(5)} = 2.00 + 2.52i \tag{3.50}$$

we cross the marginal stability wall of $\gamma_2+\gamma_4$ and $4\gamma_1+3\gamma_2$, with intersection $\langle \gamma_2+\gamma_4, 4\gamma_1+3\gamma_2\rangle = 5$ generating an $m = 5$ cohort.

In the same spirit, we have checked numerically that there is a path along which $\gamma_2 + \gamma_4$ crosses all hypermultiplets with charges $(m-1)\gamma_1 + (m-2)\gamma_2$, with pairings

$$\langle \gamma_2 + \gamma_4, (m-1)\gamma_1 + (m-2)\gamma_2\rangle = m \tag{3.51}$$

hence generating an infinite tower of cohorts. The situation gets very complicated, as these cohorts will widen and start overlapping with each other, inducing further wild wall crossing.[26]. It is worth stressing that, by the same reasoning outlined for the wall-crossing of $\gamma_2 + \gamma_4$ with $2\gamma_1 + \gamma_2$, there are no populated states between $\gamma_2 + \gamma_4$ and $(m-1)\gamma_1 + (m-2)\gamma_2$ immediately before the point where they cross. This crucial fact guarantees that in this region of the Coulomb branch m-cohorts are generated, for arbitrarily high m.

Finally, we remark that a natural question arises as to whether analogous wall-crossings happen where the integer m is negative. In fact, there is a simple physical argument that such wall-crossings cannot happen on Coulomb branches of physical theories, it goes as follows. Let us consider two charges γ_1, γ_2 with $\langle \gamma_1, \gamma_2\rangle < 0$; we would like to investigate whether there could be a chamber of the Coulomb branch, bounded by $MS(\gamma_1, \gamma_2)$, where

- $\arg Z_{\gamma_2} > \arg Z_{\gamma_1}$
- $\Omega(\gamma) = 1$ for $\gamma \in \{\pm\gamma_1, \pm\gamma_2\}$
- $\Omega(\gamma) = 0$ for all other combinations $\gamma = a\gamma_1 + b\gamma_2$.

If these conditions were realized, we would be in a situation in which the spectrum generator (defined below eq. (3.54)) contains a factor $\mathcal{K}_{\gamma_2}\mathcal{K}_{\gamma_1}$, and we stress that there would be no other $\mathcal{K}$ factors between $\mathcal{K}_{\gamma_2}$ and $\mathcal{K}_{\gamma_1}$.

We claim that this cannot happen: under sufficiently general conditions, near a wall $MS(\gamma_1, \gamma_2)$ we expect Denef's multicenter equations (for the case under consideration, they are reported below

[26] As explained in the next section, the spectrum is best studied via the *spectrum generator* technique introduced in [64]. This technique is straightforwardly applicable whenever comparing two points on the Coulomb branch, such that the lattice basis vectors have corresponding central charges all contained within a half-plane. When instead one or more of the central charges exit the half-plane, one needs to account for that by suitably modifying the spectrum generator. While moving from strong coupling into these *wilder* regions, we actually incur in such a situation.

in (3.83)) to provide a reliable description of the boundstates. It is immediately evident from such description that, in the case of negative $\langle\gamma_1,\gamma_2\rangle = m$, on the side of $MS(\gamma_1,\gamma_2)$ where $\arg Z_{\gamma_2} > \arg Z_{\gamma_1}$, there will be stable boundstates of γ_1 with γ_2 populating rays between those of Z_{γ_1} and Z_{γ_2}. In particular, inside the spectrum generator, the factors $\mathcal{K}_{\gamma_2}$ and $\mathcal{K}_{\gamma_1}$ are *necessarily* separated by other factors $\mathcal{K}_{a\gamma_1+b\gamma_2}$, for $a,b>0$, violating the conditions formulated above.

Nevertheless, it makes sense to ask what the prediction of the KSWCF would be. To learn something interesting, it is actually sufficient to consider the motivic version of the primitive WCF (see [41]). From such formula, the protected spin character (see appendix A) associated to $\gamma_1+\gamma_2$ has the simple expression

$$\Omega(\gamma_1+\gamma_2;y) := Tr_{\mathfrak{h}_m}(y)^{2J_3}(-y)^{2I_3} = \frac{y^m - y^{-m}}{y-y^{-1}} \tag{3.52}$$

corresponding (not uniquely)[27] to the following exotic representations of $so(3)\oplus su(2)_R$

$$\mathfrak{h}_m = \begin{cases} \left(\frac{1}{2},\frac{1}{2}\right)\oplus(1,0) & m=-1 \\ \left(0,\frac{1}{2}\right) & m=-2 \\ \left(\frac{-m-2}{2},\frac{1}{2}\right)\oplus\left(\frac{-m-3}{2},0\right) & m\leq -3 \end{cases} . \tag{3.53}$$

Since the no-exotics theorem is in fact fairly well established for pure $SU(K)$ gauge theories [35], this further supports the argument that such wall-crossings cannot occur on the Coulomb branch.

3.4 Some Numerical Checks on the $m=3$ Wild Spectrum

The discussion of Section 3.3 is sufficient to prove that there are wild degeneracies on the Coulomb branch of the pure $SU(3)$ theory. However, since this phenomenon is somewhat novel, we have checked the results using the "spectrum generator" in some relevant regions of the Coulomb branch. This section explains those checks.

3.4.1 The spectrum generator technique

According to the KSWCF, the phase-ordered product

$$A(\lhd) =: \prod_{\gamma,\,\arg Z_\gamma\in\lhd} \mathcal{K}_\gamma^{\Omega(\gamma)} : \tag{3.54}$$

is invariant across walls of marginal stability provided no occupied BPS rays cross into or out of the angular sector $\lhd$. Considering an angle of π corresponds to a choice of the "half plane of particles". Once this choice is made, $A(\pi)$ is called a [28] *spectrum generator* and denoted $\mathbb{S}$ [64].

[27] Albeit necessarily involving exotic representations.

[28] Several equivalent choices are related by how one chooses the half-plane in the complex plane of central charges.

The idea of the "spectrum generator technique" is that if - through some means or other - one can compute $A(\pi)$, then, by factorization one can deduce the spectrum (after computing the phase ordering of the Z_γ at that point). For example in [64] an algorithm is given for computing $A(\pi)$ without an *a priori* knowledge of the spectrum. Here our strategy will be a little different. We will derive the spectrum generator in the strong coupling chamber, where the spectrum can be easily read off from the spectral network or from quiver techniques. We then use wall-crossing to argue that $A(\pi)$ is unchanged along a particular path in the Coulomb branch (described in Section 3.3) to the wild region. Then we factorize the spectrum generator at points along that path.

An effective technique for factorizing $\mathbb{S}$ is the following. Let $\{\gamma_i\}_{i=1,\ldots,k}$ be a basis for the lattice of charges Γ, and let $\gamma = \sum a_i\gamma_i$, with $a_i > 0$. Define the height $|\gamma| := \sum_i a_i$, and $\mathbb{S}^{(r)} =: \prod_{\gamma,|\gamma|\leq r} \mathcal{K}_\gamma^{\Omega(\gamma)}$:[29]. The full spectrum generator $\mathbb{S}$ can then be factorized by studying its action on the basis formal variables[30] Y_{γ_i} for increasing values of r, by employing

$$Y_{-\gamma_i}(\mathbb{S} - \tilde{\mathbb{S}}^{(r)})Y_{\gamma_i} = -\sum_{|\gamma'|=r+1} \langle\gamma_i,\gamma'\rangle\Omega(\gamma')Y_{\gamma'} + \ldots \tag{3.55}$$

where $\tilde{\mathbb{S}}$ represents the factorization of the spectrum generator under study. The ellipses contain terms with $Y_\gamma, |\gamma| > r+1$.

3.4.2 Factorizing the spectrum generator

The spectrum in the strong coupling region can be obtained via spectral network techniques, as discussed in Section 3.3.1. According to the results presented there, the spectrum generator is

$$\mathbb{S} = \mathcal{K}_{\gamma_4}\mathcal{K}_{\gamma_3}\mathcal{K}_{\gamma_2+\gamma_4}\mathcal{K}_{\gamma_1+\gamma_3}\mathcal{K}_{\gamma_2}\mathcal{K}_{\gamma_1}, \tag{3.56}$$

in agreement with [12, 63].

We now fix a point on our path

$$u_2 = 0.56 - 0.73i, \quad u_3 = 1.94 + 1.49i, \tag{3.57}$$

corresponding to the situation exhibited in (3.48) immediately before the wall $\mathrm{MS}(\gamma_2+\gamma_4, 2\gamma_1+\gamma_2)$. The central charges corresponding to the simple roots are

$$\begin{aligned} Z_{\gamma_1} &= 8.42972 + 6.00549i \qquad Z_{\gamma_2} = 4.83278 - 0.0226871i \\ Z_{\gamma_3} &= -7.30679 + 7.50651i \quad Z_{\gamma_4} = -0.504898 + 2.53401i\,, \end{aligned} \tag{3.58}$$

[29] Recall that the ordering depends crucially on the position u on the Coulomb branch, hence we should really write $\mathbb{S}^{(r)}(u)$. To lighten the notation we do not indicate the u-dependence.

[30] i.e., it is sufficient to work with formal variables corresponding to a choice of simple roots for the lattice of charges. The choice of simple roots must be consistent with the choice of half-plane that comes with the spectrum generator.

the factorization of the spectrum generator up to $|\gamma| = 21$ reads[31]

$$\begin{aligned}
&\mathcal{K}_{\gamma_3}\mathcal{K}_{2\gamma_3+\gamma_4}\mathcal{K}_{3\gamma_3+2\gamma_4}\mathcal{K}_{4\gamma_3+3\gamma_4}\mathcal{K}_{5\gamma_3+4\gamma_4}\mathcal{K}_{6\gamma_3+5\gamma_4}\mathcal{K}_{7\gamma_3+6\gamma_4}\mathcal{K}_{8\gamma_3+7\gamma_4}\mathcal{K}_{9\gamma_3+8\gamma_4}\\
&\mathcal{K}_{10\gamma_3+9\gamma_4}\mathcal{K}_{11\gamma_3+10\gamma_4}\mathcal{K}^{-2}_{\gamma_3+\gamma_4}\mathcal{K}_{10\gamma_3+11\gamma_4}\mathcal{K}_{9\gamma_3+10\gamma_4}\mathcal{K}_{8\gamma_3+9\gamma_4}\mathcal{K}_{7\gamma_3+8\gamma_4}\mathcal{K}_{6\gamma_3+7\gamma_4}\\
&\mathcal{K}_{5\gamma_3+6\gamma_4}\mathcal{K}_{4\gamma_3+5\gamma_4}\mathcal{K}_{3\gamma_3+4\gamma_4}\mathcal{K}_{2\gamma_3+3\gamma_4}\mathcal{K}_{\gamma_3+2\gamma_4}\mathcal{K}_{\gamma_4}\mathcal{K}_{\gamma_1+\gamma_3}\mathcal{K}_{2\gamma_1+\gamma_2+2\gamma_3+\gamma_4}\\
&\mathcal{K}_{3\gamma_1+2\gamma_2+3\gamma_3+2\gamma_4}\mathcal{K}_{4\gamma_1+3\gamma_2+4\gamma_3+3\gamma_4}\mathcal{K}_{5\gamma_1+4\gamma_2+5\gamma_3+4\gamma_4}\mathcal{K}^{-2}_{\gamma_1+\gamma_2+\gamma_3+\gamma_4}\mathcal{K}_{4\gamma_1+5\gamma_2+4\gamma_3+5\gamma_4}\\
&\mathcal{K}_{3\gamma_1+4\gamma_2+3\gamma_3+4\gamma_4}\mathcal{K}_{2\gamma_1+3\gamma_2+2\gamma_3+3\gamma_4}\mathcal{K}_{\gamma_1+2\gamma_2+\gamma_3+2\gamma_4}\mathcal{K}_{\gamma_1}\mathcal{K}_{2\gamma_1+\gamma_2+\gamma_4}\mathcal{K}_{3\gamma_1+2\gamma_2+2\gamma_4}\\
&\mathcal{K}_{4\gamma_1+3\gamma_2+3\gamma_4}\mathcal{K}_{5\gamma_1+4\gamma_2+4\gamma_4}\mathcal{K}_{6\gamma_1+5\gamma_2+5\gamma_4}\mathcal{K}_{7\gamma_1+6\gamma_2+6\gamma_4}\mathcal{K}^{-2}_{\gamma_1+\gamma_2+\gamma_4}\mathcal{K}_{6\gamma_1+7\gamma_2+7\gamma_4}\\
&\mathcal{K}_{5\gamma_1+6\gamma_2+6\gamma_4}\mathcal{K}_{4\gamma_1+5\gamma_2+5\gamma_4}\mathcal{K}_{3\gamma_1+4\gamma_2+4\gamma_4}\mathcal{K}_{2\gamma_1+3\gamma_2+3\gamma_4}\mathcal{K}_{\gamma_1+2\gamma_2+2\gamma_4}\mathcal{K}_{\gamma_2+\gamma_4}\\
&\mathcal{K}_{2\gamma_1+\gamma_2}\mathcal{K}_{3\gamma_1+2\gamma_2}\mathcal{K}_{4\gamma_1+3\gamma_2}\mathcal{K}_{5\gamma_1+4\gamma_2}\mathcal{K}_{6\gamma_1+5\gamma_2}\mathcal{K}_{7\gamma_1+6\gamma_2}\mathcal{K}_{8\gamma_1+7\gamma_2}\mathcal{K}_{9\gamma_1+8\gamma_2}\\
&\mathcal{K}_{10\gamma_1+9\gamma_2}\mathcal{K}_{11\gamma_1+10\gamma_2}\mathcal{K}^{-2}_{\gamma_1+\gamma_2}\mathcal{K}_{10\gamma_1+11\gamma_2}\mathcal{K}_{9\gamma_1+10\gamma_2}\mathcal{K}_{8\gamma_1+9\gamma_2}\mathcal{K}_{7\gamma_1+8\gamma_2}\mathcal{K}_{6\gamma_1+7\gamma_2}\\
&\mathcal{K}_{5\gamma_1+6\gamma_2}\mathcal{K}_{4\gamma_1+5\gamma_2}\mathcal{K}_{3\gamma_1+4\gamma_2}\mathcal{K}_{2\gamma_1+3\gamma_2}\mathcal{K}_{\gamma_1+2\gamma_2}\mathcal{K}_{\gamma_2}
\end{aligned} \tag{3.59}$$

The spectrum exhibits four $m = 2$ cohorts, as expected from the discussion of Section 3.3.3: they include four vectormultiplets (with $\Omega = -2$), accompanied by infinite towers of hypermultiplets.

On the other side of the $m = 3$ wall, at

$$u_2 = 0.56 - 0.75i,\ u_3 = 2.00 + 1.52i, \tag{3.60}$$

central charges read

$$\begin{aligned}
Z_{\gamma_1} &= 8.52337 + 6.18454i \qquad Z_{\gamma_2} = 4.89813 - 0.18347i\\
Z_{\gamma_3} &= -7.43876 + 7.53531i \quad Z_{\gamma_4} = -0.410809 + 2.59321i.
\end{aligned} \tag{3.61}$$

[31] Color code: The factors in blue come from the hypermultiplets of the strong coupling chamber. The factors in red come from vectormultiplets. The remaining factors in black are hypermultiplets created by the wall-crossing from the strong coupling chamber.

The spectrum generator, up to $|\gamma| = 21$, is

$$
\begin{aligned}
&\mathcal{K}_{\gamma_3}\mathcal{K}_{2\gamma_3+\gamma_4}\mathcal{K}_{3\gamma_3+2\gamma_4}\mathcal{K}_{4\gamma_3+3\gamma_4}\mathcal{K}_{5\gamma_3+4\gamma_4}\mathcal{K}_{6\gamma_3+5\gamma_4}\mathcal{K}_{7\gamma_3+6\gamma_4}\mathcal{K}_{8\gamma_3+7\gamma_4}\mathcal{K}_{9\gamma_3+8\gamma_4}\\
&\mathcal{K}_{10\gamma_3+9\gamma_4}\mathcal{K}_{11\gamma_3+10\gamma_4}\mathcal{K}^{-2}_{\gamma_3+\gamma_4}\mathcal{K}_{10\gamma_3+11\gamma_4}\mathcal{K}_{9\gamma_3+10\gamma_4}\mathcal{K}_{8\gamma_3+9\gamma_4}\mathcal{K}_{7\gamma_3+8\gamma_4}\mathcal{K}_{6\gamma_3+7\gamma_4}\\
&\mathcal{K}_{5\gamma_3+6\gamma_4}\mathcal{K}_{4\gamma_3+5\gamma_4}\mathcal{K}_{3\gamma_3+4\gamma_4}\mathcal{K}_{2\gamma_3+3\gamma_4}\mathcal{K}_{\gamma_3+2\gamma_4}\mathcal{K}_{\gamma_4}\mathcal{K}_{\gamma_1+\gamma_3}\mathcal{K}_{2\gamma_1+\gamma_2+2\gamma_3+\gamma_4}\\
&\mathcal{K}_{3\gamma_1+2\gamma_2+3\gamma_3+2\gamma_4}\mathcal{K}_{4\gamma_1+3\gamma_2+4\gamma_3+3\gamma_4}\mathcal{K}_{5\gamma_1+4\gamma_2+5\gamma_3+4\gamma_4}\mathcal{K}^{-2}_{\gamma_1+\gamma_2+\gamma_3+\gamma_4}\mathcal{K}_{4\gamma_1+5\gamma_2+4\gamma_3+5\gamma_4}\\
&\mathcal{K}_{3\gamma_1+4\gamma_2+3\gamma_3+4\gamma_4}\mathcal{K}_{2\gamma_1+3\gamma_2+2\gamma_3+3\gamma_4}\mathcal{K}_{\gamma_1+2\gamma_2+\gamma_3+2\gamma_4}\mathcal{K}_{\gamma_1}\mathcal{K}_{2\gamma_1+\gamma_2+\gamma_4}\mathcal{K}_{3\gamma_1+2\gamma_2+2\gamma_4}\\
&\mathcal{K}_{4\gamma_1+3\gamma_2+3\gamma_4}\mathcal{K}_{5\gamma_1+4\gamma_2+4\gamma_4}\mathcal{K}_{6\gamma_1+5\gamma_2+5\gamma_4}\mathcal{K}_{7\gamma_1+6\gamma_2+6\gamma_4}\mathcal{K}^{-2}_{\gamma_1+\gamma_2+\gamma_4}\mathcal{K}_{6\gamma_1+7\gamma_2+7\gamma_4}\\
&\mathcal{K}_{5\gamma_1+6\gamma_2+6\gamma_4}\mathcal{K}_{4\gamma_1+5\gamma_2+5\gamma_4}\mathcal{K}_{3\gamma_1+4\gamma_2+4\gamma_4}\mathcal{K}_{2\gamma_1+3\gamma_2+3\gamma_4}\mathcal{K}_{\gamma_1+2\gamma_2+2\gamma_4}\mathcal{K}_{2\gamma_1+\gamma_2}\\
&\mathcal{K}_{6\gamma_1+4\gamma_2+\gamma_4}\mathcal{K}^{3}_{10\gamma_1+7\gamma_2+2\gamma_4}\mathcal{K}^{3}_{4\gamma_1+3\gamma_2+\gamma_4}\mathcal{K}^{-6}_{8\gamma_1+6\gamma_2+2\gamma_4}\mathcal{K}^{68}_{10\gamma_1+8\gamma_2+3\gamma_4}\mathcal{K}^{13}_{6\gamma_1+5\gamma_2+2\gamma_4}\\
&\mathcal{K}^{68}_{8\gamma_1+7\gamma_2+3\gamma_4}\mathcal{K}^{18}_{6\gamma_1+6\gamma_2+3\gamma_4}\mathcal{K}^{3}_{2\gamma_1+2\gamma_2+\gamma_4}\mathcal{K}^{-6}_{4\gamma_1+4\gamma_2+2\gamma_4}\mathcal{K}^{-84}_{8\gamma_1+8\gamma_2+4\gamma_4}\mathcal{K}^{68}_{6\gamma_1+7\gamma_2+4\gamma_4}\\
&\mathcal{K}^{13}_{4\gamma_1+5\gamma_2+3\gamma_4}\mathcal{K}^{68}_{6\gamma_1+8\gamma_2+5\gamma_4}\mathcal{K}^{18}_{6\gamma_1+9\gamma_2+6\gamma_4}\mathcal{K}^{3}_{2\gamma_1+3\gamma_2+2\gamma_4}\mathcal{K}^{-6}_{4\gamma_1+6\gamma_2+4\gamma_4}\\
&\mathcal{K}^{3}_{4\gamma_1+7\gamma_2+5\gamma_4}\mathcal{K}_{2\gamma_1+4\gamma_2+3\gamma_4}\mathcal{K}_{\gamma_2+\gamma_4}\mathcal{K}_{3\gamma_1+2\gamma_2}\mathcal{K}_{4\gamma_1+3\gamma_2}\mathcal{K}_{5\gamma_1+4\gamma_2}\mathcal{K}_{6\gamma_1+5\gamma_2}\mathcal{K}_{7\gamma_1+6\gamma_2}\\
&\mathcal{K}_{8\gamma_1+7\gamma_2}\mathcal{K}_{9\gamma_1+8\gamma_2}\mathcal{K}_{10\gamma_1+9\gamma_2}\mathcal{K}_{11\gamma_1+10\gamma_2}\mathcal{K}^{-2}_{\gamma_1+\gamma_2}\mathcal{K}_{10\gamma_1+11\gamma_2}\mathcal{K}_{9\gamma_1+10\gamma_2}\mathcal{K}_{8\gamma_1+9\gamma_2}\\
&\mathcal{K}_{7\gamma_1+8\gamma_2}\mathcal{K}_{6\gamma_1+7\gamma_2}\mathcal{K}_{5\gamma_1+6\gamma_2}\mathcal{K}_{4\gamma_1+5\gamma_2}\mathcal{K}_{3\gamma_1+4\gamma_2}\mathcal{K}_{2\gamma_1+3\gamma_2}\mathcal{K}_{\gamma_1+2\gamma_2}\mathcal{K}_{\gamma_2},
\end{aligned}
\tag{3.62}
$$

where $\mathcal{K}$-factors in green are those of the newborn $m = 3$ cohort. Notice the large values of Ω.

Both formulae (3.59), (3.62) can be recast in more suggestive forms by adopting the notation[32]

$$
\Pi^{(n,m)}(a,b) := \left(\prod_{k\nearrow n}^{\infty} \mathcal{K}_{(k+1)a+kb}\right) \mathcal{K}^{-2}_{a+b} \left(\prod_{\ell\searrow m}^{\infty} \mathcal{K}_{\ell a+(\ell+1)b}\right) \tag{3.63}
$$

Expression (3.59) is then simply the truncation to $|\gamma| = 21$ of (cf. (3.48))

$$
\Pi^{(0,0)}(\gamma_3,\gamma_4)\ \Pi^{(0,1)}(\gamma_1+\gamma_3,\gamma_2+\gamma_4)\ \Pi^{(0,0)}(\gamma_1,\gamma_2+\gamma_4)\ \Pi^{(1,0)}(\gamma_1,\gamma_2) \tag{3.64}
$$

Similarly, for (3.62) we have

$$
\begin{aligned}
&\Pi^{(0,0)}(\gamma_3,\gamma_4)\ \Pi^{(0,1)}(\gamma_1+\gamma_3,\gamma_2+\gamma_4)\ \Pi^{(0,1)}(\gamma_1,\gamma_2+\gamma_4)\\
&\Xi(2\gamma_1+\gamma_2,\gamma_2+\gamma_4)\ \Pi^{(2,0)}(\gamma_1,\gamma_2)
\end{aligned}
\tag{3.65}
$$

where $\Xi(2\gamma_1+\gamma_2,\gamma_2+\gamma_4)$ represents the contribution from the full $\mathcal{C}_3(2\gamma_1+\gamma_2,\gamma_2+\gamma_4)$ cohort, which we now analyze in greater detail.

[32] We adopt the following conventions: a product of noncommutative factors $\prod_{k\nearrow a}^{b}$ indicates that values of k increase from left to right between a and b, while $\prod_{k\searrow a}^{b}$ denotes decreasing values of k from left to right.

3.4.3 Exponential growth of the BPS degeneracies

We now focus on the part of BPS spectrum within the cohort $\mathcal{C}_3(\gamma_2+\gamma_4, 2\gamma_1+\gamma_2)$. Let

$$\mathcal{K}_{(a,b)} \equiv \mathcal{K}_{a(2\gamma_1+\gamma_2)+b(\gamma_2+\gamma_4)}, \qquad a,b\in\mathbb{Z}, \tag{3.66}$$

then, up to $a+b=15$, $\Xi(2\gamma_1+\gamma_2,\gamma_2+\gamma_4)$ reads

$$\begin{aligned}
&\mathcal{K}_{(1,0)}\mathcal{K}_{(3,1)}\mathcal{K}_{(8,3)}\mathcal{K}^{-6}_{(10,4)}\mathcal{K}^{3}_{(5,2)}\mathcal{K}^{13}_{(7,3)}\mathcal{K}^{68}_{(9,4)}\mathcal{K}^{465}_{(10,5)}\mathcal{K}^{-84}_{(8,4)}\mathcal{K}^{18}_{(6,3)}\\
&\mathcal{K}^{-6}_{(4,2)}\mathcal{K}^{3}_{(2,1)}\mathcal{K}^{2530}_{(9,5)}\mathcal{K}^{399}_{(7,4)}\mathcal{K}^{68}_{(5,3)}\mathcal{K}^{4242}_{(8,5)}\mathcal{K}^{34227}_{(9,6)}\mathcal{K}^{-478}_{(6,4)}\mathcal{K}^{13}_{(3,2)}\mathcal{K}^{4242}_{(7,5)}\\
&\mathcal{K}^{-32050}_{(8,6)}\mathcal{K}^{68}_{(4,3)}\mathcal{K}^{399}_{(5,4)}\mathcal{K}^{2530}_{(6,5)}\mathcal{K}^{16965}_{(7,6)}\mathcal{K}^{118668}_{(8,7)}\mathcal{K}^{18123}_{(7,7)}\mathcal{K}^{-2808}_{(6,6)}\mathcal{K}^{465}_{(5,5)}\\
&\mathcal{K}^{-84}_{(4,4)}\mathcal{K}^{18}_{(3,3)}\mathcal{K}^{-6}_{(2,2)}\mathcal{K}^{3}_{(1,1)}\mathcal{K}^{118668}_{(7,8)}\mathcal{K}^{16965}_{(6,7)}\mathcal{K}^{2530}_{(5,6)}\mathcal{K}^{399}_{(4,5)}\mathcal{K}^{-32050}_{(6,8)}\mathcal{K}^{68}_{(3,4)}\\
&\mathcal{K}^{4242}_{(5,7)}\mathcal{K}^{34227}_{(6,9)}\mathcal{K}^{-478}_{(4,6)}\mathcal{K}^{13}_{(2,3)}\mathcal{K}^{4242}_{(5,8)}\mathcal{K}^{68}_{(3,5)}\mathcal{K}^{399}_{(4,7)}\mathcal{K}^{2530}_{(5,9)}\mathcal{K}^{465}_{(5,10)}\mathcal{K}^{-84}_{(4,8)}\\
&\mathcal{K}^{18}_{(3,6)}\mathcal{K}^{-6}_{(2,4)}\mathcal{K}^{3}_{(1,2)}\mathcal{K}^{68}_{(4,9)}\mathcal{K}^{13}_{(3,7)}\mathcal{K}^{-6}_{(4,10)}\mathcal{K}^{3}_{(2,5)}\mathcal{K}_{(3,8)}\mathcal{K}_{(1,3)}\mathcal{K}_{(0,1)}
\end{aligned} \tag{3.67}$$

The BPS degeneracies appearing in (3.67) look rather *wild* at first sight. One way of looking at them is to consider sequences of charges (a_0+na, b_0+nb) approaching different "slopes" a/b for $n\to\infty$, and study the asymptotics of Ω for large n. As illustrated in figure 3.11, the BPS index grows exponentially with n, the asymptotic exponential behavior depends entirely on a/b and not on a_0, b_0.

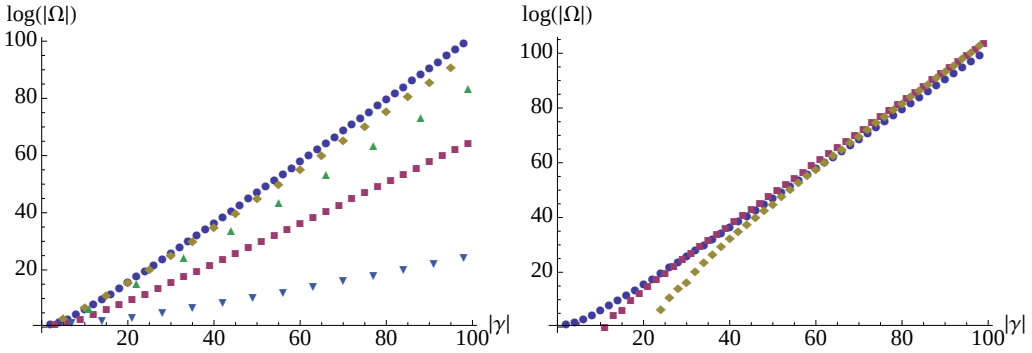

Figure 3.11: Left: values of $\log\Omega(an,bn)$ for several slopes a/b: 1 (circles), 3/2 (diamonds), 7/4 (up-triangles), 2 (squares), 5/2 (down-triangles). Right: sequences of type (a_0+an, b_0+bn) have the same asymptotics; here we show $a=b=1$ with $a_0-b_0=0,5,10$.

According to the positivity conjecture discussed below equation (A.4), BPS indices count dimensions of Hilbert subspaces, as stated more precisely in (3.95). Such exponential growth in the number of states may seem surprising in the context of a gauge theory. We will return to the physical implications below, in Section 3.6.

3.5 Relation to quivers

In addition to spectral networks, one alternative route to the BPS spectrum is the dual description in terms of quiver quantum mechanics [12, 39, 40]. The problem of counting BPS states gets mapped into that of counting cohomology classes of moduli spaces of quiver representations. These classes are organized into Lefschetz multiplets, which correspond to the $\mathfrak{so}(3)$ multiplets. The PSC $\Omega(\gamma, u; y)$ is then given by the Poincaré polynomial associated to a certain quiver representation.

The basic observation here is that an isolated wall-crossing of hypermultiplets with charges γ, γ' such that $\langle \gamma, \gamma' \rangle = m$ will produce the spectrum of the Kronecker m-quiver in the wild stability region.

3.5.1 Derivation of the Kronecker m-quivers from the strong coupling regime

Here we briefly describe how the quiver description fits in our study of the BPS spectrum of this theory. We start in the strong coupling chamber: we choose a half-plane as shown in the first frame of figure 3.12, the corresponding BPS quiver is shown in the second frame of the same figure. As we move along the path (3.44), we come to the situation shown in the third frame of figure 3.12: three MS walls have been crossed, and the corresponding $m = 2$ cohorts are indicated (this corresponds to the situation shown in the fifth frame of figure 3.10 above.). Note that no walls of the second kind[33] have been crossed, hence the same BPS quiver is still valid.

Now, while keeping the moduli fixed, we rotate the half-plane clockwise inducing a mutation on

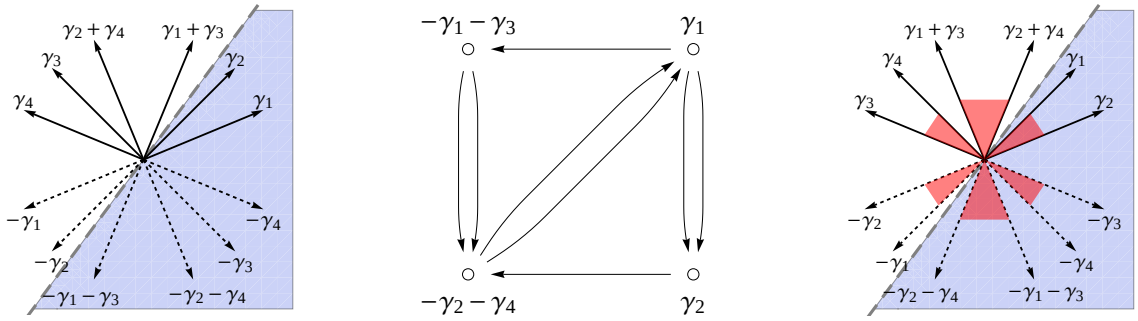

Figure 3.12: Left: the disposition of charges and choice of half plane in the strong coupling chamber. The depiction of the central charges is schematic. Center: the quiver at strong coupling. Right: central charges and cohorts after crossing the first three MS walls along our path.

the quiver, as shown in the first two frames of figure 3.13. We then proceed a little further along our path on $\mathcal{B}$, until we cross the wall $MS(\gamma_1, \gamma_2 + \gamma_4)$, again this does not involve crossing walls of

[33] In the physics literature, a wall of the second kind is, roughly speaking, the locus on the moduli space where the central charge of a populated state *exits* the half-plane associated with the quiver under study. When this happens, the quiver description changes by a mutation, for more details, see [12].

the second kind, and the same quiver is still valid. The charge disposition and cohorts are shown in the third frame of figure 3.13.

Finally, we rotate the half-plane counterclockwise, as shown in figure 3.14, inducing an inverse

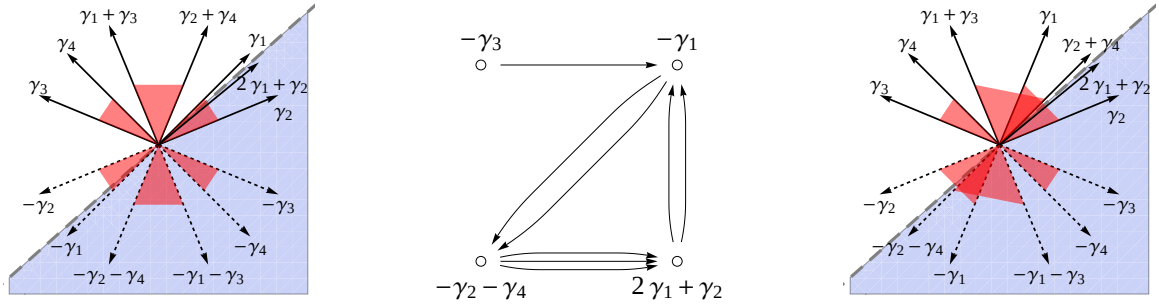

Figure 3.13: Left: a clockwise rotation of the half-plane past the ray Z_{γ_1}. Center: the corresponding BPS quiver. Right: after proceeding further on $\mathcal{B}$ we cross $MS(\gamma_1, \gamma_2+\gamma_4)$

mutation on the node $-\gamma_2-\gamma_4$, which results in the desired BPS quiver.

The two lower nodes of the quiver we just obtained manifestly exhibit the 3-Kronecker quiver

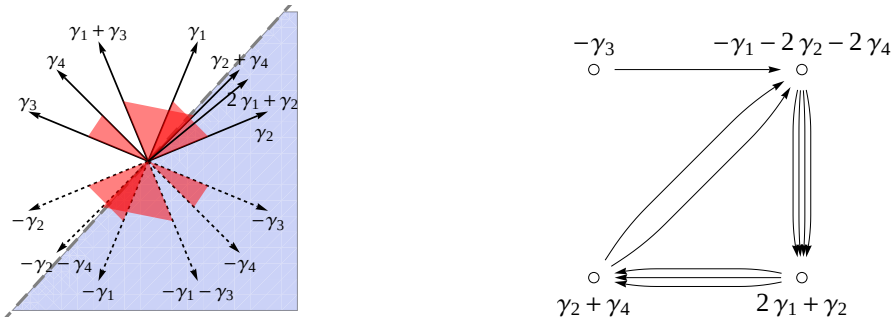

Figure 3.14: Left: a counterclockwise rotation past $Z_{\gamma_2+\gamma_4}$. Right: the corresponding BPS quiver.

involved in wild wall-crossing as a subquiver. In particular, it offers a convenient starting point for studying stable quiver representations on both sides of $MS(\gamma_2+\gamma_4, 2\gamma_1+\gamma_2)$: states with charge $a(\gamma_2+\gamma_4)+b(2\gamma_1+\gamma_2)$ correspond to particularly simple dimension vectors, in which the two upper nodes decouple leaving the pure 3-Kronecker quiver. We will not pursue the stability analysis in this paper, let us stress however that, since we have been working with stability parameters constrained by special geometry on the Coulomb branch (as opposed to working in $\mathbb{C}^4$), it should be possible to perform such analysis on both sides of the above-mentioned MS wall, thus recovering the related wild degeneracies.

The above construction generalizes easily to higher m. Consider indeed the situation in frame three of Figure 3.13: here one could rotate the half-plane clockwise up until crossing the ray of

$\gamma^{(j+1,j)} := (j+1)\gamma_1 + j\gamma_2$, resulting in a sequence of mutations leading to the quiver of Figure 3.15. Then, without crossing walls of the second kind, one can move on $\mathcal{B}$ on a continuation of our path, as discussed in Section 3.3.4, until getting past $MS((j+1)\gamma_1 + j\gamma_2, \gamma_2 + \gamma_4)$, the same quiver description still holds.

At this point, a counterclockwise rotation of the half-plane, corresponding to an inverse mutation

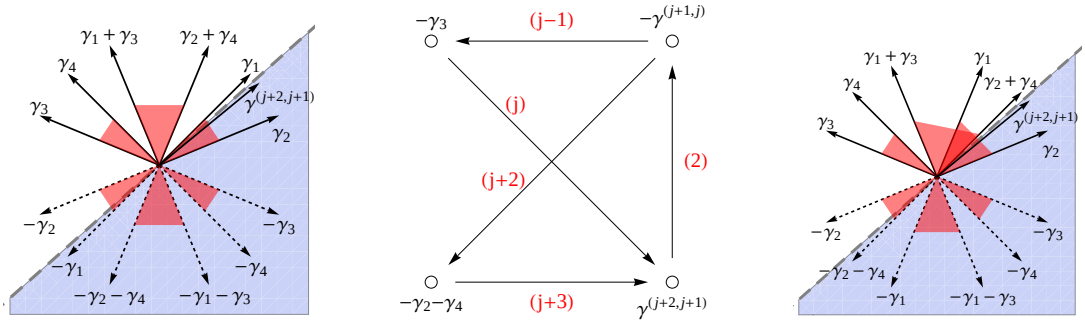

Figure 3.15: Left: a clockwise rotation of the half-plane past the ray $Z_{(j+1)\gamma_1+j\gamma_2}$. Center: the corresponding BPS quiver, arrow multiplicities are indicated in red. Right: after proceeding further on $\mathcal{B}$ we cross $MS((j+1)\gamma_1 + j\gamma_2, \gamma_2 + \gamma_4)$

on $-\gamma_2 - \gamma_4$ yields the quiver given in Figure 3.16. Again the two lower nodes exhibit the Kronecker subquiver of interest.

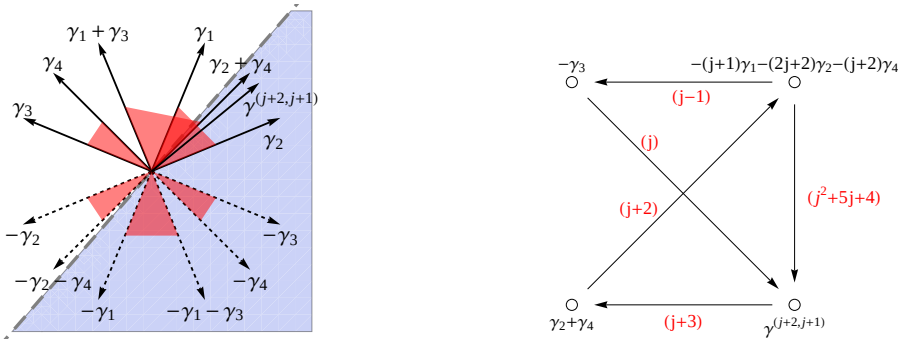

Figure 3.16: Left: a counter-clockwise rotation of the half-plane past the ray $Z_{\gamma_2+\gamma_4}$. Right: the corresponding BPS quiver, with arrow multiplicities indicated in red.

3.5.2 A nontrivial symmetry of BPS degeneracies

One very nice application of the quiver approach is that it reveals an intriguing symmetry of BPS degeneracies which would be very hard to discover using spectral networks.

Our previous analysis of the $\mathcal{C}_3$ spectrum has focused on sequences of states $(na + a_0)\gamma_1 + (nb + b_0)\gamma_2$ with fixed slope a/b as $n \to \infty$. In this section we will instead consider sequences of states

with the same BPS index.

In full generality, given two hypermultiplets with charges γ, γ' such that $\langle \gamma, \gamma' \rangle = m > 0$, we know already from the semi-primitive WCF that, across the wall $MS(\gamma, \gamma')$, a new hypermultiplet of charge $\gamma + m\gamma'$ will be a stable boundstate. The constituents γ, γ', as well as their CPT conjugates will also be stable. Now, note that $\langle -\gamma', \gamma + m\gamma' \rangle = m$, moreover we have the following relation between stability parameters

$$\text{sign}\left(\text{Im}\frac{Z_\gamma}{Z_{\gamma'}}\right) \equiv \text{sign}\left(\text{Im}\frac{Z_{-\gamma'}}{Z_{\gamma+m\gamma'}}\right). \tag{3.68}$$

Thus, any boundstate of γ, γ' can *equivalently* be described as a boundstate of $-\gamma', \gamma + m\gamma'$. Such change of *simple roots* for the $K(m)$ quiver simply corresponds[34] to a change of duality frame by

$$g_m = \begin{pmatrix} 0 & 1 \\ -1 & m \end{pmatrix} \quad \in Sp(2, \mathbb{Z}) \tag{3.69}$$

in a basis where γ, γ' are represented by column vectors $(1, 0), (0, 1)$ respectively. That is, there is a mutation of the quiver corresponding to the change of basis g_m. Since this is detectable by the semiprimitive wall crossing formula there should be a halo interpretation, see [73] for further discussion on this point.

The above is essentially an observation of [128] and it immediately implies some remarkable identities for BPS indices. The group

$$\mathcal{R} = \langle h, h' | h^2 = 1, {h'}^2 = 1 \rangle \; = \; \mathbb{Z}_2 \star \mathbb{Z}_2 \tag{3.70}$$

has an action on $\mathbb{Z}\gamma \oplus \mathbb{Z}\gamma'$ by

$$h = \begin{pmatrix} 0 & 1 \\ 1 & 0 \end{pmatrix}, \quad h' = \begin{pmatrix} -1 & m \\ 0 & 1 \end{pmatrix}, \quad g_m = h\, h', \tag{3.71}$$

then the BPS indices must have the symmetry:

$$\Omega(g \cdot \gamma) = \Omega(\gamma), \quad \forall g \in \mathcal{R}. \tag{3.72}$$

In other words, the spectrum can be organized into orbits of $\mathcal{R}$.

Remarks

- The identity (3.72) extends to the protected spin character

$$\Omega(g \cdot \gamma; y) = \Omega(\gamma; y). \tag{3.73}$$

[34] In the mathematics literature this correspondence is a known isomorphism among Kronecker moduli spaces, see for example [128], Remark 3.2.

- Consider for example $m = 3$, we call the *slope* of (a, b) the ratio a/b. The eigenvalues of g_3 are

$$\xi_{\pm} = \frac{3 \pm \sqrt{5}}{2} \tag{3.74}$$

  corresponding to the slopes limiting the cone of dense states of Fig. 3.17. All g_3 orbits are confined to lie either inside or outside of the cone, and asymptote to the limiting rays.

- The only orbits falling outside of the cone are those of "pure" hypermultiplets i.e. states with $\Omega = 1$. All the other orbits are contained within the cone.

- In the pure $SU(2)$ theory the limiting rays of the g_2 cone collapse into a single ray, which coincides with the slope of the gauge boson. In that context, the g_2 action has an interpretation in terms of a half-turn around the strong coupling chamber, combined with the residual R-symmetry, in a similar spirit to the approach of [21]. One can check that, in a suitable duality frame g_2 is a square root of the monodromy at infinity, up to an overall factor.

  For the $m = 1$ Kronecker quiver, the g_1 action simply recovers the whole spectrum.

3.5.3 Asymptotics of BPS degeneracies

For physical reasons we are often interested in the asymptotics of BPS degeneracies for large charges. There is no known simple closed formula for the degeneracies $\Omega(a\gamma_1 + b\gamma_2)$ of the 3-Kronecker quiver. In this section we discuss some aspects of the large a, b asymptotics.

The Poincaré polynomial for quivers without closed loops has been found explicitly in a closed form, as a sum over constrained partitions of corresponding quiver dimension vectors [117]. Unfortunately Reineke's formula does not lend itself well to an evaluation of the large charge asymptotics. On the other hand, use of localization techniques allows one to estimate asymptotic behavior of the Euler characteristic for moduli spaces of m-Kronecker quiver representations [127].

Weist conjectured the following. Consider a state $N\gamma + M\gamma'$ with $\langle \gamma, \gamma' \rangle = m$, in a wild region of the Coulomb branch. The corresponding BPS index equals the Euler characteristic of the moduli space of the quiver with m arrows between two nodes with spaces $\mathbb{C}^N$ and $\mathbb{C}^M$ in a wild region of stability parameters. Now consider a sequence of dimension vectors $N = an + a_0$, $M = bn + b_0$, with a, b, a_0, b_0 fixed. Weist conjectured that the asymptotic behavior of the Euler characteristic has the form

$$\begin{aligned} &\log |\Omega(N\gamma + M\gamma')| \underset{n\to\infty}{\sim} n\, C_{a,b}(m) \\ &C_{a,b}(m) = \frac{\sqrt{mab - a^2 - b^2}}{\sqrt{m-2}} \left[(m-1)^2 \log(m-1)^2 - (m^2 - 2m) \log\left(m^2 - 2m\right)\right] \end{aligned} \tag{3.75}$$

Note that $C_{1,1}(m) = c_m$ of equation (3.40).

3.5.4 Numerical check of Weist's conjecture

In section 3.4 we obtained BPS degeneracies by using an algorithmic approach, based on the KSWCF (3.46). The results are in agreement with [75]: in particular we found a sequence of degeneracies of slope 1 behaving as predicted by Reineke in [115], as well as a highly populated – suggesting dense – cone of "wild" BPS states in the complex Z_γ-plane. The region outside such cone is populated by hypermultiplets only, falling in sequences approaching the boundaries of the cone, as shown in figure 3.17.

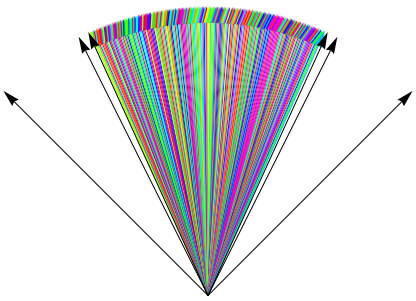

Figure 3.17: Schematic picture of BPS states charges for 3-Kronecker quiver. A dense cone is bounded by rays of slopes $a/b = (3 \pm \sqrt{5})/2$. Only hypermultiplets fall out of the cone.

Let $\gamma_{a,b}(n) = (na + a_0)\gamma_1 + (nb + b_0)\gamma_2$. Denoting by

$$\eta_{a,b} := \log |\Omega(\gamma_{a,b}(n))| \sqrt{\frac{m-2}{mab - a^2 - b^2}}, \tag{3.76}$$

Weist's conjecture says that $\eta_{ab}/n \to c_m$, $\forall \gamma \in$ dense cone as n grows (c_m is defined by formula (3.40)). In Fig. 3.11 we already noticed this kind of behavior, to some extent. In order to establish a more precise match between our data and Weist's conjecture, it is convenient to plot the behavior of $\eta_{a,b}/n$ versus the $|\gamma|$ filtration level, as in Fig. 3.18.

Different colors depict different slopes from the red for $a \gg b$ or $a \ll b$ to the blue for $a \sim b$. As the graph shows, the speed of convergence actually depends on the slope, so the degeneracies for BPS states nearest to the cone boundaries approach Weist's asymptotics in the worst way. Note that there are some charges that do not obey the general asymptotic behavior. These give the horizontal data points at the bottom of Fig. 3.18. These charges indeed lie outside the dense cone. [35]

[35] Note that, because of g_m symmetry, the figure would look rather different if we plotted the degeneracies as a function of n using $\gamma_{a,b}(n)$.

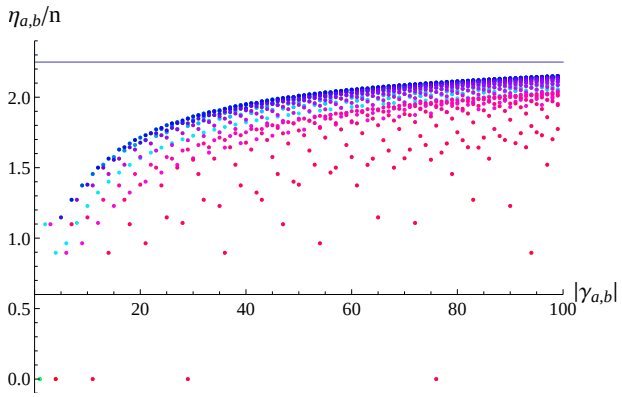

Figure 3.18: The data shown is for $m = 3$ with $(a_0, b_0) = (0.0)$. The straight horizontal line represents the Weist coefficient $c_3 = 4\log 4 - 3\log 3$. For generic values of (a, b) the BPS degeneracies indeed approach the Weist asymptotics at large $|\gamma|$.

3.6 Physical estimates and expectations

3.6.1 An apparent paradox

In this section we first present a physical argument which seems to lead to a very general bound on the behavior of the BPS index in any supersymmetric field theory. The purported bound, however, is explicitly violated by the "wild" degeneracies we have just found in the pure $SU(3)$ theory. Thus, naïvely, there is a paradox. We first explain the paradox in more detail, and then explain how this paradox is resolved.[36]

At very large energy our effective theory should approach a UV conformal fixed point. So consider a d-dimensional CFT put in a box of volume V and heated up to temperature T. Since we have only two dimensionful parameters and we assume the energy and the entropy of the system to be extensive quantities, simple dimensional analysis is enough to predict their form up to dimensionless constants (which will depend on the theory):

$$\begin{aligned} E(T,V) &= \alpha V T^d, \\ S(T,V) &= \beta V T^{d-1}. \end{aligned} \tag{3.77}$$

Eliminating the temperature dependence we derive the scaling of the entropy with the energy:

$$S(E,V) = \kappa V^{1/d} E^{(d-1)/d}. \tag{3.78}$$

This provides an estimate for the behavior of the number of microstates of energy E supported in a volume V, and gives the correct asymptotic dependence for $E \to \infty$.

[36] We thank T. Banks and S. Shenker for crucial remarks on this matter.

In order to excite massive states we can increase the temperature, thus taking into account heavier BPS states. The BPS index, being a signed sum over the states in the theory, cannot exceed the overall number of states. [37] Thus we come to the following chain of inequalities (here we take $d = 4$ and set $E = |Z_\gamma|$):

$$|\Omega(\gamma)| = \left|\mathrm{Tr}_{\mathfrak{h}^\gamma}(-1)^{2J_3}\right| \leq \frac{1}{4}\,\mathrm{Tr}_{\mathcal{H}_{BPS,\gamma}} 1 \leq \frac{1}{4}\,\mathrm{Tr}_{\mathcal{H},E}\, 1 = \frac{1}{4}e^{S(E)} \sim e^{\kappa V^{\frac{1}{4}} E^{\frac{3}{4}}}, \tag{3.79}$$

where the last estimate assumes large E. Thus the observed behavior $\log|\Omega(\gamma)| \sim E$ for large γ in the pure $SU(3)$ theory seems to give a contradiction.

The resolution of this paradox comes from taking into account the fact that our bound applies only to the theory in a finite volume. If the size of BPS states becomes large enough and they do not fit into the box of finite volume, then they do not contribute to the naïve counting of degrees of freedom. So we should instead consider a "truncated BPS index" $\check{\Omega}_V$, counting only the states which fit into a box of size V; we should expect this index to satisfy the inequality

$$|\check{\Omega}_V| = |\,\mathrm{Tr}_{\mathcal{H}_{BPS},M=|E|,R\leq V^{\frac{1}{3}}}(-1)^{2J_3}| \lesssim e^{\kappa V^{\frac{1}{4}} E^{\frac{3}{4}}} \tag{3.80}$$

with R the average size of a BPS state.

The rest of this section is devoted to arguing that the above scenario is indeed correct. We will use the semiclassical picture of BPS states given by the Denef equations, reviewed in Section 3.6.2, to give a lower bound for the average size of the semiclassical BPS states. The resolution of the paradox is spelled out in some more detail in Section 3.6.3. We give some supporting evidence for the validity of the use of the Denef equations for describing the exponentially large number of BPS states in Section 3.6.4.

3.6.2 Denef equations

In order to estimate the size of the BPS states arising in the theory, we refer to the interpretation [19, 40, 85, 93] of those BPS states that arise from wall-crossing as multi-centered solutions similar to those arising in $\mathcal{N} = 2$ supergravity [39]. We assume Denef's multicentered picture has a good $\alpha' \to 0$ limit and can be applied to field theory. Suppose we have a set of elementary BPS states with charges $\{\gamma_A\}_{A=1}^n$ placed at corresponding points $\{r_A\}_{A=1}^n$ of $\mathbb{R}^3$. This configuration is again BPS only if the following set of equations is satisfied:

$$\sum_{\substack{B=1\\B\neq A}}^{n} \frac{\langle\gamma_A,\gamma_B\rangle}{|r_A - r_B|} = 2\mathrm{Im}(e^{-i\vartheta} Z_{\gamma_A}), \tag{3.81}$$

[37] In fact, the data for the Kronecker m-quiver suggest that in this case all the summands contributing to the BPS index have the same sign, so the BPS index actually counts the number of states up to an overall sign.

where $\vartheta = \arg \sum_{A=1}^{n} Z_{\gamma_A}$.

Now let us consider a BPS state of total charge $M\gamma_1 + N\gamma_2$, with $\langle \gamma_1, \gamma_2 \rangle = m$. Let us, *for the moment*, suppose that the dominant contribution to the entropy comes from a boundstate of M elementary constituents of charge γ_1 and N elementary constituents of charge γ_2.

In the case where the charges are of the form

$$\{\underbrace{\gamma_1, \ldots, \gamma_1}_{M}, \underbrace{\gamma_2, \ldots, \gamma_2}_{N}\} \tag{3.82}$$

the equations simplify to

$$\begin{aligned} \sum_{a=1}^{N} \frac{m}{r_{ia}} &= \kappa_1 := 2\mathrm{Im}(e^{-i\vartheta} Z_{\gamma_1}), \qquad 1 \le i \le M \\ \sum_{i=1}^{M} \frac{-m}{r_{ia}} &= \kappa_2 := 2\mathrm{Im}(e^{-i\vartheta} Z_{\gamma_2}), \qquad 1 \le a \le N \end{aligned} \tag{3.83}$$

We can view the index a as running over "electrons" and i over "magnetic monopoles," in an appropriate duality frame.

Now we are interested in the size of the boundstate. Therefore we consider the sum over the first equation in (3.83). (Doing the analogous sum over the second equation produces an equivalent result.) The result is that

$$\sum_{i,a} \frac{1}{r_{ia}} = \frac{NM}{|MZ_{\gamma_1} + NZ_{\gamma_2}|} \left(\frac{2\mathrm{Im}(\bar{Z}_{\gamma_2} Z_{\gamma_1})}{m} \right) \tag{3.84}$$

We can rewrite this equation nicely in terms of the *harmonic average* of the distances r_{ia}:

$$\langle r_{ia} \rangle_h = \left(\frac{m}{2\mathrm{Im}(\bar{Z}_{\gamma_2} Z_{\gamma_1})} \right) |MZ_{\gamma_1} + NZ_{\gamma_2}|. \tag{3.85}$$

On the other hand, we can use the well-known inequality that the harmonic average is a lower bound for the ordinary average, $\langle r_{ia} \rangle_h \le \langle r_{ia} \rangle$, to conclude that

$$\left(\frac{m}{2\mathrm{Im}(\bar{Z}_{\gamma_2} Z_{\gamma_1})} \right) |MZ_{\gamma_1} + NZ_{\gamma_2}| \le \langle r_{ia} \rangle. \tag{3.86}$$

Equation (3.86) is a key result. It shows that if N or M goes to infinity then the size of the average BPS molecule grows linearly with N or M, respectively.

We have shown that boundstates of total charge $M\gamma_1 + N\gamma_2$ with constituents (3.82) become large when $N, M \to \infty$. However, other partitions of N, M can and do lead to BPS boundstates. In general, given a pair of partitions

$$M = \sum_{j=1}^{M} l_j j, \quad N = \sum_{k=1}^{N} s_k k \tag{3.87}$$

there can be other boundstates where there are l_j centers of charge $j\gamma_1$ and s_k centers of charge $k\gamma_2$. In order to deal with these cases, let us introduce, for any set of charges $\{\gamma_A\}$, the moduli space $\mathcal{M}(\{\gamma_A\})$ of solutions to the Denef equations (3.81). If there are n centers it is a subspace of $\mathbb{R}^{3n}$. Note that the moduli space for charges

$$\{\underbrace{\gamma_1,\dots,\gamma_1}_{l_1},\underbrace{2\gamma_1,\dots,2\gamma_1}_{l_2},\dots,\underbrace{\gamma_2,\dots,\gamma_2}_{s_1},\underbrace{2\gamma_2,\dots,2\gamma_2}_{s_2},\dots\} \tag{3.88}$$

is in fact a subspace of the moduli space for (3.82), where certain collections of centers r_i and r_a have (separately) collided. Nevertheless, the identity (3.85) applies uniformly throughout the moduli space and hence applies to all possible partitions. As an extreme example, the moduli space $\mathcal{M}(\{M\gamma_1, N\gamma_2\}) \cong \mathbb{R}^3 \times S^2$, where the $\mathbb{R}^3$ is the center of mass and the S^2 has a radius

$$R_{12} = \left(\frac{m}{2\mathrm{Im}(\bar{Z}_{\gamma_2} Z_{\gamma_1})}\right) |MZ_{\gamma_1} + NZ_{\gamma_2}|. \tag{3.89}$$

In any case, we can conclude that for any partition of charges such as (3.88) the average BPS state has a size bounded below by a linear expression in N and M. We call these large semiclassical BPS states *BPS giants*.

3.6.3 Resolution and Revised Bound

The giant BPS states resolve the paradox explained in Section 3.6.1 above. Indeed we can adapt the bound (3.79) by adjusting the volume of the box V in such a way that states of mass E fit in a volume $V_E := R_E^3 := E^3$. From our estimate of the sizes of BPS molecules we know that the average size indeed scales linearly with E. Therefore the new bound is

$$\log|\Omega(E)| \sim \alpha E \lesssim \kappa E^{3/4} V_E^{1/4} \sim \kappa' E^{3/2} \tag{3.90}$$

and is indeed satisfied.

In equation (3.90) κ' is a dimensionful constant, it scales as $\kappa' \sim (\text{length})^{\frac{3}{2}}$. Let us give a physical interpretation for this scale. If we consider a sequence of charges $N(a\gamma_1 + b\gamma_2)$, with $N \to \infty$ and $\gamma_p := a\gamma_1 + b\gamma_2$ primitive, then the size of an average BPS molecule behaves as $R \sim r_0 N$, where r_0 is the size of a state with charge γ_p. The energy behaves as $E = |Z_0|N$, where Z_0 is a central charge of the state with charge γ_p. Thus we can give a formula accounting for the scaling dimension of κ' in (3.90) by using

$$V_E = R_E^3 \sim (r_0 N)^3 \sim (r_0 E/|Z_0|)^3 \tag{3.91}$$

to deduce

$$\begin{aligned} E^{3/4}V_E^{1/4} &\sim \left(\frac{r_0}{|Z_0|}\right)^{3/4} E^{3/2}, \\ \Rightarrow \quad \kappa' &\sim \left(\frac{r_0}{|Z_0|}\right)^{3/4}. \end{aligned} \tag{3.92}$$

We remark that

1. The length scale $(r_0/|Z_0|)^{1/2}$ is a function of the moduli, since both r_0 and Z_0 are functions of the moduli.

2. The coefficient α in (3.90) is

$$\alpha = \frac{C_{a,b}(m)}{|Z(a\gamma_1 + b\gamma_2)|} \tag{3.93}$$

for the series of charges above eq. (3.76). As we noted in Section 3.3.4 there are points on the Coulomb branch with arbitrarily high m and

$$C_{a,b}(m) \sim \sqrt{ab}\log m^2 \tag{3.94}$$

for large m. Hence, somewhat surprisingly, the coefficient of the logarithmic growth is unbounded on the Coulomb branch.

3.6.4 Discussion of validity of the semiclassical picture

In this section we will address the question of how reliable the semiclassical approximation is. We will review some supporting evidence for the reliability of the semiclassical pictures based on the relation of an exact result for BPS degeneracies Ω to certain symplectic volumes.

As a side remark we note that numerical data for the 3-Kronecker quiver strongly suggest (cf. the discussion about positivity below (A.4)) that the BPS index actually measures the number of states

$$|\Omega(\gamma)| = \mathrm{Tr}_{\mathfrak{h}_\gamma} 1. \tag{3.95}$$

This relation is not essential to our argument but it does nicely simplify the considerations.

Let us recall the symplectic structure on Denef moduli space $\mathcal{M}(\{\gamma_A\})$. Overall translation acts on this space and the reduced space $\overline{\mathcal{M}}(\{\gamma_A\}) = \mathcal{M}(\{\gamma_A\})/\mathbb{R}^3$ is generically $2n-2$ dimensional. Moreover, the reduced space admits a symplectic form [24]:

$$\omega = \frac{1}{4}\sum_{i<j}\langle\gamma_i,\gamma_j\rangle \frac{\epsilon_{abc}dr_{ij}^a \wedge dr_{ij}^b r_{ij}^c}{r_{ij}^3}. \tag{3.96}$$

In the semiclassical approximation we identify a subspace of the space of BPS states with a set of BPS field configurations. We expect that the dimension of a subspace corresponding to a charge decomposition can be estimated, in the semiclassical approximation, by the symplectic volume

$$\mathrm{Vol}(\{\gamma_A\}) := \frac{1}{(n-1)!}\int\limits_{\mathcal{M}} \left(\frac{\omega}{2\pi}\right)^{n-1}. \tag{3.97}$$

where n is the number of centers.

Now, thanks to a result of Manschot, Pioline, and Sen [98, 99], in the example of the m-Kronecker quiver the protected spin character in the wild chamber can in fact be expressed exactly as a sum over two partitions (3.87) so that

$$\begin{aligned}\Omega(M\gamma_1 + N\gamma_2; y) = \\ = \sum_{\{l_j\},\{s_k\}} g_{\mathrm{ref}}(\{l_j\},\{s_k\}; y) \prod_{j,k} \frac{1}{l_j! j^{l_j} s_k! k^{s_k}} \left(\frac{y-y^{-1}}{y^j - y^{-j}}\right)^{l_j} \left(\frac{y-y^{-1}}{y^k - y^{-k}}\right)^{s_k}\end{aligned} \tag{3.98}$$

where g_{ref} refers to an equivariant Dirac index on the space of solutions to Denef's equations with distinguishable centers described by charge partitions $\{l_j\}$, $\{s_k\}$. If we specialize to the index at $y = 1$ [38] then g_{ref} has a very nice interpretation as the symplectic volume (3.97) of the moduli space of solutions to Denef's equations (up to a sign):

$$\Omega(M\gamma_1 + N\gamma_2) = \sum_{\{l_j\},\{s_k\}} (-1)^{mMN+1-\sum_j l_j - \sum_k s_k} \mathrm{Vol}(\{l_j\},\{s_k\}) \prod_{j,k} \frac{1}{l_j! j^{2l_j} s_k! k^{2s_k}}. \tag{3.99}$$

where $\mathrm{Vol}(\{l_j\},\{s_k\})$ is (3.97) for the charges (3.88).

We will take this relation of the exact number of BPS states to symplectic volumes as sufficient evidence for the validity of our resolution. There are, however, some further interesting aspects of this formula which we will comment on in the following Sections 3.6.4.1 and 3.6.4.2 below.

3.6.4.1 A toy example: the Hall halo

A very nice exactly solvable example of BPS configurations is provided by the Hall halo of [39]. Consider a configuration of N electric particles and a single magnetic monopole of charge m. This corresponds to the case $(M, N) = (1, N)$ in the notation above. In this case the equations (3.83) imply that the N electric particles all lie on a single sphere centered on the magnetic particle and of radius:

$$R_{12} = \left(\frac{m}{2\mathrm{Im}(\bar{Z}_{\gamma_2} Z_{\gamma_1})}\right) |Z_{\gamma_1} + N Z_{\gamma_2}|. \tag{3.100}$$

[38] In the conventions of [98] we take $y \to 1$ rather than $y \to -1$ to get the index.

Now, in this case Denef argued that to get the spin character we can just apply the usual quantum mechanics of Landau levels on a sphere with a magnetic monopole inside. Counting the ground states gives the corresponding protected spin character [124]

$$\Omega(y) = (-y)^{-(m-N)N} \frac{\prod_{j=1}^{m}(1-y^{2j})}{\prod_{j=1}^{N}(1-y^{2j}) \prod_{j=1}^{m-N}(1-y^{2j})}, \tag{3.101}$$

in perfect agreement with Reineke's general formula (see eq. (5.3) of [39]).

There are two interesting lessons we can draw from (3.101):

1. First, naive physical intuition suggests that the large size of BPS states is due to large angular momentum. This example shows that in fact this is not necessarily the case. In this case the size of the configuration is given by formula (3.100). Nevertheless this configuration contains representations of many different spins.

2. Second, we can derive the number of states in a multiplet by taking $y \to -1$. Then $\Omega = \frac{m!}{N!(m-N)!}$. In the limit $N \ll m$ the number of allowed states is much greater than the number of populated states, so quantum statistics does not play an important role, and the semiclassical approximation should work. Indeed,

$$\Omega = \frac{m!}{N!(m-N)!} \underset{N \ll m}{\sim} \frac{m^N}{N!} + \cdots \tag{3.102}$$

This confirms the semiclassical expectation that the number of states should be counted by the symplectic volume since the volume is proportional to m^N. Note however that, for fixed N the binomial coefficient is really a polynomial in m and (3.102) is only the leading term at large m. Since $1/m$ plays the role of $\hbar$ we can interpret the subleading terms as quantum corrections to the naive semiclassical reasoning.

3.6.4.2 Estimating the contribution of the maximal partition

Let us consider the contribution to the BPS degeneracy of the maximal partition (3.82) in the formula (3.99). The symplectic volume for this partition is

$$\mathrm{Vol}((N,M),\kappa_1,\kappa_2,m) := \frac{1}{(N+M-1)!} \int_{\overline{\mathcal{M}}} \Big(\frac{\omega}{2\pi}\Big)^{N+M-1} \tag{3.103}$$

where we used the fact that there are $n = N + M$ centers. We would like to estimate this volume when N, M become large.

Rescaling both $\kappa_{1,2}$ in (3.83) by $\lambda \in \mathbb{R}$ together with $r_{ij} \mapsto r_{ij}\lambda^{-1}$ shows that solutions for rescaled values of $\kappa_{1,2}$ are obtained by simply rescaling the distances. Therefore the ratio

$$H((N,M),\kappa_1/\kappa_2) := \mathrm{Vol}((N,M),\kappa_1,\kappa_2,m)/m^{N+M-1}$$

only depends on the ratio κ_1/κ_2 and on N, M. For simplicity, let us specialize to $M = N-1$. in the limit $N \to \infty$ we have

$$\begin{aligned}&\lim_{N\to\infty} \frac{1}{N} \log\left(\mathrm{Vol}((N-1,N),\kappa_1,\kappa_2,m)\right)\\ &\sim \log m^2 + F\left(\frac{\kappa_1}{\kappa_2}\right).\end{aligned}$$

Note that the second piece is independent of m.

There are two important lessons we can draw from this computation:

1. This behavior nicely coincides with the Weist coefficient, but only in the large m limit when:

$$C_{1,1}(m) \sim \log m^2 + \mathcal{O}(m^{-1}) \tag{3.104}$$

   The fact that we must take $m \to \infty$ is not terribly surprising in view of the Hall halo example discussed above.

2. It is interesting to note that at finite values of m the maximal partition does *not* fully account for the exponential growth coefficient, even in the large charge regime. Indeed, as pointed out in [128] we should take into account many other partitions to derive even the leading asymptotic behavior of the BPS index. One important (and subtle) aspect of (3.99) is that the different symplectic volumes are weighted with *signs*. This might imply some subtlety in applying the semiclassical pictures we have used, and should be understood better. In the meantime, in the formula (3.99), considering the case where the BPS ray lies in the dense cone, there can be striking cancelations between volumes of different partitions.

3.7 Spectral Moonshine

In the course of these investigations we noticed some unusual and very intriguing features in our data. We mention these here, leaving a deeper analysis and conceptual understanding of these features to future work.

3.7.1 Scaling behavior of the spin degeneracies

An interesting pattern of the spectrum emerges when we consider the distribution of spin multiplets within $\mathcal{H}_\gamma^{\rm BPS}$, the subspace of BPS states with gauge charge γ. For the definitions of the protected spin character and the spin decompositions see Appendix A.

Let $\delta_\gamma(j)$ be the number of times a spin-j multiplet[39] occurs within $\mathcal{H}_\gamma^{\rm BPS}$, as in (A.3). Numerical data suggests that *all states within the dense cone* exhibit a common δ-distribution, as shown in Fig. 3.19 (the data are in Appendix A).

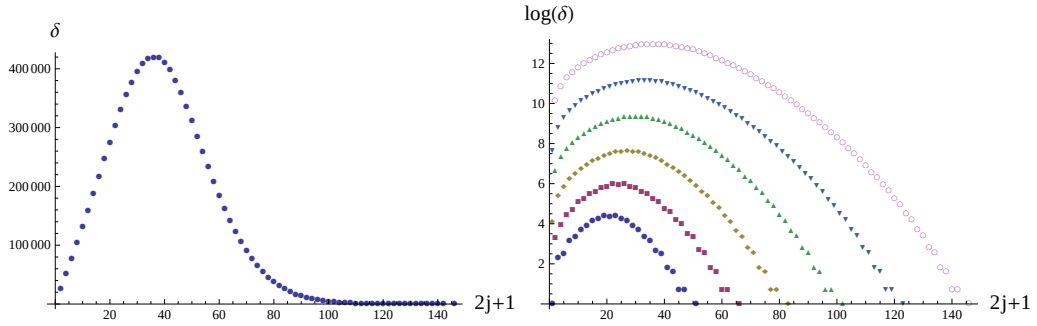

Figure 3.19: On the left: the distribution $\delta(j)$ for $\gamma = 12(\gamma_1+\gamma_2)$. On the right: the same distribution for several states $\gamma = n(\gamma_1+\gamma_2)$. This feature extends to other slopes as well, indeed all states within the dense cone exhibit such "Poisson" behavior.

More precisely, letting γ_n denote the sequence of charges $(na+a_0)\gamma_1+(nb+b_0)\gamma_2$, data collected by computer experiments strongly suggest that there are functions $\kappa_1,\kappa_2,\kappa_3,\rho,\alpha$[40] of a,b,a_0,b_0 such that, if we define $j_n(s)$ by

$$s = (2j_n(s)+1)/(\rho|\gamma_n|), \tag{3.105}$$

then the limit

$$u(s) := \lim_{n\to\infty} \kappa_3|\gamma_n|^{-\kappa_1} e^{-\kappa_2|\gamma_n|}\delta_{\gamma_n}(j_n(s))\,. \tag{3.106}$$

exists and is given by

$$u(s) = s^\alpha e^{-\alpha(s-1)} \tag{3.107}$$

(Recall that $|\gamma_n| = n(a+b)+a_0+b_0$). The numerical evidence further suggests that for $m=3$, $\alpha \approx 2$, regardless of the slope[41].

[39] Meaning a representation $\rho_{hh}\otimes(j,0)$ of $\mathfrak{so}(3)\oplus\mathfrak{su}(2)_R$.
[40] The κ_1,κ_2 employed here have nothing to do with those of section 3.6.4.2.
[41] This estimate is based on data collected for $|\gamma|<30$.

If we assume that the above scaling law holds and the limiting behavior to the scaling function is sufficiently rapid, then one can relate the parameters κ_1, κ_2 of the scaling law to the leading terms in the $n \to \infty$ asymptotic expansion

$$\log|\Omega(\gamma_n)| \sim \kappa_2|\gamma_n| + (\kappa_1+2)\log|\gamma_n| + \mathcal{O}(1) \tag{3.108}$$

where $\mathcal{O}(1)$ has a finite limit as $n \to \infty$. Indeed, comparing with the Weist asymptotics (3.75) we learn that $(a+b)\kappa_2 = C_{a,b}(m)$. Similarly, comparing with known asymptotics of $\Omega(\gamma_n)$ we can learn about the a, b, a_0, b_0 dependence of κ_1.

Regardless of the validity of the scaling law, it is worthwhile stressing that the sub-leading behavior of $\log|\Omega(\gamma_n)|$ is interesting in its own right. It is often assumed that, at large n, the BPS index is a continuous function of the slope a/b, however – somewhat surprisingly – the sub-leading correction exhibits a dependence on a_0, b_0 too. To see this, consider two different sequences approaching slope 1, namely $\gamma^{(n)} = (n, n)$ and $\tilde{\gamma}^{(n)} = (n, n+1)$, we have

$$\begin{aligned} \log|\Omega(\gamma_n)| &= nC_{1,1}(m) - \frac{5}{2}\log n + \mathcal{O}(1) \\ \log|\Omega(\tilde{\gamma}_n)| &= nC_{1,1}(m) - 2\log n + \mathcal{O}(1), \end{aligned} \tag{3.109}$$

where we used the known result[42]

$$\Omega(n, n-1) = \frac{1}{(3n+2)(2n+1)}\binom{4n+2}{n+1}. \tag{3.110}$$

The subleading dependence on $a/b, a_0, b_0$ exhibited in (3.109) also occurs at the other slopes in the same g_m orbit.

3.7.2 Partitions and relation to modular functions

Interesting features of the pattern of spin decompositions lie in the tail of the distribution. First of all, for certain sequences $\gamma^{(\alpha)}$, $\alpha = 1, 2, \ldots$ such that $|\gamma^{(\alpha)}| \stackrel{\alpha\to\infty}{\longrightarrow} \infty$, we observe the asymptotic behavior of $J_{\max}(\gamma) := \max\{j|\delta_\gamma(j) \neq 0\}$, in particular

$$J_{\max}((n,n)) = \frac{n^2+1}{2}, \qquad J_{\max}((n+1,n)) = \frac{n^2+n}{2}. \tag{3.111}$$

We can compare this behavior, as well as that of all other sequences in our data, with a prediction deriving from Kac's theorem (see e.g. [116]) about the dimensionality of the quiver varieties. More precisely, for the Kronecker m-quiver $K(m)$, Kac's theorem asserts that the dimension of the quiver variety $M_{(a,b)}(K(m))$ for indecomposable representations with dimension vectors $\gamma = (a, b)$ is

$$\dim M_{(a,b)}(K(m)) = mab - a^2 - b^2 + 1, \tag{3.112}$$

[42] Cf theorem 6.6 of [127]

therefore, noting that the Lefschez multiplet of maximal spin must be

$$j_{\max}(\gamma=(a,b))=\frac{1}{2}\dim M_{(a,b)}(K(m)) \tag{3.113}$$

we find, as a nice check, that our data agrees with this prediction. (It also confirms a prediction made in [84].)

Now, while the overall size and shape of the distribution vary with the charge, the degeneracies $\delta_\gamma(j)$ on the tail of the distribution *stabilize* to a common pattern

γ	$\delta(J_{\max})$, $\delta(J_{\max}-1)$, ...
$4\gamma_1+3\gamma_2$	$1,0,2,2,3,2,2,0,\ldots$
$7\gamma_1+6\gamma_2$	$1,0,2,2,5,6,13,14,\ldots$
$8\gamma_1+6\gamma_2$	$1,0,2,2,5,6,13,16,\ldots$
$8\gamma_1+7\gamma_2$	$1,0,2,2,5,6,13,16,\ldots$

(3.114)

As (3.114) shows, the length of the "saturated" subsequence 1,0,2,2,5,6,13,16,... increases with $|\gamma|$. Overall, the tail behavior seems to stabilize to the sequence generated by

$$g(\xi)=\prod_{m=2}^{\infty}(1-\xi^m)^{-2}=1+0\xi+2\xi^2+2\xi^3+5\xi^4+6\xi^5+13\xi^6+\ldots. \tag{3.115}$$

A slight modification yields the generating function which coefficients are the incremental sum of those in $g(\xi)$

$$\tilde{g}(\xi)=\frac{\prod_{m=2}^{\infty}(1-\xi^m)^{-2}}{(1-\xi)}=1+1\xi+3\xi^2+5\xi^3+10\xi^4+16\xi^5+29\xi^6+\ldots, \tag{3.116}$$

generating the number of planar partitions with at most two rows of the corresponding size, some examples are

No boxes		1 empty partition
1 box	1	1 partition
2 boxes	$1\ \ 1$, 2, $\begin{matrix}1\\1\end{matrix}$	3 partitions
3 boxes	3, $1\ \ 1\ \ 1$, $2\ \ 1$, $\begin{matrix}2 & 1 & 1\\1 & 1\end{matrix}$	5 partitions

This analogy suggests that the stabilized $\delta_\gamma(j)$ distribution counts some number of *constrained* partitions, only deviating from (3.115) at higher orders in ξ. This hypothesis is reminiscent of results of [98, 117].

Of course, $g(\xi)$ is also closely related to the Dedekind η-function. It is quite curious that the BPS degeneracies have some relation to modular functions. This has been long expected in supergravity [23, 40, 113] but the appearance in field theory is novel.

In fact, the above connection to the Dedekind η was noted before our work by Reineke [118], who offers a mathematical explanation. But the physical import of this strange behavior remains mysterious.

Chapter 4

Spectral Networks with Spin

4.1 Protected Spin Characters from writhe

4.1.1 Review of framed BPS states

Framed BPS states, introduced in [61], appear in the context of four-dimensional $\mathcal{N} = 2$ gauge theories with the insertion of certain line defects. In the Coulomb phase of the gauge theory, one may consider the effect of inserting a line defect L_ζ preserving a $osp(4^*|2)_\zeta$ sub-superalgebra (for notations see [61]). The preserved supercharges depend on the choice of $\zeta \in \mathbb{C}^*$, and the surviving algebra develops a new type of BPS bound

$$E + \mathrm{Re}(Z/\zeta) \geq 0\,. \tag{4.1}$$

States in the Hilbert space $\mathscr{H}_{u,L,\zeta}$ which saturate this bound are the framed BPS states, the subspace spanned by these is denoted $\mathscr{H}^{BPS}_{u,L,\zeta}$. The introduction of the line defect also modifies the usual "vanilla" grading of the BPS Hilbert space to

$$\mathscr{H}^{BPS}_{u,L,\zeta} = \bigoplus_{\gamma \in \Gamma_L} \mathscr{H}_{u,L,\zeta,\gamma} \tag{4.2}$$

where Γ_L is a torsor for the vanilla lattice gauge lattice Γ, and there is an integral-valued pairing $\langle \gamma_L, \gamma \rangle \in \mathbb{Z}$ defined for any $\gamma_L \in \Gamma_L$, $\gamma \in \Gamma$.

The framed BPS bound determines a new type of marginal stability wall, termed BPS walls:

$$\widehat{W}(\gamma) = \{(u,\zeta)\,|\,Z_\gamma(u)/\zeta \in \mathbb{R}_-\} \subset \mathcal{B} \times \mathbb{C}^*\,, \tag{4.3}$$

where Z_γ denotes the central charge of a populated vanilla BPS state of charge γ. Near these loci some framed BPS states look like halo BPS particles (with charge $\gamma_h \in \Gamma$) bound to a non-dynamical

"core charge" $\gamma_c \in \Gamma_L$. Given a choice of moduli (u, ζ) where a framed BPS state of charge $\gamma_c + \gamma_h$ is stable, its energy is

$$E = -\mathrm{Re}(Z_{\gamma_c+\gamma_h}(u)/\zeta) \leq -\mathrm{Re}(Z_{\gamma_c}(u)/\zeta) + |Z_{\gamma_h}(u)| \tag{4.4}$$

the inequality saturates at BPS walls, where boundstates become marginally stable. At BPS walls, these states mix with the continuum of vanilla BPS states, whose BPS bound is $E \geq |Z_{\gamma_h}(u)|$, the Fock space of framed states therefore gains or loses a factor, this is the halo picture of the framed wall-crossing phenomenon. Part of its importance stems from the fact that it underlies a physical derivation of the Kontsevich-Soibelman wall-crossing formula, and of its motivic counterpart [14, 61, 88, 90, 104].

As suggested by the halo picture recalled above, framed BPS states furnish representations of $\mathfrak{so}(3)$ of spatial rotations as well as of $\mathfrak{su}(2)_R$. The *framed protected spin character* (PSC) is defined as

$$\overline{\Omega}(L_\zeta, u, \gamma; y) := \mathrm{Tr}_{\mathscr{H}_{u,L,\zeta,\gamma}} y^{2J_3}(-y)^{2I_3} \tag{4.5}$$

where J_3, I_3 are Cartan generators of $\mathfrak{so}(3)$ and $\mathfrak{su}(2)_R$. Similarly, the *vanilla PSC* is defined as

$$\Omega(u, \gamma; y) := \mathrm{Tr}_{\mathfrak{h}_\gamma} y^{2J_3}(-y)^{2I_3} = \sum_{m\in\mathbb{Z}} a_m(\gamma)\,(-y)^m \tag{4.6}$$

where $\mathfrak{h}_\gamma$ is the Clifford vacuum of the BPS Hilbert space[1], $\gamma \in \Gamma$ and the last equality defines the integers $a_m(\gamma) \in \mathbb{Z}$.

It is useful to consider a generating function of framed BPS degeneracies

$$\begin{aligned} F(u, L, \zeta, \gamma_c; y) &= \sum_{\gamma_h\in\Gamma} \overline{\Omega}(u, L_\zeta, \gamma_c + \gamma_h; y)\, X_{\gamma_c+\gamma_h} \\ &= \mathrm{Tr}_{\overline{\mathcal{F}}_{\gamma_c}(u,L,\zeta)} y^{2J_3}(-y)^{2I_3}\, e^Q\,, \end{aligned} \tag{4.7}$$

where X_γ are formal variables realizing the group algebra of Γ acting on Γ_L, namely

$$X_{\gamma_c}X_{\gamma_h} = X_{\gamma_h}X_{\gamma_c} = X_{\gamma_c+\gamma_h} \qquad X_{\gamma_h}X_{\gamma_h'} = X_{\gamma_h+\gamma_h'} \qquad \forall \gamma_c \in \Gamma_L;\ \gamma_h, \gamma_h' \in \Gamma\,. \tag{4.8}$$

We denoted by $\overline{\mathcal{F}}_{\gamma_c}(u, L, \zeta)$ the Fock space of framed BPS states of core charge γ_c, while Q is a linear operator on this Fock space which evaluates to $\log X_\gamma$ on a state of charge γ. The fact that F is expressed as a trace over the Fock space of framed states, together with the halo-creation/decay mechanism explained in [61, §3.4], entail that across a BPS wall

$$F^\pm = F^\mp \prod_{\gamma_h} \prod_{m\in\mathbb{Z}} \prod_{m'=-2J_{\gamma_c,\gamma_h}}^{2J_{\gamma_c,\gamma_h}} \Big(1 + (-y)^m\, y^{m'} X_{\gamma_h}\Big)^{a_m(\gamma_h)} \tag{4.9}$$

[1] see e.g. [73, 104] for more details.

where $2J_{\gamma_c,\gamma_h}+1 = |\langle\gamma_c,\gamma_h\rangle|$ is the dimension of the $\mathfrak{so}(3)$ irrep accounting for the "orbital" degrees of freedom of the halo. It is worth noting that $a_m(\gamma) \geq 0\ \forall m$ if the vanilla BPS state in question is a fermion, while $a_m(\gamma) \leq 0\ \forall m$ for bosons[2].

Having reviewed the definition of BPS states, we shall now review how their counting goes. There are different approaches to this problem: on the one hand these states admit a semiclassical description (see [107, 126]), on the other hand the six-dimensional engineering of line defects [61, 63, 65] has been successfully exploited to derive general expressions for generating functions in class $\mathcal{S}$ theories of the A type. In the rest of this paper we will introduce and study a generalization of the second approach, we therefore end this section by reviewing this technique.

A class $\mathcal{S}$ theory of the A_k type is defined by a punctured Riemann surface C together with some data D at the punctures [59, 64, 83, 133], we will sometimes refer to A_k, C, D as the "UV data" of the theory. These objects define a classical integrable system (the Hitchin system) $\mathcal{M}_H$ together with a fibration (the Hitchin fibration) by Lagrangian tori over $\mathcal{B}_H$ (the Hitchin base). In the context of gauge theories, $\mathcal{B}_H \equiv \mathcal{B}$ is identified with the Coulomb branch of the four-dimensional theory in question. At each $u \in \mathcal{B}$, the spectral curve of the Hitchin system $\Sigma_u \subset T^*C$ is identified with the Seiberg-Witten curve which captures the low-energy dynamics of the gauge theory. The tautological 1-form λ in T^*C plays the role of the SW differential. The canonical projection $\pi : \Sigma_u \to C$ defines a ramified covering of C. To this covering is associated a one-parameter family of spectral networks $\mathcal{W}(u,\vartheta)$ [63]. Loosely speaking, a spectral network is a collection of oriented paths – termed *streets* – on C carrying certain *soliton data*; both the shape of the streets and the soliton data are determined by a set of rules; it will be important in the following that such paths can be lifted to Σ in a way dictated by the data they carry. We will not provide a review of spectral networks, we refer the reader to the original paper [63] or to [73, 106] for self-contained presentations.

Spectral networks are useful for several reasons. From the mathematical viewpoint they establish a local isomorphism between moduli spaces of flat connections known as the *nonabelianization map*. From a physical point of view they give a means to compute BPS spectra of various types, including as the "vanilla" and "framed" spectra.

Given a network with its soliton data, the counting of framed BPS degeneracies is relatively simple. Given two surface defects $\mathbb{S}_z$, $\mathbb{S}_{z'}$ [9, 49, 63, 65, 68] localized at $x^1 = x^2 = 0$ in spacetime, a UV susy interface interpolating between them is associated to a relative homotopy class[3] $\wp \subset C$. At

[2]The Clifford vacua $\mathfrak{h}_\gamma = (j, j_R)$ of bosons have j half-integer, while fermions have integer j. An interpretation for this shift can be found in [39, 40].

[3]Actually, $\wp$ is a relative homotopy class on the unit tangent bundle of C, as explained in [63]. For simplicity we suppress this detail for the moment.

fixed values of (u,ϑ) the framed degeneracies for the interface $L_\wp$ are determined by the combinatorics of "detours"

$$F(\wp,u,\vartheta)=\sum_{i,j'}\sum_{\pi\in\Gamma_{ij'}(z,z')}\overline{\Omega}(L_\wp,u,\vartheta,\pi)\,X_\pi \tag{4.10}$$

where we extended the formal X variables to take values in the *homology path algebra* (see [73, §2]). The first sum runs over all pairs of sheets of the covering Σ (a choice of local trivialization is understood), and the second sum is determined by the soliton data on the streets of $\mathcal{W}$ crossed by $\wp$. Each π is associated with a *2d-4d framed BPS state* (see [63, §4] also for the notation $\Gamma_{ij'}(z,z')$), the $\overline{\Omega}$ are the corresponding framed degeneracies.

As the parameter $\vartheta\in\mathbb{R}/2\pi\mathbb{Z}$ varies, $\mathcal{W}(u,\vartheta)$ undergoes a smooth evolution, except at special values of ϑ for which the topology of the network jumps. These jumps occur precisely when $\vartheta=\mathrm{Arg}(Z_\gamma(u))$, where γ is the charge of some populated (vanilla) BPS state. At a generic point $u\in\mathcal{B}$ this singles out a one-dimensional sublattice $\Gamma_c\subset\Gamma$. This phenomenon is key to extracting the kind of BPS degeneracies of interest to us, and occurs precisely at the BPS walls (also termed $\mathcal{K}$-walls in [63]).

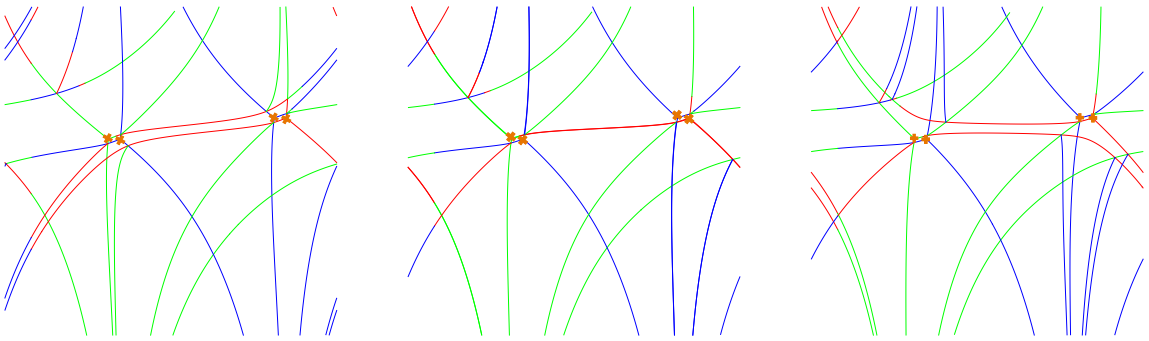

Figure 4.1: The $\mathcal{K}$-wall jump from a hypermultiplet: different colors represent streets carrying solitons of different types $(ij,jk,ki$-types).

More specifically, at a critical value $\vartheta=\vartheta_c$ a part of the network becomes "degenerate," literally two or more streets of type (ij) and (ji) overlap completely, we call this part of the network $\mathcal{W}_c\subset\mathcal{W}$. The soliton data and the topology of the subnetwork $\mathcal{W}_c$ define a discrete set (possibly infinite) of closed paths on Σ, usually indicated by $\{L(\gamma)\}_{\gamma\in\Gamma_c}$ whose homology class is

$$[L(\gamma)]=\Omega(\gamma)\cdot\gamma\,. \tag{4.11}$$

The generating functions of framed degeneracies jump across $\mathcal{K}$-walls, in a way that is captured by

a universal substitution rule of the twisted formal variables Y_a[4]

$$Y_a \quad \mapsto \quad Y_a \prod_{\gamma\in\Gamma_c} (1-Y_\gamma)^{\langle a, L(\gamma)\rangle} \,. \tag{4.12}$$

The vanilla BPS indices control the *change* of framed BPS indices with the variation of ϑ across a $\mathcal{K}$-wall. Examples illustrating this mechanism can be found in [63, 73].

4.1.2 Framed spin and writhe

4.1.2.1 Statement of the conjecture

As reviewed above, for any UV susy interface $L_\wp$ the corresponding 2d-4d framed BPS states at (u,ϑ) are associated with relative homology classes of detours $\pi \in \Gamma_{ij'}(z,z')$.

We now introduce a refinement of the classification of paths that will be of central importance for the rest of the paper. Let $I = [0,1]$ be the unit interval parametrized by t, and consider an immersion $f : I \to X$ into a Riemann surface X, namely a smooth map such that $f_* : T_tI \to T_{f(t)}X$ is injective (i.e. the path never has zero velocity). A regular homotopy between two immersions is a homotopy through immersions. For *open* paths we additionally require that the tangent directions at endpoints be constant throughout the homotopy. This defines an equivalence relation: a *regular homotopy class* is an equivalence class.

From now on we will be assuming that all self-intersections of paths are transverse. Choose $\wp$ to be any *regular homotopy class* on C^* with endpoints z, z'. We define the following spaces

$$C^* := C \setminus \{z, z'\}\,, \qquad \Sigma^* := \Sigma \setminus \pi^{-1}(\{z, z'\})\,. \tag{4.13}$$

The detours of $\wp$ can be likewise classified by regular homotopy classes on Σ^*, because the network contains more information than just relative homology for soliton paths (we will further clarify this point below). We will adopt gothic letters such as $\mathfrak{p}$ to denote regular homotopy classes of detours on Σ^*, the refinement just introduced allows us to perform the assignment

$$\mathfrak{p} \quad \mapsto \quad \mathrm{wr}(\mathfrak{p}) \tag{4.14}$$

where wr is the *writhe* of $\mathfrak{p}$, defined as a signed sum of ± 1 over transverse self-intersections of $\mathfrak{p}$. In the parametrization associated with regular homotopy $\mathfrak{p} : [0,1] \to \Sigma^*$, a self-intersection is a point where $\mathfrak{p}(t_1) = \mathfrak{p}(t_2)$. For $t_2 > t_1$ the associated sign is positive if the tangent vector $\dot{\mathfrak{p}}(t_1) \in T_{\mathfrak{p}(t_1)}\Sigma^*$ points clockwise from $\dot{\mathfrak{p}}(t_2)$ (in the short-way around); the sign is negative otherwise. Let $\mathbf{\Gamma}^*_{ij'}(z,z')$

[4]The Y are related to the X by a choice of quadratic refinement of the charge lattice(s). They obey a twisted algebra, e.g. $Y_\gamma Y_{\gamma'} = (-1)^{\langle\gamma,\gamma'\rangle} Y_{\gamma+\gamma'}$. For more details we refer the reader to [73, §2].

be the set of regular homotopy classes of paths $\mathfrak{p}$ on Σ^* which begin at $z^{(i)}$ and end at $z'^{(j')}$. There is a natural map

$$\beta:\ \mathbf{\Gamma}^*_{ij'}(z,z')\ \longrightarrow \tilde{\Gamma}^*_{ij'}(z,z') \tag{4.15}$$

which identifies different regular homotopy classes $\mathfrak{p}$ belonging to the same relative homology class π on the unit tangent bundle of Σ^*, which we denote $\widetilde{\Sigma}^*$. Correspondingly, we also define $\tilde{\Gamma}^* := H_1(\widetilde{\Sigma}^*,\mathbb{Z})$, then $\tilde{\Gamma}^*_{ij'}(z,z')$ is a torsor for this lattice[5]. We are now ready to state our conjecture on the spin of framed BPS states.

Conjecture 1. *If a framed 2d-4d BPS state for an interface determined by $\wp$ is represented by a regular homotopy class $\mathfrak{p}$ then its spin $2J_3$ is the writhe of $\mathfrak{p}$.*

Recall that the surface defects choose a direction in space and J_3 is defined as the spin around this direction. Therefore, given a spectral network $\mathcal{W}$ and an interface $\wp$, we define

$$\begin{aligned}\overline{\Omega}(L_\wp,u,\vartheta,\mathfrak{p})\ &:=\ \#\text{ of detours in class }\mathfrak{p}\,,\\ \overline{\Omega}(L_\wp,u,\vartheta,\pi;y)\ &:=\sum_{\mathfrak{p}\,|\,\beta(\mathfrak{p})=\pi} y^{\mathrm{wr}(\mathfrak{p})}\,\overline{\Omega}(L_\wp,u,\vartheta,\mathfrak{p})\,,\end{aligned} \tag{4.16}$$

together with

$$F(\wp,u,\vartheta;y):=\sum_{i,j'}\sum_{\pi\in\tilde{\Gamma}^*_{ij'}(z,z')}\overline{\Omega}(L_\wp,u,\vartheta,\pi;y)\,\hat{Y}_\pi\,, \tag{4.17}$$

where $\hat{Y}$ are formal variables associated with relative homology classes $\pi\in H_1^{rel}(\widetilde{\Sigma}^*,\widetilde{\Sigma}\setminus\widetilde{\Sigma}^*)$ as well as with homology classes in $\tilde{\gamma}\in H_1(\widetilde{\Sigma}^*,\mathbb{Z})$ subject to the relations

$$\hat{Y}_\pi\hat{Y}_{\tilde{\gamma}}=y^{\langle\pi,\tilde{\gamma}\rangle}\,\hat{Y}_{\pi+\tilde{\gamma}}\qquad \hat{Y}_{\tilde{\gamma}}\hat{Y}_\pi=y^{\langle\tilde{\gamma},\pi\rangle}\,\hat{Y}_{\pi+\tilde{\gamma}}\qquad \hat{Y}_{\tilde{\gamma}}\hat{Y}_{\tilde{\gamma}'}=y^{\langle\tilde{\gamma},\tilde{\gamma}'\rangle}\,\hat{Y}_{\tilde{\gamma}+\tilde{\gamma}'}\,, \tag{4.18}$$

as well as

$$\hat{Y}_{\pi+nH}=(-y)^n\hat{Y}_\pi\qquad \hat{Y}_{\tilde{\gamma}+nH}=(-y)^n\hat{Y}_{\tilde{\gamma}}\,, \tag{4.19}$$

where H is the generator of $H_1(\widetilde{\Sigma}^*,\mathbb{Z})$ corresponding to a cycle wrapping the fiber, going counter-clockwise (this implies a choice of orientation on Σ^*).

Although not obvious from these definitions, we will prove below in section 4.2.4 that $F(\wp,u,\vartheta;y)$ only depends on the regular homotopy class of $\wp$ on C^*.

4.1.3 Vanilla Protected Spin Characters from Spectral Networks

The main goal of this paper is to propose (vanilla/framed) PSC formulas based on spectral network data. Our approach will be to identify susy interfaces whose framed wall-crossing is described by

[5]To avoid possible confusion, let us note that if $\mathfrak{p}',\mathfrak{p}$ differ by n *counter-clockwise contractible curls* (defined below in §4.2.1) then $\mathrm{wr}(\mathfrak{p}')=\mathrm{wr}(\mathfrak{p})-n$ while $\beta(\mathfrak{p}')=\beta(\mathfrak{p})+nH$, according to our conventions.

formula (4.9). By considering the "classical limit" $y \to -1$, it is clear that this formula won't hold for generic interfaces, we therefore need to focus on a specific subset of interfaces, which we now define.

4.1.3.1 A special class of susy interfaces

To understand the motivations behind the definition to come, it is instructive to dissect and compare formulae (4.9) and (4.12).

To make a meaningful comparison, we shall take $F^- = X_{\gamma_c}$ meaning that there are no halo states with core charge γ_c at ϑ^- (here $\vartheta = \mathrm{Arg}(\zeta)$). The classical limit of (4.9) reads

$$F^+ = X_{\gamma_c} \prod_{\gamma_h} \left(1 - (-1)^{\langle \gamma_c, \gamma_h \rangle} X_{\gamma_h}\right)^{|\langle \gamma_c, \gamma_h \rangle | \Omega(\gamma_h)}, \tag{4.20}$$

switching to twisted variables [61, 73] the above reads

$$F^+ = Y_{\gamma_c} \prod_{\gamma_h} (1 - Y_{\gamma_h})^{|\langle \gamma_c, \gamma_h \rangle | \Omega(\gamma_h)}. \tag{4.21}$$

Now taking $[a] = \gamma_c$ to be a closed cycle with a basepoint on Σ, we find the expected match between the two formulae, since (4.11) ensures that

$$\langle \gamma_c, L(\gamma) \rangle \; = \; \langle \gamma_c, \gamma \rangle \cdot \Omega(\gamma). \tag{4.22}$$

On the other hand, for general a there is no relation between $\langle a, L(\gamma) \rangle$ and $\Omega(\gamma)$.

As remarked in [63, §6.4], this reflects the fact that $L(\gamma)$ contains more information than the charge of 4d BPS degeneracies, such as how they are arranged on C (the charge is a homology class, while $L(\gamma)$ are exact paths). In appendix H we suggest a physical interpretation of this phenomenon in terms of halos formed by single states of $\mathfrak{h}_\gamma$.

Now consider a critical subnetwork $\mathcal{W}_c \subset \mathcal{W}(u, \vartheta_c)$. In the British resolution ($\vartheta = \vartheta_c - \epsilon$) each two-way street $p \in \mathcal{W}_c$ carries two soliton data sets. While in [63] soliton data is classified by relative homology classes, there is much more information available in the network. The requirement of homotopy invariance regulates the propagation of soliton paths across streets of the networks, in a way described by the *six-way joint rules* [63, app.A] [73]. Keeping track of the joints involved in the propagation of a soliton path, it is therefore possible to associate to each soliton an oriented curve made of lifts of streets[6]. We consider it up to regular homotopy and refer to this refined object as a *soliton path*, while we preserve the terminology *soliton classes* for the relative homology classes.

[6] Actually, homotopy invariance is employed in [63] to establish a 2d wall-crossing formula for solitons classified by *relative homology classes* on $\widetilde{\Sigma}$. However we will show below in section 4.2.5 that the *same* set of 6-way rules – now applied to regular homotopy classes of soliton paths – follows from studying regular-homotopy invariance of a certain formal parallel transport.

Let p be an ij/ji-type two way street of $\mathcal{W}_c$, one may join any soliton path from the ij-type soliton data set with any soliton path from the ji-type data set to make a closed path. We denote by $\Pi(p)$ the set of all combinations of soliton paths from the two data sets of p, classified by regular homotopy (as closed paths, i.e. without a basepoint specified) on Σ^*. A generic element $\ell \in \Pi$ will thus be a class of closed oriented curves on Σ. By genericity its homology class will belong to the sublattice associated with the $\mathcal{K}$-wall

$$[\ell] \in \Gamma_c \,. \tag{4.23}$$

We also define

$$\Pi(\mathcal{W}_c) := \bigcup_{p \in \mathcal{W}_c} \Pi(p) \,. \tag{4.24}$$

For any UV susy interface $L_\wp$, we may consider the lifts of $\{\wp^{(i)}\} = \pi^{-1}(\wp) \subset \Sigma$. We will say that $\wp$ is *halo-saturated* if at least one of its lifts satisfies

$$\begin{aligned} &(I) \quad \langle \wp^{(i)}, \ell \rangle \neq 0 \\ &(II) \quad \frac{\langle \wp^{(i)}, \ell \rangle}{\langle \wp^{(i)}, \ell' \rangle} = \frac{[\ell]}{[\ell']} \end{aligned} \qquad \forall \ell, \ell' \in \Pi(\mathcal{W}_c) \,. \tag{4.25}$$

This is our special class of susy interfaces, their essential feature is that in a neighborhood of the $\mathcal{K}$-wall of interest, their $4d$ framed wall-crossing is the *same* as that of a suitable line *defect* (the $2d$ framed wall-crossing may be different though).

For a halo-saturated interface $\wp$, and halo charge $\gamma_h \in \Gamma$, choose any $\ell \in \Pi(\mathcal{W}_c)$ such that $[\ell] = \gamma_h$ then we define

$$J_{\wp^{(i)}, \gamma_h} := \frac{1}{2} \left(|\langle \wp^{(i)}, \ell \rangle| - 1 \right) \,. \tag{4.26}$$

4.1.3.2 The vanilla PSC formula

Let $\wp$ be a halo-saturated susy interface for $\mathcal{W}_c$, with $\wp^{(i)}$ being the lift satisfying (4.25). Note that $\wp^{(i)}$ provides a trivialization for the torsor $\tilde{\Gamma}^*_{ij'}(z, z')$ (hence an isomorphism with $\tilde{\Gamma}^*$). In particular, we may single out a certain sub-torsor $\tilde{\Gamma}^*_{c,\wp^{(i)}} \simeq [\wp^{(i)}] + \tilde{\Gamma}^*_c \subset \tilde{\Gamma}^*_{ij'}(z, z')$, where $\tilde{\Gamma}^*_c \subset \tilde{\Gamma}^*$ is the critical sublattice[7] at ϑ_c. Considering the related restriction[8] of the partition function of framed BPS states (4.17):

$$F_{\wp^{(i)}}(\wp, u, \vartheta; y) := \sum_{\pi \in \tilde{\Gamma}^*_{c,\wp^{(i)}}} \overline{\Omega}(L_\wp, u, \vartheta, \pi; y) \, \hat{Y}_\pi \,, \tag{4.27}$$

[7] Let $\tilde{\Gamma}_c$ be the preimage of Γ_c under the natural map $\tilde{\Gamma} \to \Gamma$. There is also a natural map $\tilde{\Gamma}^* \to \tilde{\Gamma}$ obtained by filling the circle fibers above $\Sigma \setminus \Sigma^*$, then $\tilde{\Gamma}^*_c$ is the preimage of $\tilde{\Gamma}_c$.

[8] An explicit example will be provided below: the first line of (4.73) contains the full partition function (hence being the ii-component of the counterpart of (4.17)), while the LHS of (4.74) is the corresponding restriction to the sub-torsor determined by $\wp^{(i)}$ (the counterpart of (4.27)). The remaining terms in (4.73) don't appear in (4.74) since they clearly do not belong to the sub-torsor: their homology classes are not of the form $[\wp^{(i)}] + \tilde{\gamma}_c$ with $\tilde{\gamma}_c \in \tilde{\Gamma}^*_c$.

we can formulate our second conjecture.

Conjecture 2. *As ϑ varies across the $\mathcal{K}$-wall there exist integers $\{a_m(\tilde{\gamma}_h)\}_{m\in\mathbb{Z}}$ such that*

$$F_{\wp^{(i)}}(\wp,u,\vartheta_c^+;y)=F_{\wp^{(i)}}(\wp,u,\vartheta_c^-;y)\left[\prod_{\tilde{\gamma}_h}\prod_{m\in\mathbb{Z}}\Phi_{n(\tilde{\gamma}_h)}\Big((-y)^m\,\hat{Y}_{\tilde{\gamma}_h}\Big)^{a_m(\tilde{\gamma}_h)}\right]^{\pm 1}, \tag{4.28}$$

moreover the $a_m(\tilde{\gamma}_h)$ only depend on γ_h, and they are precisely the Laurent coefficients of $\Omega(u,\gamma_h;y)$[9].

The $\Phi_n(\xi)$ are finite-type dilogarithms

$$\Phi_n(\xi):=\prod_{s=1}^{|n|}(1+y^{-\mathrm{sgn}(n)\,(2s-1)}\xi)\,, \tag{4.29}$$

and

$$n(\tilde{\gamma}_h)=2J_{\wp^{(i)},\tilde{\gamma}_h}+1\,. \tag{4.30}$$

The sign is determined by the direction in which the $\mathcal{K}$-wall is crossed: a framed BPS state of halo charge γ_h is stable on the side where the Denef radius $\langle\gamma_h,\wp^{(i)}\rangle\,/\,2\,\mathrm{Im}\,(Z_{\gamma_h}/e^{i\vartheta})$ is positive, the sign is therefore positive when going from the unstable side to the stable one and vice versa[10].

The practical value of this conjecture comes from taking (4.17) into account at the same time. The latter allows to compute $F(\wp,u,\vartheta_c^{\pm};y)$, while (4.28) states how to extract the $a_m(\gamma)$ (Laurent coefficients of the PSC). In Section 4.3 we will provide supporting evidence for these conjectures.

4.1.3.3 Framed spin wall-crossing of generic interfaces

Halo-saturated interfaces are just a special class of susy interfaces, it is natural to ask whether we can say something about the framed wall-crossing of more generic choices. Our conjecture 1 offers a partial answer to this: the $2J_3$ eigenvalue of a framed BPS state is still identified with the writhe of the corresponding detour. The conjecture doesn't restrict to halo-saturated interfaces.

A crucial property of our special class of interfaces is that it allows to extract the *vanilla* PSC of states associated with halo particles. Generic interfaces instead are not guaranteed to capture this information, this fact is unrelated to the counting of spin and was evident already in the classical story [63, 65, 95, 106]. The simplest example of what could go wrong is provided by a "bare" interface: tuning the moduli (u,ζ) to vary within a sufficiently small region near a $\mathcal{K}$-wall, we may choose an interface which doesn't intersect with the network for any value of the moduli; certainly as the $\mathcal{K}$-wall is crossed, this interface wouldn't capture information of vanilla PSC's, because it lacks

[9] See (4.6).

[10] further details can be found in [61].

halos of any sort. While simple, this example points to an essential difference between interfaces and defects: the pairing $\langle \gamma_c, \gamma_h \rangle$ between an (infrared) defect of charge γ_c and a halo particle of charge γ_h is a topological quantity, it can't be smoothly deformed to zero; on the contrary the intersection pairing $\langle a, \gamma_h \rangle$ between a halo charge and an (infrared) interface a is well-defined on the respective homology classes only *after* the endpoints of a are deleted from Σ. More concretely, let us look back at equation (4.12), which applies both to IR line defects and interfaces. The wall-crossing of an IR defect of charge $\gamma_0 \in \Gamma$ will be governed by $\langle \gamma_0, L(\gamma) \rangle = \Omega(\gamma) \langle \gamma_0, \gamma \rangle$ for $\gamma \in \Gamma_c$. On the other hand for an interface $\langle a, L(\gamma) \rangle$ cannot be cast into the form $\Omega(\gamma)\langle a, \gamma \rangle$, precisely because the latter pairing is not well-defined. We will come back to generic interfaces in section 4.3.4, where we analyze in some detail explicit examples.

4.2 Formal parallel transport

In this section we describe the construction of a formal parallel transport on the UV curve C, employing the data of a flat abelian connection on Σ and a spectral network. The discussion parallels closely that of [63]: the transport along a path $\wp$ on C gets corrected by "detours" corresponding to the soliton data on streets crossed by $\wp$; the novelty will consist of keeping track of a suitable refinement of the soliton data.

After defining the formal parallel transport, we show that it enjoys twisted homotopy invariance, thus reproducing the transport by a flat non-abelian connection on C. As already noticed in [63], homotopy invariance is tightly connected to pure 2d wall-crossing, in our context this will lead to a refined version of the 2d WCF.

With respect to the PSC conjectures formulated above, this section's purpose is two-fold. First, we will provide a precise definition of the generating function of framed PSC's, in terms of detours. Second, we will derive the generalization of the six-way joint rules of [63, app.A] on which the definition of soliton paths relies.

4.2.1 Twisted formal variables

Let $C, \Sigma, \mathcal{W}$ be a triplet consisting of a punctured Riemann surface C, a ramified K-fold covering $\pi : \Sigma \to C$ and a spectral network subordinate to the covering. For convenience we will sometimes label the sheets of Σ, implicitly employing a trivialization of the covering. We will restrict $\mathcal{W}$ to WKB-type spectral networks, although everything should carry over in a straightforward way to

general spectral networks (as defined in [63, §9.1]). We define

$$C^* = C \setminus \{z_1, \ldots, z_n\}\,, \qquad \Sigma^* = \Sigma \setminus \pi^{-1}\left(\{z_1, \ldots, z_n\}\right) \tag{4.31}$$

where $\{z_1, \ldots, z_n\}$ is a collection of points (away from the branching locus) with $n \geq 2$.

A *path* on Σ^* (or C^*) will be understood as a *regular homotopy class* of curves on Σ^* (resp. C^*). We will say that two paths $\mathfrak{a}, \mathfrak{b}$ are *composable* into $\mathfrak{ab}$ if $\mathrm{end}(\mathfrak{a}) = \mathrm{beg}(\mathfrak{b})$ and the corresponding tangent directions are equal at that point.

To each path $\mathfrak{a}$ we associate a formal variable $\hat{\Upsilon}_{\mathfrak{a}}$, then we consider the unital noncommutative algebra over the ring $\mathbb{Z}$ generated by the $\hat{\Upsilon}_{\mathfrak{a}}$ and subject to the following relations:

1. If $\mathfrak{a}, \mathfrak{b}$ are *regular-homotopic* (see figure 4.2) then

$$\hat{\Upsilon}_{\mathfrak{a}} = \hat{\Upsilon}_{\mathfrak{b}} \tag{4.32}$$

2. The product rule

$$\hat{\Upsilon}_{\mathfrak{a}}\hat{\Upsilon}_{\mathfrak{b}} = \begin{cases} \hat{\Upsilon}_{\mathfrak{ab}} & \text{if } \mathfrak{a}, \mathfrak{b} \text{ are composable} \\ 0 & \text{otherwise} \end{cases} \tag{4.33}$$

3. Two paths $\mathfrak{a}$ and $\mathfrak{a}'$, such that the natural pushforwards of $\beta(\mathfrak{a})$ and $\beta(\mathfrak{a}')$ to $H_1(\Sigma^*)$ coincide, are said to differ by a *contractible curl* if there exists a regular homotopy which takes $\mathfrak{a} \to \mathfrak{a}'$ except for a sub-interval of the domain $[t, t'] \subset [0, 1]$, where they differ by a curl (see figure 4.2). Contractible curls can be oriented clockwise or counterclockwise, for paths differing by a contractible curl

$$\hat{\Upsilon}_{\mathfrak{a}} = -\hat{\Upsilon}_{\mathfrak{a}'}\,. \tag{4.34}$$

Figure 4.2: On the left: $\mathfrak{a}, \mathfrak{b}$ are regular-homotopic. On the right: $\mathfrak{a}, \mathfrak{a}'$ differ by a contractible curl. Thus $\hat{\Upsilon}_{\mathfrak{a}} = \hat{\Upsilon}_{\mathfrak{b}}$ and $\hat{\Upsilon}_{\mathfrak{a}} = -\hat{\Upsilon}_{\mathfrak{a}'}$

4.2.2 Definition of $\mathfrak{F}(\wp)$: detours

Let $\wp$ be any path (in the sense specified above) on C^*, subject to the condition that

$$\{\mathrm{beg}(\wp), \mathrm{end}(\wp)\} \subset C \setminus C^*\,. \tag{4.35}$$

We associate a formal parallel transport $\mathfrak{F}(\wp)$, according to the following rules.

When $\wp \cap \mathcal{W} = \emptyset$

$$\mathfrak{F}(\wp) = \mathfrak{D}(\wp) := \sum_{i=1}^{K} \hat{\Upsilon}_{\wp^{(i)}} \,, \tag{4.36}$$

where $\wp^{(i)}$ are the lifts of $\wp$.

On the other hand, when $\wp$ intersects $\mathcal{W}$ at some point z on a one-way ij street p, it picks up contributions from soliton paths supported on p, and we have

$$\mathfrak{F}(\wp) := \mathfrak{D}(\wp) + \sum_{\mathfrak{a} \in \mathbf{\Gamma}^*_{ij}(p)} \mu_r(\mathfrak{a}, p)\, \hat{\Upsilon}_{\check{\wp}^{(i)}_+ \,\mathfrak{a}\, \check{\wp}^{(j)}_-} \,. \tag{4.37}$$

The sum runs over all regular homotopy classes with endpoints on the lift of p, the $\mu_r(\mathfrak{a}, p)$ are the refined soliton degeneracies: they are integers associated with soliton paths in each regular homotopy class $\mathfrak{a} \in \mathbf{\Gamma}^*_{ij}(z, z)$ and they are constant along p. The μ_r are uniquely determined by rules that will be presently discussed. In analogy with [63, §3.5], there is a relation between $\mathfrak{a}, \mathfrak{a}'$ which differ by a contractible curl

$$\mu_r(\mathfrak{a}, p) = -\mu_r(\mathfrak{a}', p) \,. \tag{4.38}$$

The $\check{\wp}^{(\alpha)}_{\pm}$, $\alpha = i, j$ are defined by splitting $\wp$ at z into $\wp_\pm$ and considering a deformation of the lifts that matches the initial/final tangent directions of the soliton path $\mathfrak{a}$ on sheets i, j of Σ^*; this is illustrated in figure 4.3.

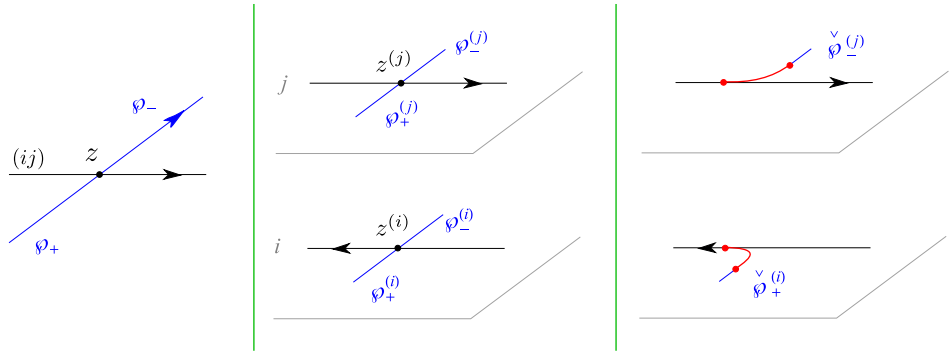

Figure 4.3: Splitting and deforming $\pi^{-1}(\wp)$.

Before moving on, let us introduce a convenient piece of notation: in order to deal with transports crossing several streets, it will sometime be convenient to rewrite (4.37) as

$$\mathfrak{F}(\wp) \;=\; \mathfrak{D}(\wp_+) \left(1 + \sum_{\mathfrak{a}} \mu_r(\mathfrak{a}, p)\, \hat{\Upsilon}_{\mathfrak{a}} \right) \mathfrak{D}(\wp_-) \,. \tag{4.39}$$

4.2.3 Twisted homotopy invariance

We now study the constraints of twisted homotopy invariance for the formal parallel transport. More precisely, for any path $\wp$ on C^*, we require $F(\wp)$ to depend only on the regular homotopy class of $\wp$. Similarly to the classical case [63], this requirement will induce constraints on the refined soliton content of the network. In fact, the whole analysis we will carry out is very close to that of [63], the only difference is that instead of relative homology classes on the circle bundle $\widetilde{\Sigma}$ (resp. $\widetilde{C}$), we work with regular homotopy classes on Σ^* (resp. C^*).

4.2.3.1 Contractible curl

Before we get to actual twisted homotopy invariance, let us briefly illustrate the meaning of "twisting". For the paths depicted in figure 4.4, we have

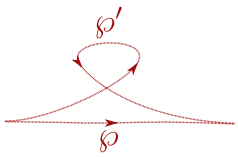

Figure 4.4: Two paths in the same relative homology class on Σ, which are not regular-homotopic.

$$\mathfrak{F}(\wp) = \mathfrak{D}(\wp) = \sum_i \hat{\Upsilon}_{\wp^{(i)}}\,, \qquad \mathfrak{F}(\wp') = \mathfrak{D}(\wp') = \sum_i \hat{\Upsilon}_{\wp'^{(i)}} \tag{4.40}$$

Where $\wp^{(i)}$, $\wp'^{(i)}$ are regular homotopy classes on Σ, corresponding to the lifts of $\wp$, $\wp'$. Since $\hat{\Upsilon}_{\wp'^{(i)}} = -\hat{\Upsilon}_{\wp^{(i)}}$, the formal transports are simply related as

$$\mathfrak{F}(\wp) = -\mathfrak{F}(\wp')\,. \tag{4.41}$$

4.2.3.2 Homotopy across streets

The simplest homotopy requirement to take into account is the one shown in figure 4.5, where a path $\wp$ is homotoped to $\wp'$ across a one-way street p of ij type.

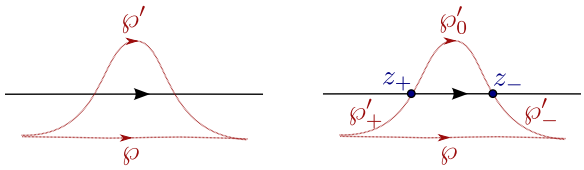

Figure 4.5: Paths differing by a regular homotopy across a street of the network.

The transports read

$$\begin{aligned}\mathfrak{F}(\wp) &= \mathfrak{D}(\wp)\\ \mathfrak{F}(\wp') &= \mathfrak{D}(\wp'_+)\Big(1+\sum_{\mathfrak{a}}\mu_r(\mathfrak{a},p)\,\hat{\Upsilon}_{\mathfrak{a}_{z_+}}\Big)\mathfrak{D}(\wp'_0)\Big(1+\sum_{\mathfrak{b}}\mu_r(\mathfrak{b},p)\,\hat{\Upsilon}_{\mathfrak{b}_{z_-}}\Big)\mathfrak{D}(\wp'_-)\\ &= \mathfrak{D}(\wp')+\sum_{\mathfrak{a}}\mu_r(\mathfrak{a},p)\left(\hat{\Upsilon}_{\wp'^{(i)}_+}\hat{\Upsilon}_{\mathfrak{a}_{z_+}}\hat{\Upsilon}_{\wp'^{(j)}_0}\hat{\Upsilon}_{\wp'^{(j)}_-}+\hat{\Upsilon}_{\wp'^{(i)}_+}\hat{\Upsilon}_{\wp'^{(i)}_0}\hat{\Upsilon}_{\mathfrak{a}_{z_-}}\hat{\Upsilon}_{\wp'^{(j)}_-}\right)\\ &= \mathfrak{D}(\wp')\end{aligned} \tag{4.42}$$

where, in the last step, we made use of (4.33) and (4.34), given that $\wp'^{(i)}_+\mathfrak{a}_{z_+}\wp'^{(j)}_0\wp'^{(j)}_-$ and $\wp'^{(i)}_+\wp'^{(i)}_0\mathfrak{a}_{z_-}\wp'^{(j)}_-$ differ precisely by a contractible curl. Since $\mathfrak{D}(\wp)\equiv\mathfrak{D}(\wp')$ by virtue of (4.32), this establishes invariance of the formal transport.

4.2.3.3 Branch Point

Homotopy invariance across branch points will provide some nontrivial constraints for *simpleton* degeneracies, just as in [63]. Considering two paths on C^* as depicted in figure 4.6, we study their transports component-wise.

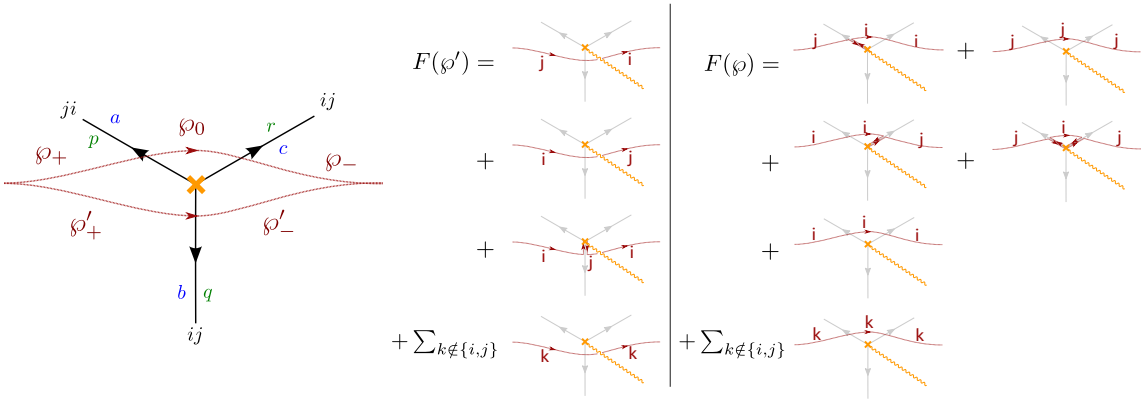

Figure 4.6: Regularly-homotopic paths across a branch point. Indicated in green are the street labels, and in blue the simpleton path labels.

Starting with the ji component[11], we have

$$\begin{aligned}\mathfrak{F}(\wp')_{ji} &= \hat{\Upsilon}_{\wp'^{(ji)}}\\ \mathfrak{F}(\wp)_{ji} &= \mu_r(\mathfrak{a},p)\,\hat{\Upsilon}_{\wp^{(j)}_+}\hat{\Upsilon}_{\mathfrak{a}}\hat{\Upsilon}_{\wp^{(i)}_0}\hat{\Upsilon}_{\wp^{(i)}_-}\end{aligned} \tag{4.43}$$

since $\wp^{(j)}_+\mathfrak{a}\wp^{(i)}_0\wp^{(i)}_-$ is regular homotopic to $\wp'^{(ji)}$, this gives

$$\mu_r(\mathfrak{a},p)=1\,. \tag{4.44}$$

[11] Notice that $\wp'$ crosses the ij branch cut, as shown on the right frame of figure 4.6.

A similar computation for the ij component reads

$$\begin{aligned}\mathfrak{F}(\wp')_{ij} &= \hat{\Upsilon}_{\wp'^{(ij)}} \\ \mathfrak{F}(\wp)_{ij} &= \mu_r(\mathfrak{c}, r)\, \hat{\Upsilon}_{\wp_+^{(i)}} \hat{\Upsilon}_{\wp_0^{(i)}} \hat{\Upsilon}_{\mathfrak{c}} \hat{\Upsilon}_{\wp_-^{(j)}}\end{aligned} \tag{4.45}$$

once again, noting that $\wp_+^{(i)} \wp_0^{(i)} \mathfrak{c} \wp_-^{(j)}$ is regular homotopic to $\wp'^{(ij)}$ yields

$$\mu_r(\mathfrak{c}, r) = 1\,. \tag{4.46}$$

Repeating with the ii components of the transports

$$\begin{aligned}\mathfrak{F}(\wp')_{ii} &= \mu_r(\mathfrak{b}, q)\, \hat{\Upsilon}_{\wp'^{(i)}_+} \hat{\Upsilon}_{\mathfrak{b}} \hat{\Upsilon}_{\wp'^{(ji)}_-} \\ \mathfrak{F}(\wp)_{ii} &= \hat{\Upsilon}_{\wp^{(i)}}\end{aligned} \tag{4.47}$$

again, we find

$$\mu_r(\mathfrak{b}, q) = 1\,. \tag{4.48}$$

Employing the results obtained so far, we can also evaluate the jj components

$$\begin{aligned}\mathfrak{F}(\wp')_{jj} &= 0 \\ \mathfrak{F}(\wp)_{jj} &= \hat{\Upsilon}_{\wp^{(j)}} + \mu_r(\mathfrak{a}, p)\mu_r(\mathfrak{c}, r)\, \hat{\Upsilon}_{\wp_+^{(j)}} \hat{\Upsilon}_{\mathfrak{a}} \hat{\Upsilon}_{\wp_0^{(i)}} \hat{\Upsilon}_{\mathfrak{c}} \hat{\Upsilon}_{\wp_-^{(j)}} \\ &= \hat{\Upsilon}_{\wp^{(j)}} + \hat{\Upsilon}_{\wp_+^{(j)}} \hat{\Upsilon}_{\mathfrak{a}} \hat{\Upsilon}_{\wp_0^{(i)}} \hat{\Upsilon}_{\mathfrak{c}} \hat{\Upsilon}_{\wp_-^{(j)}} = 0\end{aligned} \tag{4.49}$$

where we used the fact that $\wp^{(j)}$ and $\wp_+^{(j)} \mathfrak{a} \wp_0^{(i)} \mathfrak{c} \wp_-^{(j)}$ differ exactly by a contractible curl.

Finally, for the $k\ell$ components ($k, \ell \neq i, j$) we have

$$\mathfrak{F}(\wp')_{k\ell} = \mathfrak{F}(\wp)_{k\ell} \tag{4.50}$$

trivially.

4.2.3.4 Joints

Finally, let us examine homotopy invariance across joints of the network, as depicted in figure 4.7.[12]

The formal transports are computed by means of the detour rules, and read

$$\begin{aligned}\mathfrak{F}(\wp) &= \mathfrak{D}(\wp_+)\Big(1 + \sum_{\mathfrak{a}} \mu_r(\mathfrak{a}, p)\, \hat{\Upsilon}_{\mathfrak{a}}\Big)\Big(1 + \sum_{\mathfrak{b}} \mu_r(\mathfrak{b}, q)\, \hat{\Upsilon}_{\mathfrak{b}}\Big)\Big(1 + \sum_{\mathfrak{c}} \mu_r(\mathfrak{c}, r)\, \hat{\Upsilon}_{\mathfrak{c}}\Big)\mathfrak{D}(\wp_-) \\ \mathfrak{F}(\wp') &= \mathfrak{D}(\wp'_+)\Big(1 + \sum_{\mathfrak{c}} \mu_r(\mathfrak{c}, r')\, \hat{\Upsilon}_{\mathfrak{c}}\Big)\Big(1 + \sum_{\mathfrak{b}} \mu_r(\mathfrak{b}, q')\, \hat{\Upsilon}_{\mathfrak{b}}\Big)\Big(1 + \sum_{\mathfrak{a}} \mu_r(\mathfrak{a}, p')\, \hat{\Upsilon}_{\mathfrak{a}}\Big)\mathfrak{D}(\wp_-)\end{aligned} \tag{4.51}$$

[12] One should also examine joints of streets of types ij and $k\ell$, which do not involve the birth/death of new solitons. The analysis is straightforward and exactly parallel to that of [63], we omit it here and refer the reader to §5.2 of the reference.

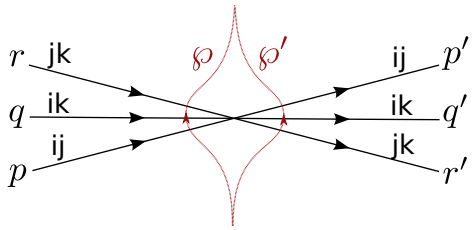

Figure 4.7: Two paths $\wp, \wp'$ within the same restricted regular homotopy class, across a branch point.

where it is understood that the detours involve suitable deformations as illustrated in figure 4.3.

Setting $F(\wp) = F(\wp')$, the ij, jk, ik components are respectively

$$\begin{aligned}
&\sum_{\mathfrak{a}} \mu_r(\mathfrak{a}, p)\, \hat{\Upsilon}_{\wp_+^{(i)}} \hat{\Upsilon}_{\mathfrak{a}} \hat{\Upsilon}_{\wp_-^{(j)}} = \sum_{\mathfrak{a}} \mu_r(\mathfrak{a}, p')\, \hat{\Upsilon}_{\wp'^{(i)}_+} \hat{\Upsilon}_{\mathfrak{a}} \hat{\Upsilon}_{\wp'^{(j)}_-} \\
&\sum_{\mathfrak{c}} \mu_r(\mathfrak{c}, r)\, \hat{\Upsilon}_{\wp_+^{(j)}} \hat{\Upsilon}_{\mathfrak{c}} \hat{\Upsilon}_{\wp_-^{(k)}} = \sum_{\mathfrak{c}} \mu_r(\mathfrak{c}, r')\, \hat{\Upsilon}_{\wp'^{(j)}_+} \hat{\Upsilon}_{\mathfrak{c}} \hat{\Upsilon}_{\wp'^{(k)}_-} \\
&\hat{\Upsilon}_{\wp_+^{(i)}} \Big(\sum_{\mathfrak{a},\mathfrak{c}} \mu_r(\mathfrak{a}, p)\mu_r(\mathfrak{c}, r)\, \hat{\Upsilon}_{\mathfrak{a}} \hat{\Upsilon}_{\mathfrak{c}} + \sum_{\mathfrak{b}} \mu_r(\mathfrak{b}, q) \hat{\Upsilon}_{\mathfrak{b}} \Big) \hat{\Upsilon}_{\wp_-^{(k)}} = \sum_{\mathfrak{b}} \mu_r(\mathfrak{b}, q')\, \hat{\Upsilon}_{\wp'^{(i)}_+} \hat{\Upsilon}_{\mathfrak{b}} \hat{\Upsilon}_{\wp'^{(k)}_-}
\end{aligned} \tag{4.52}$$

from which the following 2d wall-crossing formula follows

$$\begin{aligned}
\mu_r(\mathfrak{a}, p') &= \mu_r(\mathfrak{a}, p) \\
\mu_r(\mathfrak{c}, r') &= \mu_r(\mathfrak{c}, r) \\
\mu_r(\mathfrak{b}, q') &= \mu_r(\mathfrak{b}, q) + \sum_{\mathfrak{a},\mathfrak{b}|\mathfrak{c}} \mu_r(\mathfrak{a}, p)\mu_r(\mathfrak{c}, r)
\end{aligned} \tag{4.53}$$

where the last sum runs over $\mathfrak{a}, \mathfrak{c}$ whose concatenation $\mathfrak{a}\mathfrak{c}$ is regular-homotopic to $\mathfrak{b}$, so that $\hat{\Upsilon}_{\mathfrak{b}} = \hat{\Upsilon}_{\mathfrak{a}} \hat{\Upsilon}_{\mathfrak{c}}$[13]. This concludes the study of homotopy invariance of the formal parallel transport.

4.2.4 Invariance of $F(\wp)$ under regular homotopy

In the previous section we established the invariance of $\mathfrak{F}(\wp)$ under regular homotopy, for $\wp \subset C$ with $\{\mathrm{beg}(\wp), \mathrm{end}(\wp)\} \subset C \setminus C^*$.

Let us now choose C^* (resp. Σ^*) as in section 4.1.2.1, i.e. the set of auxiliary punctures now only includes the endpoints z, z' of $\wp$ (resp. $\pi^{-1}\{z, z'\} \subset \Sigma$). Using the detour rules, the formal parallel transport can be written in the generic form

$$\mathfrak{F}(\wp) = \sum_{ij'} \sum_{\mathfrak{p} \in \mathbf{\Gamma}^{*\,(r)}_{ij'}(z,z')} \overline{\Omega}(L_\wp, u, \vartheta, \mathfrak{p})\, \hat{\Upsilon}_{\mathfrak{p}} \tag{4.54}$$

[13] More precisely, the correct statement is that one has to concatenate $\mathfrak{a}$, $\mathfrak{c}$ by gluing an extra small arc between them to match endpoint tangents. Similarly, in order to compare $\mathfrak{a}\mathfrak{c}$ to $\mathfrak{b}$ one must further add small arcs at the endpoints of $\mathfrak{a}\mathfrak{c}$, in order to match the initial and final directions of $\mathfrak{b}$. These modifications are inessential here, since we adopt, by definition of the detour rules, paths with all the suitable modifications, and eventually we actually compare $\hat{\Upsilon}_{\wp_+^{(i)}\mathfrak{a}\mathfrak{c}\wp_-^{(k)}}$ to $\hat{\Upsilon}_{\wp_+^{(i)}\mathfrak{a}\mathfrak{b}\wp_-^{(k)}}$. Although irrelevant in this context, this issue was dealt with in Appendix B of [73].

where the sum is over all regular homotopy classes $\mathfrak{p}$ of detours of $\wp$ on C^*, and the coefficients of the series are defined by this expression. According to (4.38) and in analogy to [63, §3.5], these degeneracies obey

$$\overline{\Omega}(L_\wp, u, \vartheta, \mathfrak{a}) = -\overline{\Omega}(L_\wp, u, \vartheta, \mathfrak{a}') \tag{4.55}$$

for $\mathfrak{a}, \mathfrak{a}'$ differing by a contractible curl.

We take this as the *definition* of the refined framed degeneracies introduced in (4.16).

Since $\mathfrak{F}(\wp)$ involves exclusively paths $\mathfrak{p} \in \mathbf{\Gamma}^*(z, z') := \sqcup_{ij'} \mathbf{\Gamma}^*_{ij'}(z, z')$, we may associate to each of them its own writhe $y^{\mathrm{wr}(\mathfrak{p})}$. Then we can consider a *linear map* (it is not an algebra map!)

$$\rho(\hat{\Upsilon}_\mathfrak{p}) := y^{\mathrm{wr}(\mathfrak{p})} \hat{Y}_{\beta(\mathfrak{p})} \,, \tag{4.56}$$

in §4.5.2 below we will propose some physical intuition for this map. For convenience we adopt the following definition

$$\overline{\Omega}(L_\wp, u, \vartheta, \mathfrak{p}; y) := \overline{\Omega}(L_\wp, u, \vartheta, \mathfrak{p})\, y^{\mathrm{wr}(\mathfrak{p})} \,. \tag{4.57}$$

Collecting regular homotopy classes $\mathfrak{p}$ on Σ^* that all belong to the preimage of a relative homology class π on $\widetilde{\Sigma}^*$, the formal parallel transport maps to

$$\begin{aligned} \rho\Big(\mathfrak{F}(\wp)\Big) &= \sum_{ij'} \sum_{\pi \in \widetilde{\Gamma}^*_{ij'}(z,z')} \sum_{\mathfrak{p} \,|\, \beta(\mathfrak{p}) = \pi} \overline{\Omega}(L_\wp, u, \vartheta, \mathfrak{p}; y)\, \hat{Y}_\pi \\ &= \sum_{ij'} \sum_{\pi \in \widetilde{\Gamma}^*_{ij'}(z,z')} \overline{\Omega}(L_\wp, u, \vartheta, \pi; y)\, \hat{Y}_\pi \,. \end{aligned} \tag{4.58}$$

Since $\mathfrak{F}(\wp)$ is a (twisted) invariant of regular homotopy of $\wp$, defining

$$F(\wp) := \rho\Big(\mathfrak{F}(\wp)\Big) \tag{4.59}$$

establishes the twisted regular homotopy invariance claimed below (4.17).

4.2.5 Joint rules for two-way streets

As in [63, 73], the key to computing vanilla BPS spectra are certain equations relating the soliton content on the 2-way streets meeting at a joint. This subsection is devoted to presenting the corresponding refined version. Considering the example shown in figure B.1, there are six two-way streets, each one carrying two soliton sets. The soliton data is encoded into the generating functions denoted τ, ν, one for each street p of type ij:

$$\tau_{ij} = \sum_\mathfrak{a} \mu_r(\mathfrak{a}, p) \hat{\Upsilon}_\mathfrak{a} \qquad \nu_{ij} = \sum_\mathfrak{b} \mu_r(\mathfrak{b}, p) \hat{\Upsilon}_\mathfrak{b} \tag{4.60}$$

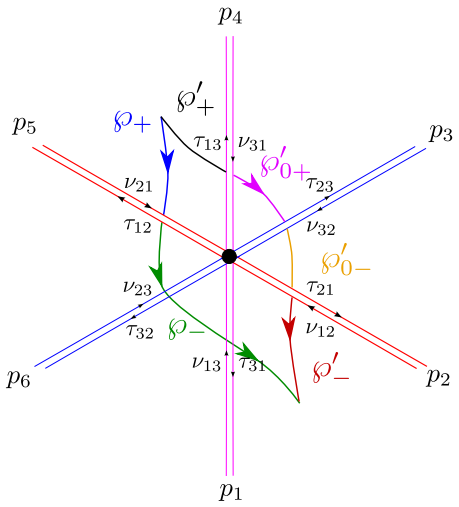

Figure 4.8: A six-way joint of 2-way streets, in the British resolution. Each 2-way street has two "lanes" (one-way streets), one of type ij and another of type ji and $i, j \in \{1, 2, 3\}$ according to the labels shown next to each street. Each lane carries its own soliton content, indicated next to it.

where $\mathfrak{a}, \mathfrak{b}$ are ij, ji solitons supported on p.

Choosing paths $\wp, \wp'$ as shown, invariance of the formal parallel transport entails, in particular

$$\mathfrak{F}_{12}(\wp) = \mathfrak{F}_{12}(\wp') \tag{4.61}$$

where, explicitly we have

$$\begin{aligned} \mathfrak{F}_{12}(\wp) &= \hat{\Upsilon}_{\wp_+^{(1)}}\, \tau_{12}\, \hat{\Upsilon}_{\wp_-^{(2)}} \\ \mathfrak{F}_{12}(\wp') &= \hat{\Upsilon}_{\wp'^{(1)}_+}\, \tau_{13}\, \hat{\Upsilon}_{\wp'^{(3)}_{0_+}}\, \nu_{32}\, \hat{\Upsilon}_{\wp'^{(2)}_{0_-}} \hat{\Upsilon}_{\wp'^{(2)}_-} + \hat{\Upsilon}_{\wp'^{(1)}_+} \hat{\Upsilon}_{\wp'^{(1)}_{0_+}} \hat{\Upsilon}_{\wp'^{(1)}_{0_-}}\, \nu_{12}\, \hat{\Upsilon}_{\wp'^{(2)}_-} \end{aligned} \tag{4.62}$$

To lighten notation, we will write the constraint of homotopy invariance simply in the form[14]

$$\tau_{12} = \nu_{12} + \tau_{13}\nu_{32}\,. \tag{4.63}$$

Similar, appropriate choices of auxiliary paths $\wp, \wp'$ allow to recover the desired joint soliton rules

$$\begin{aligned} &\tau_{12} = \nu_{12} + \tau_{13}\nu_{32}, \quad \tau_{21} = \nu_{21} + \nu_{23}\tau_{31}, \\ &\tau_{23} = \nu_{23} + \tau_{21}\nu_{13}, \quad \tau_{32} = \nu_{32} + \nu_{31}\tau_{12}, \\ &\tau_{31} = \nu_{31} + \tau_{32}\nu_{21}, \quad \tau_{13} = \nu_{13} + \nu_{12}\tau_{23}. \end{aligned} \tag{4.64}$$

these look exactly the same as the rules in [63, 73], with the only difference that we are working with regular homotopy classes on Σ^*.

[14] As noted in appendix B of [73], this expression is incomplete. It should involve a certain formal variable, called η in the reference, to account for small arcs that need to be added to match tangent directions of solitons of τ_{13} with those of ν_{32} and their composition with the solitons of ν_{12}. In our context, we suppress the η because later on, when computing generating functions for 4d BPS states, we will be actually always working with homotopy invariance of auxiliary paths $\wp, \wp'$ and such η is subsumed in the rules for deforming detour paths.

4.2.5.1 Definition of soliton paths

In section 4.1.3.1 we defined halo-saturated susy interfaces based on the notion of *soliton paths*, in this section provide more detail about the latter.

Let $p \in \mathcal{W}_c$ be a two-way street of ij-type, it may be thought of as a pair of one-way streets p_{ij} and p_{ji}. To determine the soliton paths going through street p we proceed as follows. p_{ij} has an orientation, let us denote $J[p, ij]$ the joint from which it flows out, similarly $J[p, ji]$ is the joint associated with p_{ji}. At $J[p, ij]$ we may consider the rules (B.1), expanding them in terms of *incoming* soliton generating functions, for example

$$\tau_{12} = \nu_{12} + \nu_{13}\nu_{32} + \nu_{12}\nu_{23}\nu_{32} + \nu_{12}\nu_{21}\nu_{13}\nu_{32} + \nu_{12}\nu_{23}\nu_{31}\nu_{13}\nu_{32} + \dots \tag{4.65}$$

where $\nu_{\alpha\beta} = 0$ whenever the corresponding street isn't carrying solitons.

The lift $p_{ij,\Sigma} = \pi^{-1}(p_{ij})$ contains two components, $p_{ij}^{(i)}, p_{ij}^{(j)}$. We start constructing paths by *concatenating* the lifts of streets involved in such sums, in the order dictated by the above formulae. For example, if $p = p_5$ from figure B.1 we would consider several paths:

$$\begin{aligned} &p_{5,12}^{(1)} \cdot p_{2,12}^{(1)}(\dots)\, p_{2,12}^{(2)} \cdot p_{5,12}^{(2)} \\ &p_{5,12}^{(1)} \cdot p_{1,13}^{(1)}(\dots)\, p_{1,13}^{(3)} \cdot p_{3,32}^{(3)}(\dots)\, p_{3,32}^{(2)} \cdot p_{5,12}^{(2)} \\ &\dots \end{aligned} \tag{4.66}$$

where $(\dots)$ are placeholders, which will be filled upon iteration of this procedure: namely taking into consideration the junctions at the *other* ends of the streets involved (e.g. $J[p_2, 12]$ in the first line, $J[p_1, 13]$ and $J[p_3, 32]$ in the second line, and so on). Iterating this procedure, one eventually reaches two-way streets terminating on branch-points. If the branch-point in question sources only *one* two-way street, then the $(\dots)$ are simply dropped for that street. If there is more than one two-way street ending on the branch-point, one must take into account further detours, as explained e.g. in [63, app.A]. The procedure involved is a straightforward generalization of the one for joints, we skip its description.

Thus we have constructed (possibly infinite) sets of *open* soliton paths, associated with p_{ij} and p_{ji}. Joining them pairwise produces the *closed* soliton paths employed in section 4.1.3.1.

4.3 Applications and examples

4.3.1 Vectormultiplet in $SU(2)$ SYM

The simplest nontrivial example is the spectral network of the vectormultiplet of charge γ in the weak coupling regime of $SU(2)$ SYM [64]. In order to choose a halo-saturated interface, we need

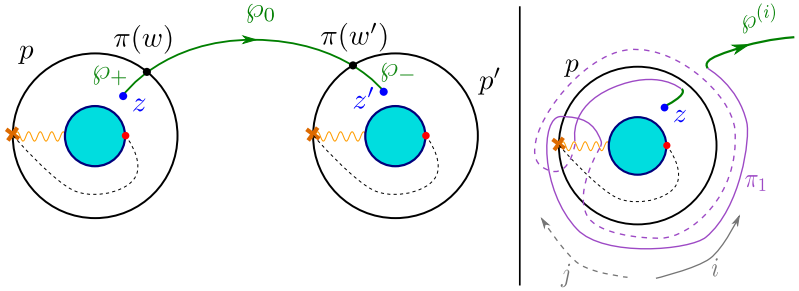

Figure 4.9: On the left, the spectral network at the critical phase; C is a cylinder, two way streets are solid lines, branch points and cuts are in orange. $z, z' \in C$ label punctures associated with UV surface defects, a choice of halo-saturated interface is shown in green. Red dots mark singularities of the WKB flow (see [64]). On the right: an example of a detour π_1; the WKB flow is indicated in grey for the two sheets of Σ.

first to construct $\Pi(\mathcal{W}_c)$. The critical sub-network $\mathcal{W}_c$ is depicted with solid black lines in figure 4.9; applying the detour rules to the branch-point of street p we find

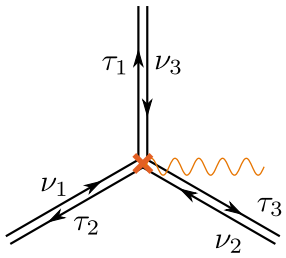

Figure 4.10: The branch point of the two way street p from figure 4.9.

$$\begin{aligned} &\nu_3 = \tau_2\, X_{\tilde{\gamma}} \qquad \nu_1 = \tau_1\, X_{\tilde{\gamma}} \qquad \nu_2 = 0 \\ &\tau_2 = X_{a_2} \qquad \tau_1 = X_{a_1} + \tau_1\, X_{\tilde{\gamma}} \end{aligned} \tag{4.67}$$

where a_1 is an ij-type soliton (it runs from sheet i to sheet j), while a_2 is of type ji. We used $\tau_n = X_{a_n} + \nu_n$ [63, app.A] with a_n denoting the *simpleton* paths sourcing from the branch point, and $\tilde{\gamma} \in \tilde{\Gamma}$ is the tangent lift of γ (which is the "critical" charge γ_c corresponding to the $\mathcal{K}$-wall, although we will be avoiding such notation to avoid confusion with the "core" charge of a halo boundstate). Therefore, let us define

$$Q(p) = 1 + \tau_1 \nu_3 = 1 + X_{a_1}\,(1 - X_{\tilde{\gamma}})^{-1}\, X_{a_2}\, X_{\tilde{\gamma}} = (1 - X_{\tilde{\gamma}})^{-1} \tag{4.68}$$

where we used[15] $X_{a_1}X_{\tilde\gamma} = X_{\tilde\gamma}X_{a_1}$ and $X_{a_1}X_{a_2} = 1$ (the closure map $\mathrm{cl}(a_1a_2) = 0 \in \tilde\Gamma^*$ is understood, see [73]); this expression for $Q(p)$ agrees with the expected one [63, 64]. A similar computation for p' reveals the same contribution. Keeping track of *soliton paths* we find that

$$\begin{aligned} \Pi(p) &= \{\ell_n\}_{n=1}^{\infty} \qquad \ell_1 = \mathring{p}_\Sigma \qquad \ell_n = \ell_{n-1}\,\ell_1\,, \\ \Pi(p') &= \{\ell'_n\}_{n=1}^{\infty} \qquad \ell'_1 = \mathring{p}'_\Sigma \qquad \ell'_n = \ell'_{n-1}\,\ell'_1\,, \end{aligned} \tag{4.69}$$

where $\mathring{p}_\Sigma$ is the regular homotopy class of the lift of street p to Σ^*, where it is understood in this example that the endpoints of the two components of the lifts are pairwise glued together (at the ramification point, see figure 4.9) into a single closed path. The notation $\ell_{n-1}\ell_1$ needs some further clarification: these are regular homotopy classes of closed curves, hence composition is ambiguous. Denote $p_\Sigma^{(i)}, p_\Sigma^{(j)}$ the two components of $\pi^{-1}(p)$. Then to construct ℓ_2 one takes two copies of p_Σ: p'_Σ, p''_Σ and glues $p'^{(i)}_\Sigma p'^{(j)}_\Sigma p''^{(i)}_\Sigma p''^{(j)}_\Sigma$, then gluing the endpoint of $p''^{(j)}_\Sigma$ with the starting point of $p'^{(i)}_\Sigma$ gives an actual closed path, ℓ_2 is the corresponding regular homotopy class. The construction generalizes straightforwardly to $\ell_{n-1}\ell_1$.

Noting that $[\ell_n] = [\ell'_n] = n\tilde\gamma$, we deduce immediately that $\wp$ as depicted in figure 4.9 satisfies both conditions (4.25).

Choose a trivialization of the cover such that τ_1 carries contributions from ij-solitons (this together with the WKB flow fixes all other sheet labels), compatibly with the right frame of fig. 4.9. Then studying the detours of $\wp$ we find

$$\begin{aligned} F_{ii}(\wp, \vartheta_c^-) &= X_{\wp^{(i)}} + X_{\wp_+^{(i)}}\Big(1 + \sum_{n=1}^{\infty} X_{a_1+n\tilde\gamma}\Big) X_{\wp_0^{(j)}} \Big(1 + \sum_{n=1}^{\infty} X_{a'_1+n\tilde\gamma}\Big) X_{\wp_-^{(i)}} \\ F_{ii}(\wp, \vartheta_c^+) &= X_{\wp_+^{(i)}}\, Q(p)\, X_{\wp_0^{(i)}}\, Q(p')\, X_{\wp_-^{(i)}} + X_{\wp_+^{(i)}}\Big(1 + \sum_{n=1}^{\infty} X_{a_1+n\tilde\gamma}\Big) X_{\wp_0^{(j)}} \Big(1 + \sum_{n=1}^{\infty} X_{a'_1+n\tilde\gamma}\Big) X_{\wp_-^{(i)}} \end{aligned} \tag{4.70}$$

where the second term of both expressions corresponds to ij detours on street p composed with ji detours on street p', while the first term in the second expression counts ii detours on both p and p'. We took into account that all 2d soliton degeneracies $\mu_\pm(a_1 + n\tilde\gamma), \mu_\pm(a'_1 + n\tilde\gamma)$ are 1 in this example. The contribution from halos of core charge $\wp^{(i)}$ undergoes the jump

$$X_{\wp^{(i)}} \quad \mapsto \quad X_{\wp^{(i)}}(1 - X_{\tilde\gamma})^{-2} \tag{4.71}$$

in agreement with $\langle \wp^{(i)}, L(\gamma)\rangle = \langle \wp^{(i)}, -p_\Sigma - p'_\Sigma\rangle = -2$.

[15] The fact that $X_{a_1}X_{a_2} = 1$ may not be obvious at first glance. This is a technical identity that reflects the choice of concatenating a_1 with a_2 the short way around, thus not going around the street p, thus giving a contractible cycle. This occurrence is dictated by the fact that we chose to indicate explicitly the parallel transport of solitons around p by factors of $X_{\tilde\gamma}$ in (4.67), accordingly it would be wrong to write $X_{a_1}X_{a_2} = X_{\tilde\gamma}$ since it would introduce extra powers of $X_{\tilde\gamma}$.

Now we take into account the writhe: first note that the writhe of ℓ_n, ℓ'_n with respect to the detour points w, w' (see figure 4.9) is

$$\mathrm{wr}(\ell_n, w) = -n \qquad \mathrm{wr}(\ell'_n, w) = n\,, \tag{4.72}$$

as clarified by the right frame of figure 4.9. Therefore we find

$$\begin{aligned} F_{ii}(\wp, \vartheta_c^-; y) &= \hat{Y}_{\wp^{(i)}} + \sum_{n,n'=0}^{\infty} y^{-n+n'}\, \hat{Y}_{\wp_+^{(i)} a_1 \wp_0^{(j)} a_1' \wp_-^{(i)} + (n+n')\tilde{\gamma}} \\ F_{ii}(\wp, \vartheta_c^+; y) &= \hat{Y}_{\wp^{(i)}} + \sum_{n=1}^{\infty} (y^{-n} + y^n)\, \hat{Y}_{\wp^{(i)} + n\tilde{\gamma}} + \sum_{n,n'=1}^{\infty} y^{-n+n'}\, \hat{Y}_{\wp^{(i)} + (n+n')\tilde{\gamma}} \\ &\quad + \sum_{n,n'=0}^{\infty} y^{-n+n'}\, \hat{Y}_{\wp_+^{(i)} a_1 \wp_0^{(j)} a_1' \wp_-^{(i)} + (n+n')\tilde{\gamma}} \end{aligned} \tag{4.73}$$

This agrees with the expected jump for $\hat{Y}_{\wp^{(i)}}$, indeed according to our conjecture we expect

$$\begin{aligned} F_{\wp^{(i)}}(\wp, \vartheta_c^-; y) = \hat{Y}_{\wp^{(i)}} \quad &\mapsto \quad \hat{Y}_{\wp^{(i)}} \left(1 - \hat{Y}_{\tilde{\gamma}}\right)^{-1} \left(1 - y^{-2}\, \hat{Y}_{\tilde{\gamma}}\right)^{-1} \\ &= \quad \hat{Y}_{\wp^{(i)}}\, \Phi_1((-y)^{-1}\, \hat{Y}_{\tilde{\gamma}})^{-1}\, \Phi_1((-y)\, \hat{Y}_{\tilde{\gamma}})^{-1} \\ &= \quad F_{\wp^{(i)}}(\wp, \vartheta_c^+; y) \end{aligned} \tag{4.74}$$

where $J_{\wp^{(i)}, \tilde{\gamma}} = 0$ in this setup, together with $a_m(\gamma) = -\delta_{m,\pm 1}$.

4.3.2 The 3 - herd

The next nontrivial example is provided by a class of critical networks known as k-herds [73]. The case $k = 1$ is trivial, while the 2-herd is just another network for the vectormultiplet studied above. The first interesting case is therefore $k = 3$, we focus on this although our analysis can be straightforwardly extended to higher integer k.

The soliton content of the 2-way streets of the 3-herd has been studied in great detail in [73]. Let $\tilde{\gamma}$ be the generator of the critical sublattice corresponding to the $\mathcal{K}$-wall. Recall that it may be constructed from $\mathcal{W}_c$ as the homology class of a weighted sum of lifts of the streets of the network, where the weights are dictated by the soliton data. Rather than describing precisely the set $\Pi(\mathcal{W}_c)$ it will be sufficient for us to note (see in particular §C.6.2 of the reference) that, for any street p and any two soliton paths $\mathfrak{a}, \mathfrak{b}$ (of ij/ji types respectively) supported on p, $\ell = \mathrm{cl}(\mathfrak{a}\mathfrak{b})$ is characterized by

$$[\ell] = n\tilde{\gamma} \quad \Leftrightarrow \quad \ell \ni \{\delta_{1,\Sigma}, \delta_{2,\Sigma}, \delta_{3,\Sigma}, \delta_{4,\Sigma}\} \quad n \text{ times}, \tag{4.75}$$

where inclusion of $\delta_{i,\Sigma}$ stands for the fact that the solitons run through the i-th ramification point n times. Street names refer to figure 4.11, and γ is the generator of the critical sublattice (with orientation fixed by ϑ_c).

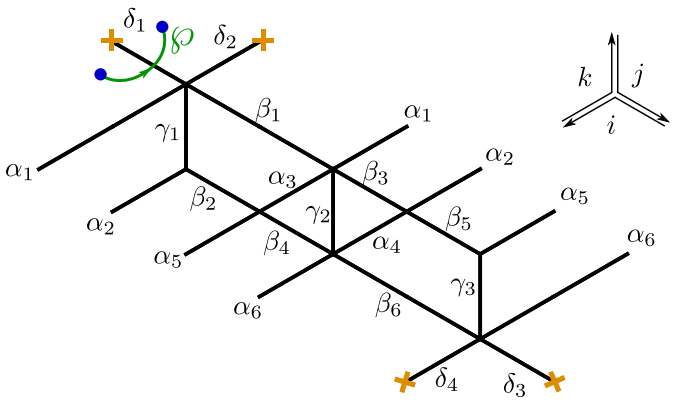

Figure 4.11: The street map of the 3-herd, on the cylinder C which has been cut. The network streets are glued according to their labeling. The schematic direction of WKB flow of the three types of streets is displayed on the upper right, for example the branch-point on the upper-left of the herd sits at the end of an ij-type street and is therefore an ij-type branchpoint.

With this information at hand, we can make a simple choice of a halo-saturated $\wp$, displayed in figure 4.11. Other choices are clearly possible. The machinery of section 4.2 establishes relations between generating functions for different halo saturated choices of $\wp$: different choices of $\wp$ within the same regular homotopy class on C^* are equivalent.

By direct inspection of soliton paths involved in detours of $\wp^{(i)}$, one finds the following framed generating functions

$$\begin{aligned}
F_{ii}(\wp,\vartheta_c^-;y) &= \hat{Y}_{\wp^{(i)}} \\
F_{ii}(\wp,\vartheta_c^+;y) &= \hat{Y}_{\wp^{(i)}} + \big(y^{-2}+1+y^2\big)\hat{Y}_{\wp^{(i)}+\tilde{\gamma}} \\
&\quad + \big(y^{-6}+2y^{-4}+3y^{-2}+3+3y^2+2y^4+y^6\big)\hat{Y}_{\wp^{(i)}+2\tilde{\gamma}} \\
&\quad + \big(y^{-12}+2y^{-10}+5y^{-8}+8y^{-6}+11y^{-4}+12y^{-2}+13 \\
&\quad + 12y^2+11y^4+8y^6+5y^8+2y^{10}+y^{12}\big)\hat{Y}_{\wp^{(i)}+3\tilde{\gamma}}+\cdots \\
&= \hat{Y}_{\wp^{(i)}} \prod_{m\in[1]} \Phi_1((-y)^m \hat{Y}_{\tilde{\gamma}}) \prod_{m'\in[5/2]} \Phi_2((-y)^{m'} \hat{Y}_{2\tilde{\gamma}})^{-1} \\
&\quad \times \prod_{m''\in[3]\oplus[5]} \Phi_3((-y)^{m''} \hat{Y}_{3\tilde{\gamma}}) \quad \cdots
\end{aligned} \tag{4.76}$$

where the notation $m\in[k]$ stands for $m\in\{-2k,-2k+2,\ldots,2k-2,2k\}$.

Due to the simplicity of $\wp$, we have $F_{ii}(\wp,\vartheta_c^\pm;y) \equiv F_{\wp^{(i)}}(\wp,\vartheta_c^\pm;y)$ (cf. (4.27)), we thus find

agreement – up to terms of order $X_{3\tilde{\gamma}}$ – with the conjectured pattern of (4.28):

$$\begin{aligned} F_{\wp^{(i)}}(\wp, \vartheta_c^-; y) = \hat{Y}_{\wp^{(i)}} \quad &\mapsto \quad \hat{Y}_{\wp^{(i)}} \prod_{n=1}^{\infty} \prod_{m\in\mathbb{Z}} \Phi_n((-y)^m \hat{Y}_{n\tilde{\gamma}})^{a_m(n\tilde{\gamma})} \\ &= \quad F_{\wp^{(i)}}(\wp, \vartheta_c^+; y)\,. \end{aligned} \tag{4.77}$$

Moreover we recover the structure

$$\mathfrak{h}_\gamma = [1]\,, \qquad \mathfrak{h}_{2\gamma} = \left[\frac{5}{2}\right]\,, \qquad \mathfrak{h}_{3\gamma} = [3]\oplus[5]\,, \tag{4.78}$$

as irreps of $\mathfrak{so}(3)$, in agreement with [73, app.A].

In section 4.4.3 below, we will provide a derivation of the generating function employed above, obtained by a careful analysis of the soliton paths involved. In fact, we will provide such data for k-herds of any value of k. Adopting the same kind of $\wp$ as in our example, the above analysis extends straightforwardly to higher k and n, allowing for a direct comparison with [73, app.A], this provides further checks of the conjectures.

4.3.3 The 3-$(2,3)$ - herd

We now move to a more complicated example, introducing a whole new type of critical network. It was shown in [73] that in higher rank gauge theories there can be wild walls on the Coulomb branch. These are marginal stability walls $MS(\gamma,\gamma')$ with $|\langle\gamma,\gamma'\rangle| > 2$ across which wild BPS states are created/lost. Wild BPS states are particularly interesting for us, because their Clifford vacua $\mathfrak{h}_{a\gamma+b\gamma'}$ typically consist of large and highly reducible representations of $\mathfrak{so}(3)$, providing rich examples for testing our conjectures.

The critical networks of wild BPS states remained largely unexplored insofar. Except for states of charge $n(\gamma+\gamma')$ whose networks – in *some* regions of the Coulomb branch – are known to be k-herds, no other cases have previously been studied. It is well known that all states of charges $a\gamma+b\gamma'$ for

$$\frac{k-\sqrt{k^2-4}}{2} < \frac{a}{b} < \frac{k+\sqrt{k^2-4}}{2} \tag{4.79}$$

are wild.

We will now fix $k=3$ and $a=2, b=3$. This kind of state appears in one of the wild chambers of $SU(3)$ SYM: choosing the same point on the Coulomb branch as in [73, §3.4], and tuning to $\vartheta = 5.22181$, the critical network of figure 4.12 appears.

By direct inspection of the soliton paths associated with each two-way street, one finds that

$$[\ell] = n\tilde{\gamma} \quad \Leftrightarrow \quad \ell \ni \{2\times\delta_{1,\Sigma}, 3\times\delta_{2,\Sigma}, 2\times\delta_{3,\Sigma}, 3\times\delta_{4,\Sigma}\} \quad n \text{ times.} \tag{4.80}$$

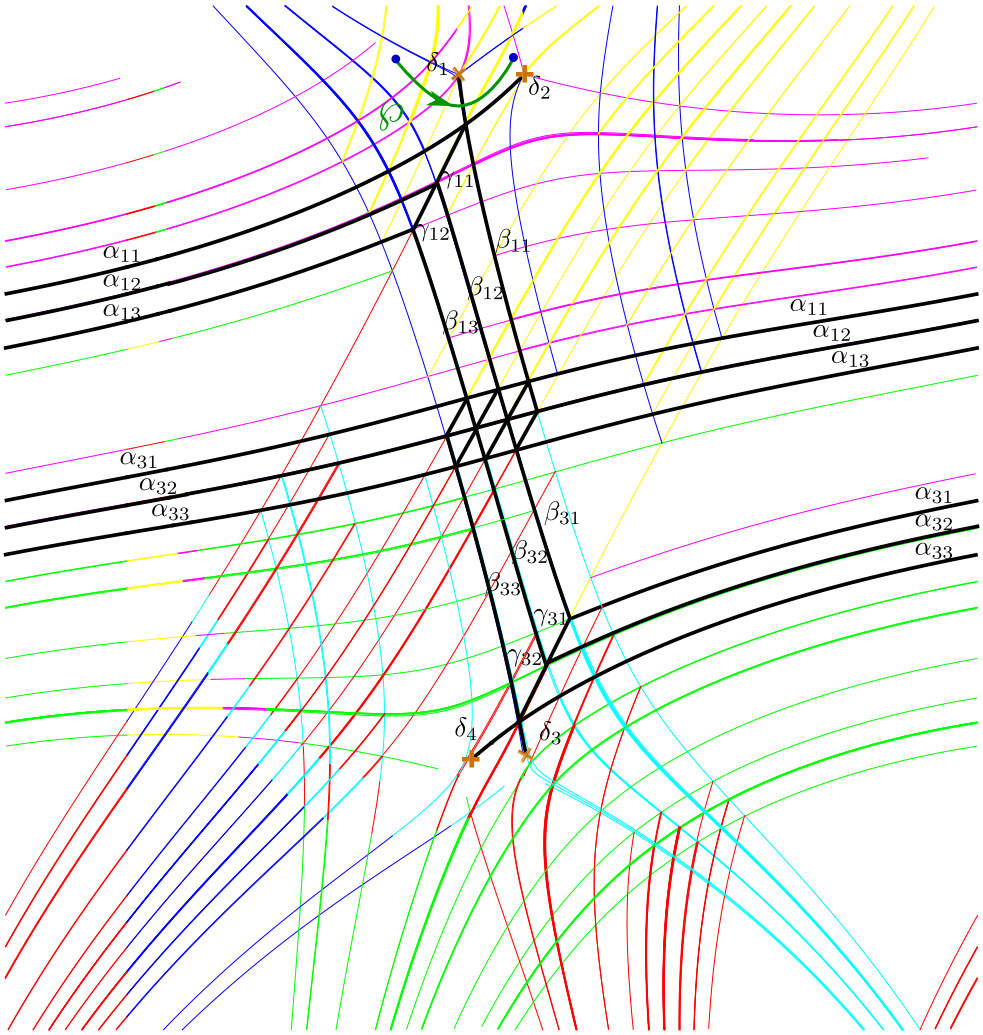

Figure 4.12: The street map of the 3-$(2,3)$-herd, on the cylinder C. Different colors denote streets carrying solitons of different types, such as ij, jk, ki-type solitons. Two-way streets are marked in black. Recall there is an identification of the far left and far right endpoints of α_{11} in the figure, and so forth.

with street names referring to figure 4.12, and γ being the generator of the critical sublattice (with orientation fixed by ϑ_c). This structure could have been expected on homological grounds, being a mild generalization of the 3-herd case.

Choosing $\wp$ as in fig 4.12 satisfies the halo-saturation condition. By direct inspection, the corresponding framed generating functions are

$$\begin{aligned} F_{ii}(\wp, \vartheta_c^-; y) &= \hat{Y}_{\wp^{(i)}} \\ F_{ii}(\wp, \vartheta_c^+; y) &= \hat{Y}_{\wp^{(i)}} + \left(y^{-7} + 2y^{-5} + 4y^{-3} + 6y^{-1} + 6y + 4y^3 + 2y^5 + y^7\right) \hat{Y}_{\wp^{(i)}+\tilde{\gamma}} + \cdots \\ &= \hat{Y}_{\wp^{(i)}} \prod_{m \in [1]\oplus[1]\oplus[3]} \Phi_2((-y)^m \hat{Y}_{\tilde{\gamma}}) \quad \times \left(\cdots\right) \end{aligned} \tag{4.81}$$

Due to the simplicity of $\wp$, we have $F_{ii}(\wp, \vartheta_c^{\pm}; y) \equiv F_{\wp^{(i)}}(\wp, \vartheta_c^{\pm}; y)$, we thus find agreement – up to terms of order $X_{\tilde{\gamma}}$ – with the conjectured pattern[16]:

$$\begin{aligned} F_{\wp^{(i)}}(\wp, \vartheta_c^{-}; y) = \hat{Y}_{\wp^{(i)}} \quad &\mapsto \quad \hat{Y}_{\wp^{(i)}} \prod_{n=1}^{\infty} \prod_{m\in\mathbb{Z}} \Phi_n((-y)^m \hat{Y}_{n\tilde{\gamma}})^{a_m(n\gamma)} \\ &= \quad F_{\wp^{(i)}}(\wp, \vartheta_c^{+}; y)\,. \end{aligned} \tag{4.82}$$

Moreover we recover the structure

$$\mathfrak{h}_\gamma = [1] \oplus [1] \oplus [3]\,, \tag{4.83}$$

as irreps of $\mathfrak{so}(3)$, in agreement with [73, app.A].

The above analysis can in principle be extended to other values of k, a, b. In appendix J we sketch the structure a large class of critical networks, which we call *off-diagonal herds*[17].

4.3.4 Generic interfaces and halos

We now come back to generic interfaces, as mentioned above in §4.1.3.3, our conjectures on the spin of framed BPS states naturally extend to these. There is a simple reason for studying generic interfaces: on the one hand they generically won't capture enough information to compute vanilla PSCs, but on the other hand their wall-crossing is of a more generic type, and studying it allows one to gain further insight into the implications of our conjectures.

In particular, the framed wall-crossing of IR line defects can be understood from a physical viewpoint in terms of a *halo picture* [61]. The fact that some framed BPS states arrange into halos is particularly important for computing (framed/vanilla) PSCs because halos furnish representations of the group of spatial rotations. Thus the halos naturally encode the spin content of framed BPS states, for this reason the halo picture played a crucial role in establishing a physical derivation of the motivic KS wall-crossing formula. Given the importance and the success of this picture, it is of particular significance to check whether predictions based on our conjectures are compatible with it.

To make the question sharper, note that in the case of generic interfaces $\mathfrak{so}(3)$ is broken to a Cartan subalgebra by the surface defects, which are stretched –say– along the x^3 axis, thus we cannot expect the same type of halos that appeared in the case of line defects. So what kind of halo picture can we expect? The breaking of the rotational symmetry will induce a distinction among the states of a vanilla multiplet according to their J_3 eigenvalue. We may then expect to have halos of

[16] Note that, given any soliton path $\ell \in \Pi(\mathcal{W}_c)$, $[\ell] = n\tilde{\gamma}$ implies that $\langle \wp^{(i)}, \ell \rangle = 2n$. Therefore $J_{\wp^{(i)}, n\tilde{\gamma}} = (2n-1)/2$ and the orbital m' runs over $2n$ different values, thus reproducing correctly the subscript of the dilogarithms. The factor of 2 comes from (4.80), had we chosen $\wp$ to cross δ_2 or δ_4, the corresponding factor would be 3 instead of 2.

[17] T. Mainiero has independently come to the picture of the off-diagonal herds and is currently studying them.

vanilla BPS states selectively binding to the interface depending on the J_3 quantum number. Before sharpening the question further, let us illustrate the latter statement with a simple example.

Consider a variant of the pure $SU(2)$ interface encountered above, as shown in figure 4.13.

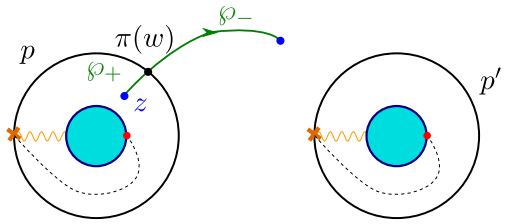

Figure 4.13: The SU(2) vectormultiplet critical network, with a different choice of susy interface $\wp$. This choice is not halo-saturated.

The removal of $\pi^{-1}(\text{end}(\wp))$ from Σ now distinguishes between closed cycles coming from lifts of p and those from lifts of p'. The sub-lattice of critical gauge charges generated by these lifts thus gets *resolved* with respect to the case of a halo saturated interface and is now two dimensional. We denote by $\tilde{\gamma}, \tilde{\gamma}'$ the generators associated with p and p' respectively[18]. It follows easily from the above analysis that we now have

$$\begin{aligned} F_{ii}(\wp, \vartheta_c^-; y) &= \hat{Y}_{\wp^{(i)}} \\ F_{ii}(\wp, \vartheta_c^+; y) &= \hat{Y}_{\wp^{(i)}} + \sum_{n=1}^{\infty} y^{-n}\, \hat{Y}_{\wp^{(i)}+n\tilde{\gamma}} = \hat{Y}_{\wp^{(i)}}\, \Phi_1((-y)^{-1}\, \hat{Y}_{\tilde{\gamma}})^{-1}\,, \end{aligned} \tag{4.84}$$

comparing with (4.74) one realizes that the interface binds not to the whole vanilla multiplet, but only a "partial" halo is formed, as if the interface is binding only to vanilla states with $2J_3 = -1$. Introducing the quantum-dilogarithms

$$\Phi(\xi) := \prod_{k=1}^{\infty} (1 + y^{2k-1}\xi)^{-1}\,, \tag{4.85}$$

the above can be recast into the suggestive form

$$\begin{aligned} F_{ii}(\wp, \vartheta_c^+; y) &= \Phi((-y)^{-1}\hat{Y}_{\tilde{\gamma}})^{a_{-1}(\gamma)} F_{ii}(\wp, \vartheta_c^-; y)\, \Phi((-y)^{-1}\, \hat{Y}_{\tilde{\gamma}})^{-a_{-1}(\gamma)} \\ &= \mathcal{O}\, F_{ii}(\wp, \vartheta_c^-; y)\, \mathcal{O}^{-1} \\ \mathcal{O} &= \Phi((-y)^{+1}\hat{Y}_{\tilde{\gamma}'})^{a_{+1}(\gamma)} \Phi((-y)^{-1}\hat{Y}_{\tilde{\gamma}})^{a_{-1}(\gamma)} \end{aligned} \tag{4.86}$$

[18] A one-dimensional sub-lattice obviously has two possible generators, however the choice of ϑ_c canonically lifts the degeneracy.

with $a_{\pm 1}(\gamma) = -1$ (cf. (4.74)) and where in the first line we used identity (K.2) as well as the equivalence $\Phi_n(z) = \Phi_{-n}(y^{-2n}z)$. In the second line we used the fact that $\langle \wp^{(i)}, \tilde{\gamma}' \rangle = 0$ hence $\hat{Y}_{\tilde{\gamma}'}\hat{Y}_{\wp^{(i)}} = \hat{Y}_{\wp^{(i)}}\hat{Y}_{\tilde{\gamma}'}$.

We will say that *the framed wall-crossing of a generic interface is compatible with the halo picture if the $\mathcal{K}$-wall jump of the generating function of framed PSCs can be expressed as a conjugation by quantum dilogarithms*[19].

As the next example will illustrate, it is not at all obvious that this criterion will be satisfied in general. Let us consider a different choice of interface for the 3-herd, as shown in figure 4.14.

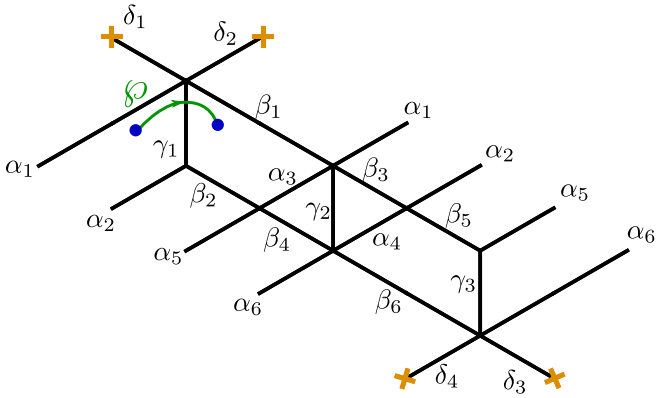

Figure 4.14: The 3-herd critical network, with a different choice of $\wp$. This choice is not halo-saturated.

After removing endpoints of $\wp$ from C and their lifts from Σ, there are two basic refined homology classes that we need to consider. They obey

$$\langle \wp^{(j)}, \tilde{\gamma}_1 \rangle = -1 \qquad \langle \wp^{(j)}, \tilde{\gamma}_2 \rangle = 0 \qquad \tilde{\gamma}_1 - \tilde{\gamma}_2 = \tilde{\gamma}_f \tag{4.87}$$

where $\tilde{\gamma}_f$ corresponds to a small cycle circling end($\wp^{(j)}$) clockwise. $\tilde{\gamma}_f$ is in the annihilator of $\langle\,,\,\rangle$ when restricted to $\tilde{\Gamma}^*$. We will refer to it as a "technical flavor charge".

By direct inspection we find the following detour generating functions

$$\begin{aligned} F_{jj}(\wp, \vartheta_c^-; y) &= \hat{Y}_{\wp^{(j)}} \\ F_{jj}(\wp, \vartheta_c^+; y) &= \hat{Y}_{\wp^{(j)}} + y^2\, \hat{Y}_{\wp^{(j)}+\tilde{\gamma}_1} + (y + y^5)\hat{Y}_{\wp^{(j)}+\tilde{\gamma}_1+\tilde{\gamma}_2} + 2y^4\hat{Y}_{\wp^{(j)}+2\tilde{\gamma}_1} \\ &\quad + 5y^6\hat{Y}_{\wp^{(j)}+3\tilde{\gamma}_1} + (5y^7 + 5y^3)\hat{Y}_{\wp^{(j)}+2\tilde{\gamma}_1+\tilde{\gamma}_2} \\ &\quad + (y^{10} + 2y^8 + y^4 + y^{-2} + 2)\hat{Y}_{\wp^{(j)}+\tilde{\gamma}_1+2\tilde{\gamma}_2} + \cdots \end{aligned} \tag{4.88}$$

[19]The choice of this criterion, as opposed to just demanding some jump of the form (4.84), is more stringent. It is relatively easy to find an expression for a $\mathcal{K}$-wall jump as a product of finite-type dilogs, but not all finite-type dilogs correspond to conjugation by quantum dilogs.

this jump of $F(\wp)$ presents a little puzzle: as explained in appendix K it cannot be immediately expressed as conjugation by quantum dilogarithms. This would seem to indicate some tension between our conjectures and the halo picture, for the case of generic interfaces.

However, by introducing a technical assumption on certain "flavor charges" associated with the endpoints of the interface, we found that the above expression *can* be massaged into a factorizable form. We will presently provide the details of this computation. While it is not clear to us what the generalization to generic interfaces should be, we expect one to exist. To recover the halo picture, we start with the identity

$$\begin{aligned} \hat{Y}_{\tilde{\gamma}_1} = \hat{Y}_{\tilde{\gamma}_2}\hat{Y}_{\tilde{\gamma}_f} = \hat{Y}_{\tilde{\gamma}_f}\hat{Y}_{\tilde{\gamma}_2} \;\Rightarrow\; \hat{Y}_{\wp^{(j)}+n_1\tilde{\gamma}_1+n_2\tilde{\gamma}_2} &= y^{-n_2}\hat{Y}_{\wp^{(j)}+(n_1+n_2)\tilde{\gamma}_1}\hat{Y}_{-n_2\tilde{\gamma}_f} \\ &= y^{n_2}\hat{Y}_{-n_2\tilde{\gamma}_f}\hat{Y}_{\wp^{(j)}+(n_1+n_2)\tilde{\gamma}_1} \end{aligned} \tag{4.89}$$

to turn the above into

$$\begin{aligned} F_{jj}(\wp,\vartheta_c^+;y) = \hat{Y}_{\wp^{(j)}} &+ y^2\,\hat{Y}_{\wp^{(j)}+\tilde{\gamma}_1} + (y^2+y^6)\hat{Y}_{-\tilde{\gamma}_f}\hat{Y}_{\wp^{(j)}+2\tilde{\gamma}_1} + 2y^4\hat{Y}_{\wp^{(j)}+2\tilde{\gamma}_1} \\ &+ 5y^6\hat{Y}_{\wp^{(j)}+3\tilde{\gamma}_1} + (5y^8+5y^4)\hat{Y}_{-\tilde{\gamma}_f}\hat{Y}_{\wp^{(j)}+3\tilde{\gamma}_1} \\ &+ (y^{12}+2y^{10}+y^6+1+2y^2)\hat{Y}_{-2\tilde{\gamma}_f}\hat{Y}_{\wp^{(j)}+3\tilde{\gamma}_1} + \cdots \end{aligned} \tag{4.90}$$

then (this is our technical assumption[20]) taking $\hat{Y}_{\tilde{\gamma}_f}\to 1$

$$\begin{aligned} F_{jj}(\wp,\vartheta_c^+;y) &= \hat{Y}_{\wp^{(j)}}\Big(1 + y^3\,\hat{Y}_{\tilde{\gamma}_1} + (y^4+2y^6+y^8)\,\hat{Y}_{2\tilde{\gamma}_1} \\ &\quad + (y^{15}+2y^{13}+5y^{11}+6y^9+5y^7+2y^5+y^3)\,\hat{Y}_{\wp^{(j)}+3\tilde{\gamma}_1} + \cdots\Big) \\ &= \mathcal{O}\,\hat{Y}_{\wp^{(j)}}\,\mathcal{O}^{-1} \end{aligned} \tag{4.91}$$

with

$$\begin{aligned} \mathcal{O} &= \Phi((-y)^2\hat{Y}_{\tilde{\gamma}_1})\,\Phi((-y)^3\hat{Y}_{2\tilde{\gamma}_1})^{-1}\,\Phi((-y)^5\hat{Y}_{2\tilde{\gamma}_1})^{-1} \\ &\quad\times\Phi\left((-y)^{10}\hat{Y}_{3\tilde{\gamma}_1}\right)\Phi\left((-y)^8\hat{Y}_{3\tilde{\gamma}_1}\right)\Phi\left((-y)^6\hat{Y}_{3\tilde{\gamma}_1}\right)^2 \\ &\quad\times\Phi\left((-y)^4\hat{Y}_{3\tilde{\gamma}_1}\right)\Phi\left((-y)^2\hat{Y}_{3\tilde{\gamma}_1}\right)\cdots \\ &= \prod_{n>0}\prod_{m\in\mathbb{Z}}\Phi((-y)^m\,\hat{Y}_{n\tilde{\gamma}_1})^{c_{n,m}}\,. \end{aligned} \tag{4.92}$$

All values of m appearing in the factorization are compatible with the vanilla spin content (4.78), moreover the exponents satisfy

$$0 \le \frac{c_{n,m}}{a_m(n\tilde{\gamma}_1)} \le 1 \tag{4.93}$$

[20]Recall that $\tilde{\gamma}_f$ is a "technical" flavor charge, arising from the removal of endpoints of the interface from Σ. It is therefore natural to assume that formal variables –which should be related to holonomies of a flat connection on a line bundle over Σ– should resemble trivial holonomy around this cycle.

for $a_m(n\tilde{\gamma}_1)$ defined by (4.28), this is compatible with the interpretation that each dilog is the contribution to the Framed Fock space by $|c_{n,m}|$ vanilla oscillators of corresponding charge and $2J_3$ eivgenvalue. Hence we recover the picture that the generic interface interacts unevenly with different states within a vanilla multiplet, as in the previous $SU(2)$ example. Only some of the vanilla states bind to the interface as the $\mathcal{K}$-wall is crossed, while another part of the vanilla multiplet does not.

It is worth mentioning that, based on the observations and the conjecture of appendix H, it should be possible to enhance (4.92) with dilog factors corresponding to other states in the vanilla multiplet as well, in the same fashion as in (4.86). This would reinforce the picture of a generic interface interacting selectively with vanilla states depending on their J_3 quantum number: the "phantom" quantum dilogs would be those of states that do not couple to the interface. For *halo-saturated* interfaces on the other hand all states of a multiplet contribute to the jump, there are no "phantoms", hence the choice of terminology. We will not pursue the study of generic interfaces further, although it would certainly be interesting to gain a systematic understanding of these phenomena.

To sum up, we have given a sharp criterion to determine whether our conjectures are compatible with the halo picture, based on whether the $\mathcal{K}$-wall jump of the related generating function of framed states can be expressed in terms of conjugation by quantum dilogarithms. However we do not have a general proof that this is always the case, and we have seen that it takes some care to check that the halo picture is recovered even in simple examples. It would be good to clarify these matters further.

4.4 m-herds

Herds, already encountered above, are a class of critical networks occurring in higher rank gauge theories [73]. As reviewed in section 4.3.3, these theories have wild chambers on their moduli space of vacua, where BPS particles of charges γ, γ' with $\langle \gamma, \gamma' \rangle > 2$ can form stable wild BPS boundstates. Herd networks correspond to "slope 1" boundstates, i.e. states with charge of the form $n(\gamma + \gamma')$ with $n \geq 1$.

In this section we study the refined soliton content of herds, relying on equations (B.1). From the refined soliton data, vanilla PSCs of wild BPS states can be extracted. The main result is a *functional equation* for the generating function of PSCs. Our analysis applies to m-herds for any positive integer m.

4.4.1 The horse and other preliminaries

m-herds are constructed by gluing together m copies of an elementary subnetwork called *the horse* (a.k.a. the 1-herd, with suitable boundary conditions [73]), shown in figure 4.15. We therefore start by studying the soliton content of the horse, and then move on to $m > 1$.

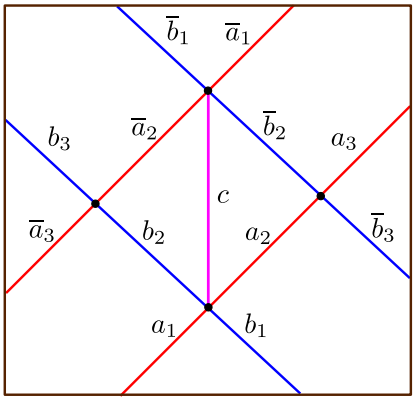

Figure 4.15: The horse. All streets are assumed to be 2-way (in some cases certain streets are actually one-way, but this case is automatically handled by our setup) and directions correspond to conventions explained in the text. We stress that $p, \bar{p}$ are distinct streets and are not identified: while the bar stresses the symmetry of the equations, we do not impose particular boundary conditions.

The lift of this kind of network involves 3 sheets of the cover $\pi : \Sigma \to C$, say i, j, k; there are then three types of two-way streets: ij, jk, ik marked by blue, red and purple colors on the figure respectively.

Recall that each two-way street can be thought of as a pair of one-way streets flowing in opposite directions. Therefore to each two-way street p we associate a refined soliton generating function D_p (resp. U_p) for the one-way street flowing downwards (resp. upwards). We fix conventions such that one-way streets of types ij, jk, ik flow upwards (they carry solitons of the U-type), while ji, kj, ki flow downwards (they carry solitons of the D-type).

Without loss of generality we choose the British resolution, then applying the 6-way joint rules (B.1) to all four joints, we find the following set of identities

$$\begin{aligned} D_{\bar{b}_2} = D_{\bar{b}_1}, \quad D_c = D_{\bar{a}_1} D_{\bar{b}_1}, \quad D_{\bar{a}_2} = D_{\bar{a}_1} \hat{Q}(\bar{b}_2) \\ U_{b_2} = U_{b_1}, \quad U_c = U_{b_1} U_{a_1}, \quad U_{a_2} = \hat{Q}(b_2) U_{a_1} \\ D_{\bar{b}_3} = D_{\bar{b}_2}, \quad U_{a_3} = \hat{Q}(\bar{b}_3) U_{a_2} \\ U_{b_3} = U_{b_2}, \quad D_{\bar{a}_3} = D_{\bar{a}_2} \hat{Q}(b_3) \end{aligned} \tag{4.94}$$

To each street we may associate two generating functions

$$\hat{Q}^{(\alpha)}(p) := 1 + D_p U_p \qquad \hat{Q}^{(\beta)}(p) := 1 + U_p D_p \tag{4.95}$$

where $\alpha = j, k, k$ and $\beta = i, j, i$ respectively for the three types of streets. In (4.94) we suppressed the superscripts, but it is understood that the suitable choice of $\hat{Q}^{(\star)}$ appears: this is determined by compatibility of concatenation of paths with those within the D, U they multiply.

In the same way as equations (B.1) were derived from homotopy invariance of off-diagonal terms of the formal parallel transport, there is a corresponding set of equations descending from homotopy invariance of diagonal terms (the story is closely parallel to [63, eq.s (6.18)-(6.19)]). These may be cast into the form of a "conservation law" for different streets coming into one joint, for example referring to figure B.1 we have for the sheet-1 component

$$\hat{\Upsilon}_{\wp_+^{(1)}} \hat{Q}^{(1)}(p_1) \hat{\Upsilon}_{\wp_0^{(1)}} \hat{Q}^{(1)}(p_2) \hat{\Upsilon}_{\wp_-^{(1)}} = \hat{\Upsilon}_{\wp'^{(1)}_+} \hat{Q}^{(1)}(p_5) \hat{\Upsilon}_{\wp'^{(1)}_0} \hat{Q}^{(1)}(p_4) \hat{\Upsilon}_{\wp'^{(1)}_-} \tag{4.96}$$

where $\wp, \wp'$ are here understood to be broken apart into pieces compatibly with the necessary concatenations. Analogous expressions hold for other streets and sheets combinations.

To keep track properly of the writhe of detours, it is more convenient to express the above rule with a richer notation. Consider a path χ with endpoints on $\Sigma \backslash \Sigma^*$, intersecting $\pi^{-1}(\mathcal{W}_c)$ somewhere. An example is provided in fig.4.11, where the path χ may be taken to be $\wp^{(i)}$. Let p be one of the streets whose lift is crossed by χ, the intersection splits χ into two pieces denoted $\chi_\pm$. Associated with χ we can construct a "corrected" detour generating function $Q_\chi(p)$ defined by the following relation

$$\hat{Y}_{\beta(\chi)} Q_\chi(p, y, z) := \rho\left(\hat{\Upsilon}_{\chi_+} \hat{Q}(p) \hat{\Upsilon}_{\chi_-}\right) \tag{4.97}$$

where $z = y \hat{Y}_{\gamma_c}$ and ρ was defined in (4.56). Where we implicitly made use of the fact that all detours' homology classes can be decomposed as $\pi = \beta(\chi) + n\gamma_c$. As will be evident in the following, the "correction" by χ consists of extra units of writhe induced by possible intersections of $\chi_\pm$ with the soliton detours to which they concatenate.

Moreover, it is easy to show that the "conservation rule" (4.96) carries over through the map ρ:

$$Q_\chi(p_1, y, z) Q_\chi(p_2, y, z) = Q_\chi(p_4, y, z) Q_\chi(p_5, y, z) \tag{4.98}$$

in fact, choosing the auxiliary paths as in fig. I.1, multiplying both sides of (4.96) by $\hat{\Upsilon}_{\chi_+}$ and $\hat{\Upsilon}_{\chi_-}$ from the left and from the right respectively, accounting for the regular homotopy classes[21] of

[21] More precisely, the δ_p are open regular homotopy classes on Σ^* consisting of concatenations of ij solitons with ji solitons supported on p.

detours δ_p from each street p, and applying the morphism ρ, we find

$$\sum_{\delta_{p_1},\delta_{p_2}} y^{\mathrm{wr}(\chi_+\delta_{p_1}\delta_{p_2}\chi_-)} Y_{\beta(\chi)+\beta(\delta_{p_1})+\beta(\delta_{p_2})} = \sum_{\delta_{p_4},\delta_{p_5}} y^{\mathrm{wr}(\chi_+\delta_{p_5}\delta_{p_4}\chi_-)} Y_{\beta(\chi)+\beta(\delta_{p_5})+\beta(\delta_{p_4})} \tag{4.99}$$

Noting that the mutual intersections of the detours paths δ_{p_i} all vanish, it is easy to see that both sides factorize into

$$\begin{aligned} &Y_{\beta(\chi)} \left(\sum_{\delta_{p_1}} y^{\mathrm{wr}(\chi_+\delta_{p_1}\chi_-)} y^{\langle [\chi],[\delta_{p_1}]\rangle} Y_{\beta(\delta_{p_1})} \right) \left(\sum_{\delta_{p_2}} y^{\mathrm{wr}(\chi_+\delta_{p_2}\chi_-)} y^{\langle [\chi],[\delta_{p_2}]\rangle} Y_{\beta(\delta_{p_2})} \right) = \\ &= Y_{\beta(\chi)} \left(\sum_{\delta_{p_4}} y^{\mathrm{wr}(\chi_+\delta_{p_4}\chi_-)} y^{\langle [\chi],[\delta_{p_4}]\rangle} Y_{\beta(\delta_{p_4})} \right) \left(\sum_{\delta_{p_5}} y^{\mathrm{wr}(\chi_+\delta_{p_5}\chi_-)} y^{\langle [\chi],[\delta_{p_5}]\rangle} Y_{\beta(\delta_{p_5})} \right) \end{aligned} \tag{4.100}$$

establishing eq.4.98.

The above derivation keeps holding if we start moving the point where the path χ is connected to the street p, while preserving the homotopy class of the detours. In this way we can simultaneously uniquely assign generating functions to each street whose lift to the i-th sheet is contained in a contractible chart on Σ^*.

In the following we will omit the subscript χ, leaving understood that we will always be working with such "corrected" generating functions.

4.4.2 Herds

An m-herd is a critical network consisting of a sequence of horses glued together, see for example figure 4.16. The outer legs of each horse are either glued to external legs of neighboring horses, or terminate on branching points, as displayed. Just like horses, herds lift to a triple of sheets i, j, k, we adopt the same sheet labels and color conventions for the streets of herds as we used for the horse. Thus, for example, branch points $\mathfrak{a}$ and $\mathfrak{d}$ are of type (ij), while $\mathfrak{b}$, $\mathfrak{c}$ are of type (jk).

Denoting the formal variables of the four simpletons by $\hat{\Upsilon}_{\mathfrak{a}}$, ..., $\hat{\Upsilon}_{\mathfrak{d}}$ (cf. figure 4.16), these soliton paths can be propagated through the m-herd by using the rules derived in the previous section together with gluing rules

$$\begin{aligned} D_{\alpha_1} &= \hat{\Upsilon}_{\mathfrak{b}} \hat{Q}(\beta_1), \qquad & D_{\alpha_n} &= D_{\alpha_{n-1}} \hat{Q}(\beta_n) \hat{Q}(\bar{\beta}_{n-1}) \,, \\ U_{\bar{\alpha}_{m-1}} &= \hat{Q}(\bar{\beta}_{m-1}) \hat{\Upsilon}_{\mathfrak{c}}, \qquad & U_{\bar{\alpha}_{n-1}} &= \hat{Q}(\bar{\beta}_{n-1}) \hat{Q}(\beta_n) U_{\bar{\alpha}_n} \,, \\ D_{\beta_n} &= \hat{\Upsilon}_{\mathfrak{a}}, \qquad & U_{\bar{\beta}_n} &= \hat{\Upsilon}_{\mathfrak{d}} \,. \end{aligned} \tag{4.101}$$

These are obtained by applying (4.94) to the network, for example

$$D_{\alpha_2} = D_{\alpha_1} \, \hat{Q}(\bar{\beta}_2) \, \hat{Q}(\beta_1) \tag{4.102}$$

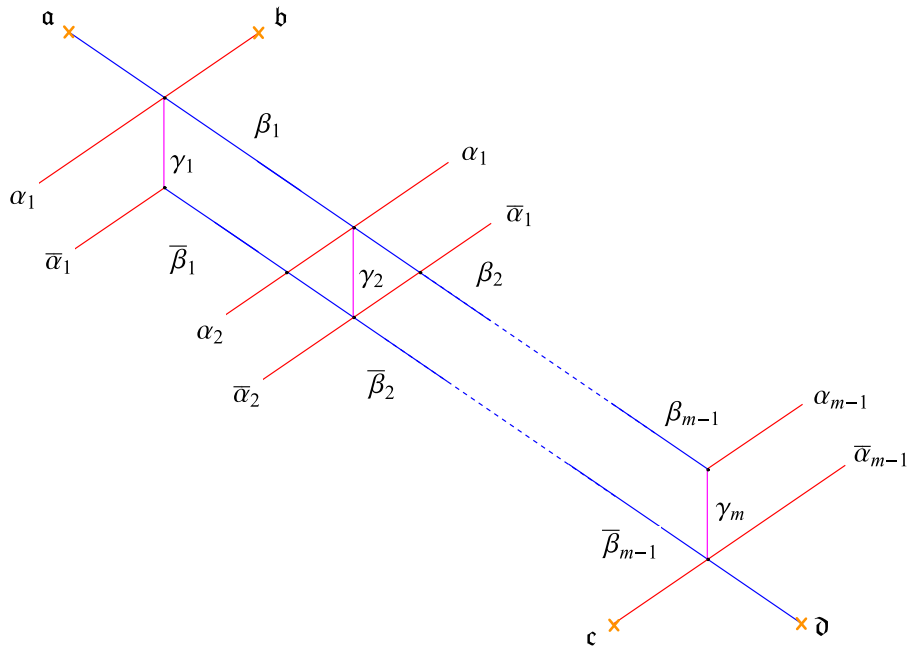

Figure 4.16: The m-herd, the streets are glued together according to labels. Typically the herd "wraps" a tube of C, in the picture the tube has been cut along a spiral and opened up.

is derived from

$$D_{\bar{a}_3} = D_{\bar{a}_2}\,\hat{Q}(b_3) = \left(D_{\bar{a}_1}\,\hat{Q}(\bar{b}_2)\right)\hat{Q}(b_3)\,. \tag{4.103}$$

Thus we find the following expression for the generating function of a generic *vertical* 2-way street γ_n

$$\begin{aligned}\hat{Q}(\gamma_n) &= 1 + D_{\alpha_{n-1}} D_{\beta_{n-1}} U_{\bar{\beta}_n} U_{\bar{\alpha}_n} = \\ &= 1 + \hat{\Upsilon}_{\mathfrak{b}}\hat{Q}(\beta_1)\left(\prod_{j=2}^{n-1}\hat{Q}(\beta_j)\hat{Q}(\bar{\beta}_{j-1})\right)\hat{\Upsilon}_{\mathfrak{a}}\hat{\Upsilon}_{\mathfrak{d}}\left(\prod_{j=n}^{m-2}\hat{Q}(\bar{\beta}_j)\hat{Q}(\beta_{j+1})\right)\hat{Q}(\bar{\beta}_{m-1})\hat{\Upsilon}_{\mathfrak{c}}\,.\end{aligned} \tag{4.104}$$

It is easily seen that each $\hat{Q}$ generating function is a formal power series in a single word, then we consider assigning an *algebraic generating function* to each $\hat{Q}$, as follows. For example,

$$\begin{aligned}\hat{Q}(\beta) &= \sum_{n\in\mathbb{N}} \omega_n(y,\beta)\left(\hat{\Upsilon}_{\mathfrak{a}}\hat{\Upsilon}_{\mathfrak{d}}\hat{\Upsilon}_{\mathfrak{c}}\hat{\Upsilon}_{\mathfrak{b}}\right)^n, \quad Q(\beta,y,z) = \sum_{n\in\mathbb{N}}\omega_n(y,\beta)z^n \\ \hat{Q}(\bar{\beta}) &= \sum_{n\in\mathbb{N}} \omega_n(y,\bar{\beta})\left(\hat{\Upsilon}_{\mathfrak{c}}\hat{\Upsilon}_{\mathfrak{b}}\hat{\Upsilon}_{\mathfrak{a}}\hat{\Upsilon}_{\mathfrak{d}}\right)^n, \quad Q(\bar{\beta},y,z) = \sum_{n\in\mathbb{N}}\omega_n(y,\bar{\beta})z^n\end{aligned} \tag{4.105}$$

where ω_n are Laurent polynomials in y arising after casting the $\hat{Q}$ into this form by means of (4.33) and (I.6). It is important to note that the two words made of simpleton variables (in the expressions for $\beta, \bar{\beta}$ respectively) are *different*. Moreover, in constructing these functions we hid the involvement of necessary transition functions which actually extend the simpleton paths across the herd (see [73,

app.C]). We fix a prescription for the transport of soliton paths as follows: the transport must be carried out along streets of the same soliton type (for example to join $\mathfrak{a},\mathfrak{d}$ we can continue them across the β-type streets) plus any one of the vertical streets of γ-type.

In particular, the generating functions of vertical γ-streets $\hat{Q}(\gamma_n)$ are formal series in the single word $\hat{\Upsilon}_{\mathfrak{b}}\hat{\Upsilon}_{\mathfrak{a}}\hat{\Upsilon}_{\mathfrak{d}}\hat{\Upsilon}_{\mathfrak{c}}$. Performing the due substitutions of the generating functions $\hat{Q}(\beta),\hat{Q}(\bar{\beta})$ into the expression for $\hat{Q}(\gamma_n)$ we end up with an expression in which different words are *scrambled*. To make some order, we employ a trick explained in appendix I, manipulating the expressions of $\hat{Q}(\gamma_n)$ by means of the equivalence

$$\big(\hat{\Upsilon}_{\mathfrak{a}}\hat{\Upsilon}_{\mathfrak{d}}\big)\big(\hat{\Upsilon}_{\mathfrak{c}}\hat{\Upsilon}_{\mathfrak{b}}\big)\doteq y^{2\langle \mathrm{cl}(\mathfrak{ad}),\mathrm{cl}(\mathfrak{cb})\rangle}\,\big(\hat{\Upsilon}_{\mathfrak{c}}\hat{\Upsilon}_{\mathfrak{b}}\big)\big(\hat{\Upsilon}_{\mathfrak{a}}\hat{\Upsilon}_{\mathfrak{d}}\big)\,, \tag{4.106}$$

the symbol $\doteq$ means that both sides have the same image under ρ.

For an m-herd, we have simply $\langle \mathrm{cl}(\mathfrak{ad}),\mathrm{cl}(\mathfrak{cb})\rangle = m$. Taking this into account, we may rewrite the equations for the formal series $\hat{Q}$ in terms of algebraic ones which include corrections from generic auxiliary paths χ

$$\begin{aligned} &Q_\chi(\gamma_n,y,z) = 1 + z\,y^{\mathrm{wr}(\chi_+\mathfrak{b}\mathfrak{a}\gamma_n\mathfrak{d}\mathfrak{c}\chi_-)}\times \\ &\times\left(\prod_{j=1}^{n-1} Q_\chi(\beta_j,y,z)\right)\left(\prod_{j=n+1}^{m-1} Q_\chi(\beta_j,y,zy^{-2m})\right)\left(\prod_{j=n}^{m-1} Q_\chi(\bar{\beta}_j,y,z)\right)\left(\prod_{j=1}^{n-2} Q_\chi(\bar{\beta}_j,y,zy^{2m})\right) \end{aligned} \tag{4.107}$$

where in $\mathfrak{b}\mathfrak{a}\gamma_n\mathfrak{d}\mathfrak{c}$ it is understood that simpletons are propagated through the network in the way explained above, and the extra powers of y in the arguments of Q's account for due reorderings. Here the path χ intersects the 2-way street γ_n on sheet i and the factor γ_n inside $y^{\mathrm{wr}(\chi_+\mathfrak{b}\mathfrak{a}\gamma_n\mathfrak{d}\mathfrak{c}\chi_-)}$ means a lift of this 2-way street to another sheet.

Switching to "universal" generating functions, all corresponding to a specific path $\chi=\wp^{(i)}$ as drawn in fig.4.11, gives simply

$$\mathrm{wr}\,(\chi_+\mathfrak{b}\mathfrak{a}\gamma_n\mathfrak{d}\mathfrak{c}\chi_-) = 2n-1-m \tag{4.108}$$

Applying homotopy invariance (4.98) thus yields

$$\begin{aligned} Q(\mathfrak{a},y,z) = Q(\mathfrak{d},y,z) &= \prod_{j=1}^{m-1} Q(\gamma_j,y,z), \\ Q(\beta_n,y,z) = \prod_{j=n+1}^{m-1} Q(\gamma_j,y,z), \qquad & Q(\bar{\beta}_n,y,z) = \prod_{j=1}^{n-1} Q(\bar{\beta}_j,y,z) \end{aligned} \tag{4.109}$$

After substitution of the ansatz

$$Q(\gamma_n,y,z) = P(zy^{2n-1-m},y) \tag{4.110}$$

into (4.107) all the equations in this system turns into the same single equation with a parameter z shifted by powers of y in different ways. This defining equation reads

$$P(z,y) = 1 + z \prod_{s=-(m-2)}^{m-2} P(zy^{2s}, y)^{m-1-|s|} \,. \tag{4.111}$$

This is a *functional* equation for power series in z, with Laurent polynomials in y as their coefficients.

In the limit $y^2 \to 1$ all terms in the product on the r.h.s. become the same, then powers just sum up to $(m-1)^2$, properly reproducing the *algebraic* herd equation found in [73, eq.(1.2)]. It therefore generalizes Prop.3.1 of [115] and the defining equation of (1.4) of [75] to the "refined" case.

Given a solution to the functional equation (4.111), generating functions on other 2-way streets follow simply by

$$\begin{aligned} Q(\mathfrak{a},y,z) = Q(\mathfrak{d},y,z) &= \prod_{s=-\frac{m-1}{2}}^{\frac{m-1}{2}} P(zy^{2s},y), \\ Q(\gamma_n,y,z) &= P(zy^{2n-1-m},y) \end{aligned} \tag{4.112}$$

where the product is assumed to be taken either over integers or over half-integers.

Finally, we should note that, due to choice of (commutative) variables in this section, there is a controlled shift in powers of y as compared[22] to the expected factorization (4.28):

$$Q(\mathfrak{a},y,z) = \prod_{\tilde{\gamma}_h} \prod_{m\in\mathbb{Z}} \Phi_{n(\tilde{\gamma}_h)}\Big((-y)^m y^{n(\tilde{\gamma}_h)} z^{n(\tilde{\gamma}_h)}\Big)^{a_m(\tilde{\gamma}_h)} \,. \tag{4.113}$$

4.4.3 Herd PSC generating functions

To conclude our discussion of herds, we examine some explicit solutions to the functional equation (4.111).

2-herd: Eq.(4.111) is algebraic in this case and can be solved explicitly

$$P(z,y) = (1-z)^{-1} \,. \tag{4.114}$$

Thus

$$Q(\mathfrak{a},y,z) = Q(\mathfrak{b},y,z) = Q(\mathfrak{c},y,z) = Q(\mathfrak{d},y,z) = (1-zy)(1-zy^{-1}) \,, \tag{4.115}$$

corresponding to the expected vectormultiplet

$$\Omega(\gamma_c,y) = y + y^{-1}, \quad \Omega(n\gamma_c,y) = 0,\ n \geq 2 \tag{4.116}$$

[22] More precisely, the extra y^n factor is omitted in (4.28) because it is reproduced by $\hat{Y}_{\wp^{(i)}}\hat{Y}_{n\tilde{\gamma}_h} = y^n\, \hat{Y}_{\wp^{(i)}+n\tilde{\gamma}_h}$.

3-herd: $m = 3$ provides the first non-trivial example, since in this case (4.111) is no longer algebraic. Nevertheless one can study its solutions perturbatively, introducing the series

$$P(z,y) = 1 + \sum_{n=1}^{\infty} \omega_n^{(m)}(y) z^n \,. \tag{4.117}$$

We find the following perturbative solution

$$\begin{aligned}
P(z,y) &= 1 + z + \left(y^{-2} + 2 + y^2\right) z^2 + \left(y^{-6} + 2y^{-4} + 5y^{-2} + 6 + 5y^2 + 2y^4 + y^6\right) z^3 + \\
&+ \left(y^{-12} + 2y^{-10} + 5y^{-8} + 10y^{-6} + 16y^{-4} + 23y^{-2} + 26 + 23y^2 + 16y^4 + 10y^6\right. \\
&+ \left. 5y^8 + 2y^{10} + y^{12}\right) z^4 + O(z^5) \\
&= \Phi_1(yz)\Phi_2\left((-y)^{-1}y^2z^2\right)^{-1}\Phi_2\left((-y)y^2z^2\right)^{-1}\Phi_3\left((-y)^{-4}y^3z^3\right)\Phi_3\left((-y)^{-2}y^3z^3\right) \\
&\times \Phi_3\left(y^3z^3\right)^2\Phi_3\left((-y)^2y^3z^3\right)\Phi_3\left((-y)^4y^3z^3\right)\Phi_4\left((-y)^{-9}y^4z^4\right)^{-1}\Phi_4\left((-y)^{-7}y^4z^4\right)^{-1} \\
&\times \Phi_4\left((-y)^{-5}y^4z^4\right)^{-3}\Phi_4\left((-y)^{-3}y^4z^4\right)^{-4}\Phi_4\left((-y)^{-1}y^4z^4\right)^{-5}\Phi_4\left((-y)y^4z^4\right)^{-5} \\
&\times \Phi_4\left((-y)^3y^4z^4\right)^{-4}\Phi_4\left((-y)^5y^4z^4\right)^{-3}\Phi_4\left((-y)^7y^4z^4\right)^{-1}\Phi_4\left((-y)^9y^4z^4\right)^{-1}(1+O(z^5))\,.
\end{aligned} \tag{4.118}$$

Relations (4.112) and (4.113) allow to extract the corresponding PSCs: denoting $\chi_s(y) = (y^{2s+1} - y^{-(2s+1)})/(y - y^{-1})$

$$\begin{aligned}
\Omega(\gamma_c, y) &= \chi_1(y) \\
\Omega(2\gamma_c, y) &= \chi_{\frac{5}{2}}(y) \\
\Omega(3\gamma_c, y) &= \chi_3(y) + \chi_5(y) \\
\Omega(4\gamma_c, y) &= \chi_{\frac{5}{2}}(y) + 2\chi_{\frac{9}{2}}(y) + \chi_{\frac{11}{2}}(y) + 2\chi_{\frac{13}{2}}(y) + \chi_{\frac{17}{2}}(y)
\end{aligned} \tag{4.119}$$

as anticipated in (4.78). These results agree in fact with the ones derived by means of the *motivic Kontsevich-Sobeilman wall-crossing formula* [73, Appendix A.2].

4.5 Extra remarks

4.5.1 Kac's theorem and Poincaré polynomial stabilization

Kac's theorem. As discussed in [73, §8.2], Kac's theorem (see e.g. [116]) implies a charge-dependent bound on the highest-spin irreps in the Clifford vacua of BPS states. The highest admissible spin is related to the dimensionality of the corresponding quiver variety. In the case of interest to us, m-Kronecker quivers, the maximal spin for a state of charge (n,n) is

$$2J_{\max}^{(\text{quiver})}(n) = (m-2)n^2 + 1 \tag{4.120}$$

Recall that Laurent decomposition of the PSC reads

$$\Omega_n(y) = \sum_{m=-2J_{\max}}^{2J_{\max}} a_m(n)\,(-y)^m\,, \tag{4.121}$$

also note that the highest power of y for the z^k term of the generating function comes from

$$\Phi_k((-y)^{2J_{\max}(k)}y^k z^k) \sim z^k y^{k-1+2J_{\max}(k)} + \dots\,. \tag{4.122}$$

Then let us study the maximal power of y for the z^k term of m-herd generating functions, as predicted by equation (4.111). To do so, we consider the series expansion (4.117), where coefficients ω_k are Laurent polynomials in y. For an m-herd, the first two read

$$\omega_1^{(m)}(y) = 1, \qquad \omega_2^{(m)}(y) = \frac{y^{2(m-1)} + y^{-2(m-1)} - 2}{(y + y^{-1} - 2)\,(y + y^{-1} + 2)}\,. \tag{4.123}$$

Equation (4.111) implies a recursion relation for the coefficients of (4.117). The contribution to a particular Taylor coefficient in front of z can be represented as a sum over partitions $t_{s,j}$. We label non-negative integers $t_{s,j}$ by a pair of integers (s, j); s corresponds to a contribution of a term with a shift controlled by s in (4.111), while j distinguishes formally between the terms with the same s gathered into powers in (4.111). We sum over all possible values of $t_{s,j}$ inserting a Kronecker symbol, so that only a few contribute. The recursion relation reads

$$\omega_k^{(m)}(y) = \sum_{t_{s,j}=0}^{\infty} y^{2\sum_{s,j} s t_{s,j}} \left(\prod_{s=-(m-2)}^{m-2} \prod_{j=1}^{m-1-|s|} \omega_{t_{s,j}}^{(m)}(y) \right) \delta_{k-1,\sum_{s,j} t_{s,j}} \tag{4.124}$$

The highest power of y is contributed by $t_{m-2,1} = k-1$ with all the others t's set to zero, therefore we may recast the above as a recursion relation for the the maximal power α_k for y in $\omega_k^{(m)}(y)$, together with a boundary condition:

$$\alpha_k = \alpha_{k-1} + 2(m-2)(k-1), \qquad \alpha_1 = 0\,, \tag{4.125}$$

which is solved by

$$\alpha_k = (m-2)k(k-1)\,. \tag{4.126}$$

Since Q is related to P by (4.112), the highest power of y in the coefficient of z^k is $\alpha_k + (m-1)k$. Hence, finally, the highest spin for the (n, n) state reads

$$2J_{\max}^{(\text{herds})}(k) + k - 1 = \alpha_k + (m-1)k\,. \tag{4.127}$$

This entails a beautiful agreement of our formula (4.111) with previously known results from quiver representation theory

$$2J_{\max}^{(\text{herds})}(n) = 2J_{\max}^{(\text{quiver})}(n) = (m-2)n^2 + 1\,. \tag{4.128}$$

Poincaré polynomial stabilization. The relation between quiver representation theory and BPS state counting extends to Poincaré polynomials. In our particular example the representation of the Kronecker quiver with m arrows and a dimensional vector (n, n) is a collection of m elements of $\mathrm{End}(\mathbb{C}^n)$ [89, 118]:

$$R = \mathrm{Hom}\,(\mathbb{C}^n, \mathbb{C}^n)^{\oplus m} \tag{4.129}$$

It has a natural action of the gauge group $G = GL(n, \mathbb{C}) \times GL(n, \mathbb{C})$. The BPS states are associated with G-equivariant cohomologies of the quiver representations.

The relation between the Poincaré polynomial and the PSC reads [23]

$$\begin{aligned} \chi_n^{(m)}(y) :=& \sum_k \beta_{n,k}^{(m)} y^{2k} \\ =& y^{2J_{\max}(n)} \Omega^{(m)}(y, n\gamma_c) \end{aligned} \tag{4.130}$$

where $\beta_{n,k}^{(m)}$ $(k = 0, \ldots, \dim \mathcal{M})$ are corresponding suitably defined[24] Betti numbers of the moduli space of representations, and $\Omega^{(m)}(y, n\gamma_c)$ denotes the PSC of a BPS state of charge (n, n), with m being the charge pairing of elementary constituents.

Explicit computations [73] of the Betti numbers suggest that they *stabilize*: there is a well-defined limit

$$\lim_{n \longrightarrow \infty} \beta_{n,k}^{(m)} = \beta_{\infty,k}^{(m)}\,, \tag{4.131}$$

which can be recast as a limit for a polynomial

$$\lim_{n \longrightarrow \infty} \chi_n^{(m)}(y) = \chi_\infty^{(m)}(y)\,. \tag{4.132}$$

Moreover, by direct inspection, this limit turns out to be independent of m: $\chi_\infty^{(m)}(y) = \chi(y)$ for all m; this observation implies *another* interesting limit

$$\lim_{m \longrightarrow \infty} \chi_n^{(m)}(y) = \chi_n^{(\infty)}(y)\,. \tag{4.133}$$

It turns out that these limiting polynomials are known. In fact they correspond to the Poincaré polynomials of the classifying space $B\left((GL_n \times GL_n)/\mathbb{C}^*\right)$ where $\mathbb{C}^*$ is the subgroup of elements $(\lambda\,\mathbb{I}, \lambda^{-1}\,\mathbb{I})$ [118].

---

[23] It would be more precise to call quantity $\chi_n^{(m)}(y)$ a χ_y-genus, though if the moduli space is smooth it can be identified with the Poincaré polynomial (see the discussion in [35, section 2.5]).

[24] The BPS indices for generalized m-herds are not simple Euler-characteristics (of stable or semi-stable moduli). The reason is that the contributions to $\Omega(n\gamma)$ for $n > 1$ involve contributions from threshold bound states, or, in the language of quivers, from semi-stable representations of the Kronecker quiver.

The failure can be seen most drastically for the m-herd: where the Euler characteristic $\chi(n)$ for the moduli space of stable representations of the Kronecker m-quiver, with dimension vector (n, n), vanishes for $n > 1$ (see the proof of the m-herd functional equation in [115]). See also discussion in [118, s.6.5, s.7].

We thank T. Mainiero for this valuable remark.

Numerical experiments indicate that Betti numbers satisfy an interesting inequality $\beta_{n,k}^{(m)} \leq \beta_{n,k}^{(m+1)}$, implying in turn

$$\beta_{\infty,k}^{(m)} \leq \beta_{\infty,k}^{(\infty)} \tag{4.134}$$

though it remains unclear why Betti numbers saturate this bound for every $m \geq 3$.

It is interesting to investigate how this convergence interplays with the equation for the generating function (4.111). As a preliminary remark, notice that the expansion of the dilog product in the generating function allows one to relate coefficients in the formal series to the PSC

$$\omega_n^{(m)}(y) = y^{\alpha_n - 2J_{\max}(n)} \frac{1-y^{2n}}{1-y^2} \Omega^{(m)}(y, n\gamma_c) \left(1 + O(y^{(m-1)n})\right) . \tag{4.135}$$

and by $O(y^p)$ we denote a formal series in y, starting with a term of degree p. It is simple to observe this relation since $\Phi_n(\xi) = 1 + y^{1-2n}\frac{1-y^{2n}}{1-y^2}\xi + O(\xi)$

$$\prod_{k\in\mathbb{Z}} \Phi_n\left((-y)^k y^n z^n\right)^{a_k(\tilde{\gamma}_h)} = 1 + y^{1-n}\frac{1-y^{2n}}{1-y^2}\left(\sum_{k\in\mathbb{Z}} a_k(\tilde{\gamma}_h)(-y)^k\right) z^n + O(z^{n+1}) \tag{4.136}$$

and corrections from lower dilogarithms can be estimated by lowest values of the powers of y they bring in.

Introducing the series

$$\tilde{\chi}_n^{(m)}(y) := y^{-(m-2)n(n-1)} \omega_n^{(m)}(y) , \tag{4.137}$$

we can focus on its stabilization since (assuming $|y| < 1$)

$$\begin{aligned} \lim_{n\to\infty} \tilde{\chi}_n^{(m)}(y) &= (1-y^2)^{-1} \chi_\infty^{(m)}(y) , \\ \lim_{m\to\infty} \tilde{\chi}_n^{(m)}(y) &= \frac{1-y^{2n}}{1-y^2} \chi_n^{(\infty)}(y) . \end{aligned} \tag{4.138}$$

Performing the substitution $\omega_n^{(m)}(y) \mapsto \tilde{\chi}_n^{(m)}(y) y^{(m-2)n(n-1)}$, $s \mapsto s-(m-2)$ into (4.124) we arrive at the following recursion relation

$$\begin{aligned} \tilde{\chi}_k^{(m)}(y) = \sum_{t_{s,j}=0}^{\infty} y^{2\sum_{s,j} s t_{s,j} + (m-2) \sum_{(s,j)\neq(s',j')} t_{s,j} t_{s',j'}} \times \\ \times \left(\prod_{s=0}^{2(m-2)} \prod_{j=1}^{m-1-|s-(m-2)|} \tilde{\chi}_{t_{s,j}}^{(m)}(y) \right) \delta_{k-1, \sum_{s,j} t_{s,j}} \end{aligned} \tag{4.139}$$

where the second summation in the power of y goes over different pairs of indices. In the limit $m \to \infty$, precisely that summation causes a *localization* (assuming $|y| < 1$ and noticing that the power is non-negative) on partitions of $k-1$ satisfying $\sum_{(s,j)\neq(s',j')} t_{s,j} t_{s',j'} = 0$, these are partitions consisting of just one $t_{s,j} = k-1$ with all the others being zero. Thus we are eventually left with a summation over positions (s,j)

$$\tilde{\chi}_k^{(\infty)}(y) = \sum_{s=0}^{\infty} (1+s) y^{2s(k-1)} \tilde{\chi}_{k-1}^{(\infty)}(y) . \tag{4.140}$$

This reproduces the result from quiver representation theory

$$\chi(y, B\left((GL_n \times GL_n)/\mathbb{C}^*\right)) = \frac{1-y^2}{(1-y^2)^{2n}}\tilde{\chi}_n^{(\infty)}(y) = \frac{1-y^2}{\prod_{j=1}^{n}(1-y^{2j})^2}\,, \tag{4.141}$$

the corresponding limiting Poincaré series reads

$$\chi(y) = \frac{1-y^2}{\prod_{j=1}^{\infty}(1-y^{2j})^2}\,. \tag{4.142}$$

4.5.2 Chern-Simons, formal variables and the writhe

In this section we propose a different perspective on the formal variables introduced in §4.2.1, together with a natural explanation for the appearance of the writhe and of the map ρ introduced in (4.56), two prominent characters of our story.

The formal variables $\hat{\Upsilon}$ employed above have a natural interpretation in terms of a quantized twisted flat connection. Before turning to the twisted connection, let us consider a classical flat abelian $\mathbb{C}$-valued connection on Σ, subject to certain boundary conditions at punctures. We take the logarithm of the holonomy to be fixed to $\mathfrak{m}_s$ at the puncture z_s. Let $\mathcal{X}_\gamma$ be coordinates on the moduli space $\mathcal{M}_{ab} \simeq Hom(\pi_1(\Sigma), \mathbb{C}^\times)$ with fixed choices of $\mathfrak{m}$, obeying

$$\{\mathcal{X}_\gamma, \mathcal{X}_{\gamma'}\} = \langle\gamma, \gamma'\rangle \mathcal{X}_\gamma \mathcal{X}_{\gamma'}\,, \qquad \mathcal{X}_\gamma \mathcal{X}_{\gamma'} = \mathcal{X}_{\gamma+\gamma'}\,. \tag{4.143}$$

These coordinates are holonomies

$$\mathcal{X}_\gamma = \exp \oint_\gamma \mathcal{A}^{ab}\,, \tag{4.144}$$

where $\mathcal{A}^{ab}$ is required to have canonical structure

$$\{\mathcal{A}^{ab}_\mu(w), \mathcal{A}^{ab}_\nu(w')\} = \frac{1}{k}\,\epsilon_{\mu\nu}\,\delta^{(2)}(w-w')\,, \tag{4.145}$$

where w, w' are local coordinates on Σ and we have used $k=1$ in (4.145). $\epsilon_{\mu\nu}$ is the Levi-Civita symbol normalized to $\epsilon_{12}=1$. Given a flat connection with this Poisson bracket, its transports indeed obey (4.143). This also coincides with the algebra of Darboux coordinates of [60] (cf eq. (2.3) of [64]).

Notice that the canonical structure of this flat connection coincides with the equal-time Poisson bracket of a Chern-Simons gauge field on Σ, with noncompact gauge group $\mathbb{C}^\times$. In the spirit of this observation, it is easy to see that promoting the Poisson bracket to a commutator

$$[\hat{A}_\mu(w), \hat{A}_\nu(w')] = 2\log y\,\epsilon_{\mu\nu}\delta^{(2)}(w-w'), \tag{4.146}$$

produces corresponding "quantum" noncommutative holonomies obeying precisely the algebra of our y-twisted formal variables

$$\overline{Y}_\gamma = \exp \oint_\gamma \hat{A}\,, \qquad\qquad \overline{Y}_\gamma \overline{Y}_{\gamma'} = y^{\langle \gamma, \gamma' \rangle} \overline{Y}_{\gamma+\gamma'}\,. \tag{4.147}$$

Honest gauge invariant holonomies should be path-ordered, however if a closed path does not self-intersect, then path-ordering has no effect since the commutator (4.146) only contributes to transverse (self-)intersections. On the other hand, if the path does contain self-intersections, the path-ordered transport will depend on a choice of basepoint $p \in \gamma$

$$\overline{\Upsilon}_{\gamma_p} = P \exp \oint_p^p \hat{A}\,. \tag{4.148}$$

Closed self-intersecting curves on surfaces are also known as *singular knots*, Wilson lines associated to singular knots on the plane in abelian Chern-Simons theory were studied in [50], where it was shown that the algebra of $\overline{\Upsilon}_{\gamma_p}$ matches that of $y^{\mathrm{wr}(\gamma_p)}\,\overline{Y}_\gamma$, this motivates (4.56), and offers a *natural explanation for the appearance of the writhe as a consequence of path-ordering* of quantum holonomies. In particular this relation reveals that the $\overline{Y}$ also enjoy gauge invariance, being proportional to the $\overline{\Upsilon}$ up to a constant. There is an analogous story for open paths[25].

In the proofs of twisted homotopy invariance of §4.2.3, it was crucial to deal with a *twisted* flat connection, concretely we repeatedly used the fact that holonomy around a contractible cycle[26] equals $-y$, resulting in (4.34). At the classical level, one way to construct such a connection is to consider the unit circle bundle $\widetilde{\Sigma} \to \Sigma$ with a flat $U(1)$ connection having fixed holonomy equal to -1 around the circle fiber; then to each path on Σ one associates the transport of this connection along the *tangent framing lift* of the path to $\widetilde{\Sigma}$. To the best of our knowledge, quantum twisted flat connections have not been discussed in the literature. A reasonable approach to quantizing a twisted flat connection is to leave the holonomy on the fiber fixed to a constant, while quantizing the holonomies on Σ in a way consistent with the symplectic structure. Alternatively, using the data of a spin structure we can identity the moduli space of twisted flat connections with the moduli space of ordinary flat connections and quantize the latter. Either way we produce transports obeying the twisted algebra of our formal variables $\hat{\Upsilon}$.

The above discussion of quantum flat connections is only meant to provide an heuristic motivation for the definition of formal variables in section §4.2.1. In particular, it ignores the important subtleties associated with the quantization of Chern-Simons connections with noncompact gauge

[25] Although open Wilson lines aren't gauge invariant, they are gauge covariant and this is enough to ensure that their algebra is gauge invariant.

[26] For contractible curls winding counter-clockwise

group. A more thorough investigation of how our formal variables can be modeled on quantum holonomies of a Chern-Simons connection should clearly be possible, given a number of works available in the literature on noncompact Chern-Simons (see e.g. [20, 44, 131, 132]). We leave this for future work.

We expect that quantum Chern-Simons theory will provide an interesting perspective on the key formula, equation (4.54). We recall from [63, §10] that given the data of a spectral network one can construct a "nonabelianization map," taking a flat $\mathbb{C}^*$-connection $\nabla^{\rm ab}$ on Σ to a flat $GL(K,\mathbb{C})$-connection $\nabla^{\rm nonab}$ on C. The key formula defining this map expresses the parallel transport of $\nabla^{\rm nonab}$ along a path $\wp$ on C in terms of a sum of parallel transports by $\nabla^{\rm ab}$ on Σ, weighted by framed BPS degeneracies. (See, for example, equation (16.17) of [106].) In the quantum setting, $P\exp\int_\wp \nabla^{\rm nonab}$ and $P\exp\int_{\gamma_{ij'}} \nabla^{\rm ab}$ become quantum operators on Chern-Simons theory Hilbert spaces $\mathscr{H}^{\rm nonab}(C)$ and $\mathscr{H}^{\rm ab}(\Sigma)$, respectively. We conjecture that there is an isomorphism between these Hilbert spaces $\phi : \mathscr{H}^{\rm nonab}(C) \to \mathscr{H}^{\rm ab}(\Sigma)$ allowing us to interpret equation (4.54) as a quantum version of the nonabelianization map[27]:

$$\phi\left(\mathrm{Tr}\, P\exp\oint_\wp \nabla^{\rm nonab}\right)\phi^{-1} = \sum_{\mathfrak{a}} \overline{\Omega}(\wp,\mathfrak{a};y)\exp\oint_{\mathfrak{a}} \nabla^{\rm ab} \tag{4.149}$$

We stress that this is a conjecture, motivated by the present paper, and further work is needed to make precise sense of the formula. We hope to return to this topic and make these ideas more precise in future work.

An interpretation of y-twisted formal variables in terms of deformation quantization of the above Poisson brackets was already suggested in [61, §6.2]. The relation of BPS states of class $\mathcal{S}$ theories to Chern-Simons Wilson lines was already pointed out in [30, 31]. In those works Chern-Simons theory appeared when considering compactifications of M5 branes in certain backgrounds, via the duality of Chern-Simons theory to open topological strings (see also [6, 8]). Although we didn't find a straightforward connection to our setup, we take such results as supporting evidence that our formal variables can be related to quantum parallel transports.

We expect there will also be very interesting further connections with non-compact WZW models and Toda theories [119, 125], using the theory of Verlinde operators [9, 49] and β-ensembles. See [5] for a recent review of the current state of the art. Closely related to this is the theory of check operators [10, 71] which should provide new perspectives on the quantum version of the Darboux expansion alluded to above.

[27] Related considerations have appeared in [29] and [111].

Chapter 5

The BPS Spectrum of $SU(2)$ $\mathcal{N} = 2^*$

5.1 Review of $SU(2)$ $\mathcal{N} = 2^*$ theory

5.1.1 Classical Description

In $\mathcal{N} = 2$ language, the field content consists of a vectormultiplet together with one hypermultiplet, both are in the adjoint representation of $SU(2)$. The $\mathcal{N} = 2$ vectormultiplet contains $\mathcal{N} = 1$ vectormultiplets V^a, with gauge index $a = 1, 2, 3$, together with chiral multiplets Φ^a. For fixed a, the gauge field and the scalar transform as singlets under $SU(2)_R$ while the fermions in V^a and Φ^a rotate into each other in the fundamental representation. The hypermultiplet features chiral superfields Q^a together with anti-chiral ones $\widetilde{Q}^a$, here the fermions are singlets of $SU(2)_R$ while the complex scalars mix with each other as a fundamental doublet. The action can be expressed in $\mathcal{N} = 1$ language as

$$\begin{aligned}\mathcal{L} = \frac{1}{8\pi}\text{Im Tr}\left[\tau\left(\int d^2\theta\, W^\alpha W_\alpha + 2\int d^4\theta\, \Phi^\dagger e^{-2V}\Phi\right)\right] \\ + \text{Tr}\left[\int d^4\theta\left(Q^\dagger e^{-2V}Q + \widetilde{Q}e^{2V}\widetilde{Q}^\dagger\right) + \left(\int d^2\theta\left(\sqrt{2}\,\widetilde{Q}\Phi Q + m\widetilde{Q}Q\right) + h.c.\right)\right]\end{aligned} \tag{5.1}$$

where the first row is the pure $\mathcal{N} = 2$ SYM kinetic term for the vector multiplet, while the second row contains the hyper multiplet's kinetic terms with coupling to V, Φ together with its mass terms.

5.1.2 Seiberg-Witten low energy description

The $SU(2)\,\mathcal{N} = 2^*$ theory may be regarded as $\mathcal{N} = 4$ SYM explicitly broken by a mass term down to $\mathcal{N} = 2$. From this perspective one might ask whether S-duality is preserved by the mass term. A nontrivial check is provided by the Seiberg-Witten curve of the theory [121] which can be presented in a manifestly $SL(2, \mathbb{Z})$ invariant way: in conventions where the W bosons carry unit electric charge

the equation of the curve is

$$y^2 = (x - e_1\widetilde{u} - \frac{1}{4}{e_1}^2 m^2)(x - e_2\widetilde{u} - \frac{1}{4}{e_2}^2 m^2)(x - e_3\widetilde{u} - \frac{1}{4}{e_3}^2 m^2) \tag{5.2}$$

where $e_i(\tau)$ are the roots of $4\,x^3 - g_2\,x - g_3$, where in terms of Eisenstein series $g_2 = 60\,\pi^{-4}\,G_4(\tau)$ and $g_3 = 140\,\pi^{-6}\,G_6(\tau)$ characterizing the auxiliary elliptic curve with modular parameter τ. All coefficients of the curve are modular forms: the e_i and $\widetilde{u}$ have modular weight 2, while x, y have weights 4 and 6 respectively. To be precise, the e_i are not modular forms for $SL(2,\mathbb{Z})$, but only for certain subgroups of it, however $SL(2,\mathbb{Z})$ permutes them, and this presentation of the SW curve is manifestly invariant under permutations of the e_i. The parameter $\widetilde{u}$ is related to the gauge-invariant Coulomb branch-coordinate $u = \langle \mathrm{Tr}\,\phi^2 \rangle$ by

$$u = \widetilde{u} + \frac{1}{8} e_1 m^2. \tag{5.3}$$

As argued in [121], a weak coupling analysis indicates the presence of a singularity at $u \approx \frac{1}{4}m^2$ where a component of the adjoint hypermultiplet becomes massless, while flowing to low energies one expects the theory to evolve to the pure $SU(2)$ theory which is well known to have two singularities. Overall one expects therefore three singularities on the Coulomb branch, at each of these two branch points collide, indicating the presence of three distinct hypermultiplets, each with monodromy conjugate to T^2. At a generic point in the coupling parameter space the precise positions of the singularities can be read off eq. (5.2) to be

$$u_1 = \frac{3}{8}\,m^2\,e_1, \qquad u_{2,3} = \pm\frac{1}{8}\,m^2\,(e_3 - e_2). \tag{5.4}$$

The two dyons becoming massless at $u_{2,3}$ are exchanged under the $\mathbb{Z}_2$ symmetry of the pure $SU(2)$ Coulomb branch, identifying u_1 as the singularity due to the new adjoint hypermultiplet.

The flow to the pure $SU(2)$ theory involves sending the mass to infinity together with taking the weak coupling limit: more precisely, letting $q = e^{2\pi i \tau}$ and sending $\tau \to i\infty$, $m \to \infty$ while keeping $\Lambda_0 = 2q^{1/2}m^2$ fixed, takes the curve (5.2) to

$$y^2 = (\widetilde{x} - u)(\widetilde{x} - \Lambda_0^2)(\widetilde{x} + \Lambda_0^2) \tag{5.5}$$

where $\widetilde{x} = x - \frac{1}{2}e_1 u + \frac{1}{8}m^2{e_1}^2$ is an optional shift in the x plane that highlights the $u \to -u$ symmetry.

5.1.3 $SU(2)$ $\mathcal{N} = 2^*$ theory as a theory of class $\mathcal{S}$

Following [59] we may engineer the $\mathcal{N} = 2^*$ theory as a superconformal $SU(2)$ quiver gauge theory with a single node and a single bifundamental massive hypermultiplet (this viewpoint was first

adopted in [133]). The UV parameter space of marginal deformations of this theory then coincides with the parameter space of a once-punctured torus C. C arises by gluing together two punctures of a three-holed sphere, this corresponds to gauging two of the three $SU(2)$ flavor symmetries on the trinion into a single $SU(2)$ node, leaving a hypermultiplet in the bifundamental of the gauge group, with the remaining $SU(2)$ flavor symmetry. Turning on the mass parameter, which is represented by the Cartan generator of $SU(2)$, will eventually break the flavor symmetry down to the expected $U(1)$. The bifundamental of $SU(2)$ reduces to the direct sum of an adjoint and a singlet, the singlet decouples, leaving $\mathcal{N} = 2$ $SU(2)$ SYM coupled to and adjoint-valued hypermultiplet. When $m = 0$ this field content actually enjoys more supersymmetry, and the theory really corresponds to maximally supersymmetric gauge theory. When the mass deformation is instead turned on this is also known as $\mathcal{N} = 2^*$ theory. The moduli space of marginal deformations, modulo S-duality, coincides with the moduli space of elliptic curves with a marked point, which is just is the fundamental domain of the modular group. The Seiberg-Witten curve of this theory is a ramified double-covering of C, with Seiberg-Witten differential (see for example [61])

$$\lambda^2 = \left(\widetilde{u} + \widetilde{m}^2 \wp(z|\tau)\right) (dz)^2 \tag{5.6}$$

where $\wp$ is the Weierstrass elliptic function and z is a holomorphic coordinate on the elliptic curve $C \sim \mathbb{C}/\Lambda$, and Λ is the lattice generated by $(1, \tau)$. $\wp : C \to \mathbb{C}$ has a double pole at $z = 0$, where is behaves as $\wp \sim 1/z^2$. Then the SW differential exhibits a simple pole at the origin with $\mathrm{Res}_{z=0}\lambda = \widetilde{m}$, and has two branch points on the torus. The Seiberg-Witten curve is then a genus-two Riemann surface with two punctures.

Let us briefly comment on the relation between this description of the SW curve and that of equation 5.2. First, recall that $\wp$ and satisfies

$$\wp(z) = \wp(z + 1) = \wp(z + \tau) = \wp(-z) \tag{5.7}$$

in particular this means that each point on $\mathbb{C}$ has two preimages on C, with the exception of the three points $e_i(\tau)$, $i = 1, 2, 3$ whose preimages are three vanishing loci of $\wp'$: $1/2, \tau/2, (1+\tau)/2$. The e_i have the property that $e_1 + e_2 + e_3 = 0$, which we'll make use of. Starting from expression (5.7), changing variable from z to $x = \wp(z)$

$$\lambda^2 = \frac{(\widetilde{m}^2\, x + \widetilde{u})(dz)^2}{4x^3 - g_2 x - g_3} \tag{5.8}$$

the equation of the elliptic curve described as a branched covering of the x plane is obtained by looking at $\partial\lambda/\partial u \equiv dx/y$. Scaling $y = y'\, 2i\widetilde{m}$ we have the curve

$$y'^2 = \left(x + \frac{\widetilde{u}}{\widetilde{m}^2}\right)(x - e_1)(x - e_2)(x - e_3) \tag{5.9}$$

where e_i depend on τ and are simply the roots of $4x^3 - g_2 x - g_3$. Now employ the change of variable $x \mapsto x' = T_{(e_1,e_2,e_3)}(x)$ with

$$T_{(a,b,c)}(z) := \frac{(z-a)(b-c)}{(z-b)(a-c)} \tag{5.10}$$

giving

$$w^2 = x'(x'-1)(x'-v) \qquad v = \frac{(\tilde{u}+e_1\tilde{m}^2)(e_2-e_3)}{(\tilde{u}+e_2\tilde{m}^2)(e_1-e_3)} \tag{5.11}$$

now employ an affine transformation on the x plane $x'' = ax' + b$ with

$$\begin{aligned} a &= (e_1-e_3)\left(\widetilde{u} + \frac{1}{4}(e_1+e_3)m^2)\right) \\ b &= e_3\widetilde{u} + \frac{1}{4}e_3^2 m^2 \end{aligned} \tag{5.12}$$

and where $m = 2i\tilde{m}$, together with a rescaling $y'' = wa^{3/2}$, overall this gives

$$y''^2 = \prod_{i=1}^{3}(x'' - e_i\tilde{u} - \frac{1}{4}e_i^2 m^2) \tag{5.13}$$

this is precisely equation (5.2).

5.2 The spectrum generator

In this section we derive explicit expressions for those functions that correspond to the action of the spectrum generator (1.19) on a basis of WKB coordinates, establishing the following relations between WKB coordinates before and after an *omnipop*

$$\mathcal{X}_{\gamma_i}^{\vartheta+\pi} \;=\; \mathbb{S}\,\mathcal{X}_{\gamma_i}^{\vartheta} \;=\; S_i\,\mathcal{X}_{\gamma_i}^{\vartheta}, \qquad i = 1,2,3\,. \tag{5.14}$$

In order to determine the S_i, we shall follow closely the algorithm presented in [64]. The only ingredient in the computation is the WKB triangulation. In the context of $SU(2)$ $\mathcal{N} = 2^*$ we are dealing with a triangulation of a once-punctured torus and the typical $T^{\vartheta}_{\mathrm{WKB}}$ for generic ϑ is of the type shown in figure 5.1.

To each edge E_i of $T^{\vartheta}_{\mathrm{WKB}}$ we associate a polynomial Σ_i (these are precisely the same polynomials we already encountered in chapter 2, see equation (2.9); normally there would be two distinct ones, but in this theory they coincide)

$$\begin{aligned} \Sigma_1 &= 1 + \mathcal{X}_{\gamma_2} + \mathcal{X}_{\gamma_2+\gamma_3} + \mathcal{X}_{\gamma_2+\gamma_3+\gamma_1} + \mathcal{X}_{2\gamma_2+\gamma_3+\gamma_1} + \mathcal{X}_{2\gamma_2+2\gamma_3+\gamma_1} \\ \Sigma_2 &= 1 + \mathcal{X}_{\gamma_3} + \mathcal{X}_{\gamma_3+\gamma_1} + \mathcal{X}_{\gamma_3+\gamma_1+\gamma_2} + \mathcal{X}_{2\gamma_3+\gamma_1+\gamma_2} + \mathcal{X}_{2\gamma_3+2\gamma_1+\gamma_2} \\ \Sigma_3 &= 1 + \mathcal{X}_{\gamma_1} + \mathcal{X}_{\gamma_1+\gamma_2} + \mathcal{X}_{\gamma_1+\gamma_2+\gamma_3} + \mathcal{X}_{2\gamma_1+\gamma_2+\gamma_3} + \mathcal{X}_{2\gamma_1+2\gamma_2+\gamma_3} \end{aligned} \tag{5.15}$$

upon defining

$$A_i := \frac{\mathcal{X}_{\gamma_i}\,{\Sigma_i}^2}{(1-\mu^2)^2}, \qquad i = 1,2,3 \tag{5.16}$$

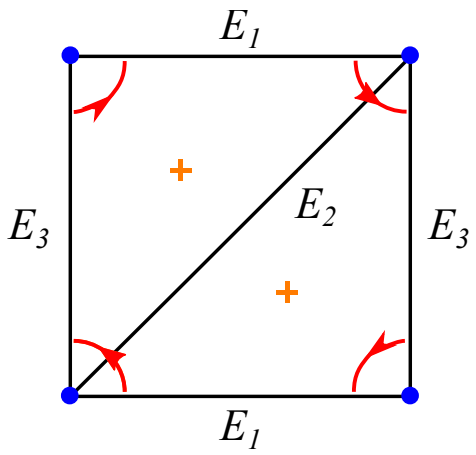

Figure 5.1: The triangulation of C for the $\mathcal{N}=2^*$ theory: C is a torus obtained by identifying parallel edges pairwise. The edges E_i of the WKB triangulation are shown, the elements γ_i of the charge lattice are the corresponding dual cycles. The puncture on C is indicated by the thick blue dot, branch points are indicated by orange crosses. The path for computing Σ_1 is indicated in red.

with $\mu^2 = \mathcal{X}_{2\gamma_1+2\gamma_2+2\gamma_3}$, the spectrum generating functions can be readily expressed as

$$S_1 = \left(\frac{1+A_2}{1+A_3}\right)^2, \qquad S_2 = \left(\frac{1+A_3}{1+A_1}\right)^2, \qquad S_3 = \left(\frac{1+A_1}{1+A_2}\right)^2. \tag{5.17}$$

This set of functions uniquely encodes the full BPS spectrum of the theory, our next step is to prove that that our ansatz for $\mathbb{S}$ correctly reproduces the S_i just derived.

5.3 A special decomposition of $\mathbb{S}$

5.3.1 Review of $SU(2)$ wall-crossing

Before dealing with our ansatz for the $\mathcal{N}=2^*$ spectrum, it will be useful to review some aspects of the well known wall crossing formula of the pure $SU(2)$ theory, as this will provide us with some necessary tools. The two factorizations of the spectrum generator in the different regimes of strong- and weak-coupling are related by the renowned wall crossing formula of [88]

$$\mathcal{K}_{\gamma_1}\mathcal{K}_{\gamma_2} \;=\; \Pi_1 \; \mathcal{K}^{-2}_{\gamma_1+\gamma_2} \; \Pi_2 \tag{5.18}$$

where $\langle\gamma_1,\gamma_2\rangle = 2$ and we set

$$\begin{aligned} \Pi_1 &= \mathcal{K}_{\gamma_2}\mathcal{K}_{\gamma_1+2\gamma_2}\cdots\mathcal{K}_{n\gamma_1+(n+1)\gamma_2}\cdots \\ \Pi_2 &= \cdots\mathcal{K}_{(n+1)\gamma_1+n\gamma_2}\cdots\mathcal{K}_{2\gamma_1+\gamma_2}\mathcal{K}_{\gamma_1} \end{aligned} \tag{5.19}$$

the physical interpretation of this formula (first observed by Frederik Denef) was described in [60]. The purpose of this subsection is to derive explicit expressions in closed form for the action of Π_1, Π_2

on $\mathcal{X}_{\gamma_1}$ and $\mathcal{X}_{\gamma_2}$. For the sake of clarity we will denote by $\mathcal{X}_\gamma^{(0)}$ the Darboux coordinates before acting on them with $\mathbb{S}$, together with

$$\begin{aligned}\mathcal{X}_\gamma^{(I)} &= \Pi_2 \mathcal{X}_\gamma^{(0)},\\ \mathcal{X}_\gamma^{(II)} &= \mathcal{K}^{-2}_{\gamma_1+\gamma_2}\mathcal{X}_\gamma^{(I)},\\ \mathcal{X}_\gamma^{(III)} &= \Pi_1 \mathcal{X}_\gamma^{(II)}.\end{aligned} \tag{5.20}$$

Adopting a trick employed[1] in the appendix of [60], we introduce a reparameterization of the $\mathcal{X}_\gamma$'s in terms of two auxiliary variables $a, b \in \mathbb{C}$. For that purpose let us introduce the following countably infinite set of variables

$$x_n = \frac{\cosh^2(an+b)}{\sinh^2 a} \tag{5.21}$$

enjoying the recursion relation $x_{n+1}x_{n-1} = (1+x_n)^2$. Without loss of generality we choose

$$\mathcal{X}^{(0)}_{\gamma_1} = x_1^{-1}, \qquad \mathcal{X}^{(0)}_{\gamma_2} = x_0. \tag{5.22}$$

The advantage of using the auxiliary x_n description will now become clear, consider the action of Π_2

$$\left\{\begin{array}{l}\mathcal{X}^{(0)}_{\gamma_1} = x_1^{-1}\\ \mathcal{X}^{(0)}_{\gamma_1+\gamma_2} = x_0 x_1^{-1}\end{array}\right. \xrightarrow{\mathcal{K}_{\gamma_1}} \left\{\begin{array}{l}\mathcal{X}^{(1)}_{2\gamma_1+\gamma_2} = x_2^{-1}\\ \mathcal{X}^{(1)}_{\gamma_1+\gamma_2} = x_1 x_2^{-1}\end{array}\right. \xrightarrow{\mathcal{K}_{2\gamma_1+\gamma_2}} \left\{\begin{array}{l}\mathcal{X}^{(2)}_{3\gamma_1+2\gamma_2} = x_3^{-1}\\ \mathcal{X}^{(2)}_{\gamma_1+\gamma_2} = x_2 x_3^{-1}\end{array}\right. \cdots \tag{5.23}$$

in particular, acting with the first n KS operators within Π_2 yields $\mathcal{X}^{(n)}_{\gamma_1+\gamma_2} = x_n x_{n+1}^{-1}$, $\mathcal{X}^{(n)}_{(n+1)\gamma_1+n\gamma_2} = x_{n+1}$. If, say, $\operatorname{Re} a, \operatorname{Re} b > 0$, then the limit $n \to \infty$ is finite for $\mathcal{X}^{(n)}_{\gamma_1}$, $\mathcal{X}^{(n)}_{\gamma_2}$ and gives

$$\Pi_2 : \left\{\begin{array}{l}\mathcal{X}^{(0)}_{\gamma_1} = \frac{\sinh^2 a}{\cosh^2(a+b)}\\ \mathcal{X}^{(0)}_{\gamma_2} = \frac{\cosh^2 b}{\sinh^2 a}\end{array}\right. \mapsto \left\{\begin{array}{l}\mathcal{X}^{(I)}_{\gamma_1} = e^{-2b}(1-e^{-2a})^2\\ \mathcal{X}^{(I)}_{\gamma_2} = e^{2(b-a)}(1-e^{-2a})^{-2}\end{array}\right. , \tag{5.24}$$

hence $\mathcal{X}^{(I)}_{\gamma_1+\gamma_2} = e^{-2a}$. Acting with $K^{-2}_{\gamma_1+\gamma_2}$ then gives

$$\begin{aligned}\mathcal{X}^{(II)}_{\gamma_1} &= e^{-2b}(1-e^{-2a})^{-2}\\ \mathcal{X}^{(II)}_{\gamma_2} &= e^{2(b-a)}(1-e^{-2a})^{2}\end{aligned} \tag{5.25}$$

In order to study the action of Π_1 on these Darboux coordinates, it is convenient to work backwards: by employing the strong-coupling side of the pure $SU(2)$ wall crossing formula on the $X^{(0)}_\gamma$, one can readily derive that $\mathcal{X}^{(III)}_{\gamma_1} = x_{-1}$, $\mathcal{X}^{(III)}_{\gamma_2} = x_{-2}^{-1}$. Although this is all we need to know, for the sake of completeness we show that the wall crossing formula closes correctly: consider the action of Π_1^{-1}

[1] Notice that our definition of the x_n differs from theirs by a sign. This sign modifies the recursion relation of the x_n, this in turn is necessary when working with the pure $SU(2)$ wall crossing formula while taking into account the quadratic refinement $\sigma(\gamma)$ within each $\mathcal{K}_\gamma$ factor, which was later introduced in [64].

on the $\mathcal{X}_\gamma^{(III)}$

$$\left\{\begin{array}{ll}\mathcal{X}^{(III)}_{\gamma_2}=x_{-2}^{-1} & \overset{\mathcal{K}^{-1}_{\gamma_2}}{\longrightarrow}\\ \mathcal{X}^{(III)}_{\gamma_1+\gamma_2}=x_{-1}x_{-2}^{-1} & \overset{\mathcal{K}_{\gamma_2}}{\longleftarrow}\end{array}\right.\left\{\begin{array}{ll}\mathcal{X}^{(-1)}_{\gamma_1+2\gamma_2}=x_{-3}^{-1} & \overset{\mathcal{K}^{-1}_{\gamma_1+2\gamma_2}}{\longrightarrow}\\ \mathcal{X}^{(-1)}_{\gamma_1+\gamma_2}=x_{-2}x_{-3}^{-1} & \overset{\mathcal{K}_{\gamma_1+2\gamma_2}}{\longleftarrow}\end{array}\right.\left\{\begin{array}{l}\mathcal{X}^{(-2)}_{2\gamma_1+3\gamma_2}=x_{-4}^{-1}\\ \mathcal{X}^{(-2)}_{\gamma_1+\gamma_2}=x_{-3}x_{-4}^{-1}\end{array}\right.\cdots \tag{5.26}$$

the n-th iteration yields $\mathcal{X}^{(-n)}_{\gamma_1+\gamma_2}=x_{-(n+1)}x^{-1}_{-(n+2)}$, $\mathcal{X}^{(-n)}_{n\gamma_1+(n+1)\gamma_2}=x^{-1}_{-(n+2)}$. In the limit $n\to\infty$ we recover

$$\begin{aligned}\mathcal{X}^{(-n)}_{\gamma_1+\gamma_2} &\longrightarrow e^{-2a}\equiv\mathcal{X}^{(II)}_{\gamma_1+\gamma_2}\\ \mathcal{X}^{(-n)}_{\gamma_1} &\longrightarrow e^{-2b}(1-e^{-2a})^{-2}\equiv\mathcal{X}^{(II)}_{\gamma_1}\,.\end{aligned} \tag{5.27}$$

Overall, we found

$$\Pi_1:\left\{\begin{array}{l}\mathcal{X}^{(II)}_{\gamma_1}=e^{-2b}(1-e^{-2a})^2\\ \mathcal{X}^{(II)}_{\gamma_2}=e^{2(b-a)}(1-e^{-2a})^{-2}\end{array}\right.\mapsto\left\{\begin{array}{l}\mathcal{X}^{(III)}_{\gamma_1}=\frac{\cosh^2(b-a)}{\sinh^2 a}\\ \mathcal{X}^{(III)}_{\gamma_2}=\frac{\sinh^2 a}{\cosh^2(b-2a)}\end{array}\right.\,, \tag{5.28}$$

By inverting the LHS of the above relation, we find $e^{-2a}=\mathcal{X}^{(II)}_{\gamma_1+\gamma_2}$ and $e^{-2b}=\mathcal{X}^{(II)}_{\gamma_1}(1-\mathcal{X}^{(II)}_{\gamma_1+\gamma_2})^2$. Replacing these on the right-hand side, we find the action of Π_1 on the WKB basis coordinates

$$\begin{aligned}\mathcal{X}^{(III)}_{\gamma_1} &= \mathcal{X}^{(II)}_{\gamma_1}\frac{(1+\mathcal{X}^{(II)}_{\gamma_2}(1+\mathcal{X}^{(II)}_{\gamma_1}(-2+\mathcal{X}^{(II)}_{\gamma_1+\gamma_2})))^2}{(1-\mathcal{X}^{(II)}_{\gamma_1+\gamma_2})^4}\\ \mathcal{X}^{(III)}_{\gamma_2} &= \mathcal{X}^{(II)}_{\gamma_2}\frac{(1-\mathcal{X}^{(II)}_{\gamma_1+\gamma_2})^4}{(1+\mathcal{X}^{(II)}_{\gamma_1+\gamma_2}(-2+\mathcal{X}^{(II)}_{\gamma_2}+\mathcal{X}^{(II)}_{\gamma_1+\gamma_2}))^2},.\end{aligned} \tag{5.29}$$

This is the expression we were after, as we will see shortly, it will enable us to express the Poisson transformation given by equations (1.19) and (1.18) in closed form. An analogous expression for Π_2 can be obtained by the same method.

5.3.2 The spectrum at the special locus

Let us consider the low energy theory at some point $u\in\mathcal{E}_3$ where $\operatorname{Arg}Z(\gamma_2)>\operatorname{Arg}Z(\gamma_1)$, our ansatz for the spectrum generator reads

$$\mathbb{S}\;=\;\Pi_1\;\mathcal{K}_{\gamma_f-(\gamma_1+\gamma_2)}\mathcal{K}^{-2}_{\gamma_1+\gamma_2}\mathcal{K}_{\gamma_f+(\gamma_1+\gamma_2)}\;\Pi_2 \tag{5.30}$$

notice that the central charges corresponding to the three $\mathcal{K}$ operators in the middle have exactly the same phase, a fact that could potentially introduce an ambiguity of the ordering. The ambiguity is absent in this case, because the three operators commute. Adopting a notation analogous to that of the previous subsection, we will denote by $\mathcal{X}^{(0)}_\gamma$ the set of WKB coordinates before acting on them

with $\mathbb{S}$, together with

$$\begin{aligned}
\mathcal{X}_\gamma^{(I)} &= \Pi_2 \mathcal{X}_\gamma^{(0)}, \\
\mathcal{X}_\gamma^{(II)} &= \mathcal{K}_{\gamma_0-(\gamma_1+\gamma_2)} \mathcal{K}_{\gamma_1+\gamma_2}^{-2} \mathcal{K}_{\gamma_0+(\gamma_1+\gamma_2)} \mathcal{X}_\gamma^{(I)}, \\
\mathcal{X}_\gamma^{(III)} &= \Pi_1 \mathcal{X}_\gamma^{(II)}.
\end{aligned} \tag{5.31}$$

Unlike in the previous subsection, we are now working with a rank 3 lattice generated by $\gamma_1, \gamma_2, \gamma_3$ with intersection pairing $\langle \gamma_i, \gamma_{i+1} \rangle = 2$ (the index i here runs cyclically from 1 to 3). Nevertheless, notice that $\mathcal{X}_{\gamma_f} = \mathcal{X}_{\gamma_1+\gamma_2+\gamma_3}$ remains unchanged by each of the $\mathcal{K}_\gamma$, we shall rename this distinguished coordinate as μ (compatibly with the definition below eq. (5.16)). This means that, at any stage during the computation, we only need to compute the action of $\mathcal{K}$ operators on $\mathcal{X}_{\gamma_1}, \mathcal{X}_{\gamma_2}$, while $\mathcal{X}_{\gamma_3}$ will follow as

$$\mathcal{X}_{\gamma_3}^{(K)} = \frac{\mu}{\mathcal{X}_{\gamma_1}^{(K)} \mathcal{X}_{\gamma_2}^{(K)}}. \tag{5.32}$$

Once again, we will employ the auxiliary variables x_n, and choose $\mathcal{X}_{\gamma_1}^{(0)} = x_1^{-1}$, $\mathcal{X}_{\gamma_2}^{(0)} = x_0$ to begin with. We already know the action of Π_2 from (5.24), hence we start from the $\mathcal{X}_\gamma^{(I)}$ and act on them with $\mathcal{K}_{\gamma_0-(\gamma_1+\gamma_2)} \mathcal{K}_{\gamma_1+\gamma_2}^{-2} \mathcal{K}_{\gamma_0+(\gamma_1+\gamma_2)}$, this yields

$$\begin{aligned}
\mathcal{X}_{\gamma_1}^{(II)} &= e^{-2b} \frac{\left(1+e^{-2a}\mu\right)^2}{\left(1-e^{-2a}\right)^2 \left(1+e^{2a}\mu\right)^2} \\
\mathcal{X}_{\gamma_2}^{(II)} &= e^{2(b-a)} \left[\frac{\left(1+e^{-2a}\mu\right)^2}{\left(1-e^{-2a}\right)^2 \left(1+e^{2a}\mu\right)^2}\right]^{-1} \\
\mathcal{X}_{\gamma_1}^{(II)} &= e^{2a}\mu
\end{aligned} \tag{5.33}$$

Then, acting with Π_1 is achieved by employing (5.29), which gives

$$\begin{aligned}
\mathcal{X}_{\gamma_1}^{(III)} &= e^{-2b} \frac{\left(e^{4a}+e^{2(a+b)}+2e^{2a}\mu+2e^{4a+2b}\mu+\mu^2+e^{6a+2b}\mu^2\right)^2}{\left(1-e^{2a}\right)^2 \left(e^{2a}+\mu\right)^2 \left(1+e^{2a}\mu\right)^2} \\
\mathcal{X}_{\gamma_2}^{(III)} &= e^{2(a-b)} \frac{\left(1-e^{2a}\right)^2 \left(e^{2a}+\mu\right)^2 \left(1+e^{2a}\mu\right)^2}{\left(e^{4a}+e^{2b}+2e^{2a}\mu+2e^{2(a+b)}\mu+\mu^2+e^{4a+2b}\mu^2\right)^2} \\
\mathcal{X}_{\gamma_3}^{(III)} &= e^{2a}\mu \frac{\left(e^{4a}+e^{2b}+2e^{2a}\mu+2e^{2(a+b)}\mu+\mu^2+e^{4a+2b}\mu^2\right)^2}{\left(e^{4a}+e^{2(a+b)}+2e^{2a}\mu+2e^{4a+2b}\mu+\mu^2+e^{6a+2b}\mu^2\right)^2}
\end{aligned} \tag{5.34}$$

At this point one could solve equations (5.22) for a, b and substitute into the above ones, to express the $\mathcal{X}_\gamma^{(III)}$ in terms of the original basis $\mathcal{X}_\gamma^{(0)}$. Since this would be cumbersome, we will instead employ equations (5.22) to express the S_i in terms of a, b, μ and show that they match with our

result (5.34). From the discussion of §5.2, in our current notation the S_i are given by (5.17) with

$$\begin{aligned} A_1 &:= \mathcal{X}^{(0)}_{\gamma_1} \frac{\left(1+\mathcal{X}^{(0)}_{\gamma_2}+\mathcal{X}^{(0)}_{\gamma_2+\gamma_3}+\mathcal{X}^{(0)}_{\gamma_2+\gamma_3+\gamma_1}+\mathcal{X}^{(0)}_{2\gamma_2+\gamma_3+\gamma_1}+\mathcal{X}^{(0)}_{2\gamma_2+2\gamma_3+\gamma_1}\right)^2}{(1-\mu^2)^2} \\ A_2 &:= \mathcal{X}^{(0)}_{\gamma_2} \frac{\left(1+\mathcal{X}^{(0)}_{\gamma_3}+\mathcal{X}^{(0)}_{\gamma_3+\gamma_1}+\mathcal{X}^{(0)}_{\gamma_3+\gamma_1+\gamma_2}+\mathcal{X}^{(0)}_{2\gamma_3+\gamma_1+\gamma_2}+\mathcal{X}^{(0)}_{2\gamma_3+2\gamma_1+\gamma_2}\right)^2}{(1-\mu^2)^2} \\ A_3 &:= \mathcal{X}^{(0)}_{\gamma_3} \frac{\left(1+\mathcal{X}^{(0)}_{\gamma_1}+\mathcal{X}^{(0)}_{\gamma_1+\gamma_2}+\mathcal{X}^{(0)}_{\gamma_1+\gamma_2+\gamma_3}+\mathcal{X}^{(0)}_{2\gamma_1+\gamma_2+\gamma_3}+\mathcal{X}^{(0)}_{2\gamma_1+2\gamma_2+\gamma_3}\right)^2}{(1-\mu^2)^2} \end{aligned} \tag{5.35}$$

Together with (5.22), these entail

$$\begin{aligned} \mathcal{X}^{(0)}_{\gamma_1} S_1 &= e^{-2b} \frac{\left(e^{4a}+e^{2(a+b)}+2e^{2a}\mu+2e^{4a+2b}\mu+\mu^2+e^{6a+2b}\mu^2\right)^2}{\left(1-e^{2a}\right)^2\left(\mu+e^{4a}\mu+e^{2a}\left(1+\mu^2\right)\right)^2}, \\ \mathcal{X}^{(0)}_{\gamma_2} S_2 &= e^{2b} \frac{\left(1+\mu^2+\mu(e^{2a}+e^{-2a})\right)^2(e^a-e^{-a})^2}{\left(2\left(1+e^{2b}\right)\mu+\left(1+e^{2b}\right)\left(1+\mu^2\right)(e^{2a}+e^{-2a})/2+\left(1-e^{2b}\right)\left(1-\mu^2\right)(e^{2a}-e^{-2a})/2\right)^2}, \\ \mathcal{X}^{(0)}_{\gamma_3} S_3 &= e^{2a}\mu \frac{\left(e^{4a}+e^{2b}+2e^{2a}\mu+2e^{2(a+b)}\mu+\mu^2+e^{4a+2b}\mu^2\right)^2}{\left(e^{4a}+e^{2(a+b)}+2e^{2a}\mu+2e^{4a+2b}\mu+\mu^2+e^{6a+2b}\mu^2\right)^2}. \end{aligned} \tag{5.36}$$

The first and third lines coincide with (5.34). A little algebra shows that the middle line also coincides, as claimed.

5.4 Wall crossing to other chambers

So far we discussed the BPS spectrum at some very particular loci on the Coulomb branch. As we will see, the spectrum becomes much more complicated as we move away from those loci. In particular, an infinitesimally small perturbation in u will induce wall crossing and produce an *infinite* amount of BPS vector multiplets, together with their cohorts of hypermultiplets.

Recall that the central charges of the lattice basis are related by

$$Z(\gamma_1)+Z(\gamma_2)+Z(\gamma_3)=m \tag{5.37}$$

Let us now consider an infinitesimal perturbation away from the condition $\operatorname{Arg} Z(\gamma_1+\gamma_2)=\operatorname{Arg} m=\vartheta_0$, more precisely, consider moving on the Coulomb branch along an infinitesimal path away from $\mathcal{E}_3$, where $Z(\gamma_2)$ remains unchanged and $Z(\gamma_1)$ changes by $\rho\, e^{i\phi}$, $0<\rho\ll|Z(\gamma_i)|$, $\phi=\operatorname{Arg} Z(\gamma_1)+\pi/2$. In other words, we consider a perturbation which "closes" slightly the wedge between $Z(\gamma_1)$ and $Z(\gamma_2)$, while leaving $Z(\gamma_2)$ unchanged (recall that $\operatorname{Arg} Z(\gamma_1)<\operatorname{Arg} Z(\gamma_2)$). Since m does not depend on u, then $Z(\gamma_3)$ rotates clockwise to $Z(\gamma_3)-\rho\, e^{i\phi}$ by a phase $\delta\phi_3$. Conversely, $Z(\gamma_1+\gamma_2)$ and $Z(\gamma_f+\gamma_1+\gamma_2)$ will undergo infinitesimal counter-clockwise rotations by respective phases $\delta\phi_{12}$ and $\delta\phi_{\bar{3}}$, furthermore $\delta\phi_{\bar{3}}<\delta\phi_{12}$.

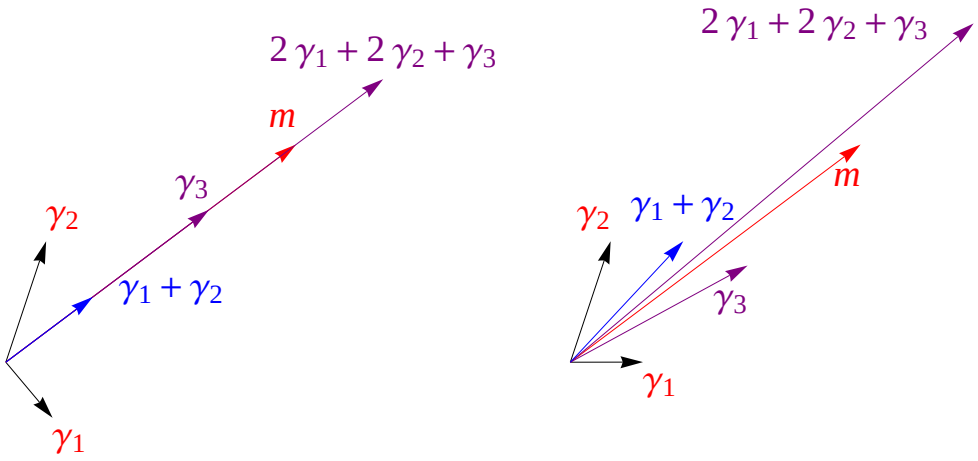

Figure 5.2: On the left: the configuration of central charges on the locus $\mathcal{E}_3$. On the right: the central charges after perturbing away from the special locus

Accordingly, the spectrum generator evolves to

$$\Pi_1 \mathcal{K}^{-2}_{\gamma_1+\gamma_2} \cdots ?? \cdots \mathcal{K}_{\gamma_f+(\gamma_1+\gamma_2)} \cdots ?? \cdots \mathcal{K}_{\gamma_3} \mathcal{K}_{(n'+1)\gamma_1+n'\gamma_2} \cdots \mathcal{K}_{2\gamma_1+\gamma_2} \mathcal{K}_{\gamma_1} \tag{5.38}$$

where n' is the largest positive integer such that $\mathrm{Arg}\, Z((n'+1)\gamma_1 + n'\gamma_2) < \mathrm{Arg}\, Z(\gamma_3)$. The central charges of BPS hypermultiplets within Π_2 accumulate at the phase of $Z(\gamma_1+\gamma_2)$, therefore as we perturb away from the situation of §5.3.2 the $\mathcal{K}_{\gamma_3}$ factor will cross infinitely many $\mathcal{K}$ factors within Π_2, stopping at a "finite distance" of n' operators from the right end. It is important that $\mathcal{K}_{\gamma_3}$ leads the way in front of $\mathcal{K}_{\gamma_f+(\gamma_1+\gamma_2)}$, this ensures that at each wall of marginal stability crossed by γ_3 one has $\langle \gamma_3, (m+1)\gamma_1 + m\gamma_2 \rangle = 2$. In other words, upon crossing each wall, the portion of $\mathbb{S}$ affected by wall crossing of γ_3 will change as prescribed by the pure $SU(2)$ wall crossing formula. This occurs (countably) infinitely many times: as $\mathcal{K}_{\gamma_3}$ proceeds across the MS walls of the charges in Π_2 it leaves behind a wake of vector multiplets of charges $(n+1)\gamma_1 + n\gamma_2 + \gamma_3$ for $n > n'$ and relative cohorts of hypermultiplets. The advance of $\mathcal{K}_{\gamma_3}$ is followed by that of $\mathcal{K}_{\gamma_f+(\gamma_1+\gamma_2)}$, this operator will find on its way the remnants of the infinitely many wall crossings caused by its predecessor. These are harder to follow systematically, because there could in principle be walls of marginal stability where two charges have arbitrarily large (positive or negative, though always even) intersection pairing. Extensive experimentation suggests that the only type of wall crossing actually occurring is the one encountered in pure $SU(2)$ SYM, although we don't have a proof of this.

In keeping with our approach of pairwise permuting adjacent $\mathcal{K}$-operators of $\mathbb{S}$, it should be noted that the products of the infinitely many wall crossing formulae will interact among themselves, giving rise to new "second generation" wall crossing phenomena. There is no good reason to think that this

should stop at the second generation of BPS states, hence we expect the structure to be extremely intricate as we move further away from the $\mathcal{E}_i$. Given the complexity of this structure, the absence

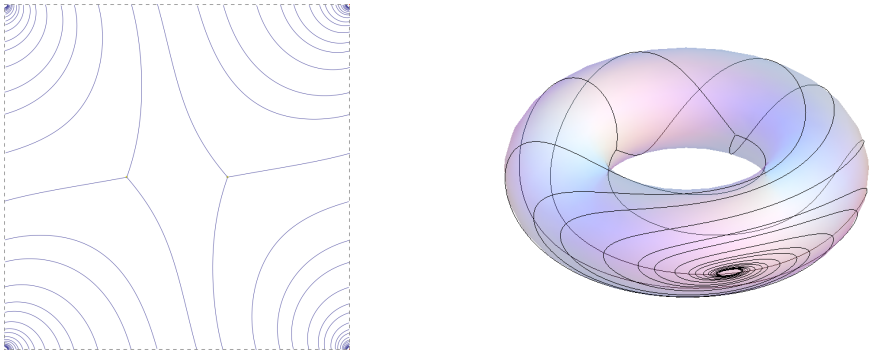

Figure 5.3: A spectral network $\mathcal{W}_\zeta$ of the $SU(2)$ $\mathcal{N}=2^*$ theory. Away from the exceptional loci, it is difficult to study the spectrum systematically by keeping track directly of the jumps of the network, as these occur for infinitely many values of the phase ζ. While in the example of $SU(2)$ pure SYM (which also exhibits an infinite sequence of jumps) there is a clear pattern for the cycles involved in the jumps, there is no evidence of a general pattern in this theory, save for the exceptional locus $\mathcal{E}$.

of wild chambers on $\mathcal{B}$ appears to be rather nontrivial, and worthy of further investigation.

We should also point out that, if we started perturbing in the opposite direction, i.e. "opening" the wedge between Z_{γ_1} and Z_{γ_2}, we would just have encountered a mirror situation. Once again $\mathcal{K}_{\gamma_3}$ leads the way through the infinitely many hyper multiplet's $\mathcal{K}_\gamma$ within Π_1, with $\mathcal{K}_{\gamma_f+(\gamma_1+\gamma_2)}$ following. In this case, just like in the previous one, the wall crossing formula of the pure $SU(2)$ theory governs the wall crossing phenomena induced by $\mathcal{K}_{\gamma_3}$, since $\langle m\gamma_1+(m+1)\gamma_2,\gamma_3\rangle=2$.

In conclusion, it seems difficult to give an explicit exact description of the spectrum away from the exceptional locus $\mathcal{E}$, at least within the approach of explicitly keeping track of the phase-reordering of $\mathcal{K}$ operators in $\mathbb{S}$, which would be induced by varying u. The main difficulties are presented by the rapid proliferation of 2-cohorts as we move away from the special locus, and by their "mutual interactions[2]". Nevertheless, thanks to the exact expression of the spectrum generating functions (5.17), a *truncated* version of the spectrum can be obtained *algorithmically*[3] for arbitrary values of the moduli, to arbitrary precision.

[2]The non-commutivity of the $\mathcal{K}$ operators from different, but overlapping (in the central charge plane), cohorts.
[3]An illustration of such an algorithm was given above, in section 3.4.1.

Chapter 6

Future Directions

We conclude with a collection of questions and new directions suggested by our work.

6.1 Open Problems

1. It is natural to guess that wild degeneracies will be a common feature among higher rank theories of class S. Strictly speaking, the only examples we have given are for gauge group $SU(3)$, but we fully expect that the phenomenon will persist for $SU(K)$ with $K > 3$. This is strongly suggested by the quiver analysis of Section 3.5, but a fully rigorous proof would require that one demonstrate that the path exhibited in the moduli space of stability parameters of the the Fiol quiver, which leads to wild wall crossing for $K > 3$, actually can be chosen in the moduli space of physical stability parameters. (While not fully mathematically rigorous, a compelling physical argument that this is indeed the case is that we could consider a hierarchy of symmetry breaking where $SU(K)$ is much more strongly broken to $SU(3) \times U(1)^{K-3}$ than the $SU(3)$ is broken to $U(1)^2$.)

2. Another open problem along similar lines is how the presence of, say, matter multiplets affects the existence of wild degeneracies.

3. It should be noted that the explicit point on the Coulomb branch illustrated in Figure 3.5 is in fact different from the region explored in Section 3.3.2. Nevertheless, using the techniques of Appendix C we have checked that the same crucial algebraic equation (4.111) governing the street factors of herds indeed appears in the spectral networks that arise in this region. These networks are very similar to but not quite the same as the m-herds. One might ask for a succinct test to see whether a degenerate spectral network leads to m-wild degeneracies.

4. It would be nice to understand better the physics of the curious invariance of the BPS degeneracies under the transformation by the g_m matrix discussed in Section 3.5.2 above. To the extent that the relation to quivers is physical, a physical understanding is indeed provided by the arguments in Section 3.5. However, we would like to suggest an alternative interpretation using the halo picture of BPS states. If we consider a core particle γ with halo particles of charge γ' then the replacement of the hypermultiplet of charge γ for the hypermultiplet $\gamma+m\gamma'$ is simply flipping the Fermi sea of the halo Fock space. (See, e.g. Section 3.5 of [13] for a similar transformation.) Perhaps then a physical derivation of the symmetry could proceed by using Fermi flips to establish such a symmetry for framed BPS states and then using recursion relations between framed and unframed BPS states to deduce it for general degeneracies. This symmetry also raises the interesting possibility that the mutation method for determining BPS degeneracies can be extended to higher spin states.

5. The g_m symmetry of Kronecker quivers makes a surprising prediction about two well-known formulae: Reineke's formula for Poincaré polynomials of quiver varieties [117], and the Manschot-Pioline-Sen wall-crossing formula [98, 99]. These formulae involve sums over certain partitions. For certain charges, there is rather extensive cancelation between terms in these formulae implied by the g_m symmetry of the BPS degeneracies. Since the individual terms in the sum in the MPS formulae have a simple geometrical interpretation [99] the g_m symmetry together with the MPS formula imply nontrivial identities on equivariant Dirac indices. For a simple and dramatic example we can choose $m = 3$ and note that that $(1, 1)$ has a very simple PSC, but

$$(g_3)^k \cdot \begin{pmatrix} 1 \\ 1 \end{pmatrix} = \begin{pmatrix} F_{2k-1} \\ F_{2k+1} \end{pmatrix} \tag{6.1}$$

(where F_n is the n^{th} Fibonacci number) involves arbitrarily large charges. Clearly there are many terms in the MPS formula (3.99) and, as we just said, their coefficients have a beautiful geometrical interpretation as equivariant indices of Dirac operators on the Denef moduli spaces. So the identity[1]

$$\Omega((F_{2k-1}, F_{2k+1}); y) = \Omega((1, 1); y) = [3]_y \tag{6.2}$$

is a very remarkable set of identities for these indices. It would be interesting to understand better these identities (and their analogues for $m > 3$) from a geometrical point of view.

[1] We use the notation $[n]_y := \frac{y^n - y^{-n}}{y - y^{-1}}$

6. Returning to the key algebraic equation (4.111), a natural question is whether there is a physical interpretation of the other roots of this equation. We expect that there will be. For example, choose a small path $\wp$ crossing a c-street in an m-herd. The corresponding supersymmetric interface has a vev when wrapped on the circle in $\mathbb{R}^3 \times S^1$ given by

$$\langle L_\zeta(\wp)\rangle_m = \begin{pmatrix} q(m,\zeta) & 0 & 0 \\ 0 & 1 & 0 \\ 0 & 0 & q(m,\zeta) \end{pmatrix} \tag{6.3}$$

where m is a point in Hitchin moduli space $\mathcal{M}$, $\zeta \in \mathbb{C}^*$ has phase $\operatorname{Arg}\zeta = \operatorname{Arg} Z(\gamma+\gamma')$, and $q(m,\zeta) = Q(c)|_{X_{\gamma_c}\to\mathcal{Y}_{\gamma_c}}$, where $\mathcal{Y}_{\gamma_c}$ is a function on the twistor space of the Hitchin moduli space $\mathcal{M}$ constructed in [60, 63]. It therefore makes sense to ask about the physical meaning of the analytic behavior of $\langle L_\zeta(\wp)\rangle$, and this might well involve the other roots of (4.111). Exploring this point further is beyond the scope of this paper.

7. A closely related point to the previous one is that the exponential growth of Ω for certain charges implies a similar exponential growth for μ and therefore for $\overline{\underline{\Omega}}$. We expect this will have important implications for the construction of hyperkahler metrics of associated Hitchin systems proposed in [60] and for the definition of the nonabelianization map of [63, 70]. Again, we leave this important point for future work.

8. The implications of our conjectures on the spin of framed BPS states in presence of "generic interfaces" raised some interesting questions. For one thing, compatibility with the halo picture required the introduction of auxiliary "flavor charges", these played the role of a refinement in the homological classification of paths on Σ, in particular accounting for important corrections to the writhe of detours. We also noticed how the jumps of $\mathfrak{F}(\wp,\vartheta;y)$ may be understood in terms of boundstates of the interface with *part* of the vanilla BPS multiplets, leading to the notion of *phantom halos*. While this interpretation fits nicely with the data extracted from spectral networks, a better understanding of these mechanisms may be achieved by studying physical models of framed wall crossing of interfaces. One example of such a model was considered in appendix D.2 of [65].

9. The interpretation of the formal $\hat{\Upsilon}$ variables as line operators of an abelian Chern-Simons theory on $\Sigma \times \mathbb{R}$, played the role of an effective guiding principle in formulating a consistent algebra. However, there are a few hints suggesting to take this analogy more seriously. One of them is the observation [56–58] that $4d$ $\mathcal{N}=2$ theories on $S^3 \times S^1$ are dual to q-deformed $2d$

Yang-Mills, which can also be viewed as an analytic continuation of a Chern-Simons theory away from integer rank [7]. Likewise, the appearance of complex Chern-Simons in $3d$ compactifications of the $(2,0)$ theory [37, 94] may be taken as another compelling argument for pursuing this analogy further. At any rate, from this perspective, the formal parallel transport $\mathfrak{F}$ may be interpreted as an explicit relation between algebras of observables of two different quantum theories of flat connections: one involving an abelian connection on Σ, the other involving a non-abelian connection on C. The statement about this duality can be formulated rather sharply, thanks to the precise rules involved in our construction of $\mathfrak{F}$. It would be interesting to check this correspondence directly, for example by explicitly constructing the Hilbert spaces associated with flat connections on C and Σ, as well as the corresponding line operators.

10. While it is true that the spectrum generator of $SU(2)$ $\mathcal{N} = 2^*$, together with the algorithm of section 3.4.1, allows to determine the spectrum to arbitrary accuracy in any region of $\mathcal{B}$, a more explicit description remains elusive. Away from the exceptional locus $\mathcal{E}$ the structure of the spectrum appears to be in general rather intricate, and particularly difficult to describe in the language of "cohorts". The shortfall is due to the infinite number of $\mathcal{K}$ operators undergoing phase-reordering within $\mathbb{S}$, as we perturb away from the exceptional locus. This is in contrast with familiar situations where phase-adjacent $\mathcal{K}$ operators are permuted pairwise in a controllable way. We believe that a more suitable language to describe this spectrum may exist, this would likely involve conceiving a suitable generalization of the concept of "cohort" for the case of simultaneous multi-$\mathcal{K}$ reshuffling within $\mathbb{S}$. We regard this as an interesting question, since finding such a description would likely lead to a broader understanding of the workings of the Kontsevich-Soiberlman wall crossing formula, and vice versa. The spectrum generator technique provides a vast amount of potentially important clues towards this goal.

11. Another lesson we take away from the $\mathcal{N} = 2^*$ story, is how important it is to have an algorithm for computing $\mathbb{S}$ from the topology of a *single* WKB triangulation. As we mentioned, it would have been extremely difficult to guess the full spectrum generator by simply studying the jumps of the spectral network in a generic chamber of the Coulomb branch. However, such a prescription for deriving the spectrum generator only exists for the vanilla and 2d-4d BPS spectra of A_1-type theories of class $\mathcal{S}$ [64, 95]. We do not see any obvious obstruction to the existence of such a relation of $\mathbb{S}$ to generic spectral networks, finding it would significantly enhance the effectiveness of the spectral network technique for studying BPS spectra.

6.2 Taking stock

A natural question to ask at this point is: *how much have we learned about BPS spectra?* Our viewpoint is that there are still important open questions that have been only partially answered by the recent major breakthroughs in BPS spectroscopy [11, 12, 63, 64, 99] and the subsequent developments.

For example, we may consider the interpretation of vanilla $4d$ BPS states as supersymmetric configuration of M2 branes suspended between M5 branes. The geometry of such membranes was studied long ago [80, 102, 103] for the simplest cases of BPS hypermultiplets and vector-multiplets, but the discovery of wild spectra immediately raises the question the classification of infinitely many new states. Of course, critical spectral networks such as m-herds and $m-(p,q)$-herds offer precious clues for answering this question.

The sector of *pure flavor* $4d$ BPS states is another aspect demanding further attention. In fact, while these states are successfully detected by jumps of spectral networks, the KS wall crossing formula is "blind" to them. This is because $\mathcal{K}_{\gamma_f}$ commutes with any $\mathcal{K}_\gamma$ operator, since γ_f has vanishing $\langle\cdot,\cdot\rangle$ pairing with any cycle γ. Thus, the wall crossing behavior of pure flavor states remains undetermined: for example, in a theory with a wall of marginal stability $MS(\gamma,\gamma')$ such that $\gamma+\gamma'=\gamma_f$, the KS formula doesn't tell us whether the BPS index $\Omega(\gamma_f)$ undergoes a jump, or not. As a hint to the potential interest of these states, it's worth recalling that the main characters of this work, namely "vanilla" $4d$ BPS states themselves, appeared precisely as *pure flavor* states from the viewpoint of $2d$ BPS spectra on surface operators in coupled $2d$-$4d$ systems.

A third direction awaiting to be explored, is the extension of spectral networks beyond $S[A_n,C,D]$ theories with spectral covers in the defining representation. Generalizing the construction of spectral networks both to other simply-laced Lie algebras, and to higher-dimensional representations for the spectral cover, requires to deal with some rather nontrivial new features [62, 97]. On the one hand, the generalization to D,E-type Lie algebras seems to involve novel propagation rules of 2d solitons across joints, possibly leading to critical networks with novel topologies, and to corresponding algebraic/functional equations of a new type. On the other hand, the physical meaning of going beyond the defining representation is an interesting open question, especially from the viewpoint of the brane construction of $2d$-$4d$ coupled

systems and their $2d$-$4d$ BPS states. This subject is being actively investigated at the time of this writing [97].

Appendix A

Protected spin characters of the 3-Kronecker quiver

In this subsection we discuss some data for the "refined BPS degeneracies," or, more properly, the "protected spin character." First, we recall some definitions. Then we present the data.

A.1 Spin decompositions

Short irreducible representations of the $\mathcal{N}=2$ superalgebra take the general form [104, 129]

$$\rho_{hh} \otimes \mathfrak{h} \tag{A.1}$$

where $\rho_{hh} = (1/2, 0) \oplus (0, 1/2)$ is the *half-hypermultiplet* representation of $\mathfrak{so}(3) \oplus \mathfrak{su}(2)_R$, and $\mathfrak{h}$ is the *Clifford vacuum*. It has been shown recently in [35] that the Clifford vacuum is actually a singlet of $\mathfrak{su}(2)_R$, this fact had been previously known as the *no-exotics conjecture*.

In order to extract information about the spin decomposition of the BPS index, we study a refinement known as the *protected spin character* (see e.g. [61, 106])

$$\begin{aligned} \Omega(\gamma, u; y) &= \mathrm{Tr}_{\mathfrak{h}_\gamma} y^{2J_3} (-y)^{I_3} \\ &= \sum_m a_m(\gamma, u) \, (-y)^m, \end{aligned} \tag{A.2}$$

where J_3, I_3 are Cartan elements of $\mathfrak{so}(3)$, $\mathfrak{su}(2)_R$ respectively, and the last line defines the coefficients a_m. The PSC reduces to the BPS index in the limit $y \to -1$.

For a given charge γ, $\mathfrak{h}_\gamma$ has an isotypical decomposition into $\mathfrak{so}(3)$ reps:

$$\mathfrak{h}_\gamma = \bigoplus_j \Big(D_j \otimes (j, 0) \Big) \tag{A.3}$$

where the degeneracy space D_j is a complex vector space of dimension $\delta_\gamma(j)$. Therefore

$$\Omega(\gamma) = \sum_j (-1)^{2j} \delta_\gamma(j)(2j+1). \tag{A.4}$$

The numerical evidence given below suggests that the degeneracies $\delta_\gamma(j)$ for the 3-Kronecker quiver satisfy the following property: for fixed γ, $\delta_\gamma(j) \neq 0$ only for $2j$ of a definite parity.[1] For such spin degeneracies note that

$$(-1)^{2j}\Omega(\gamma) = \dim \mathcal{H}_\gamma. \tag{A.5}$$

Of course, knowing $\Omega(\gamma)$ does not determine the isotypical decomposition. In order to determine that we need to employ a generalization of the KSWCF known in the physics literature as the "motivic" KSWCF [42, 61, 87, 88, 90]. We introduce a set of non-commutative formal variables obeying

$$\hat{Y}_\gamma \hat{Y}_{\gamma'} = y^{\langle \gamma, \gamma' \rangle} \hat{Y}_{\gamma+\gamma'}, \qquad \forall \gamma, \gamma' \in \Gamma\,. \tag{A.6}$$

The generalization of (3.30) is then (for details, see [61])

$$\hat{\mathcal{K}}_\gamma^{\Omega(\gamma;y)} : \hat{Y}_{\gamma_0} \mapsto \hat{Y}_{\gamma_0} \prod_{m\in\mathbb{Z}} \left(\Phi_{\langle \gamma_0, \gamma \rangle}((-y)^m \hat{Y}_\gamma) \right)^{a_m \, (\mathrm{sign}\langle \gamma_0, \gamma \rangle)} \tag{A.7}$$

where the a_m are defined according to (A.2), and

$$\Phi_n(\xi) := \prod_{s=1}^{|n|} (1 + y^{-\,\mathrm{sign}(n)(2s-1)}\xi). \tag{A.8}$$

Let us now apply this formalism to the case at hand, namely the 3-Kronecker quiver. The motivic version of the wall crossing identity is

$$\hat{\mathcal{K}}_{\gamma_2} \hat{\mathcal{K}}_{\gamma_1} =: \prod_{\substack{a\gamma_1 + b\gamma_2 \\ a,b\geq 0}} \hat{\mathcal{K}}_\gamma^{\Omega(a\gamma_1+b\gamma_2;y)} : \tag{A.9}$$

The RHS admits a *unique* decomposition with the required charge orderings and hence this equation fully determines the $\Omega(a\gamma_1 + b\gamma_2; y)$.

In practical terms the protected spin characters can be extracted from this formula as follows. First, acting with the operator on the LHS of (A.9) on the formal variable $\hat{Y}_{\gamma_1}$, yields [2]

$$\hat{Y}_{\gamma_1} + \left(y^{-2} + 1 + y^2\right) \hat{Y}_{\gamma_1+\gamma_2} + \left(y^{-2} + 1 + y^2\right) \hat{Y}_{\gamma_1+2\gamma_2} + \hat{Y}_{\gamma_1+3\gamma_2}. \tag{A.10}$$

with a similar formula for the action on $\hat{Y}_{\gamma_2}$. Then, we apply an inductive procedure directly analogous to that used in (3.55) for the ordinary BPS indices.

We report the resulting PSCs in A.2, for charges up to $a + b \leq 15$.

[1] Indeed the data suggests that $2j$ must be odd for $\gamma = a\gamma_1 + b\gamma_2$ with a, b both even and $2j$ must be even otherwise.

[2] As a side note, this implies that a line defect with charge γ_1 would support halo configurations of vanilla hypermultiplets, with overall halo charges $\gamma_h = k\gamma_2$, $k = 0, 1, 2, 3$. The $\mathfrak{so}(3)$ representations of the respective framed BPS states would have spin $j = 0, 1, 1, 0$ (see [61, 106]). These can also be thought of as the Hall-halo configurations of [39].

A.2 The data

The following tables report the content of BPS boundstates corresponding to the 3-Kronecker quiver, only a quarter of the spectrum is given[3] , the rest is determined by symmetry. For convenience, boundstates are ordered according to the phase of the central charge. Here j labels the $\mathfrak{so}(3)$ irrep of the Clifford vacuum, while δ counts the number of occurrences of such irreps.

γ	j	δ
γ_1	0	1
$3\gamma_1+\gamma_2$	0	1
$8\gamma_1+3\gamma_2$	0	1
$10\gamma_1+4\gamma_2$	5/2	1
$5\gamma_1+2\gamma_2$	1	1
$7\gamma_1+3\gamma_2$	3	1
	5	1
$9\gamma_1+4\gamma_2$	0	2
	1	2
	2	3
	3	2
	4	2
	6	1
$2\gamma_1+\gamma_2$	1	1
$4\gamma_1+2\gamma_2$	5/2	1
$6\gamma_1+3\gamma_2$	3	1
	5	1
$8\gamma_1+4\gamma_2$	5/2	1
	9/2	2
	11/2	1
	13/2	2
	17/2	1
$10\gamma_1+5\gamma_2$	1	1
	3	2
	4	2
	5	4
	6	4
	7	5
	8	4
	9	4
	10	2
	11	2
	13	1

γ	j	δ
$9\gamma_1+5\gamma_2$	0	7
	1	25
	2	30
	3	38
	4	32
	5	31
	6	23
	7	21
	8	12
	9	11
	10	6
	11	5
	12	2
	13	2
	15	1
$7\gamma_1+4\gamma_2$	0	5
	1	5
	2	11
	3	7
	4	9
	5	4
	6	5
	7	2
	8	2
	10	1
$5\gamma_1+3\gamma_2$	0	2
	1	2
	2	3
	3	2
	4	2
	6	1

γ	j	δ
$8\gamma_1+5\gamma_2$	0	17
	1	32
	2	55
	3	55
	4	61
	5	48
	6	44
	7	30
	8	25
	9	15
	10	12
	11	6
	12	5
	13	2
	14	2
	16	1
$3\gamma_1+2\gamma_2$	1	2
	3	1
$6\gamma_1+4\gamma_2$	1/2	4
	3/2	7
	5/2	11
	7/2	7
	9/2	10
	11/2	5
	13/2	5
	15/2	2
	17/2	2
	21/2	1

[3] I.e. one half of the *particle* spectrum, namely dimension vectors with non-negative entries.

γ	j	δ
$9\gamma_1+6\gamma_2$	0	31
	1	125
	2	173
	3	241
	4	251
	5	279
	6	255
	7	244
	8	201
	9	177
	10	129
	11	109
	12	74
	13	58
	14	37
	15	29
	16	15
	17	13
	18	16
	19	5
	20	2
	21	2
	23	1
$7\gamma_1+5\gamma_2$	0	17
	1	32
	2	55
	3	55
	4	61
	5	48
	6	44
	7	30
	8	25
	9	15
	10	12
	11	6
	12	5
	13	2
	14	2
	16	1

γ	j	δ
$4\gamma_1+3\gamma_2$	0	2
	1	2
	2	3
	3	2
	4	2
	6	1
$8\gamma_1+6\gamma_2$	1/2	94
	3/2	171
	5/2	242
	7/2	263
	9/2	291
	11/2	263
	13/2	252
	15/2	203
	17/2	179
	19/2	128
	21/2	109
	23/2	71
	25/2	58
	27/2	35
	29/2	29
	31/2	15
	33/2	13
	35/2	6
	37/2	5
	39/2	2
	41/2	2
	45/2	1
$5\gamma_1+4\gamma_2$	0	5
	1	5
	2	11
	3	7
	4	9
	5	4
	6	5
	7	2
	8	2
	10	1

γ	j	δ
$6\gamma_1+5\gamma_2$	0	7
	1	25
	2	30
	3	38
	4	32
	5	31
	6	23
	7	21
	8	12
	9	11
	10	6
	11	5
	12	2
	13	2
	15	1
$7\gamma_1+6\gamma_2$	0	23
	1	95
	2	119
	3	160
	4	150
	5	157
	6	131
	7	124
	8	91
	9	83
	10	57
	11	49
	12	31
	13	26
	14	14
	15	13
	16	6
	17	5
	18	2
	19	2
	21	1

γ	j	δ
$8\gamma_1 + 7\gamma_2$	0	135
	1	353
	2	562
	3	677
	4	765
	5	762
	6	752
	7	679
	8	619
	9	522
	10	455
	11	363
	12	304
	13	231
	14	188
	15	135
	16	109
	17	73
	18	57
	19	36
	20	28
	21	16
	22	13
	23	6
	24	5
	25	2
	26	2
	28	1

γ	j	δ
$\gamma_1 + \gamma_2$	1	1
$2\gamma_1 + 2\gamma_2$	5/2	1
$3\gamma_1 + 3\gamma_2$	3	1
	5	1
$4\gamma_1 + 4\gamma_2$	5/2	1
	9/2	2
	11/2	1
	13/2	2
	17/2	1
$5\gamma_1 + 5\gamma_2$	1	1
	3	2
	4	2
	5	4
	6	4
	7	5
	8	4
	9	4
	10	2
	11	2
	13	1
$6\gamma_1 + 6\gamma_2$	1/2	1
	3/2	2
	5/2	5
	7/2	5
	9/2	11
	11/2	9
	13/2	18
	15/2	15
	17/2	20
	19/2	15
	21/2	18
	23/2	9
	25/2	11
	27/2	5
	29/2	5
	31/2	2
	33/2	2
	37/2	1

γ	j	δ
$7\gamma_1 + 7\gamma_2$	0	1
	1	10
	2	12
	3	23
	4	28
	5	41
	6	48
	7	63
	8	68
	9	79
	10	77
	11	79
	12	68
	13	63
	14	48
	15	41
	16	29
	17	23
	18	14
	19	12
	20	6
	21	5
	22	2
	23	2
	25	1

Appendix B

The Six-Way Junction

For reference, we present some basic conditions on soliton generating functions as enforced by the homotopy invariance of the framed 2D-4D generating functions $F(\wp, \vartheta)$. First, using the convention described in Section 3.1.2.1, we assign every two-way street an orientation. If the network in question is degenerate, we resolve all two-way streets into "constituent one-way streets" using the *British resolution*: let p be a two-way street; using the orientation on p, we resolve p into two one-way

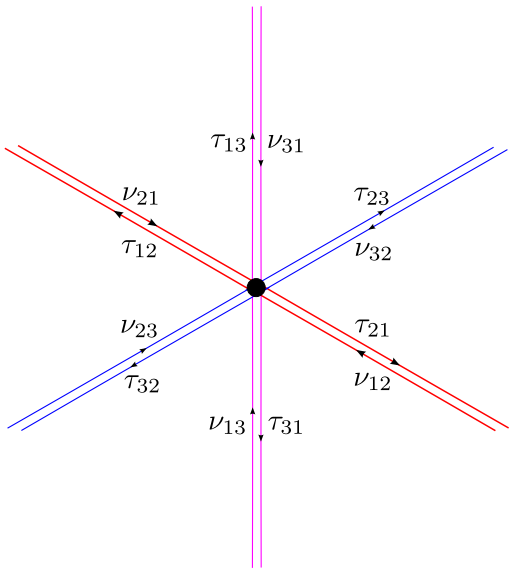

Figure B.1: A six-way junction. Two-way streets are resolved into one-way constituent streets using the British resolution. Streets of type 12 are red, type 23 are blue, and type 13 are fuchsia. A soliton generating function attached to a (one-way constituent) street is shown adjacent to its respective street. Subscripts on the soliton generating functions are ordered pairs $ij \in \{1, 2, 3\}^2$ denoting the type of solitons that the generating function "counts".

streets running in opposite directions, infinitesimally displaced from one another, and such that the street pointing along the orientation of p is to the *left* of the street running against the orientation. If p is a two-way street of type ij (i.e. composed of coincident streets of type ij and type ji), then (after resolving) the street on the left is of type ij and the street on the right is of type ji.

Just as with Kirchoff's circuit laws it is most convenient to express our equations locally around each joint (or branch point). Hence, rather than expressing them in terms of the street-dependent Υ/Δ notation introduced in (3.13)-(3.14), we will temporarily adopt a joint-dependent notation.

Definition Let $v \in C$ be a joint or branch point, then τ_{ij} will denote the soliton generating function attached to a constituent one-way street of type ij running *out* of v, and ν_{ij} will denote the soliton generating function attached to a constituent one-way street of type ij running *into* v.

In a full spectral network, the joint dependent τ, ν notation can become redundant; so we will eventually revert back to the Υ/Δ notation in Appendix C.

To define products of soliton generating functions properly we introduce the following.

Definition Let η be a formal variable that acts on each formal variable X_a in the homology path algebra via

$$\eta X_a = X_{a^{\rm tw}},$$

where, at the level of 1-chains, $a^{\rm tw}$ is the 1-chain produced by inserting a half-twist along the circle fiber of $\widetilde{\Sigma} \to \Sigma$ at some point[1] along a.

Remark It is immediate that $\forall G \in \mathcal{A}$

$$\eta^2 G = X_H G = -G.$$

We now consider a general type of joint, that can occur for a spectral network subordinate to a branched cover with $K \geq 3$ sheets, where six (possibly two-way) streets meet. The situation is shown in Fig. B.1: the (relevant) sheets of the cover are labeled from 1 to 3, and the soliton generating functions attached to a constituent one-way street (under the British resolution of all possible two-way streets) are shown adjacent to their corresponding sheet. Using homotopy invariance of $F(\wp, \vartheta)$,

[1] Up to homotopy (rel endpoints) the insertion point does not matter; hence, it is irrelevant for relative homology.

one arrives at the six-way junction equations:[2]

$$\begin{aligned} \tau_{12} &= \nu_{12} + \eta\tau_{13}\nu_{32}, \quad & \tau_{21} &= \nu_{21} + \eta^{-1}\nu_{23}\tau_{31}, \\ \tau_{23} &= \nu_{23} + \eta\tau_{21}\nu_{13}, \quad & \tau_{32} &= \nu_{32} + \eta^{-1}\nu_{31}\tau_{12}, \\ \tau_{31} &= \nu_{31} + \eta\tau_{32}\nu_{21}, \quad & \tau_{13} &= \nu_{13} + \eta^{-1}\nu_{12}\tau_{23}. \end{aligned} \tag{B.1}$$

At a branch point of type ij, we will assume that there is at most one two-way street, of type ij, emanating from the branch point; on this two-way street we will take

$$\tau_{ij} = X_{a_{ij}}$$

where a_{ij} is the charge of a simpleton.[3] As described at the end of Section 3.1.2, fixing a point z near the branch point, such a simpleton is represented by a path which runs from the lift of z on sheet i to the lift of z on sheet j. In [63] one can find a more general rule accommodating the situation of three two-way streets emanating from the branch point; however, we will not need this generalized rule for m-herds.

[2] In [63] these equations were erroneously written without the factors η, η^{-1}.

[3] The coefficient of $\mu(a_{ij}) = 1$ in front of $X_{a_{ij}}$ is a result of the soliton input data (3.12).

Appendix C

m-Herds in Detail

C.1 Notational Definitions

We will consider four distinct branch points of a branched cover $\Sigma \to C$ of degree $K \geq 3$. On any local region on C', where the cover may be trivialized, only three sheets will be relevant and we will label the relevant sheets from 1 to 3. Label the branch points from 1 to 4 such that branch points 1 and 3 are branch points of type 12, while branch points 2 and 4 are branch points of type 23. For each branch point $i \in \{1, \cdots, 4\}$ we will choose a simpleton (cf. the end of Section 3.1.2) s_i with endpoints on distinct lifts of some $z_i \in C'$ close to the ith branch point. s_1 and s_2 will be simpletons of type 12 and 23, respectively, while s_3 and s_4 will be of type 21 and 32, respectively. We denote the charges of these simpletons by

$$\begin{aligned} a_* &= [s_1] \in \Gamma_{12}(z_1, z_1) \\ b_* &= [s_2] \in \Gamma_{23}(z_2, z_2) \\ \overline{a}_* &= [s_3] \in \Gamma_{21}(z_3, z_3) \\ \overline{b}_* &= [s_4] \in \Gamma_{32}(z_4, z_4). \end{aligned} \tag{C.1}$$

More often, however, computations are performed in the "$\mathbb{Z}/2\mathbb{Z}$-extended" sets $\widetilde{\Gamma}(\widetilde{z}, -\widetilde{z})$, $\widetilde{z} \in \widetilde{C'}$ where we define

$$\begin{aligned} a &= [\widehat{s_1}] \in \widetilde{\Gamma}_{12}(\widetilde{z}_1, -\widetilde{z}_1) \\ b &= [\widehat{s_2}] \in \widetilde{\Gamma}_{23}(\widetilde{z}_2, -\widetilde{z}_2) \\ \overline{a} &= [\widehat{s_3}] \in \widetilde{\Gamma}_{21}(\widetilde{z}_3, -\widetilde{z}_3) \\ \overline{b} &= [\widehat{s_4}] \in \widetilde{\Gamma}_{32}(\widetilde{z}_4, -\widetilde{z}_4). \end{aligned} \tag{C.2}$$

where $\widehat{(\cdot)}$ denotes the *tangent framing lift* (first discussed in Section 3.1.2.3) and the $\widetilde{z}_i \in \widetilde{C}$ are the unit tangent vectors at the starting points of the tangent framing lifts.

In a slight abuse of notation, horse streets[1] (which may be two-way), will be denoted by decorated latin letters: a_i, $\overline{a}_i$ are streets of type 12, b_i, $\overline{b}_i$ are of type 23, and c is of type 13. The subscripts, denoted by $i \in \{1, 2, 3\}$, denote which street is in question and the use of overlines are just a notational exploit of the duality operation described below in C.2.

Furthermore, in contrast with the "joint-dependent" τ, ν notation of Appendix B, we will (more naturally) denote soliton generating functions[2] "streetwise." The point $z \in p \subset C$ in the definition of soliton generating functions will be dropped for notational convenience. As mentioned in a remark at the end of Section 3.1.2.2: for any $z, z' \in p$ the generating functions $\Upsilon_z(p)$ and $\Upsilon_{z'}(p)$ are related by parallel transport (similarly for $\Delta_z(p)$ and $\Delta_{z'}(p)$).

For the sake of readability, we will modify our notation slightly from Section 3.1.2.2 and write streets as subscripts.

Definition Let p be a street, the generating function of solitons on p which *agree* with the orientation of p is denoted Υ_p, the generating function of solitons which *disagree* with the orientation of p is denoted Δ_p. In all figures in this paper streets are oriented in an upward direction (upsilon is for "up" and delta is for "down").

We now wish to associate the street factor (a generating function) Q_p to each street p. To do so, it is convenient to pass through the definition of a closely related auxiliary function.

Definition

For each street p, we define the function

$$\mathcal{Q}_p := 1 + \Upsilon_p \Delta_p \in \mathcal{A}_C \tag{C.3}$$

To produce a formal series in the X_γ, $\gamma \in \Gamma$, we use the "basepoint-forgetting" closure map.

Definition

$$Q_p := \mathrm{cl}\,[\mathcal{Q}_p] \in \mathbb{Z}[\![\widetilde{\Gamma}]\!].$$

We now make some important technical remarks about the use of $\mathcal{Q}_p$ vs. Q_p.

[1] See the definition in Section 4.4.

[2] We refer to Section 3.1.2.2 for the detailed definitions of generating functions and formal variables.

Remarks If p is a street of type ij, then $\mathcal{Q}_p$ is a formal series in formal variables over Γ_{ii}. In particular, let $a \in \Gamma_{kl}$, then this means

$$\mathcal{Q}_p X_a = \begin{cases} 0 & \text{if } k \neq i \\ Q_p X_a = X_a Q_p & \text{if } k = i \end{cases},$$

$$X_a \mathcal{Q}_p = \begin{cases} 0 & \text{if } l \neq i \\ X_a Q_p = Q_p X_a & \text{if } l = i \end{cases}.$$

Hence, if the (left or right) action of $\mathcal{Q}_p$ on a soliton function of type kl is nonvanishing, then it can be replaced with the (commutative) action of Q_p. In the following derivations, the action of $\mathcal{Q}_p$ happens to be always nonvanishing; hence, it will almost always be replaced by Q_p, except in cases where we resist such replacements for the sake of precision and pedagogy.

Terminology Occassionally we will use the term *spectral data* to refer to the collection of soliton generating functions, street factors, and the functions $\mathcal{Q}_p$ supported on a particular collection of streets.

C.2 Duality

As an oriented graph embedded in a disk, Fig. 4.15 is invariant under an involution given by rotating the diagram 180 degrees, and reversing all orientations; we denote this involution on streets p via an overline

$$p \mapsto \overline{p}, \tag{C.4}$$

for $p \in \{a_i, \overline{a_i}, b_i, \overline{b_i}, c : i = 1, 2, 3\}$. As the terminology suggests, this involution satisfies $\overline{\overline{p}} = p$ for every street p and $\overline{c} = c$. We claim that this geometric involution actually induces a duality operation on all spectral data, i.e. generating functions. In particular, on any equations involving soliton generating functions, the replacements

$$\begin{aligned} \Upsilon_p &\leftrightarrow \Delta_{\overline{p}} \\ \eta &\leftrightarrow \eta^{-1}, \end{aligned} \tag{C.5}$$

with all products taken in reverse order, will also yield a valid equation. This claim can be verified by brute-force checking. Note, in particular, applying the duality operation to the definition of $\mathcal{Q}_p$ in (C.3) will yield $\mathcal{Q}_{\overline{p}}$.

C.3 The Horse as a Machine

Recall the definition of a horse is given as a condition on the subset of two-way streets of a spectral network in an open disk region (see Section 4.4). For convenience we restate the definition.

Definitions

1. A *horse street* $p \in \{a_1, a_2, a_3, b_1, b_2, b_3, c, \overline{a_1}, \overline{a_2}, \overline{a_3}, \overline{b_1}, \overline{b_2}, \overline{b_3}\}$ is one of the streets of Fig. 4.15 (left frame).

2. Let N be a spectral network (subordinate to some branched cover $\Sigma \to C$) and $U \subset C'$ be an open disk region. Then $U \cap N$ is a horse if a subset of its streets can be identified with Fig. 4.15 in a way such that

   a) Every two-way street is a horse street.

   b) There is always a two-way street identified with the street labeled c.

It may happen, however, that on a horse there are "background" non-horse streets that cannot be identified with those of Fig. 4.15; by definition, these are one-way streets. The following claim ensures that the computation of soliton generating functions on the streets of a horse are independent of the details of the non-horse streets.

Claim The equations for soliton generating functions on horse streets, induced by (B.1), close on themselves. I.e., the equations for the soliton generating functions on a given horse street can be written entirely in terms of the soliton generating functions on horse streets.

Proof. Let us temporarily denote the four joints in Fig. 4.15 (left frame) as *horse joints*. We split non-horse streets into two classes:

(A) Streets that have no endpoints on a horse joint.

(B) Streets that have a single endpoint on a horse joint.

Let us first consider streets of class (A). The claim is trivial for (A)-streets that do not intersect a horse street. Thus, we turn our attention to a joint where an (A)-street meets a horse street. The most general picture of such a joint[3] is depicted in Fig. C.1. In this figure: i, j, k label any permutation of the sheets $1, 2, 3$, the streets of type jk and ki label background one-way streets,

[3]By the "most general picture" we mean a six-way junction equipped with the weakest possible constraints on incoming soliton degeneracy functions, compatible with the condition that only the streets of type ij (for some fixed pair ij) are two-way. Using (B.1), one finds that the most general picture is Fig. C.1.

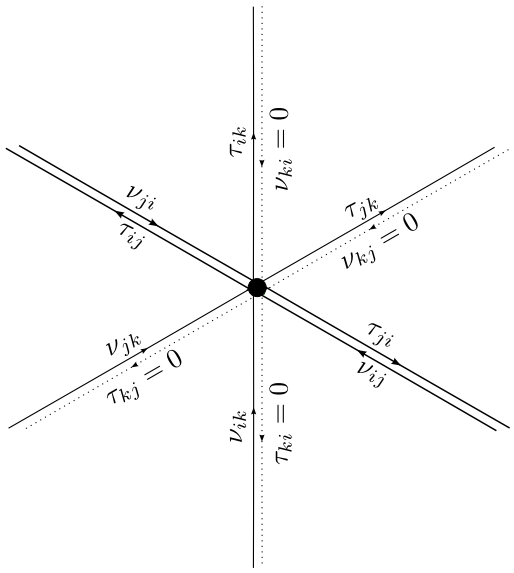

Figure C.1: The most general type of joint where non-horse streets of class (A) meets a horse street (which may be two-way). As in Fig. B.1, streets are resolved into one-way constituents using the British resolution. Soliton generating functions vanish on the dotted streets. The labels i, j, k are a permutation of the sheets $1, 2, 3$.

and the streets of type ij compose the the horse street (after being split into two streets by the joint). The soliton generating functions on the horse street are (in the "joint-wise" notation of Section B) τ_{ji}, ν_{ij}, τ_{ij}, and ν_{ji}. The claim (for (A)-streets) is then equivalent to the statement that $\tau_{ij} = \nu_{ij}$, $\tau_{ji} = \nu_{ji}$; we will show this is the case. Indeed, by the six-way joint equations (B.1):

$$\tau_{ij} = \nu_{ij} + \begin{cases} \eta\tau_{ik}\nu_{kj}, & \text{if } ij \in \{12,\, 23,\, 31\} \\ \eta^{-1}\nu_{ik}\tau_{kj}, & \text{if } ij \in \{21,\, 32,\, 13\} \end{cases}$$

$$\tau_{ji} = \nu_{ji} + \begin{cases} \eta^{-1}\nu_{jk}\tau_{ki}, & \text{if } ij \in \{12,\, 23,\, 31\} \\ \eta\tau_{jk}\nu_{ki}, & \text{if } ij \in \{21,\, 32,\, 13\} \end{cases}$$

but $\nu_{kj} = 0$, $\tau_{kj} = 0$, $\nu_{ki} = 0$, and $\tau_{ki} = 0$. Hence,

$$\tau_{ij} = \nu_{ij}$$

$$\tau_{ji} = \nu_{ji}.$$

Now, via inspection of Fig. 4.15, streets of class (B) are of type 13. If a (B)-street meets a horse street at a non-horse joint, then we apply the same argument used for (A)-streets to see that the (equations for) soliton generating functions on horse streets do not depend on the (B)-street soliton generating function. Thus, we focus our attention on the horse joint.

If a (B)-street meets a horse joint, then (B.1) requires the equations for soliton generating functions, on the horse streets meeting the joint, to depend on the soliton generating function of the (B)-street. We will show that the soliton generating function on the (B) street can be rewritten in terms of generating functions on the horse streets. First, note that if a (B)-street meets the horse joint where a_1 and b_1 meet, or the joint where $\overline{a}_1$ and $\overline{b}_1$ meet, then it must be outgoing with respect to the horse joint. Indeed, the constraint that c is two-way requires the presence of outgoing streets of type 13 at the horse joints meeting c; if the (B)-street were incoming, it would combine with one of these outgoing streets to form a two-way street, violating the horse condition. Without loss of generality, assume the (B) street meets the horse joint where a_1 and b_1 meet; denote the soliton generating function on the (B)-street by $\Upsilon_{(B)}$. Then, using (B.1), it follows that $\Upsilon_{(B)} = \eta^{-1}\Upsilon_{a_1}\Upsilon_{b_1}$; so its soliton generating function is a function of the soliton generating functions on horse streets.

If a (B)-street meets one of the other two horse joints (where b_3 and $\overline{a}_3$ meet or where a_3 and $\overline{b}_3$ meet), then there are two situations: the horse streets at the horse joint are both two-way, or only one of the horse streets at the horse joint is two-way. The former situation is equivalent to the situation where the (B)-street meets the horse joint where a_1 and b_1 meet. To resolve the latter situation we repeat the same argument used for (A)-streets. □

We divide the soliton generating functions supported on horse streets into elements of three subspaces: incoming data, outgoing data, and internal data.

Incoming data

Incoming data is defined as the spectral data which flows into the internal joints of the horse and is supported on the external streets. Here, the space of such data is composed of four soliton generating functions and their duals:

$$\text{Incoming-Data} = \left\{ \begin{pmatrix} \Upsilon_{a_1}, & \Upsilon_{b_1}, & \Delta_{a_3}, & \Delta_{b_3}, \\ \Delta_{\overline{a_1}}, & \Delta_{\overline{b_1}}, & \Upsilon_{\overline{a_3}}, & \Upsilon_{\overline{b_3}} \end{pmatrix} \in \mathcal{A}_S^{\times 8} \right\}. \tag{C.6}$$

It will prove useful to subdivide this space of data further into generating functions of solitons that agree with the orientation of the diagram, Incoming-Data$^+$, and those that disagree, Incoming-Data$^-$:

$$\text{Incoming-Data}^+ = \left\{ \left(\Upsilon_{a_1}, \Upsilon_{b_1}, \Upsilon_{\overline{a_3}}, \Upsilon_{\overline{b_3}} \right) \in \mathcal{A}_S^{\times 4} \right\},$$

$$\text{Incoming-Data}^- = \left\{ \left(\Delta_{\overline{a_1}}, \Delta_{\overline{b_1}}, \Delta_{a_3}, \Delta_{b_3} \right) \in \mathcal{A}_S^{\times 4} \right\}.$$

Outgoing data

Similarly, outgoing data is defined as the spectral data which flows out of the internal joints and is supported on external streets. This consists of the space of soliton generating functions,

$$\text{Outgoing-Data} = \left\{ \begin{pmatrix} \Delta_{a_1}, & \Delta_{b_1}, & \Upsilon_{a_3}, & \Upsilon_{b_3}, \\ \Upsilon_{\overline{a_1}}, & \Upsilon_{\overline{b_1}}, & \Delta_{\overline{a_3}}, & \Delta_{\overline{b_3}} \end{pmatrix} \in \mathcal{A}_S^{\times 8} \right\}. \tag{C.7}$$

As with the incoming data, we can similarly subdivide this data into generating functions of solitons that agree or disagree with the overall orientation:

$$\begin{aligned} \text{Outgoing-Data}^+ &= \left\{ \left(\Upsilon_{\overline{a_1}}, \Upsilon_{\overline{b_1}}, \Upsilon_{a_3}, \Upsilon_{b_3} \right) \in \mathcal{A}_S^{\times 4} \right\}, \\ \text{Outgoing-Data}^- &= \left\{ \left(\Delta_{a_1}, \Delta_{b_1}, \Delta_{\overline{a_3}}, \Delta_{\overline{b_3}} \right) \in \mathcal{A}_S^{\times 4} \right\}. \end{aligned} \tag{C.8}$$

Internal/Bound data

The internal data of the diagram is composed of the ten soliton generating functions defined on the internal streets a_2, b_2, $\overline{a_2}$, $\overline{b_2}$:

$$\text{Internal-Data} = \left\{ \begin{pmatrix} \Upsilon_{a_2}, & \Upsilon_{b_2}, & \Upsilon_{\overline{a_2}}, & \Upsilon_{\overline{b_2}}, & \Upsilon_c, \\ \Delta_{\overline{a_2}}, & \Delta_{\overline{b_2}}, & \Delta_{a_2}, & \Delta_{b_2}, & \Delta_c. \end{pmatrix} \in \mathcal{A}_S^{\times 10} \right\} \tag{C.9}$$

However, as far as the results of this paper are concerned, all that is relevant are the street factors Q_p, for p an internal street, which are derived from the soliton generating functions above:

$$\text{Internal-Data} \rightsquigarrow \left\{ \begin{pmatrix} Q_{a_2}, & Q_{b_2}, & Q_{\overline{a_2}}, & Q_{\overline{b_2}}, & Q_c \end{pmatrix} \in \mathbb{Z}[\![\widetilde{\Gamma}]\!]^{\times 5} \right\}. \tag{C.10}$$

We then view a horse as a scattering-matrix machine that eats incoming solitons and spits out outgoing solitons + "bound"/internal solitons:

$$\text{Horse} : \text{Incoming-Data} \to \text{Outgoing-Data} \times \text{Internal-Data},$$

or in other words, we can determine Outgoing-Data and Internal-Data as a function of Incoming-Data; to do so we utilize the six-way junction equations (B.1) to give[4]

$$\begin{aligned}
\Upsilon_{a_2} &= \Upsilon_{a_1} + \eta \Upsilon_c \Delta_{b_2} \\
\Upsilon_{a_3} &= \Upsilon_{a_2} + \eta \left(\eta^{-1} \Upsilon_{a_2} \Upsilon_{\overline{b_2}} \right) \Delta_{\overline{b_2}} \\
&= \Upsilon_{a_2} \mathcal{Q}_{\overline{b_2}} \\
\Upsilon_{b_2} &= \Upsilon_{b_1} \\
\Upsilon_{b_3} &= \Upsilon_{b_2} \\
\Upsilon_c &= \eta^{-1} \Upsilon_{a_1} \Upsilon_{b_1} \\
\Delta_{a_1} &= \Delta_{a_2} + \eta^{-1} \Upsilon_{b_1} \left(\Delta_c + \eta \Delta_{b_1} \Delta_{a_2} \right) \\
&= \mathcal{Q}_{b_1} \Delta_{a_2} + \eta^{-1} \Upsilon_{b_1} \Delta_c \\
\Delta_{a_2} &= \Delta_{a_3} + \eta^{-1} \Upsilon_{\overline{b_3}} \left(\eta \Delta_{\overline{b_3}} \Delta_{a_3} \right) \\
&= \mathcal{Q}_{\overline{b_3}} \Delta_{\overline{a_3}} \\
\Delta_{b_1} &= \Delta_{b_2} + \eta^{-1} \Delta_c \Upsilon_{a_2} \\
\Delta_{b_2} &= \Delta_{b_3} .
\end{aligned} \tag{C.11}$$

By applying the duality operation of Section C.2 to each equation above, we produce the rest of the six-way junction equations.

We wish to solve for the outgoing and internal (blue) quantities in terms of the incoming (red) quantities.

[4]When using the six-way junction equations on the four relevant joints of a horse, pictured in the left panel of Fig. 4.15, one must take into account one-way streets of type 13 that flow out of these joints. However, as shown in the proof of the claim of Section C.3, the soliton generating functions on these one-way streets can be written in terms of soliton generating functions on the horse streets.

C.3.1 Outgoing Soliton Generating Functions

Starting from a_1 and moving counter-clockwise around the edge of Fig. 4.15, we have

$$\begin{aligned}
\Delta_{a_1} &= \left(1+\Upsilon_{b_1}\Delta_{\overline{b_1}}\Delta_{\overline{a_1}}\Upsilon_{a_1}\right)\left(1+\Upsilon_{b_1}\Delta_{b_3}\right)\left(1+\Upsilon_{\overline{b_3}}\Delta_{\overline{b_1}}\right)\Delta_{a_3}+\Upsilon_{b_1}\Delta_{\overline{b_1}}\Delta_{\overline{a_1}}\\
\Delta_{b_1} &= \Delta_{b_3}+\Delta_{\overline{b_1}}\Delta_{\overline{a_1}}\Upsilon_{a_1}\left(1+\Upsilon_{b_1}\Delta_{b_3}\right)\\
\Delta_{\overline{b_3}} &= \Delta_{\overline{b_1}}\\
\Upsilon_{a_3} &= \Upsilon_{a_1}\left(1+\Upsilon_{b_1}\Delta_{b_3}\right)\left(1+\Upsilon_{\overline{b_3}}\Delta_{\overline{b_1}}\right)\\
\Upsilon_{\overline{a_1}} &= \Upsilon_{\overline{a_3}}\left(1+\Delta_{\overline{a_1}}\Upsilon_{a_1}\Upsilon_{b_1}\Delta_{\overline{b_1}}\right)\left(1+\Upsilon_{\overline{b_3}}\Delta_{\overline{b_1}}\right)\left(1+\Upsilon_{b_1}\Delta_{b_3}\right)+\Upsilon_{a_1}\Upsilon_{b_1}\Delta_{\overline{b_1}}\\
\Upsilon_{\overline{b_1}} &= \Upsilon_{\overline{b_3}}+\left(1+\Upsilon_{\overline{b_3}}\Delta_{\overline{b_1}}\right)\Delta_{\overline{a_1}}\Upsilon_{a_1}\Upsilon_{b_1}\\
\Upsilon_{b_3} &= \Upsilon_{b_1}\\
\Delta_{\overline{a_3}} &= \left(1+\Upsilon_{\overline{b_3}}\Delta_{\overline{b_1}}\right)\left(1+\Upsilon_{b_1}\Delta_{b_3}\right)\Delta_{\overline{a_1}}.
\end{aligned}$$

C.3.2 Outgoing Street Factors

We remark that all outgoing street factors can be expressed in terms of the internal street factors. Hence, starting from a_1 and moving counter-clockwise around the edge of the diagram, we have

$$\begin{aligned}
Q_{a_1} &= Q_c Q_{a_2}\\
Q_{b_1} &= Q_c Q_{b_2}\\
Q_{\overline{b_3}} &= Q_{\overline{b_2}}\\
Q_{a_3} &= Q_{a_2}\\
Q_{\overline{a_1}} &= Q_c Q_{\overline{a_2}}\\
Q_{\overline{b_1}} &= Q_c Q_{\overline{b_2}}\\
Q_{b_3} &= Q_{b_2}\\
Q_{\overline{a_3}} &= Q_{\overline{a_2}}.
\end{aligned}$$

C.3.3 Internal Street Factors

We now state the internal street factors in terms of the incoming soliton generating functions. These equations follow from (C.11) and are:

$$\mathcal{Q}_c = 1 + \Upsilon_{a_1}\Upsilon_{b_1}\Delta_{\overline{b_1}}\Delta_{\overline{a_1}}$$
$$\mathcal{Q}_{a_2} = 1 + \Upsilon_{a_1}Q_{b_2}Q_{\overline{b_2}}\Delta_{a_3}$$
$$\mathcal{Q}_{\overline{b_2}} = 1 + \Upsilon_{\overline{b_3}}\Delta_{\overline{b_1}}$$
$$\mathcal{Q}_{\overline{a_2}} = 1 + \Upsilon_{\overline{a_3}}Q_{b_2}Q_{\overline{b_2}}\Delta_{\overline{a_1}}$$
$$\mathcal{Q}_{b_2} = 1 + \Upsilon_{b_1}\Delta_{b_3}.$$

By applying the closure map cl one produces the corresponding Q_p functions.

Remark We note that in all the equations of sections C.3.1 - C.3.2 there is an almost magical cancellation of the half-twists η; this cancellation will ultimately ensure that the coefficients of the degeneracy generating functions Q_p (as polynomials in some formal variable $X_{\widehat{\gamma_c}}$, yet to be identified) are all positive.

Special Cases

We now cite two important special cases of incoming data for a horse.

Definitions

1. A lower-sourced horse is a horse along with exactly "two-sources from below," i.e. it is a horse restricted to the subset of Incoming-Data where a point in Incoming-Data$^+$ is specified:

$$\text{Incoming-Data}^+_{\text{LSH}} = \left\{ \begin{pmatrix} \Upsilon_{a_1} = X_a \\ \Upsilon_{b_1} = X_b \\ \Upsilon_{\overline{a_3}} = 0 \\ \Upsilon_{\overline{b_3}} = 0. \end{pmatrix} \right\} \subset \text{Incoming-Data}^+. \tag{C.12}$$

2. An upper-sourced horse is dual to a lower-sourced horse, i.e. it is a horse restricted to the subset of Incoming-Data where a point in Incoming-Data$^-$ is specified:

$$\text{Incoming-Data}^-_{\text{USH}} = \left\{ \begin{pmatrix} \Delta_{\overline{a_1}} = X_{\overline{a}} \\ \Delta_{\overline{b_1}} = X_{\overline{b}} \\ \Delta_{a_3} = 0 \\ \Delta_{b_3} = 0. \end{pmatrix} \right\} \subset \text{Incoming-Data}^-. \tag{C.13}$$

Remark Inserting the lower-sourced horse conditions into the equations of Section C.3.3, the most important of the resulting equations are

$$Q_{\overline{a_2}} = Q_{\overline{b_2}} = 1; \tag{C.14}$$

which, furthermore, via (C.3.2) require

$$Q_{\overline{a_3}} = Q_{\overline{b_3}} = 1. \tag{C.15}$$

The upper-sourced horse conditions yield the dual equations,

$$Q_{a_2} = Q_{a_3} = Q_{b_2} = Q_{b_3} = 1. \tag{C.16}$$

With this technology, we can define an m-herd on an arbitrary oriented real surface C as a collection of m-horses glued together using the relations (3.18), beginning with a lower-sourced horse coming from a pair of branch points, and ending with an upper-sourced horse near another pair of branch points (which, for the purposes of this paper, we will take to be disjoint from the lower-sourced branch points).

Definition Let N be a spectral network subordinate to some branched cover $\Sigma \to C$ and let $H \subset N$ be the set of two-way streets of N. Then N is an m-herd if the following conditions are satisfied.

***Horses*:** There exists a collection of open embedded disks $\{U_l\}_{l=1}^m \subset C'$ forming a covering of H, with $U_l \cap U_k \neq \emptyset$ iff $l = k \pm 1$, and each $N \cap U_l$ is:

- a lower-sourced horse if $l = 1$,
- a horse if $1 < l < m$,
- an upper-sourced horse if $l = m$.

***Gluing*:** Each horse satisfies particular gluing conditions: let $p^{(l)}$ denote a horse street[5] on $N \cap U_l$. Then, for $l = 2, \cdots, m-1$, we have the conditions

$$\begin{aligned} a_1^{(l)} &= a_3^{(l-1)} \\ b_1^{(l)} &= b_3^{(l-1)} \\ \overline{a_1}^{(l)} &= \overline{a_3}^{(l+1)} \\ \overline{b_1}^{(l)} &= \overline{b_3}^{(l+1)}. \end{aligned} \tag{3.18}$$

***No Holes*:** For $l = 1, \cdots, m-1$, the oriented loops traced out by the words

[5] Using our previous naming convention: $p \in \{a_1, a_2, a_3, b_1, b_2, b_3, c, \overline{a_1}, \overline{a_2}, \overline{a_3}, \overline{b_1}, \overline{b_2}, \overline{b_3}\}$.

- $\left(\overline{a}_2^{(l)}\right)\left(\overline{b}_1^{(l)}\right)\left(a_2^{(l+1)}\right)^{-1}\left(b_3^{(l)}\right)^{-1}$,
- $\left(\overline{b}_2^{(l)}\right)\left(\overline{a}_1^{(l)}\right)\left(b_2^{(l+1)}\right)^{-1}\left(a_3^{(l)}\right)^{-1}$

are each the oriented boundary of (separate) disks on C' (see Fig. C.2).

Remarks

- Note that a 1-herd is the spectral network for a saddle: indeed, via the above definition it consists of a single horse which is both lower and upper-sourced. The picture of a saddle is formed by viewing only the two-way streets remaining after "removing" the horse streets constrained to be one-way according to (C.14) - (C.16).

- Let Incoming-Data$^{\pm}(l)$ (Outgoing-Data$^{\pm}(l)$) be the domain of incoming (range of outgoing) data associated to the lth horse of an m-herd. Via the definition, Incoming-Data$^{+}(1)$ and Incoming-Data$^{+}(m)$ are specified by the lower sourced horse conditions (C.12) and upper-sourced horse conditions (C.13) respectively:

$$\begin{aligned}\text{Incoming-Data}^{+}(1) &= \left\{\begin{pmatrix}\Upsilon^{(1)}_{a_1} = X_a\\ \Upsilon^{(1)}_{b_1} = X_b\\ \Upsilon^{(1)}_{\overline{a_3}} = 0\\ \Upsilon^{(1)}_{\overline{b_3}} = 0.\end{pmatrix}\right\},\\ \text{Incoming-Data}^{-}(m) &= \left\{\begin{pmatrix}\Delta^{(m)}_{\overline{a_1}} = X_{\overline{a}}\\ \Delta^{(m)}_{\overline{b_1}} = X_{\overline{b}}\\ \Delta^{(m)}_{a_3} = 0\\ \Delta^{(m)}_{b_3} = 0.\end{pmatrix}\right\}.\end{aligned} \tag{C.17}$$

  Further, for $l = 2, \cdots, m-1$, the gluing conditions (3.18) force[6]

$$\begin{aligned}\text{Incoming-Data}^{+}(l) &= \text{Outgoing-Data}^{+}(l-1),\\ \text{Incoming-Data}^{-}(l) &= \text{Outgoing-Data}^{-}(l+1).\end{aligned} \tag{C.18}$$

  In fact, as we will discover, all spectral data on an m-herd can be determined recursively from (C.18) using the initial conditions (C.17).

- The technical *No Holes* condition excludes cases where there are "holes" between adjacent streets when gluing together horses. This condition is essential for our proof of Prop. 3.2.2, as

[6] We have omitted the parallel transport map (on the RHS of (C.18)), detailed in Section C.4, that transports spectral data on the $(l-1)$th horse to the lth horse.

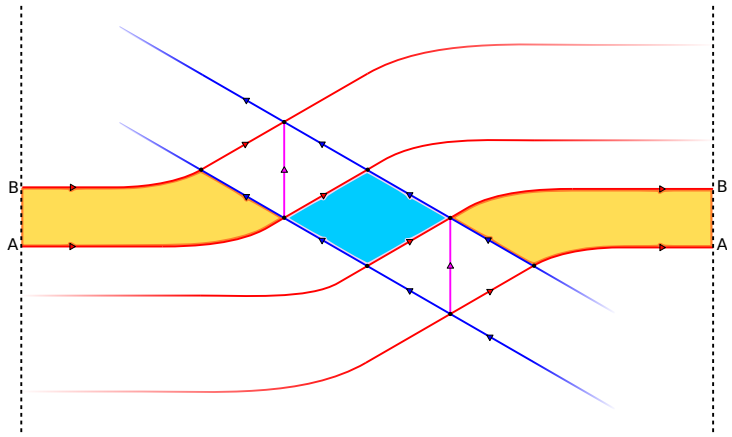

Figure C.2: A picture of two horses (cf. Fig. 4.15) glued together using the *Gluing* conditions and satisfying the *No Holes* condition; the dotted lines are identified, and we assign the "horse-indices" l and $l+1$ to the bottom and top horses respectively. The aqua-blue region is a disk with boundary traced out by the word $\left(\overline{a}_2^{(l)}\right)\left(\overline{b}_1^{(l)}\right)\left(a_2^{(l+1)}\right)^{-1}\left(b_3^{(l)}\right)^{-1}$; the yellow region is a disk with boundary traced out by the word $\left(\overline{b}_2^{(l)}\right)\left(\overline{a}_1^{(l)}\right)\left(b_2^{(l+1)}\right)^{-1}\left(a_3^{(l)}\right)^{-1}$. Two examples for which the *No Holes* condition fails can be pictured by either inserting a puncture, or connect summing with a torus (inserting a "handle"), inside of the colored regions.

such holes create obstructions to auxiliary streets introduced in the proof. Furthermore, the *No Holes* condition is utilized in Prop. 3.2.1 in order to produce an explicit expression for the charge $\widehat{\gamma}_c$ (defined in (C.45)) that appears in the formal variable z, but the condition is not necessary to derive the algebraic equation (4.111).[7]

C.4 A Global Interlude

The following is a technical subsection dedicated to a proper definition of the symbols $\rho_*^{(k,l)}$ that appear throughout the proof of Prop. 3.2.1. Readers who wish to avoid this technical detour may skip this section and interpret the symbols $\rho_*^{(l,l\pm1)}$ as parallel transport maps along an appropriate path, from the lth horse to the $(l\pm1)$th horse, along the graph of the m-herd living on C'; further, the $R^{(k,l)}$ can be replaced by parallel transport maps from the lth horse to the kth horse.

First, we will define the local system of soliton charges over $\widetilde{C'}$.

Definition Let $\mathfrak{s}:\bigcup_{\widetilde{z}\in\widetilde{C'}}\widetilde{\Gamma}(\widetilde{z},-\widetilde{z})\to\widetilde{C'}$ be the projection map with fibers $\mathfrak{s}^{-1}(\widetilde{z})=\widetilde{\Gamma}(\widetilde{z},-\widetilde{z})$.

[7] In particular, the *No Holes* condition is used in the definition of the parallel transport maps $\rho_*^{(l,l\pm1)}$ of Section C.4. One could use a more general notation for parallel transport in a situation without the *No Holes* condition and the proof of the algebraic equation would follow similarly, although, the final expression for z would be modified.

Remark $\mathfrak{s}$ defines a local system of $\widetilde{\Gamma}$-sets (a locally constant sheaf of $\widetilde{\Gamma}$-sets) over $\widetilde{C'}$, when equipped with a parallel transport map defined by a lifted version of the parallel transport of solitons (3.6). More explicitly, for any path $\ell : [0,1] \to \widetilde{C'}$, the parallel transport map $\widetilde{P}_\ell : \widetilde{\Gamma}(\ell(0), -\ell(0)) \to \widetilde{\Gamma}(\ell(1), -\ell(1))$ is given by

$$\widetilde{P}_\ell s = (s' + [\ell\{j\}] - [\ell\{i\}]) \bmod 2H,\ s \in \widetilde{\Gamma}_{ij}(\ell(0), -\ell(0)). \tag{C.19}$$

where

- s' is a lift of s to a relative homology cycle[8] on $\widetilde{\Sigma}$,
- $\ell\{n\}$ is the lift of ℓ to a path on $\widetilde{\Sigma}$ given by lifting $\ell(0)$ to sheet n,
- $[\ell\{n\}]$ is the relative homology class of $\ell\{n\}$
- $(\cdot) \bmod 2H : G(\ell(1), -\ell(1)) \to \widetilde{\Gamma}(\ell(1), -\ell(1))$ is the quotient map (where the subset of relative homology classes $G(\ell(1), -\ell(1))$ is defined in (3.7)).

By construction, $\widetilde{P}_\ell$ only depends on the homotopy class of ℓ (rel endpoints).

Let $\xi : \widetilde{C'} \to C'$ be the unit tangent bundle projection map (previously denoted $\xi^{C'}$). We now make an important observation.

Observation The monodromy of $\widetilde{P}_\ell$ around any loop that wraps the circle fibers of ξ is trivial. I.e., let $z \in C'$ and choose $\ell : S^1 \to (\xi)^{-1}(z) \subset \widetilde{C'}$ to be a closed loop supported on the circle fiber $\xi^{-1}(z)$, then the monodromy $\widetilde{P}_\ell$ is the identity map.

Proof. The proof is immediate: if ℓ is such a loop, then for any sheet n, we have $\mathrm{cl}([\ell\{n\}]) = H$; the result follows from (C.19). □

Definition Let S be any topological space; $\pi_1(S; z_1, z_2)$ is the set of homotopy (rel endpoints) classes of paths $p : [0,1] \to S$ with $p(0) = z_1$ and $p(1) = z_2$.

Corollary C.4.1. *Let $\ell : [0,1] \to \widetilde{C'}$ be a path. Then $\widetilde{P}_\ell : \widetilde{\Gamma}(\ell(0), -\ell(0)) \to \widetilde{\Gamma}(\ell(1), -\ell(1))$ is completely specified by the homotopy class (rel endpoints) of the projected path $\xi \circ \ell : [0,1] \to C'$.*

In particular, given $q \in \pi_1(C', z_1, z_2)$ along with lifts $\widetilde{z}_1 \in \xi^{-1}(z_1)$, $\widetilde{z}_2 \in \xi^{-1}(z_2)$, we may associate a parallel transport map $\widetilde{P}_\ell : \widetilde{\Gamma}(\widetilde{z}_1, -\widetilde{z}_1) \to \widetilde{\Gamma}(\widetilde{z}_2, -\widetilde{z}_2)$ where $\ell : [0,1] \to \widetilde{C'}$ is a lift of any path representative of the class q such that $\ell(0) = \widetilde{z}_1$, $\ell(1) = \widetilde{z}_2$. By the corollary this association $(q, \widetilde{z}_1, \widetilde{z}_2) \rightsquigarrow \widetilde{P}_\ell$ is well-defined.

[8] Recall from (3.8): $\widetilde{\Gamma}(\widetilde{z}, -\widetilde{z})$ is defined as a quotient of the the subset $G(\widetilde{z}, -\widetilde{z})$ (consisting of relative homology classes on $\widetilde{\Sigma}$).

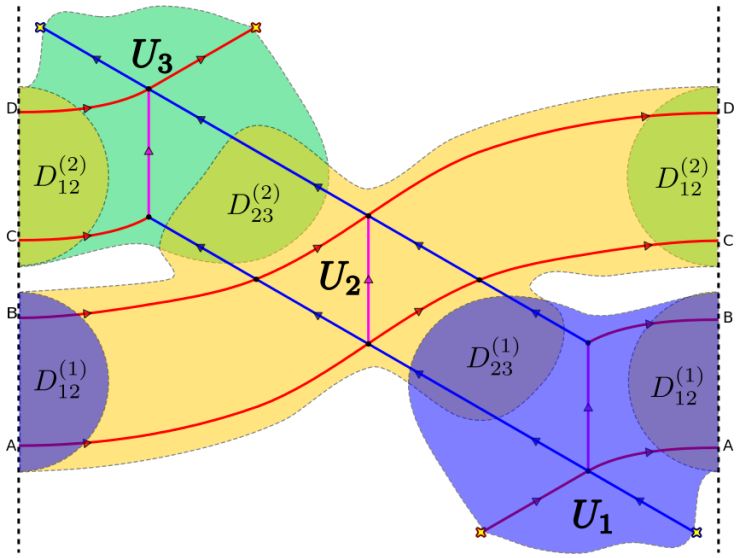

Figure C.3: A 3-herd, on $C = \mathbb{R} \times S^1$, equipped with a (two-way street) cover $\{U_l\}_{l=1}^3$ satisfying the *Horses* condition along with (C.20)-(C.21).

Definition Let $q \in \pi_1(C'; z_1, z_2)$ and $\widetilde{z}_1 \in \xi^{-1}(z_1)$, $\widetilde{z}_2 \in \xi^{-1}(z_2)$, then $\widetilde{P}_{(q,\widetilde{z}_1,\widetilde{z}_2)} : \widetilde{\Gamma}(\widetilde{z}_1, -\widetilde{z}_1) \to \widetilde{\Gamma}(\widetilde{z}_2, -\widetilde{z}_2)$ is the unique parallel transport map assigned to $(q, \widetilde{z}_1, \widetilde{z}_2)$.

To simplify matters of computation, without ignoring global issues, we will develop a notation, suitable to combinatorics, for parallel transport on an m-herd. As each horse is embedded in a contractible region of C, it suffices to keep track of parallel transport of paths *between the horses* of an m-herd: our notation need not keep track of parallel transport between points in an individual horse as suggested by the following remark.

Remark Let $\{U_l\}_{l=1}^m$ be an open cover of disks (on C') satisfying the *Horses* condition for an m-herd, then all paths running between points z_1, $z_2 \in U_l$ and contained within U_l are homotopic (rel endpoints). Thus, by Cor. C.4.1, for each pair of points $\widetilde{z}_1 \in \xi^{-1}(z_1)$, $\widetilde{z}_2 \in \xi^{-1}(z_2)$, there is a unique parallel transport map assigned to all paths running from $\widetilde{z}_1$ to $\widetilde{z}_2$ and contained in $\xi^{-1}(U_l)$.

Now, let us turn our attention to parallel transport of paths running between horses; in particular, paths contained in $U_l \cup U_{l+1}$ for some $l = 1, \cdots, m-1$. First, note that each non-vanishing intersection $U_l \cap U_{l+1}$, $l = 1, \cdots, m-1$, will consist of some number of disconnected disks. However, on an m-herd, the *No Holes* condition allows us to modify our cover such that $U_l \cap U_{l+1}$ contains exactly *two* components:

$$U_l \cap U_{l+1} = D_{12}^{(l)} \sqcup D_{23}^{(l)}, \tag{C.20}$$

where the $D_{ij}^{(l)}$ are disks such that for $l = 1, \cdots, m-1$

$$\begin{gathered}\left(\overline{a}_1^{(l)} = \overline{a}_3^{(l+1)}\right) \cap (U_l \cap U_{l+1}) \subset D_{12}^{(l)}, \left(a_3^{(l)} = a_1^{(l+1)}\right) \cap (U_l \cap U_{l+1}) \subset D_{12}^{(l)} \\ \left(\overline{b}_1^{(l)} = \overline{b}_3^{(l+1)}\right) \cap (U_l \cap U_{l+1}) \subset D_{23}^{(l)}, \left(b_3^{(l)} = b_1^{(l+1)}\right) \cap (U_l \cap U_{l+1}) \subset D_{23}^{(l)};\end{gathered} \tag{C.21}$$

an example of such a cover is shown in Fig. C.3 for the case of a 3-herd on $\mathbb{C} = \mathbb{R} \times S^1$. Thus, fixing a pair of points $\widetilde{z}_1 \in \xi^{-1}(U_l)$, $\widetilde{z}_2 \in \xi^{-1}(U_{l+1})$, our interest lies in two homotopy classes (rel endpoints) of paths that run from $\widetilde{z}_1$ to $\widetilde{z}_2$, and are contained in $U_l \cup U_{l+1}$. In particular, denoting these two classes by $q_{12}, q_{23} \in \pi_1(U_l \cup U_{l+1}; z_1, z_2)$,

1. q_{12} has a path representative given by a simple curve running from $\widetilde{z}_1$ to $\widetilde{z}_2$ and passing through $D_{12}^{(l)}$ (but not $D_{23}^{(l)}$) exactly once,

2. q_{23} has a path representative given by a simple curve running from $\widetilde{z}_1$ to $\widetilde{z}_2$ and passing through $D_{23}^{(l)}$ (but not $D_{12}^{(l)}$) exactly once.

Definition Let $z_1 \in U_l$, $z_2 \in U_{l+1}$, and take q_{ij} ($ij \in \{12, 23\}$) to be the homotopy classes described above. Then, for a choice of lifts $\widetilde{z}_1 \in \xi^{-1}(z_1)$ and $\widetilde{z}_2 \in \xi^{-1}(z_2)$,

$$\begin{aligned}\rho_{ij}^{(l,l+1)}(\widetilde{z}_1, \widetilde{z}_2) &:= \widetilde{P}_{(q_{ij}, \widetilde{z}_1, \widetilde{z}_2)} : \widetilde{\Gamma}(\widetilde{z}_1, -\widetilde{z}_1) \to \widetilde{\Gamma}(\widetilde{z}_2, -\widetilde{z}_2), \\ \rho_{ij}^{(l+1,l)}(\widetilde{z}_1, \widetilde{z}_2) &:= \widetilde{P}_{(q_{ij}^{-1}, \widetilde{z}_2, \widetilde{z}_1)} : \widetilde{\Gamma}(\widetilde{z}_2, -\widetilde{z}_2) \to \widetilde{\Gamma}(\widetilde{z}_1, -\widetilde{z}_1) = \left[\rho_{ij}^{(l,l+1)}(\widetilde{z}_1, \widetilde{z}_2)\right]^{-1}.\end{aligned} \tag{C.22}$$

Notation In the following computations we will just write $\rho_{ij}^{(l,l+1)}$, dropping the explicit dependence on the endpoints $\widetilde{z}_1 \in \xi^{-1}(U_l)$ and $\widetilde{z}_2 \in \xi^{-1}(U_{l+1})$; this notation will be sufficiently unambiguous for our purposes. Indeed, let $\widetilde{w}_1 \in \xi^{-1}(U_l)$, $\widetilde{w}_2 \in \xi^{-1}(U_{l+1})$ be another choice of endpoints with projections $w_i = \xi(\widetilde{w}_i)$, $i = 1, 2$; then, by a remark above, $\exists!$ homotopy classes $q_1 \in \pi_1(U_l; w_1, z_1)$ and $q_2 \in \pi_1(U_{l+1}, z_2, w_2)$ such that

$$\rho_{ij}^{(l,l+1)}(\widetilde{w}_1, \widetilde{w}_2) = \widetilde{P}_{(q_2, \widetilde{z}_2, \widetilde{w}_2)} \left(\rho_{ij}^{(l,l+1)}(\widetilde{z}_1, \widetilde{z}_2)\right) \widetilde{P}_{(q_1, \widetilde{w}_1, \widetilde{z}_1)},\ ij \in \{12, 23\}.$$

Now, on an m-herd, (C.21) indicates that only solitons of type 12 or 21 will be transported via $\rho_{12}^{(l,l+1)}$, and only solitons of type 23 or 32 will be transported via $\rho_{23}^{(l,l+1)}$. With this in mind, for the sake of readability, it will prove convenient to make further notation simplifying definitions.

Definitions

1. Let $\widetilde{z} \in \xi^{-1}(U_l)$, then

$$\rho_*^{(l,l+1)} a := \begin{cases} \rho_{12}^{(l,l+1)} a & \text{if } a \in \widetilde{\Gamma}_{12}(\widetilde{z}, -\widetilde{z}) \cup \widetilde{\Gamma}_{21}(\widetilde{z}, -\widetilde{z}) \\ \rho_{23}^{(l,l+1)} a & \text{if } a \in \widetilde{\Gamma}_{23}(\widetilde{z}, -\widetilde{z}) \cup \widetilde{\Gamma}_{32}(\widetilde{z}, -\widetilde{z}) \end{cases}, \tag{C.23}$$

and $\rho_*^{(l-1,l)} := \left(\rho_*^{(l-1,l)}\right)^{-1}$.

2.
$$R^{(k,n)} := \begin{cases} \rho_*^{(n-1,n)} \cdots \rho_*^{(k+1,k+2)} \rho_*^{(k,k+1)} & \text{if } k < n \\ \rho_*^{(n+1,n)} \cdots \rho_*^{(k-1,k-2)} \rho_*^{(k,k-1)} & \text{if } n < k. \end{cases} \tag{C.24}$$

Remarks

1. The $\rho_*^{(l,k)}$ extend their action to formal variables X_a via
$$\rho_*^{(l,k)} X_a = X_{\rho_*^{(l,k)} a}.$$

2. $R^{(k,n)}$ is a parallel transport map, on the local system $\mathfrak{s}$, from the kth horse to the nth horse associated to a path that passes through each l-horse between k and n exactly once. If $R^{(k,n)}$ acts on a soliton of charge 12 or 21, this path passes through the sets $D_{12}^{(l)}$ (but never $D_{23}^{(l)}$) for $\min\{k,n\} < l < \max\{k,n\}$; if $R^{(k,n)}$ acts on a soliton of charge 23 or 32 the path passes through the sets $D_{23}^{(l)}$ (but never $D_{12}^{(l)}$) for $\min\{k,n\} < l < \max\{k,n\}$.

We make one final observation that will be of use in Section C.7.

Remark Let $\mathfrak{r} : \bigcup_{z\in C} \Gamma(z,z) \to C'$ be the projection map with $\mathfrak{r}^{-1}(z) = \Gamma(z,z)$; this forms a local system over C' when equipped with the parallel transport map

$$P_q s_* = s_* + [q\{j\}] - [q\{i\}],\ s_* \in \Gamma_{ij}(q(0), q(0)). \tag{C.25}$$

The parallel transport on $\mathfrak{r}$ is compatible with the parallel transport (C.19) on the local system $\mathfrak{s}$ in the sense that for any $q \in \pi_1(C', z_1, z_2)$ and $\widetilde{z}_1 \in \xi^{-1}(z_1)$, $\widetilde{z}_2 \in \xi^{-1}(z_2)$, we have

$$\xi_*^\Sigma \left(\widetilde{P}_{(q,\widetilde{z}_1,\widetilde{z}_2)} s \right) = P_q \left(\xi_*^\Sigma s \right), \tag{C.26}$$

where, recall, $\xi^\Sigma : \widetilde{\Sigma} \to \Sigma$ is the unit tangent bundle projection map.

Now, we may define the analog of the parallel transport operators $R^{(k,n)}$ for $\mathfrak{r}$.

Definition Let $s_* \in \bigsqcup_{ij\in\{12,21,23,32\}} \Gamma_{ij}(z,z)$ for some $z \in U_k$, then

$$R_{\mathfrak{r}}^{(k,n)} s_* := \xi_*^\Sigma R^{(k,n)} s, \tag{C.27}$$

where $s \in \bigsqcup_{ij\in\{12,21,23,32\}} \widetilde{\Gamma}_{ij}(\widetilde{z}, -\widetilde{z})$ is any lift of s_* (i.e. $s_* = \xi_*^\Sigma s$).

(C.26) ensures that (C.27) is a well-defined (lift-independent) statement.

C.5 Identifications of Generating Functions

Using the notation developed in Section C.4, we can express (C.18) explicitly as

$$\begin{aligned}
\Upsilon^{(l)}_{a_1} &= \rho_*^{(l-1,l)}\Upsilon^{(l-1)}_{a_3}, \quad & \Delta^{(l)}_{\overline{a_1}} &= \rho_*^{(l+1,l)}\Delta^{(l+1)}_{\overline{a_3}}, \\
\Upsilon^{(l)}_{b_1} &= \rho_*^{(l-1,l)}\Upsilon^{(l-1)}_{b_3}, \quad & \Delta^{(l)}_{\overline{b_1}} &= \rho_*^{(l+1,l)}\Delta^{(l+1)}_{\overline{b_3}}, \\
\Upsilon^{(l)}_{\overline{a_3}} &= \rho_*^{(l-1,l)}\Upsilon^{(l-1)}_{\overline{a_1}}, \quad & \Delta^{(l)}_{a_3} &= \rho_*^{(l+1,l)}\Delta^{(l+1)}_{a_1}, \\
\Upsilon^{(l)}_{\overline{b_3}} &= \rho_*^{(l-1,l)}\Upsilon^{(l-1)}_{\overline{b_1}}, \quad & \Delta^{(l)}_{b_3} &= \rho_*^{(l+1,l)}\Delta^{(l+1)}_{b_1}.
\end{aligned} \tag{C.28}$$

In particular,

$$\begin{aligned}
Q^{(l)}_{a_1} &= Q^{(l-1)}_{a_3}, \quad & Q^{(l)}_{\overline{a_1}} &= Q^{(l+1)}_{\overline{a_3}}, \\
Q^{(l)}_{b_1} &= Q^{(l-1)}_{b_3}, \quad & Q^{(l)}_{\overline{b_1}} &= Q^{(l+1)}_{\overline{b_3}}.
\end{aligned} \tag{C.29}$$

C.6 Proof of Proposition 3.2.1

C.6.1 Proof of Equations (3.20)

Using the recursion relations (C.29), in conjunction with the equations listed in Sections C.3.3 and C.3.2, we first solve for the internal street factors $Q^{(l)}_{a_2}$, $Q^{(l)}_{\overline{a_2}}$, $Q^{(l)}_{b_2}$, $Q^{(l)}_{\overline{b_2}}$ in terms of street factors on the lower/upper-sourced horses at $l = 1$ or $l = m$. As we noticed in Section C.3.2, all other street factors can be written in terms of the internal ones.

Now, via (C.29), and the equations of Section (C.3.2),

$$\begin{aligned}
Q^{(l)}_{a_2} &= Q^{(l)}_{a_3} \\
&= Q^{(l+1)}_{a_1} \\
&= Q^{(l+1)}_{c} Q^{(l+1)}_{a_2}.
\end{aligned} \tag{C.30}$$

Similarly, we find

$$Q^{(l)}_{\overline{a_2}} = Q^{(l-1)}_{c} Q^{(l-1)}_{\overline{a_2}} \tag{C.31}$$

$$Q^{(l)}_{b_2} = Q^{(l+1)}_{c} Q^{(l+1)}_{b_2} \tag{C.32}$$

$$Q^{(l)}_{\overline{b_2}} = Q^{(l-1)}_{c} Q^{(l-1)}_{\overline{b_2}}. \tag{C.33}$$

This leads us to the following.

Lemma C.6.1. *For $l = 1, \dots, m$, we have*

$$Q^{(l)}_{a_2} = Q^{(l)}_{b_2} = \prod_{r=l+1}^{m+1} Q^{(r)}_c \tag{C.34}$$

$$Q^{(l)}_{\overline{a_2}} = Q^{(l)}_{\overline{b_2}} = \prod_{r=0}^{l-1} Q^{(r)}_c. \tag{C.35}$$

with the convention that $Q^{(m+1)}_c = Q^{(0)}_c = 1$.

Proof. From the upper-sourced horse conditions (C.13) we have

$$Q^{(m)}_{a_2} = Q^{(m)}_{b_2} = 1; \tag{C.16}$$

so (C.34) follows via (C.30) and (C.32). Similarly, from the lower-sourced horse conditions (C.12) we have

$$Q^{(1)}_{\overline{a_2}} = Q^{(1)}_{\overline{b_2}} = 1; \tag{C.14}$$

so (C.35) follows via (C.31) and (C.33). □

To reduce (C.34) - (C.35) further, we must compute some soliton generating functions.

Computing $\Upsilon^{(l)}_{b_1}$

Via (C.28)

$$\begin{aligned} \Upsilon^{(l)}_{b_1} &= \rho_*^{(l-1,l)} \Upsilon^{(l-1)}_{b_3} \\ &= \rho_*^{(l-1,l)} \Upsilon^{(l-1)}_{b_1}. \end{aligned} \tag{C.36}$$

Thus, propagating the lower sourced horse conditions (C.12) through this recursion relation,

$$\Upsilon^{(l)}_{b_1} = \left(\prod_{r=1}^{l} \rho_*^{(r-1,r)} \right) X_b \tag{C.37}$$

$$= R^{(1,l)} X_b. \tag{C.38}$$

Computing $\Delta^{(l)}_{\overline{b_1}}$

The idea is dual to above; indeed

$$\begin{aligned} \Delta^{(l)}_{\overline{b_1}} &= \rho_*^{(l+1,l)} \Delta^{(l+1)}_{\overline{b_3}} \\ &= \rho_*^{(l+1,l)} \Delta^{(l+1)}_{\overline{b_1}}. \end{aligned} \tag{C.39}$$

Using the upper-sourced horse conditions (C.13),

$$\begin{aligned}\Delta_{\overline{b_1}}^{(l)} &= \left(\prod_{r=l}^{m} \rho_*^{(r+1,r)}\right) X_{\overline{b}} \\ &= R^{(m,l)} X_{\overline{b}}. \end{aligned} \tag{C.40}$$

Computing $\Upsilon_{a_1}^{(l)}$

Via (C.28) and the equation for Υ_{a_3} in Section C.3.1,

$$\begin{aligned}\Upsilon_{a_1}^{(l)} &= \rho_*^{(l-1,l)} \Upsilon_{a_3}^{(l-1)} \\ &= \rho_*^{(l-1,l)} \Upsilon_{a_1}^{(l-1)} \left(1 + \Upsilon_{\overline{b_3}}^{(l-1)} \Delta_{\overline{b_1}}^{(l-1)}\right) \left(1 + \Upsilon_{b_1}^{(l-1)} \Delta_{b_3}^{(l-1)}\right) \\ &= \rho_*^{(l-1,l)} \Upsilon_{a_1}^{(l-1)} Q_{\overline{b_2}}^{(l-1)} Q_{b_2}^{(l-1)}. \end{aligned} \tag{C.41}$$

Using the lower-sourced horse conditions (C.12),

$$\begin{aligned}\Upsilon_{a_1}^{(l)} &= \left(\prod_{r=1}^{l} \rho_*^{(r-1,r)} X_a\right) \left(\prod_{r=1}^{l} \rho_*^{(r-1,r)} Q_{\overline{b_2}}^{(r-1)} Q_{b_2}^{(r-1)}\right) \\ &= R^{(1,l)} X_a \left(\prod_{r=0}^{l-1} Q_{\overline{b_2}}^{(r)} Q_{b_2}^{(r)}\right). \end{aligned} \tag{C.42}$$

Computing $\Delta_{\overline{a_1}}^{(l)}$

Again, the computation is dual to that for $\Upsilon_{a_1}^{(l)}$,

$$\begin{aligned}\Delta_{\overline{a_1}}^{(l)} &= \rho_*^{(l+1,l)} \Delta_{\overline{a_3}}^{(l+1)} \\ &= \rho_*^{(l+1,l)} \left[\left(1 + \Upsilon_{\overline{b_3}}^{(l+1)} \Delta_{\overline{b_1}}^{(l+1)}\right) \left(1 + \Upsilon_{b_1}^{(l+1)} \Delta_{b_3}^{(l+1)}\right) \Delta_{\overline{a_1}}^{(l+1)}\right] \\ &= \rho_*^{(l+1,l)} Q_{\overline{b_2}}^{(l+1)} Q_{b_2}^{(l+1)} \Delta_{\overline{a_1}}^{(l+1)}. \end{aligned} \tag{C.43}$$

So, using the upper-sourced horse conditions (C.13),

$$\begin{aligned}\Delta_{\overline{a_1}}^{(l)} &= \left(\prod_{r=l}^{m} \rho_*^{(r+1,l)} Q_{\overline{b_2}}^{(r+1)} Q_{b_2}^{(r+1)}\right) X_a \\ &= \left(\prod_{r=l+1}^{m+1} Q_{\overline{b_2}}^{(r)} Q_{b_2}^{(r)}\right) R^{(m,l)} X_a. \end{aligned} \tag{C.44}$$

These computations lead us to the following key lemma that allows all street factors Q_p to be reduced to powers of a single function.

Lemma C.6.2.

$$Q_c^{(l)} = Q_c^{(1)}, \forall l = 1, \cdots, m.$$

Proof. Recall (C.36), (C.39), (C.41), and (C.43)

$$\begin{aligned}
\Upsilon_{b_1}^{(l)} &= \rho_*^{(l-1,l)} \Upsilon_{b_1}^{(l-1)} \\
\Delta_{\overline{b_1}}^{(l)} &= \rho_*^{(l+1,l)} \Delta_{\overline{b_1}}^{(l+1)} \\
\Upsilon_{a_1}^{(l)} &= \rho_*^{(l-1,l)} Q_{\overline{b_2}}^{(l-1)} Q_{b_2}^{(l-1)} \Upsilon_{a_1}^{(l-1)} \\
\Delta_{\overline{a_1}}^{(l)} &= \rho_*^{(l+1,l)} Q_{\overline{b_2}}^{(l+1)} Q_{b_2}^{(l+1)} \Delta_{\overline{a_1}}^{(l+1)};
\end{aligned}$$

we can rewrite the equations for $\Delta_{\overline{b_1}}^{(l)}$ and $\Delta_{\overline{a_1}}^{(l)}$ as

$$\begin{aligned}
\Delta_{\overline{b_1}}^{(l)} &= \rho_*^{(l-1,l)} \Delta_{\overline{b_1}}^{(l-1)} \\
\Delta_{\overline{a_1}}^{(l)} &= \rho_*^{(l-1,l)} \frac{\Delta_{\overline{a_1}}^{(l-1)}}{Q_{\overline{b_2}}^{(l)} Q_{b_2}^{(l)}}.
\end{aligned}$$

Using the equation for $\mathcal{Q}_c$ in Section C.3.3

$$\begin{aligned}
\mathcal{Q}_c^{(l)} &= 1 + \Upsilon_{a_1}^{(l)} \Upsilon_{b_1}^{(l)} \Delta_{\overline{b_1}}^{(l)} \Delta_{\overline{a_1}}^{(l)} \\
&= 1 + \left(\rho_*^{(l-1,l)} Q_{\overline{b_2}}^{(l-1)} Q_{b_2}^{(l-1)} \Upsilon_{a_1}^{(l-1)} \right) \left(\rho_*^{(l-1,l)} \Upsilon_{b_1}^{(l-1)} \right) \left(\rho_*^{(l-1,l)} \Delta_{\overline{b_1}}^{(l-1)} \right) \left(\rho_*^{(l-1,l)} \frac{\Delta_{\overline{a_1}}^{(l-1)}}{Q_{\overline{b_2}}^{(l)} Q_{b_2}^{(l)}} \right) \\
&= 1 + \left(\mathcal{Q}_c^{(l-1)} - 1 \right) \left(\frac{Q_{\overline{b_2}}^{(l-1)} Q_{b_2}^{(l-1)}}{Q_{\overline{b_2}}^{(l)} Q_{b_2}^{(l)}} \right);
\end{aligned}$$

where, on the last line, the cancellation of the $\rho_*^{(l-1,l)}$ (parallel transport) actions[9] can be seen by working through its definition in equations (C.19), (C.22), and (C.23). Applying the closure map we obtain

$$Q_c^{(l)} = 1 + \left(Q_c^{(l-1)} - 1 \right) \left(\frac{Q_{\overline{b_2}}^{(l-1)} Q_{b_2}^{(l-1)}}{Q_{\overline{b_2}}^{(l)} Q_{b_2}^{(l)}} \right).$$

Using (C.34) and (C.35), then

$$\begin{aligned}
Q_c^{(l)} &= 1 + \left(Q_c^{(l-1)} - 1 \right) \left(\frac{\prod_{r \neq l-1} Q_c^{(r)}}{\prod_{r \neq l} Q_c^{(r)}} \right) \\
&= 1 + \left(Q_c^{(l-1)} - 1 \right) \frac{Q_c^{(l)}}{Q_c^{(l-1)}} \\
&= 1 + Q_c^{(l)} - \frac{Q_c^{(l)}}{Q_c^{(l-1)}}.
\end{aligned}$$

Hence,

$$Q_c^{(l)} = Q_c^{(l-1)}, \; l = 2, \cdots, m.$$

□

[9] This is consistent with the fact that, according to (C.19), parallel transport acts trivially on charges of type *ii*.

The above proposition motivates the following simplified notation.

Definition

$$P_m := Q_c^{(1)}.$$

Now, when lemmata C.6.1 and C.6.2 are combined, we have

Corollary C.6.3.

$$Q_{a_2}^{(l)} = Q_{b_2}^{(l)} = (P_m)^{m-l}$$
$$Q_{\overline{a_2}}^{(l)} = Q_{\overline{b_2}}^{(l)} = (P_m)^{l-1}.$$

The above corollary, combined with the equations of Section C.3.2, is enough to express the remainder of the street factors in terms of P_m,

$$(P_m)^{m-l} = Q_{a_3}^{(l)} = Q_{b_3}^{(l)}$$
$$(P_m)^{l-1} = Q_{\overline{a_3}}^{(l)} = Q_{\overline{b_3}}^{(l)}$$
$$(P_m)^{m-l+1} = Q_{a_1}^{(l)} = Q_{b_1}^{(l)}$$
$$(P_m)^{l} = Q_{\overline{a_1}}^{(l)} = Q_{\overline{b_1}}^{(l)}.$$

This completes the proof of (3.20) in Prop. 3.1.

C.6.2 Proof of the Algebraic Equation (4.111)

Via the equation for $\mathcal{Q}_c$ in Section C.3.3 along with (C.38)-(C.42),

$$\begin{aligned}
\mathcal{Q}_c^{(l)} &= 1 + \Upsilon_{a_1}^{(l)} \Upsilon_{b_1}^{(l)} \Delta_{\overline{b_1}}^{(l)} \Delta_{\overline{a_1}}^{(l)} \\
&= 1 + \left[\left(\prod_{r=0}^{l-1} Q_{\overline{b_2}}^{(r)} Q_{b_2}^{(r)} \right) R^{(1,l)} X_a \right] \left[R^{(1,l)} X_b \right] \left[R^{(m,l)} X_{\overline{b}} \right] \left[\left(\prod_{r=l+1}^{m+1} Q_{\overline{b_2}}^{(r)} Q_{b_2}^{(r)} \right) R^{(m,l)} X_a \right] \\
&= 1 + \left(\prod_{r \neq l} Q_{\overline{b_2}}^{(r)} Q_{b_2}^{(r)} \right) \left(R^{(1,l)} X_a \right) \left(R^{(1,l)} X_b \right) \left(R^{(m,l)} X_{\overline{b}} \right) \left(R^{(m,l)} X_a \right) \\
&= 1 + (P_m)^{(m-1)^2} \left(R^{(1,l)} X_a \right) \left(R^{(1,l)} X_b \right) \left(R^{(m,l)} X_{\overline{b}} \right) \left(R^{(m,l)} X_{\overline{a}} \right);
\end{aligned}$$

where, on the last line we utilized Corollary C.6.3.

Remark We note that,

$$R^{(1,l)} a + R^{(1,l)} b + R^{(m,l)} \overline{b} + R^{(m,l)} \overline{a}$$

represents a soliton charge of type 11 on the open set $\xi^{-1}(U_l) \subset \widetilde{C'}$. Thus, we may apply the map cl to this expression to produce an element of $\widetilde{\Gamma}$.

This leads us to the following definition.

Definition We define

$$\widehat{\gamma}_c := \mathrm{cl}\left[R^{(1,l)}a + R^{(1,l)}b + R^{(m,l)}\overline{b} + R^{(m,l)}\overline{a}\right] \in \widetilde{\Gamma} \tag{C.45}$$

and corresponding formal variable

$$z := X_{\widehat{\gamma}_c}. \tag{C.46}$$

(We will show below that, in fact, (C.45) does not depend on l; thus, this definition is sensible.)

With the above definitions we have

$$Q_c^{(l)} = 1 + zP_m^{(m-1)^2}$$

hence, by Lemma C.6.2, P_m satisfies the algebraic equation

$$P_m = 1 + zP_m^{(m-1)^2}. \tag{4.111}$$

This completes the proof of the algebraic equation in Prop. 3.2.1.

Remark As we will show in Section C.7, $\widehat{\gamma}_c$ is the sum of two tangent framing lifts of simple closed curves with corresponding homology classes γ, $\gamma' \in \Gamma$. In fact, we will show that (C.46) can be rewritten in the form stated in Prop. 3.2.1: $z = (-1)^m X_{\widetilde{\gamma}+\widetilde{\gamma}'}$, where $\widetilde{(\cdot)} : \Gamma \to \widetilde{\Gamma}$ is defined in Section (3.1.2.3) and discussed further in Section E.

C.7 Proof of the Decomposition of $\widehat{\gamma}_c$

We begin with an example (which may be skipped for the more general proof below).[10]

C.7.1 Example: $\widehat{\gamma}_c$ for m-herds on the cylinder

We consider generalizations (to arbitrary m) of the herds shown in Fig. 3.4 for $m = 1, \cdots, 4$. Assume we are equipped with a branched 3-cover of the cylinder $C = S^1 \times \mathbb{R}$ with four branch points. Now, consider an m-herd such that it is contained in a presentation of the cylinder as an identification space of $[0,1] \times \mathbb{R}$: the streets of type 23 lie entirely in the interior of $(0,1) \times \mathbb{R}$, while the streets of type 12 involved in the identifications (3.18) pass through the identified boundary. First, each of the charges a, $b, \overline{a}$, $\overline{b}$ can be thought of as flat sections of the local system $\mathfrak{s} : \bigcup_{\widetilde{z} \in \widetilde{C'}} \widetilde{\Gamma}(\widetilde{z}, -\widetilde{z}) \to \widetilde{C'}$, locally defined around their respective branch points. The two-way streets are contained within

[10] The following sections rely on the ideas of Section C.4.

the open set $U := \bigcup_{l=1}^{m} U_l$, which is homeomorphic to $S^1 \times I$ for $I \cong (0,1)$ an open interval. Let $U^c \cong (0,1)^2$ be the open set formed by removing the vertical line[11] $(\{0\} \times \mathbb{R}) \cap U \sim (\{1\} \times \mathbb{R}) \cap U$ from U. $\mathfrak{s}$ is trivial over the open set $\xi^{-1}(U^c) \cong (0,1)^2 \times S^1$ in $\widetilde{C'}$; so, we can extend a, $b, \overline{a}$, $\overline{b}$ to flat sections over all of $\xi^{-1}(U^c)$.

Now, let $q_{\text{cyl}} : [0,1] \to U \subset C'$ denote a loop winding once around the S^1 direction of U, and oriented such that the upper-sourced horse branch points sit to its "left," while the lower-sourced horse branch points sit to its "right"; $\widehat{q}_{\text{cyl}} : [0,1] \to \widetilde{C'}$ will denote the tangent framing lift of q_{cyl}.

Working through the definition of the parallel transport maps $R^{(k,l)}$ in (C.19), (C.22)-(C.24), we have

$$\widehat{\gamma}_c = \text{cl}\left(a + b + \overline{b} + \overline{a}\right) + (m-1)\left([\hat{q}_{\text{cyc}}\{2\}] - [\hat{q}_{\text{cyc}}\{1\}]\right);$$

the expression in the closure map is defined by evaluating the sections a, $b, \overline{a}$, $\overline{b}$ at some point $\widetilde{z} \in \xi^{-1}(U^c \cap U_l)$ and taking their sum to define an element in $\widetilde{\Gamma}_{11}(\widetilde{z}, -\widetilde{z})$.

Observe that we can decompose $\widehat{\gamma}_c$ as $\widehat{\gamma}_c = \widehat{\gamma} + \widehat{\gamma}'$ where,

$$\begin{aligned}
\widehat{\gamma} &= \text{cl}\left(b + \overline{b}\right) \\
\widehat{\gamma}' &= \text{cl}\left(a + \overline{a}\right) + (m-1)\left([\hat{q}_{\text{cyc}}\{2\}] - [\hat{q}_{\text{cyc}}\{1\}]\right).
\end{aligned}$$

Now, note that we can realize $\widehat{\gamma}$ the tangent framing lift of a simple closed curve on Σ. Indeed, consider an auxiliary street of type 23, realized as a straight line on $U \cup \{\text{branch pts.}\}$, running between the two branch points of type 23 (beginning at the branch point emitting the charge b and ending at the branch point emitting the charge $\overline{b}$). The lift of this street to Σ is a simple closed curve; the tangent framing lift is a representative of $\text{cl}\left(b + \overline{b}\right)$. Similarly, we can realize $\text{cl}\left(a + \overline{a}\right)$ with the tangent framing lift of a simple closed curve ℓ_a on $U \cup \{\text{branch pts.}\}$ and so $\widehat{\gamma}'$ can be realized as a modification of ℓ_a by smoothly "detouring" along the lifts (to sheets 1 and 2) of a curve that winds $m-1$ times around the S^1 direction of U. The resulting curve is the tangent framing lift of a simple closed curve. Furthermore, project these simple-closed curves to Σ; then letting γ and γ' be the homology classes of our projections, with their representative curves it is clear that $\langle \gamma, \gamma' \rangle = m$.

Now, using different techniques, let us proceed on with the general proof of the decomposition $\widehat{\gamma}_c = \widehat{\gamma} + \widehat{\gamma}'$, described in the example above, for an m-herd on a general oriented curve C.

[11] Here $\sim$ denotes the identification of the boundary of $[0,1] \times \mathbb{R}$ to form the cylinder. The removed vertical line is given by the (identified) dotted lines in Fig. 3.4.

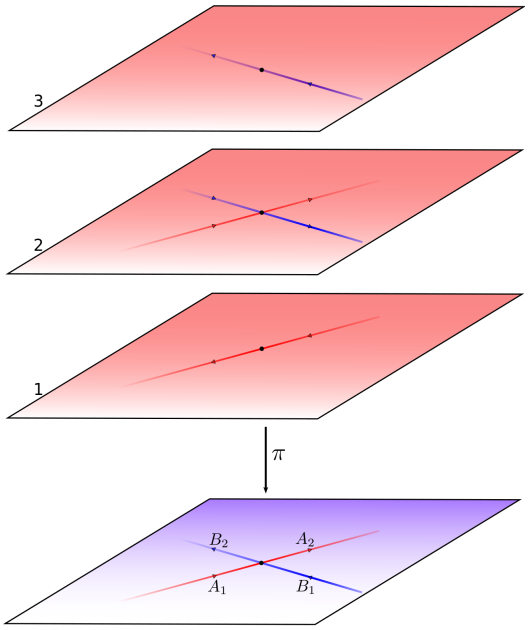

Figure C.4: A pony and its lift to Σ. Red streets are of type 12, blue streets are of type 23.

C.7.2 General Proof

Let $\xi^\Sigma : \widetilde{\Sigma} \to \Sigma$ be the unit tangent bundle projection.

Definition

$$\gamma_c := \xi^\Sigma_* \widehat{\gamma}_c \in \Gamma.$$

To derive an explicit expression for γ_c in terms of simpleton charges (C.1) in $\bigcup_{z\in C} \Gamma(z,z)$, we "pushforward" the expression (C.45) via ξ^Σ. From the definitions (C.1), (C.2), and (C.45) it follows that

$$\gamma_c = \mathrm{cl}\left[R^{(1,l)}_{\mathfrak{r}} a_* + R^{(1,l)}_{\mathfrak{r}} b_* + R^{(m,l)}_{\mathfrak{r}} \overline{b}_* + R^{(m,l)}_{\mathfrak{r}} \overline{a}_*\right] \tag{C.47}$$

where $R^{(k,n)}_{\mathfrak{r}}$ are the "pushforward" of the parallel transport operators $R^{(k,n)}$ defined in (C.27).

We will construct a decomposition $\gamma_c = \gamma + \gamma'$ with $\langle \gamma, \gamma' \rangle = m$ roughly by shrinking the $c^{(l)}$ streets of the herd to points. To be precise, we introduce some definitions.

Definitions

1. A pony is a partial spectral network as shown in Fig. C.4. Upper and lower-sourced ponies are defined similar to upper and lower sourced horses.

2. The string of ponies S_m associated to an m-herd H_m is the spectral network constructed by placing

a) A lower sourced pony on U_1

b) Ponies on U_l, $1 < l < m$

c) An upper-sourced pony on U_m,

where the U_m are a good open cover satisfying the *Horses* condition for H_m, and forcing the identifications

$$A_1^{(l+1)} = A_2^{(l)}$$
$$B_1^{(l+1)} = B_2^{(l)}$$

on each $U_l \cap U_{l+1}$.

Remarks

1. S_m is only defined up to homotopy on each disk U_l.
2. The interpretation of S_m as a spectral network is overkill for our discussion and we introduce it as such mainly for notational convenience: all that will be necessary is the graph of the lift $\text{Lift}(S_m) \subset \Sigma$. However, in the wall-crossing interpretation of m-herds discussed in Section 4.4, the spectral network S_m is expected to appear on the wall of marginal stability where two hypermultiplets of intersection number m have coincident central charge phase. In fact, the procedure of deforming such a picture is what motivated the construction of m-herds.

Definition Let $p^{(l)}$ be a street of type ij, then $\mathbf{m}p^{(l)} \in C_1(\Sigma;\mathbb{Z})$ is the 1-chain on Σ representing the lift[12] of $p^{(l)}$ as a street of type ij (using the orientation discussed in Section 3.1.2).

If we define,

$$\gamma = \left[\sum_{l=1}^{m} \left(\mathbf{m}B_1^{(l)} + \mathbf{m}B_2^{(l)}\right)\right] \in H_1(\Sigma;\mathbb{Z})$$
$$\gamma' = \left[\sum_{l=1}^{m} \left(\mathbf{m}A_1^{(l)} + \mathbf{m}A_2^{(l)}\right)\right] \in H_1(\Sigma;\mathbb{Z}),$$

then, as shown in Fig. C.4, γ and γ' intersect once in each $\pi^{-1}(U_l)$, $l = 1, \cdots m$; hence,

$$\langle \gamma, \gamma' \rangle = m.$$

Now

[12] If $p^{(l)}$ connects two joints, this lift has two components. If $p^{(l)}$ connects a joint to a branch point of type ij, then the two components combine to form a connected 1-chain between sheets i and j.

- $\sum_{l=1}^{m-1}\left(\mathbf{m}A_1^{(l)}+\mathbf{m}A_2^{(l)}\right)$ is a 1-chain representative of the parallel transported charge $R_{\mathfrak{r}}^{(1,m-1)}a_*$.
- $\sum_{l=1}^{m-1}\left(\mathbf{m}B_1^{(l)}+\mathbf{m}B_2^{(l)}\right)$ is a 1-chain representative of $R_{\mathfrak{r}}^{(1,m-1)}b_*$.
- $\mathbf{m}A_1^{(m)}+\mathbf{m}A_2^{(m)}$ is a 1-chain representative of $\overline{a}_*$.
- $\mathbf{m}B_1^{(m)}+\mathbf{m}B_2^{(m)}$ is a 1-chain representative of $\overline{b}_*$.

Hence,

$$\gamma_c=\gamma+\gamma'.$$

Now, each of the 1-chains $\mathbf{m}A_i^{(l)}$, $\mathbf{m}B_i^{(l)}$ have well-defined tangent framing lifts $\widehat{\mathbf{m}A}_i^{(l)}$, $\widehat{\mathbf{m}B}_i^{(l)}$ when thought of as oriented paths on $\mathrm{Lift}(S_m)\subset\Sigma$. Similarly, γ and γ' have obvious representative curves on $\mathrm{Lift}(S_m)$ that allow us to produce tangent framing lifts $\widehat{\gamma}$, $\widehat{\gamma}'$. In fact,

$$\widehat{\gamma}=\left[\sum_{l=1}^{m}\left(\widehat{\mathbf{m}B}_1^{(l)}+\widehat{\mathbf{m}B}_2^{(l)}\right)\right]\in H_1(\widetilde{\Sigma};\mathbb{Z})$$
$$\widehat{\gamma}'=\left[\sum_{l=1}^{m}\left(\widehat{\mathbf{m}A}_1^{(l)}+\widehat{\mathbf{m}A}_2^{(l)}\right)\right]\in H_1(\widetilde{\Sigma};\mathbb{Z}).$$

Via similar arguments to above, along with the definition of $\widehat{\gamma}_c$ in (C.45), we have

$$\widehat{\gamma}_c=\widehat{\gamma}+\widehat{\gamma}'.$$

Alternatively, we can lift $\gamma_c=\gamma+\gamma'$ using the map $\widetilde{(\cdot)}:\Gamma\to\widetilde{\Gamma}$ defined in (E.1) of Appendix E. Indeed, as the curves representing γ and γ' intersect m times, we have

$$\widetilde{\gamma}_c=\widehat{\gamma}+\widehat{\gamma}'+mH=\widehat{\gamma}_c+mH.$$

Thus,

$$z=X_{\widehat{\gamma}_c}=(-1)^mX_{\widetilde{\gamma}_c}.$$

C.8 Proof of Proposition 3.2.2

We wish to compute the homology class of the 1-chain $L(n\gamma_c)$. First we introduce a few notational definitions that differ slightly from the main body of the paper.

Definition $\mathbf{m}p^{(l,r)} \in C_1(\Sigma;\mathbb{Z})$ is the component of $\mathbf{m}p^{(l)} \in C_1(\Sigma;\mathbb{Z})$ on the rth sheet. If $p^{(l)}$ is a street of type ij, then

$$\mathbf{m}p^{(l,r)} = \begin{cases} +\left(\text{1-chain representing the lift of } p^{(l)} \text{ to the } r\text{th sheet}\right), & \text{if } r = j \\ -\left(\text{1-chain representing the lift of } p^{(l)} \text{ to the } r\text{th sheet}\right), & \text{if } r = i \\ 0 & \text{otherwise} \end{cases} .$$

Now,

$$\begin{aligned} L(n\gamma_c) &= \sum_{l=1}^{m} \sum_{p^{(l)}} \alpha_n(p,l)\mathbf{m}p^{(l)} \\ &= \alpha_n \sum_{l=1}^{m} \Big\{ \mathbf{m}c^{(l)} + (m-l)\left(\mathbf{m}a_2{}^{(l)} + \mathbf{m}a_3{}^{(l)} + \mathbf{m}b_2{}^{(l)} + \mathbf{m}b_3{}^{(l)}\right) \\ &+ (l-1)\left(\mathbf{m}\overline{a_2}^{(l)} + \mathbf{m}\overline{a_3}^{(l)} + \mathbf{m}\overline{b_2}^{(l)} + \mathbf{m}\overline{b_3}^{(l)}\right) + \\ &+ (m-l+1)\left(\mathbf{m}a_1{}^{(l)} + \mathbf{m}b_1{}^{(l)}\right) + l\left(\mathbf{m}\overline{a_1}^{(l)} + \mathbf{m}\overline{b_1}^{(l)}\right)\Big\}. \end{aligned} \tag{3.36}$$

after using the results of Prop. 3.2.1 and the definition of α_n given in equation (3.35).

For the sake of readability we introduce some simplifying notation.

Notational Definition We denote,

$$\begin{aligned} \mathbf{m}a_{12} &:= \mathbf{m}a_1^{(l)} + \mathbf{m}a_2^{(l)} \\ \mathbf{m}a_{23} &:= \mathbf{m}a_2^{(l)} + \mathbf{m}a_3^{(l)} \\ \mathbf{m}a_{123} &:= \mathbf{m}a_1^{(l)} + \mathbf{m}a_2^{(l)} + \mathbf{m}a_3^{(l)}; \end{aligned}$$

and similarly, for $\mathbf{m}\overline{a}_i$, $\mathbf{m}b_i$, and $\mathbf{m}\overline{b}_i$.

Using this notation, we can rewrite our sum in slightly more illuminating form,

$$\begin{aligned} L(n\gamma_c) = \alpha_n \sum_{l=1}^{m} \Big\{ &(m-l)\left(\mathbf{m}a_{123}^{(l)} + \mathbf{m}b_{123}^{(l)}\right) + l\left(\mathbf{m}\overline{a}_{123}^{(l)} + \mathbf{m}\overline{b}_{123}^{(l)}\right) \\ &+ \mathbf{m}a_1{}^{(l)} + \mathbf{m}b_1{}^{(l)} + \mathbf{m}c^{(l)} - \mathbf{m}\overline{a_{23}}^{(l)} - \mathbf{m}\overline{b_{23}}^{(l)}\Big\}. \end{aligned}$$

This form suggests we should try to find a homological equivalence taking the terms multiplying the factor l, to the terms multiplying the factor $(m-l)$. We introduce extra 1-chains to aid in our computation. To define them, it is helpful to think of them as lifts of auxiliary streets. However, the interpretation as lifts of streets on C is only a notational tool: these streets are not part of any spectral network.

Definition Let $\{U_l\}_{l=1}^m$ be an open covering satisfying the *Horses* condition for an m-herd. On each horse we define auxiliary streets as in Fig. C.5: $e_1^{(l)}, e_2^{(l)} \subset U_l$ of type 12, and $f_1^{(l)}$, $f_2^{(l)} \subset U_l$, of type 23 ; such that,

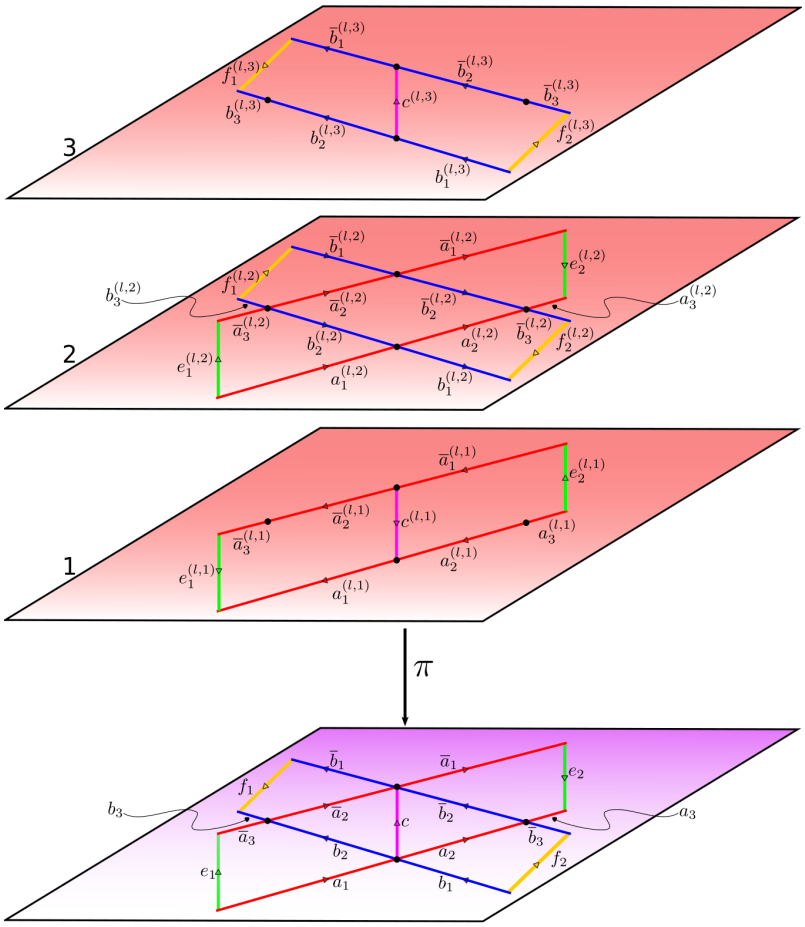

Figure C.5: Lift of a horse with extra 1-chains, pictured here as the lift of some auxiliary streets on C. For the sake of readability, the "horse label" (l) is suppressed on the base C.

$(C1)$:

$$e_1^{(l+1)} = -e_2^{(l)}$$
$$f_2^{(l+1)} = -f_1^{(l)},$$

where "$-$" indicates orientation reversal.

$(C2)$: $e_1^{(1)}$ and $f_2^{(1)}$ end on the branch points of type 12 and 23 (respectively) of the lower-sourced horse, while $e_2^{(m)}$ and $f_1^{(m)}$ end on the branch points of type 12 and 23 (respectively) of the upper-sourced horse.

Remark The *No Holes* condition removes any obstruction to condition $(C1)$.

The 1-chains that will aid in our proof are the lifts of the auxiliary streets.

Remark Keeping with the (previously defined) convention for lifts of streets, there are 1-chains (on Σ) $\mathbf{m}e_1^{(l)}$, $\mathbf{m}e_2^{(l)}$, $\mathbf{m}f_1^{(l)}$, and $\mathbf{m}f_2^{(l)}$ (also depicted in Fig. C.5). It follows that, via (*C1*),

$$\begin{aligned} \mathbf{m}e_1^{(l+1)} &= -\mathbf{m}e_2^{(l)} \\ \mathbf{m}f_2^{(l+1)} &= -\mathbf{m}f_1^{(l)}. \end{aligned} \tag{C.48}$$

for $l = 1, \cdots, m-1$.

Lemma C.8.1. *Let $\sim$ denote homological equivalence. Then for each $l = 1, \cdots, m$: on the first (locally defined) sheet,*

$$0 \sim \mathbf{m}\overline{a}_{23}^{(l,1)} + \mathbf{m}e_1^{(l,1)} - \mathbf{m}a_1^{(l,1)} - \mathbf{m}c^{(l,1)} \tag{C.49}$$

$$0 \sim \mathbf{m}\overline{a}_1^{(l,1)} + \mathbf{m}c^{(l,1)} - \mathbf{m}a_{23}^{(l,1)} + \mathbf{m}e_2^{(l,1)}. \tag{C.50}$$

On the second sheet,

$$0 \sim \mathbf{m}\overline{a}_{123}^{(l,2)} + \mathbf{m}e_2^{(l,2)} - \mathbf{m}a_{123}^{(l,2)} + \mathbf{m}e_1^{(l,2)} \tag{C.51}$$

$$0 \sim \mathbf{m}\overline{b}_{123}^{(l,2)} + \mathbf{m}f_2^{(l,2)} - \mathbf{m}b_{123}^{(l,2)} + \mathbf{m}f_1^{(l,2)} \tag{C.52}$$

$$0 \sim \mathbf{m}\overline{a}_3^{(l,2)} + \mathbf{m}b_2^{(l,2)} - \mathbf{m}a_1^{(l,2)} + \mathbf{m}e_1^{(l,2)} \tag{C.53}$$

$$0 \sim \mathbf{m}a_2^{(l,2)} + \mathbf{m}\overline{b}_3^{(l,2)} + \mathbf{m}f_2^{(l,2)} - \mathbf{m}b_1^{(l,2)} \tag{C.54}$$

$$0 \sim \mathbf{m}b_2^{(l,2)} + \mathbf{m}a_2^{(l,2)} - \mathbf{m}\overline{b}_2^{(l,2)} - \mathbf{m}\overline{a}_2^{(l,2)}. \tag{C.55}$$

On the third sheet,

$$0 \sim \mathbf{m}b_1^{(l,3)} + \mathbf{m}c^{(l,3)} - \mathbf{m}\overline{b}_{23}^{(l,3)} - \mathbf{m}f_2^{(l,3)} \tag{C.56}$$

$$0 \sim \mathbf{m}\overline{b}_1^{(l,3)} + \mathbf{m}f_1^{(l,3)} - \mathbf{m}b_{23}^{(l,3)} + \mathbf{m}c^{(l,3)}. \tag{C.57}$$

Proof. The lemma follows by inspection of Fig. C.5. Each of the listed sum of 1-chains is the boundary of an oriented disk. □

In particular, it follows from the lemma that

$$\begin{aligned} \mathbf{m}\overline{a}_{123}^{(l)} &\sim \mathbf{m}a_{123}^{(l)} - \mathbf{m}e_1^{(l)} - \mathbf{m}e_2^{(l)} \\ \mathbf{m}\overline{b}_{123}^{(l)} &\sim \mathbf{m}b_{123}^{(l)} - \mathbf{m}f_1^{(l)} - \mathbf{m}f_2^{(l)}. \end{aligned}$$

Hence,

$$\begin{aligned} L(n\gamma_c) &\sim \alpha_n \sum_{l=1}^{m} \left\{ (m-l) \left(\mathbf{m}a_{123}^{(l)} + \mathbf{m}b_{123}^{(l)} \right) + l \left(\mathbf{m}a_{123}^{(l)} + \mathbf{m}b_{123}^{(l)} \right) \right\} + \alpha_n R_1 + \alpha_n R_2 \\ &\sim m\alpha_n \sum_{l=1}^{m} \left(\mathbf{m}a_{123}^{(l)} + \mathbf{m}b_{123}^{(l)} \right) + \alpha_n R_1 + \alpha_n R_2 \end{aligned} \tag{C.58}$$

where

$$R_1 = -\sum_{l=1}^{m} l\left\{\mathbf{m}e_1^{(l)} + \mathbf{m}e_2^{(l)} + \mathbf{m}f_1^{(l)} + \mathbf{m}f_2^{(l)}\right\}$$
$$R_2 = \sum_{l=1}^{m}\left\{\mathbf{m}a_1{}^{(l)} + \mathbf{m}b_1{}^{(l)} + \mathbf{m}c^{(l)} - \mathbf{m}\overline{a_{23}}^{(l)} - \mathbf{m}\overline{b_{23}}^{(l)}\right\}.$$

Using (C.48), the first of these sums can be simplified,

$$\begin{aligned}
R_1 &= -\sum_{l=1}^{m} l\left(\mathbf{m}e_1^{(l)} + \mathbf{m}f_2^{(l)}\right) - \sum_{l=1}^{m} l\left(\mathbf{m}e_2^{(l)} + \mathbf{m}f_1^{(l)}\right)\\
&= -\sum_{l=1}^{m} l\left(\mathbf{m}e_1^{(l)} + \mathbf{m}f_2^{(l)}\right) + \sum_{l=1}^{m-1} l\left(\mathbf{m}e_1^{(l+1)} + \mathbf{m}f_2^{(l+1)}\right) - m\left(\mathbf{m}e_2^{(m)} + \mathbf{m}f_1^{(m)}\right)\\
&= -\sum_{l=1}^{m} l\left(\mathbf{m}e_1^{(l)} + \mathbf{m}f_2^{(l)}\right) + \sum_{l=2}^{m}(l-1)\left(\mathbf{m}e_1^{(l)} + \mathbf{m}f_2^{(l)}\right) - m\left(\mathbf{m}e_2^{(m)} + \mathbf{m}f_1^{(m)}\right)\\
&= -\left(\mathbf{m}e_1^{(1)} + \mathbf{m}f_2^{(1)}\right) - m\left(\mathbf{m}e_2^{(m)} + \mathbf{m}f_1^{(m)}\right) - \sum_{l=2}^{m}\left(\mathbf{m}e_1^{(l)} + \mathbf{m}f_2^{(l)}\right)\\
&= -m\left(\mathbf{m}e_2^{(m)} + \mathbf{m}f_1^{(m)}\right) - \sum_{l=1}^{m}\left(\mathbf{m}e_1^{(l)} + \mathbf{m}f_2^{(l)}\right). \qquad \text{(C.59)}
\end{aligned}$$

To reduce R_2, we use the following lemma.

Lemma C.8.2.

$$\mathbf{m}a_1{}^{(l)} + \mathbf{m}b_1{}^{(l)} + \mathbf{m}c^{(l)} - \mathbf{m}\overline{a_{23}}^{(l)} - \mathbf{m}\overline{b_{23}}^{(l)} \sim \mathbf{m}e_1^{(l)} + \mathbf{m}f_2^{(l)}.$$

Proof. On sheet 1,

$$\mathbf{m}a_1^{(l,1)} + \mathbf{m}b_1^{(l,1)} + \mathbf{m}c^{(l,1)} - \mathbf{m}\bar{a}_{23}^{(l,1)} - \mathbf{m}\bar{b}_{23}^{(l,1)} = \mathbf{m}a_1^{(l,1)} + \mathbf{m}c^{(l,1)} - \mathbf{m}\bar{a}_{23}^{(l,1)}.$$

Using (C.49),

$$\begin{aligned}
&\sim \mathbf{m}a_1^{(l,1)} + \mathbf{m}c^{(l,1)} + \left(\mathbf{m}e_1^{(l,1)} - \mathbf{m}a_1^{(l,1)} - \mathbf{m}c^{(l,1)}\right)\\
&\sim \mathbf{m}e_1^{(l,1)}.
\end{aligned}$$

Similarly, on sheet 3, using (C.56) appropriately,

$$\begin{aligned}
\mathbf{m}a_1^{(l,3)} + \mathbf{m}b_1^{(l,3)} + \mathbf{m}c^{(l,3)} - \mathbf{m}\bar{a}_{23}^{(l,3)} - \mathbf{m}\bar{b}_{23}^{(l,1)} &= \mathbf{m}b_1^{(l,3)} + \mathbf{m}c^{(l,3)} - \mathbf{m}\bar{b}_{23}^{(l,3)}\\
&\sim \mathbf{m}b_1^{(l,3)} + \mathbf{m}c^{(l,3)} + \left(\mathbf{m}f_2^{(l,3)} - \mathbf{m}b_1^{(l,3)} - \mathbf{m}c^{(l,3)}\right)\\
&\sim \mathbf{m}f_2^{(l,3)}.
\end{aligned}$$

On sheet 2

$$\mathbf{m}a_1^{(l,2)} + \mathbf{m}b_1^{(l,2)} + \mathbf{m}c^{(l,2)} - \mathbf{m}\bar{a}_{23}^{(l,2)} - \mathbf{m}\bar{b}_{23}^{(l,2)} = \mathbf{m}a_1^{(l,2)} + \mathbf{m}b_1^{(l,2)} - \mathbf{m}\bar{a}_{23}^{(l,2)} - \mathbf{m}\bar{b}_{23}^{(l,2)}.$$

Now, via (C.53) and (C.54)

$$\begin{aligned}\mathbf{m}a_1^{(l,2)} &\sim \mathbf{m}\bar{a}_3^{(l,2)} + \mathbf{m}b_2^{(l,2)} + \mathbf{m}e_1^{(l,2)} \\ \mathbf{m}b_1^{(l,2)} &\sim \mathbf{m}a_2^{(l,2)} + \mathbf{m}\bar{b}_3^{(l,2)} + \mathbf{m}f_2^{(l,2)}.\end{aligned}$$

Hence,

$$\begin{aligned}&\mathbf{m}a_1^{(l,2)} + \mathbf{m}b_1^{(l,2)} + \mathbf{m}c^{(l,2)} - \mathbf{m}\bar{a}_{23}^{(l,2)} - \mathbf{m}\bar{b}_{23}^{(l,2)} \\ &\qquad\sim \left(\mathbf{m}\bar{a}_3^{(l,2)} + \mathbf{m}b_2^{(l,2)} + \mathbf{m}e_1^{(l,2)}\right) \\ &\qquad + \left(\mathbf{m}a_2^{(l,2)} + \mathbf{m}\bar{b}_3^{(l,2)} + \mathbf{m}f_2^{(l,2)}\right) - \mathbf{m}\bar{a}_{23}^{(l,2)} - \mathbf{m}\bar{b}_{23}^{(l,2)} \\ &\qquad\sim \mathbf{m}b_2^{(l,2)} + \mathbf{m}a_2^{(l,2)} - \mathbf{m}\bar{b}_2^{(l,2)} - \mathbf{m}\bar{a}_2^{(l,2)} + \mathbf{m}e_1^{(l,2)} + \mathbf{m}f_2^{(l,2)} \\ &\qquad\sim \mathbf{m}e_1^{(l,2)} + \mathbf{m}f_2^{(l,2)},\end{aligned}$$

where the last reduction is due to (C.55). □

Thus,

$$R_2 \sim \sum_{l=1}^{m} \left(\mathbf{m}e_1^{(l)} + \mathbf{m}f_2^{(l)}\right);$$

so, with (C.59), we have

$$R_1 + R_2 = -m\left(\mathbf{m}e_2^{(m)} + \mathbf{m}f_1^{(m)}\right).$$

Substituting this result into (C.58),

$$L(n\gamma) \sim m\alpha_n \sum_{l=1}^{m-1} \left(\mathbf{m}a_{123}^{(l)} + \mathbf{m}b_{123}^{(l)}\right) + m\alpha_n \left[\left(\mathbf{m}a_{123}^{(m)} + \mathbf{m}b_{123}^{(m)}\right) - \left(\mathbf{m}e_2^{(m)} + \mathbf{m}f_1^{(m)}\right)\right].$$

After inspecting Fig. C.5, by deforming slightly on the mth horse we can convince ourselves this is precisely a 1-chain representing γ_c.

To make this claim precise, let $\mathbf{m}q$ be a 1-chain on Σ such that $\partial\mathbf{m}q \subset \pi^{-1}(z)$ for some $z \in C'$, and define $[\mathbf{m}q]_R$ as the corresponding equivalence class in $\bigcup_{z\in C'} \Gamma(z,z)$. Then, for any $k = 1, \cdots, m$

$$\begin{aligned}R_{\mathfrak{r}}(1,k)a_* &= \left[\sum_{l=1}^{k} \mathbf{m}a_{123}\right]_R \\ R_{\mathfrak{r}}(1,k)b_* &= \left[\sum_{l=1}^{k} \mathbf{m}b_{123}\right]_R.\end{aligned}$$

Furthermore, by parallel transporting the endpoints of $\overline{a}$ and $\overline{b}$ along an appropriate path contained in the mth horse[13]

$$\begin{aligned}\overline{a}_* &= \left[\left(\mathbf{m}a_{123}^{(m)} - \mathbf{m}e_2^{(m)}\right)\right]_R \\ \overline{b}_* &= \left[\left(\mathbf{m}b_{123}^{(m)} - \mathbf{m}f_1^{(m)}\right)\right]_R .\end{aligned}$$

Thus,

$$[L(n\gamma_c)]_R = m\alpha_n \left[R_{\mathfrak{r}}^{(1,k)} a_* + R_{\mathfrak{r}}^{(1,k)} b_* + \overline{a}_* + \overline{b}_*\right]_R .$$

Applying the closure map to both sides, by (C.47) the proposition holds:

$$[L(n\gamma_c)] = m\alpha_n\gamma_c \in H_1(\Sigma;\mathbb{Z}).$$

C.9 Table of m-herd BPS indices $\Omega(n\gamma_c)$, for low values of n and m

Table C.1: Values of $\Omega(n\gamma_c)$ for low n and m

	n						
	1	2	3	4	5	6	7
$m=1$	1	0	0	0	0	0	0
$m=2$	-2	0	0	0	0	0	0
$m=3$	3	-6	18	-84	465	-2808	18123
$m=4$	-4	-16	-144	-1632	-21720	-318816	-5018328
$m=5$	5	-40	600	-12400	300500	-8047440	231045220
$m=6$	-6	-72	-1800	-58800	-2251500	-95312880	-4325917260
$m=7$	7	-126	4410	-208740	11579925	-710338104	46716068007

[13] As per our notation motivated in Section C.4, we do not write this parallel transport map explictly.

Appendix D

Proof of Proposition 3.2.4

Define the sequence

$$b_l := \binom{(m-1)^2 l}{l};$$

we will show

$$\lim_{n\to\infty} \frac{\Omega(n\gamma_c)}{(-1)^{mn+1}\left(\frac{m}{(m-1)^2n^2}\right) b_n} = 1. \tag{D.1}$$

Indeed, from (3.38),

$$\frac{\Omega(n\gamma_c)}{(-1)^{mn+1}\left(\frac{m}{(m-1)^2n^2}\right) b_n} = 1 + \overbrace{\sum_{\substack{d|n \\ d<n}} (-1)^{m(n+d)} \mu\left(\frac{n}{d}\right)\left(\frac{b_d}{b_n}\right)}^{R(n)},$$

but

$$|R(n)| \leq \sum_{\substack{d|n \\ d<n}} \frac{b_d}{b_n}.$$

Now, from the bounds

$$\sqrt{2\pi} n^{n+\frac{1}{2}} e^{-n} < n! \leq n^{n+\frac{1}{2}} e^{1-n}$$

it follows that

$$\frac{b_d}{b_n} < \left(\frac{e}{\sqrt{2\pi}}\right)^3 \left(\frac{n}{d}\right)^{1/2} e^{c_m(d-n)},$$

where c_m is the constant defined in (3.40). Hence,

$$|R(n)| < \left(\frac{e}{\sqrt{2\pi}}\right)^3 \left(n^{1/2} e^{-c_m n}\right) \sum_{\substack{d|n \\ d<n}} d^{-1/2} e^{c_m d}.$$

Now, the next largest divisor of n, other than n itself, is $\leq n/2$. Using this fact, the observation that $d^{-1/2}e^{c_m d}$ is a monotonically increasing function of d, and the crude bound that number of divisors

of n is $\leq n$, we have

$$\sum_{\substack{d|n \\ d<n}} d^{-1/2} e^{c_m d} \leq n \left(\left(\frac{n}{2} \right)^{-1/2} e^{c_m n/2} \right) = \sqrt{2n} e^{c_m n/2};$$

so

$$|R(n)| < \sqrt{2} \left(\frac{e}{\sqrt{2\pi}} \right)^3 n e^{-c_m n/2},$$

which vanishes as $n \to \infty$, verifying (D.1). In other words, the $n \to \infty$ asymptotics of $\Omega(n\gamma_c)$ are given by the asymptotics of the largest term b_n of (3.38) inside the sum over divisors:

$$\Omega(n\gamma_c) \sim (-1)^{mn+1} \left(\frac{m}{(m-1)^2} \right) n^{-2} b_n.$$

Equation (3.39) follows by using Stirling's asymptotics on the binomial coefficient b_n: as $n \to \infty$,

$$b_n \sim \frac{1}{\sqrt{2\pi}} \left(\frac{m-1}{\sqrt{m(m-2)}} \right) n^{-1/2} e^{c_m n}.$$

Appendix E

A sign rule

In this appendix we discuss a subtle point about signs which was not treated correctly in the first version of [63].

The issue concerns the proper way of extracting 4D BPS degeneracy information from the generating functions $Q(p)$ defined in (3.1.2.2). What we want to do is factorize $Q(p)$ as we wrote in (3.15), but to do so, we need a way of choosing the lifts $\tilde{\gamma} \in \tilde{\Gamma}$ of classes $\gamma \in \Gamma$.

We propose the following rule. First, represent γ as a sum of k smooth closed curves β_m on Σ. Each such curve has a canonical lift $\hat{\beta}_m$ to $\tilde{\Sigma}$ just given by the tangent framing. Then we define

$$\tilde{\gamma} = \sum_{m=1}^{k} (\hat{\beta}_m + H) + \sum_{m \leq n} \#(\beta_m \cap \beta_n) H. \tag{E.1}$$

We need to check that $\tilde{\gamma}$ so defined is independent of the choice of how we represent γ as a union of β_m. First we check that $\tilde{\gamma}$ is stable under creation/deletion of a null-homologous loop. If β denotes such a loop then $\hat{\beta} = H$ modulo $2H$ (indeed, suppose β bounds a subsurface S; S admits a vector field extending $\hat{\beta}$, with $\chi(S)$ signed zeroes in the interior; this vector field gives a 2-chain on $\tilde{\Sigma}$ which shows $\hat{\beta}$ is homologous on $\tilde{\Sigma}$ to $\chi(S)H$; but $\chi(S)$ is odd since S has a single boundary component.) Thus the extra term $\hat{\beta} + H$ added to $\tilde{\gamma}$ is zero modulo $2H$. Next we check $\tilde{\gamma}$ is stable under resolution of an intersection: indeed this changes $\sum_{m \leq n} \#(\beta_m \cap \beta_n)$ by -1, and changes k by ± 1, while not changing $\sum \hat{\beta}_m$; it thus changes $\tilde{\gamma}$ by either 0 or $-2H$, which is in either case trivial mod $2H$. Finally we note that any representation of γ as a union of smooth closed curves can be related to any other by repeated application of these two operations and their inverses. It follows that $\tilde{\gamma}$ is indeed well defined.

Moreover, this rule has the following property:

$$\tilde{\gamma} + \tilde{\gamma}' = \widetilde{\gamma + \gamma'} + \langle \gamma, \gamma' \rangle H. \tag{E.2}$$

It follows that the corresponding formal variables

$$Y_\gamma = X_{\widetilde{\gamma}} \tag{E.3}$$

obey the twisted product rule

$$Y_\gamma Y_{\gamma'} = (-1)^{\langle \gamma, \gamma' \rangle} Y_{\gamma+\gamma'}. \tag{E.4}$$

In turn it follows (using the arguments of [61, 63]) that, if we use this particular lifting rule to extract the 4D BPS degeneracies, all the wall-crossing relations (and in particular the KSWCF for the pure 4D degeneracies) will come out as they should.

Appendix F

Spectral networks and algebraic equations

It has been noted by Kontsevich that the generating functions of Donaldson-Thomas invariants are often solutions of algebraic equations. The equation (1.15) is one example. This equation determines the BPS degeneracies $\Omega(n\gamma_c)$ corresponding to an m-cohort. As we have seen in this paper, this equation can be derived from a close analysis of the spectral network corresponding to an m-herd.

While finding the precise equation (1.15) involved some hard work, the bare fact that the BPS generating function obeys *some* algebraic equation is not so mysterious. Indeed, this seems to be a general phenomenon, which we expect to occur for *any* theory of class S. Let us briefly explain why.

The junction equations (B.1) involve variables ν and τ attached to each street of the network. These variables lie *a priori* in the noncommutative algebra $\mathcal{A}_S$. However, one can replace them by variables lying in the commutative algebra $\mathcal{A}_C$ simply by choosing local trivializations of the torsors $\tilde{\Gamma}(\tilde{z}, -\tilde{z})$; indeed such a trivialization gives an embedding of $\mathcal{A}_S$ into the algebra of $K \times K$ matrices over $\mathcal{A}_C$; taking the individual matrix components then gives equations where all of the variables lie in $\mathcal{A}_C$. These equations alone do not quite determine ν and τ — there are not quite enough of them. However, once one supplements them with the "branch point" equations from [63] (which are also algebraic), one then has one equation for each variable.

In principle the spectral network may involve infinitely many streets and joints, so at this stage we may have an infinite set of algebraic equations in an infinite number of variables. However, in all examples we have considered, only finitely many of these equations are relevant for determining any particular BPS generating function. Indeed, in these examples the set of "two-way streets" is always supported in some compact set K obtained by deleting small discs around punctures on C; the intersection $\mathcal{W} \cap K$ only involves finitely many streets; and there are no streets which enter K from outside. It seems likely that these properties hold for *all* spectral networks, although we have

not proven it. In any case, taking these properties for granted, it follows that the finitely many variables ν and τ attached to the finitely many streets in $\mathcal{W} \cap K$ are indeed determined by a finite set of algebraic equations.

The functions $Q(p)$ in turn are algebraic combinations of the ν and τ, as are the BPS generating functions $\prod_p Q(p)^{\langle \bar{a}, p_\Sigma \rangle}$. Thus we expect that the BPS generating functions in any theory of class S always satisfy algebraic equations, which gives a natural explanation of Kontsevich's observation, at least in those theories.

Appendix G

Generating function detailed calculation

In this Appendix we present a simple technique allowing one to calculate the writhe effectively for soliton paths encoded by certain graphs on branched spectral covers, and show its application to a direct computation of several first terms in expansions like (4.118).

G.1 Singular writhe technique

Schematically, the spectral network may be though of as a graph. We would like to adapt the usual notion of writhe for smooth curves to the singular[1] curves arising in this setting. In order to compute the writhe it will be necessary to keep track of the order in which the path runs (in different transverse directions) through a self-intersection. For this purpose, we will resolve paths pictorially by drawing under/over-crossing. The path-ordering convention is that what runs below runs first.

For example, consider a self-intersection through which a single path runs multiple times as shown in figure G.1). We can slightly resolve the critical angle ϑ_c to get the picture on the left hand side, then it is simple to notice that the four segments give contributions to the writhe by pairs, so it is enough to sum these contributions pairwise for the thick intersections. The contribution for this particular case is -2.

Another interesting possible issue are "half-intersections". They occur when two lines going first parallel split and go in different directions, this happens due to splitting of intersections as depicted in fig.G.2. From these pictures it is clear that we can assign half-contributions to half-intersections assuming that these half-contributions will be summed up to an integer result.

[1] Here *singular* does not denote the presence of self-intersections as, for instance, in the math literature on knots. We refer instead to discontinuities of the tangent vector of solitons paths, these occur in correspondence of (lifts of) joints.

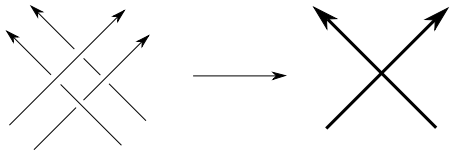

Figure G.1: Resolved intersection

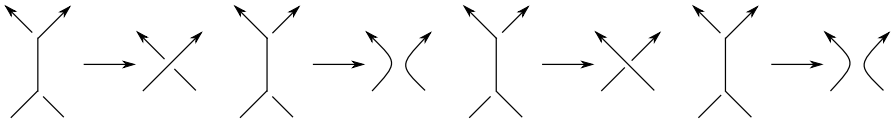

Figure G.2: On the singular writhe calculation. At junctions, soliton paths may intersect somewhat ambiguously, with "half-integer" units of intersections to be taken into account. Upon summation the contributions from *all junctions* involved, intersection numbers can eventually be correctly computed and found to be integers. From left to right we show the addition of half-integer intersection numbers at pairs of junctions: $-\frac{1}{2}-\frac{1}{2}=-1$, $-\frac{1}{2}+\frac{1}{2}=0$, $+\frac{1}{2}+\frac{1}{2}=+1$, $+\frac{1}{2}-\frac{1}{2}=0$

Thus to compute the "singular writhe" we choose a base point, in each self-intersection lines come in with some tangent vectors $\vec{v}_k$ at corresponding "times" t_k, so, finally the formula for the writhe reads

$$\begin{aligned}\mathrm{wr}(\gamma) = &-\sum_{i\in \mathrm{int's}}\sum_{k,m}\mathrm{sign}(t_k^{(i)}-t_m^{(i)})\mathrm{sign}\left[\vec{v}_k^{(i)},\vec{v}_m^{(i)}\right]+\\ &-\frac{1}{2}\sum_{i\in \frac{1}{2}\mathrm{int's}}\sum_{k,m}\mathrm{sign}(t_k^{(i)}-t_m^{(i)})\mathrm{sign}\left[\vec{v}_k^{(i)},\vec{v}_m^{(i)}\right]\end{aligned} \tag{G.1}$$

G.2 Diagram rules

In the next subsection we present results for detour writhe calculations in the cases of 2-herds and 3-herds. We schematize the corresponding detours by diagrams denoting resolutions of paths in 6-way joints.

In this way we can reformulate the 6-way joint rules in a pictorial form. As an example, consider

$\tau_{ki}(p_S) =$ 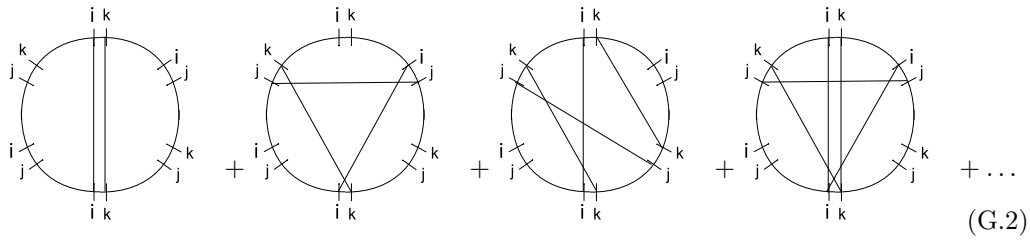 (G.2)

here we describe the outgoing soliton generating function for the street p_S (S is for *South*) attached to the bottom gate of the joint: solitons of type ki start from this gate on sheet k going upwards

and end up on sheet i going downwards to return back to the bottom gate. What happens in between is described by following the lines connecting the various gates. For example, in the first term we simply have straight connections to the upper gate, this corresponds to solitons contributed from $\nu_{ki}(p_N)$ (the street at the northern gate). In the second term we have solitons starting on sheet k on the south gate, propagating on sheet k to the NW gate, then propagating through the network, then coming back to the NW gate on sheet j, then propagating to the NE gate on sheet j and going once more through the network and coming back to the NE gate on sheet i and finally propagating back to the S gate, and on p_S on sheet i. Solitons in the second term are those encoded into $\nu_{kj}(p_{NW})\nu_{ji}(p_{NE})$. Further terms bear analogous interpretations.

We present whole detour diagrams, calculate corresponding writhes and restore the generating function $Q(\mathfrak{d}, y, z)$ (eq.(4.112)). The results will be:

$$Q^{(2-\text{herd})}(\mathfrak{d}, y, z) = 1 + (y + y^{-1})z + (y^2 + 1 + y^{-2})z^2 + O(z^3)$$
$$Q^{(3-\text{herd})}(\mathfrak{d}, y, z) = 1 + (y^2 + 1 + y^{-2})z + (y^6 + 2y^4 + 3y^2 + 3 + 3y^{-2} + 2y^{-4} + y^{-6})z^2 + O(z^3) \tag{G.3}$$

Diagram rules:

- Green lanes go along ith sheet, red lanes go along jth sheet, blue lanes go along kth sheet
- Green and blue lanes go from right to left, red lanes go from left to right
- We calculate the generating function for $\mathfrak{d}$ branching point street, thus we always start computing writhe from $\mathfrak{d}$ branching point from kth sheet.
- For n-th order contributions (meaning that the detour's homology class is n times the generator of the critical lattice), in order to keep things tidy, we split the picture into n layers. To reconstruct the path one has to glue the layers back together, the endpoints of a piece of path drawn on a layer are marked by thick red and blue dots. The red dot is where the jump to the next layer begins, the blue dot is where the jump from the previous layer lands. For example, see figure G.5. On those diagrams where dots are missing layers are glued in the point $\mathfrak{d}$.

G.3 2-herd diagrams

G.3.1 Diagrams for order one

We now introduce a diagrammatic representation of detours. We draw the joints of a critical network as circles and mark the six gates of each joint. The two herd has four joints: two for each horse,

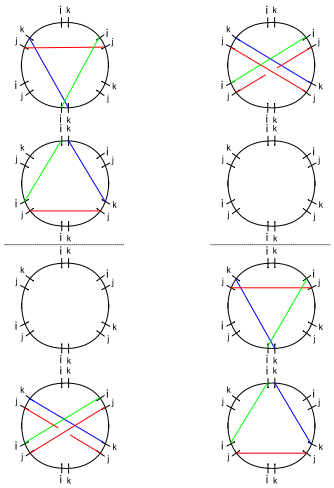

Figure G.3: The two diagrams for order one in the 2-herd

these are shown in each column of figure G.3: focusing on the left column, the upper two joints correspond to the joints of the upper horse, while the lower two joints are the joints of the lower horse (see fig. G.4), the horizontal dashed line separating them denotes the distinction of joints of a horse from those of the other. The topology of the network determines how the different gates are mutually connected by two-way streets, or whether they attach to streets ending on branch points. Each column describes a detour path on Σ, the path is constructed out of the segments shown in the figure (each color corresponds to a sheet of Σ) as well as of lifts of streets attached to the gates on which segments end. All paths are conventionally taken with a basepoint on sheet i on the terminal 2-way streets on the SW branch-point of the herd, they are constructed starting from the basepoint and following segments through joints, and connecting streets from one joint to the next one. As an example, in figure G.4 we reproduce in full detail the path described by the diagram on the left of fig. G.3.

diag #	1	2
contribution	y^{-1}	y

G.3.2 Diagrams for order two

diag #	1	2	3
contribution	y^{-2}	y^2	1

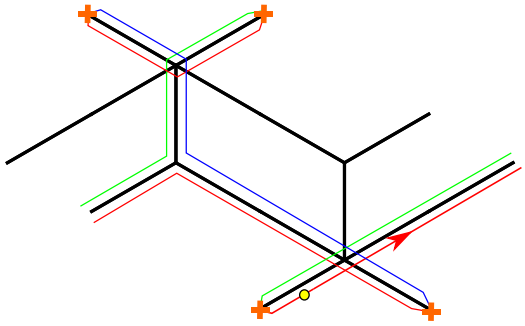

Figure G.4: The path corresponding to the diagram on the left of figure G.3. Recall that the endpoints of streets on the far left are identified with endpoints of streets on the far right, as the herd wraps a tube of the Riemann surface C. The starting point of the detour is indicated by a yellow dot, there is only one self-intersection at the lowest joint, where two red lines (both run on sheet i) cross each other. The overall writhe of this detour is therefore -1.

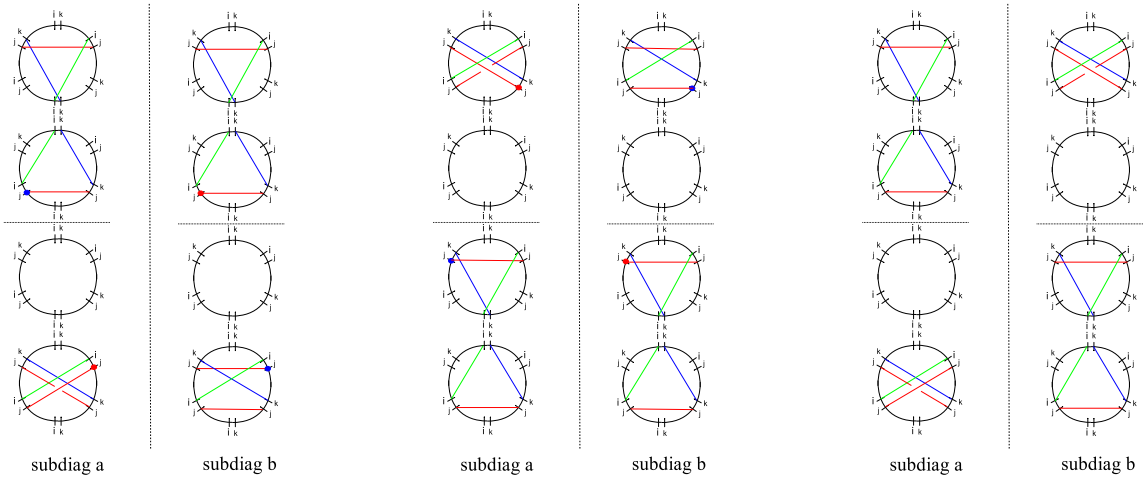

Figure G.5: Diagrams of order two in the 2-herd. Since each path goes twice around the herd, we split the path into two and represented each piece separately, the dashed vertical line separates two pieces of the same path, the thick dot indicates where one piece joins the other.

G.4 3-herd diagrams

G.4.1 Diagrams for order one

diag #	1	2	3
contribution	y^{-2}	1	y^2

G.4.2 Diagrams for order two

diag #	1	2	3	4	5	6	7	8	9	10	11	12	13
contribution	1	$2y^2$	y^4	y^4	y^{-6}	y^6	y^{-4}	y^{-4}	$2y^{-2}$	1	y^{-2}	1	y^2

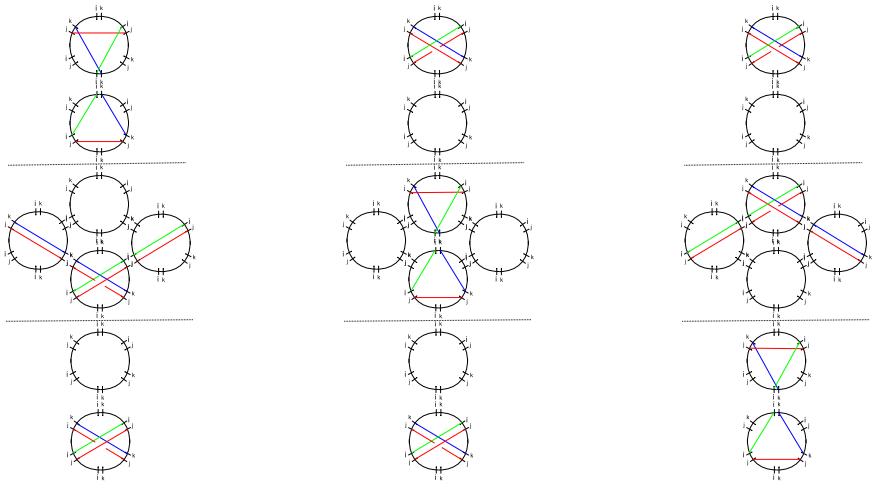

Figure G.6: Diagrams for the order one in 3-herd

Notice that diagrams of type #2 and type #9 come into play twice, so the total number of diagrams with multiplicities is 15. All the diagrams except #5, 6 are independent of the order along what subdiagram one goes first, though for diagrams #5, 6 this choice may switch the sign of the index to the opposite. The right choice in this case can be extracted from the order of crossing cuts what coincides with the order of simpleton generating functions in the final generating function expression.

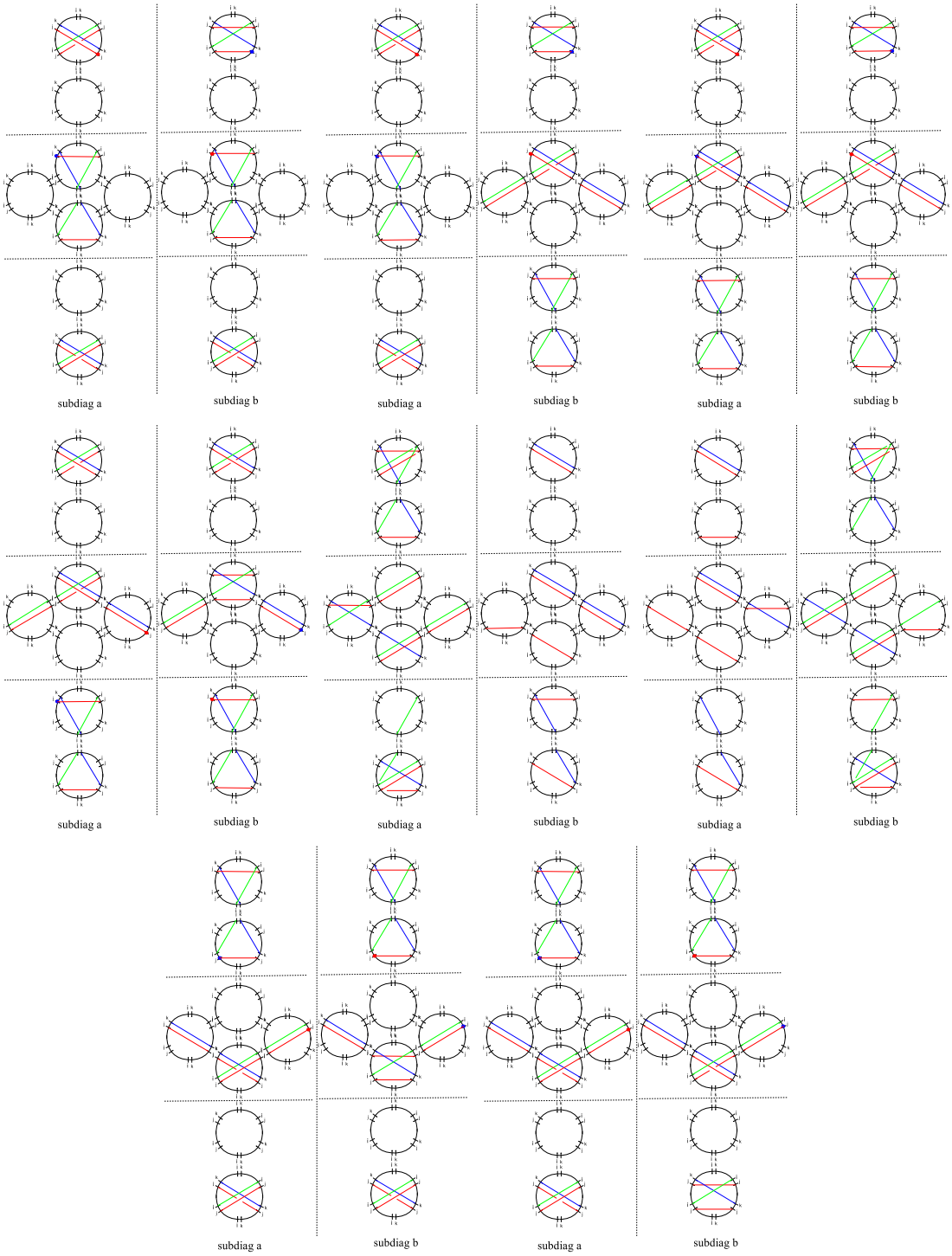

Figure G.7: Diagrams #1-8 for the order two in 3-herd

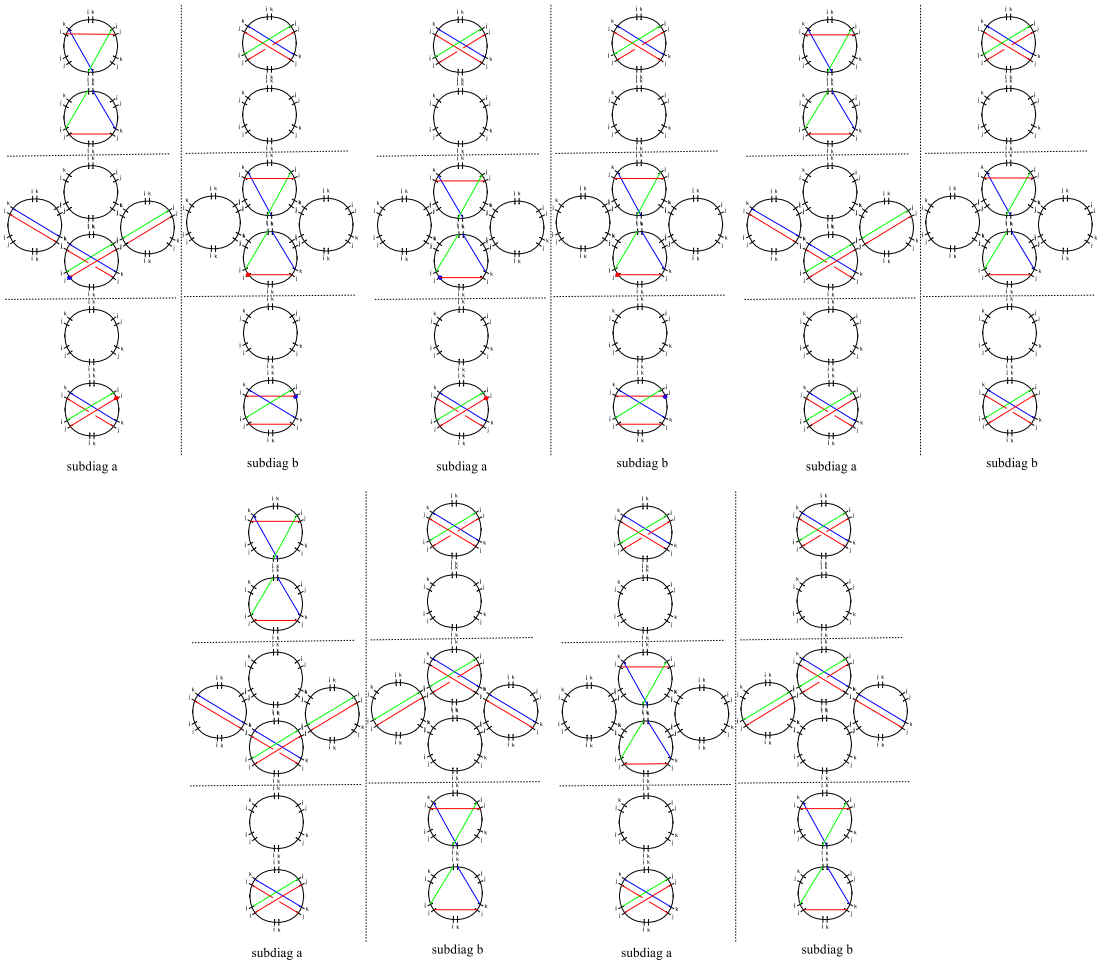

Figure G.8: Diagrams #9-13 for the order two in 3-herd

Appendix H

Vanilla states from refined charges

In section 4.1.3.1 we motivated the definition of halo-saturated interfaces by noting that the framed wall-crossing of generic IR interfaces differs from that of IR line defects, due to the lack of a relation such as (4.11) for generic interfaces. It is interesting to study the soliton combinatorics involved in contributions to $\langle \mathfrak{a}, L(\gamma)\rangle$ for a generic interface labeled by the regular homotopy class $\mathfrak{a}$ on Σ^*. In fact, since here we are interested in intersections of $\mathfrak{a}$ with closed homology classes, it will be sufficient to consider the relative homology class of $\mathfrak{a}$ on Σ^*, which will be denoted a.

H.1 Refinement of halo charges

In the classical K-wall formula of [63, 65], the enhanced 2d-4d degeneracies $\omega(\gamma, a)$ keep track of the effects of the *refinement* of 4d charges induced by the removal of points corresponding to the 2d vacua $z^{(i)}$, $z'^{(j')}$ (the endpoints of a). In the context of spectral networks, this is identified with

$$\omega(\gamma, a) = \langle L(\gamma), a\rangle \,. \tag{H.1}$$

When positivity holds[1], it tells us that $|\Omega(\gamma)| = \dim(\mathfrak{h}_\gamma)$, in other words the BPS index really counts the number of oscillators generating the corresponding vanilla Fock sub-space. We conjecture that there exists a unique splitting

$$L(\gamma) = \sum_{r=1}^{|\Omega(\gamma)|} L_r(\gamma)\,, \tag{H.2}$$

with each term satisfying

$$L_r(\gamma) = \sum_{p\in\mathcal{W}_c} \alpha_{r,\gamma}(p)\, p_\Sigma, \qquad \partial L_r(\gamma) = 0\,, \qquad [L_r(\gamma)] = \mathrm{sgn}(\Omega(\gamma))\cdot\gamma\,, \tag{H.3}$$

[1] In [73] evidence was found, somewhat surprisingly, that positivity seems to hold for BPS boundstates corresponding to stable irreps of the m-Kronecker quiver.

where $\alpha_{r,\gamma}(p)$ are integers determined by a set of rules which we will presently explain. Heuristically, each $L_r(\gamma)$ should be associated with a 1-particle vanilla BPS state in the multiplet $\mathfrak{h}_\gamma$, then $\omega(\gamma, a)$ counts the number of 4d vanilla as well as orbital oscillators contributing to the Fock space of *framed* BPS states.

To present our construction of the L_r, we introduce a new homology lattice, naturally related to a classification of supersymmetric interfaces. Given a network at a critical phase $\mathcal{W}(\vartheta_c)$, consider the space $C \setminus \mathcal{W}(\vartheta_c)$, it will be a disconnected union of various components. Choose a point from each component, let R be the set of these points. Then we define

$$C^* := C \setminus R \qquad \Sigma^* := \Sigma \setminus \pi^{-1}(R) \qquad \Gamma^* = H_1(\Sigma^*, \mathbb{Z}) \tag{H.4}$$

we will call Γ^* the *refined lattice*, while we denote by $H_1(\Sigma^*, \mathbb{Z}; \pi^{-1}(R))$ the Γ^*-torsor of relative homology classes on Σ^* with endpoints in $\pi^{-1}(R)$. We define Γ_c^* to be the (not necessarily one-dimensional) sublattice which projects to $\Gamma_c \subset \Gamma$ upon filling the punctures at $\pi^{-1}(R)$. We also denote by γ_c the generator of the one-dimensional lattice Γ_c (the sign ambiguity is fixed by ϑ_c).

Any IR interface labeled by $a \in H_1(\Sigma^*, \mathbb{Z}; \pi^{-1}(R))$, enjoys a well-defined pairing $\langle \tilde{\gamma}, a \rangle$ with any $\tilde{\gamma} \in \Gamma^*$. The L_r – so far defined as *actual paths* – can be clearly associated to homology classes of Γ^*, we define $\tilde{\gamma}_{n,r} := [L_{r,n\gamma_c}]_{\Gamma^*} \operatorname{sgn}(\Omega(n\gamma_c))$.

Correspondingly, we introduce a new set of formal variables $\tilde{X}$ associated with (relative) homology classes on Σ^*, satisfying

$$\tilde{X}_{\tilde{\gamma}} \tilde{X}_{\tilde{\gamma}'} = \tilde{X}_{\tilde{\gamma}+\tilde{\gamma}'} \qquad \tilde{X}_a \tilde{X}_{\tilde{\gamma}'} = \tilde{X}_{a+\tilde{\gamma}} \,. \tag{H.5}$$

Now, choose a to be any relative homology class on Σ^* with endpoints in $\pi^{-1}(R)$, and consider the generating function of its framed BPS states with halo charges in Γ_c^* (cf. 4.27, where a is played by $\wp^{(i)}$)

$$\sum_{\tilde{\gamma} \in \Gamma_c^*} \tilde{X}_{a+\tilde{\gamma}} \tag{H.6}$$

Conjecture 3. *the series (H.6) admits a factorization of the form*

$$\tilde{X}_a \prod_{n,r} \left(1 + \sigma(n\gamma_c) \tilde{X}_{\tilde{\gamma}_{n,r}}\right)^{\langle a, \tilde{\gamma}_{n,r} \rangle} \tag{H.7}$$

where $\sigma(n\gamma_c) = \operatorname{sgn}(\Omega(n\gamma_c))$, $[\tilde{\gamma}_{n,r}]_\Gamma = n\gamma_c$ *and* $r = 1, \ldots, |\Omega(n\gamma_c)|$.

Because of our choice of Γ^*, the refined homology classes $\tilde{\gamma}^*$ uniquely determine the $L_r(\gamma)$ (i.e. the $\alpha_{r,\gamma}(p)$). This is our definition of the L_r, it relies on the conjectural factorization. We conclude by presenting some nontrivial evidence for the conjecture.

H.2 The 3-herd

For the 3-herd, the BPS indices read

$$\Omega(\gamma_c) = 3, \quad \Omega(2\gamma_c) = -6, \quad \Omega(3\gamma_c) = 18, \quad \dots \tag{H.8}$$

We know that $L_{n,r}$ must run through each terminal street n times, for all r, for homological reasons. Thus we expect for the halo generating function (H.7) of an interface crossing one terminal street (cf. fig.4.11)

$$\begin{aligned}
&\tilde{X}_a\,(1+\tilde{X}_{\tilde{\gamma}_{1,1}})(1+\tilde{X}_{\tilde{\gamma}_{1,2}})(1+\tilde{X}_{\tilde{\gamma}_{1,2}}) \\
&\times(1-\tilde{X}_{\tilde{\gamma}_{2,1}})^{-2}(1-\tilde{X}_{\tilde{\gamma}_{2,2}})^{-2}(1-\tilde{X}_{\tilde{\gamma}_{2,3}})^{-2}(1-\tilde{X}_{\tilde{\gamma}_{2,4}})^{-2}(1-\tilde{X}_{\tilde{\gamma}_{2,5}})^{-2}(1-\tilde{X}_{\tilde{\gamma}_{2,6}})^{-2} \\
&\times(1+\tilde{X}_{\tilde{\gamma}_{3,1}})^{3}(1+\tilde{X}_{\tilde{\gamma}_{3,2}})^{3}\ \cdots\ (1-X_{\tilde{\gamma}_{3,18}})^{3} \\
&\times\cdots
\end{aligned} \tag{H.9}$$

According to our conjecture, this *predicts the following form for generating function of framed states (H.6)*

$$\begin{aligned}
\tilde{X}_a\Big[&1+\Big(\tilde{X}_{\tilde{\gamma}_{1,1}}+\tilde{X}_{\tilde{\gamma}_{1,2}}+\tilde{X}_{\tilde{\gamma}_{1,2}}\Big) \\
&+\Big(\tilde{X}_{\tilde{\gamma}_{1,1}+\tilde{\gamma}_{1,2}}+\tilde{X}_{\tilde{\gamma}_{1,1}+\tilde{\gamma}_{1,3}}+\tilde{X}_{\tilde{\gamma}_{1,2}+\tilde{\gamma}_{1,3}}+2\sum_{r=1}^{6}\tilde{X}_{\tilde{\gamma}_{2,r}}\Big) \\
&+\Big(X_{\tilde{\gamma}_{1,1}+\tilde{\gamma}_{1,2}+\tilde{\gamma}_{1,3}}+2\sum_{r=1}^{3}\sum_{r'=1}^{6}\tilde{X}_{\tilde{\gamma}_{1,r}+\tilde{\gamma}_{2,r'}}+3\sum_{r=1}^{18}\tilde{X}_{\tilde{\gamma}_{3,r}}\Big) \\
&+\cdots\Big]
\end{aligned} \tag{H.10}$$

Indeed, by studying the detours, *we find exactly the predicted structure*, with the identifications (labels refer to the street map of figure 4.11, the lifts of streets carry the orientations dictated by the WKB flow for each component of the lift)

$$\begin{aligned}
L_{1,1} =&\pi^{-1}(\gamma_1+\delta_1+\alpha_2+\beta_2+\delta_2+\delta_3+\alpha_4+\beta_4+\delta_4+\alpha_6+\beta_6) \\
L_{1,2} =&\pi^{-1}(\alpha_1+\beta_1+\delta_1+\gamma_2+\delta_2+\delta_3+\delta_4+\alpha_6+\beta_6) \\
L_{1,3} =&\pi^{-1}(\alpha_1+\beta_1+\delta_1+\delta_2+\alpha_3+\beta_3+\gamma_3+\delta_3+\delta_4+\alpha_5+\beta_5)
\end{aligned} \tag{H.11}$$

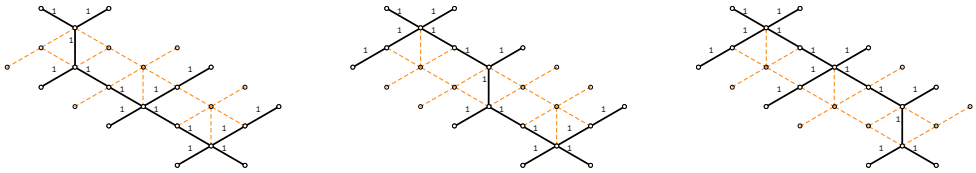

Figure H.1: The set of $L_{1,r}$. Values of the $\alpha_r(p)$ are displayed.

$$
\begin{aligned}
L_{2,1} =& \pi^{-1}(2(\alpha_1+\beta_1+\delta_1+\gamma_2+\delta_2+\delta_3+\delta_4+\alpha_6+\beta_6)) \\
L_{2,2} =& \pi^{-1}(\alpha_1+\beta_1+\gamma_1+2\delta_1+\alpha_2+\beta_2+\gamma_2+2\delta_2+2\delta_3+\alpha_4+\beta_4+2\delta_4+2\alpha_6+2\beta_6) \\
L_{2,3} =& \pi^{-1}(2\alpha_1+2\beta_1+2\delta_1+\gamma_2+2\delta_2+\alpha_3+\beta_3+\gamma_3+2\delta_3+2\delta_4+\alpha_5+\beta_5+\alpha_6+\beta_6) \\
L_{2,4} =& \pi^{-1}(2(\gamma_1+\delta_1+\alpha_2+\beta_2+\delta_2+\delta_3+\alpha_4+\beta_4+\delta_4+\alpha_6+\beta_6)) \\
L_{2,5} =& \pi^{-1}(\alpha_1+\beta_1+\gamma_1+2\delta_1+\alpha_2+\beta_2+2\delta_2+\alpha_3+\beta_3+\gamma_3+2\delta_3+\alpha_4+\beta_4+2\delta_4 \\
&+\alpha_5+\beta_5+\alpha_6+\beta_6) \\
L_{2,6} =& \pi^{-1}(2(\alpha_1+\beta_1+\delta_1+\delta_2+\alpha_3+\beta_3+\gamma_3+\delta_3+\delta_4+\alpha_5+\beta_5))
\end{aligned}
\tag{H.12}
$$

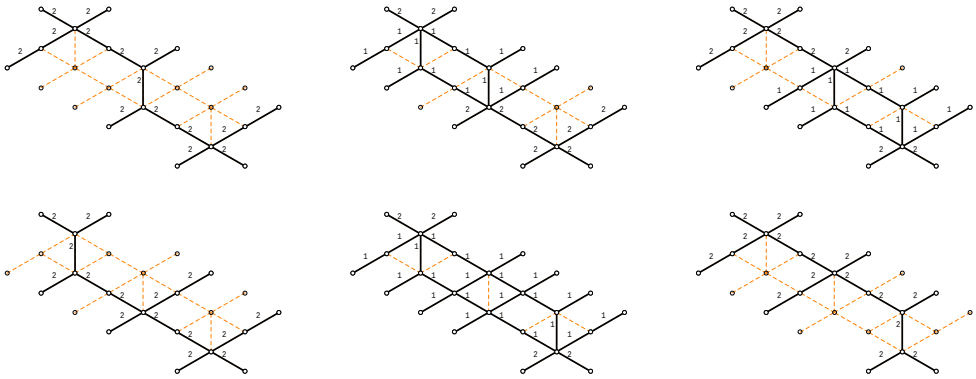

Figure H.2: The set of $L_{2,r}$. Values of the $\alpha_r(p)$ are displayed.

$$
\begin{aligned}
L_{3,1} &= \pi^{-1}(3(\alpha_1+\beta_1+\delta_1+\gamma_2+\delta_2+\delta_3+\delta_4+\alpha_6+\beta_6))\\
L_{3,2} = L_{3,3} &= \pi^{-1}(2\alpha_1+2\beta_1+\gamma_1+3\delta_1+\alpha_2+\beta_2+2\gamma_2+3\delta_2+3\delta_3+\alpha_4\\
&\quad +\beta_4+3\delta_4+3\alpha_6+3\beta_6)\\
L_{3,4} = L_{3,5} &= \pi^{-1}(3\alpha_1+3\beta_1+3\delta_1+2\gamma_2+3\delta_2+\alpha_3+\beta_3+\gamma_3+3\delta_3+3\delta_4\\
&\quad +\alpha_5+\beta_5+2\alpha_6+2\beta_6)\\
L_{3,6} = L_{3,7} = L_{3,8} &= \pi^{-1}(2\alpha_1+2\beta_1+\gamma_1+3\delta_1+\alpha_2+\beta_2+\gamma_2+3\delta_2+\alpha_3+\beta_3\\
&\quad +\gamma_3+3\delta_3+\alpha_4+\beta_4+3\delta_4+\alpha_5+\beta_5+2\alpha_6+2\beta_6)\\
L_{3,9} = L_{3,10} &= \pi^{-1}(\alpha_1+\beta_1+2\gamma_1+3\delta_1+2\alpha_2+2\beta_2+\gamma_2+3\delta_2+3\delta_3+2\alpha_4\\
&\quad +2\beta_4+3\delta_4+3\alpha_6+3\beta_6) \qquad \text{(H.13)}\\
L_{3,11} = L_{3,12} &= \pi^{-1}(3\alpha_1+3\beta_1+3\delta_1+\gamma_2+3\delta_2+2\alpha_3+2\beta_3+2\gamma_3+3\delta_3+3\delta_4\\
&\quad +2\alpha_5+2\beta_5+\alpha_6+\beta_6)\\
L_{3,13} = L_{3,14} &= \pi^{-1}(2\alpha_1+2\beta_1+\gamma_1+3\delta_1+\alpha_2+\beta_2+3\delta_2+2\alpha_3+2\beta_3+2\gamma_3\\
&\quad +3\delta_3+\alpha_4+\beta_4+3\delta_4+2\alpha_5+2\beta_5+\alpha_6+\beta_6)\\
L_{3,15} = L_{3,16} &= \pi^{-1}(\alpha_1+\beta_1+2\gamma_1+3\delta_1+2\alpha_2+2\beta_2+3\delta_2+\alpha_3+\beta_3+\gamma_3\\
&\quad +3\delta_3+2\alpha_4+2\beta_4+3\delta_4+\alpha_5+\beta_5+2\alpha_6+2\beta_6)\\
L_{3,17} &= \pi^{-1}(3(\gamma_1+\delta_1+\alpha_2+\beta_2+\delta_2+\delta_3+\alpha_4+\beta_4+\delta_4+\alpha_6+\beta_6))\\
L_{3,18} &= \pi^{-1}(3(\alpha_1+\beta_1+\delta_1+\delta_2+\alpha_3+\beta_3+\gamma_3+\delta_3+\delta_4+\alpha_5+\beta_5))
\end{aligned}
$$

The check can be extended to detours on all streets of the critical network (considering a short interface crosing only a single 2-way street). We checked that the correspondence between (H.7) and (H.6) holds: taking an interface crossing the lift of a single 2-way street, we find that the halo generating function gets contributions only from those $L_{n,r}$ which contain the street itself.

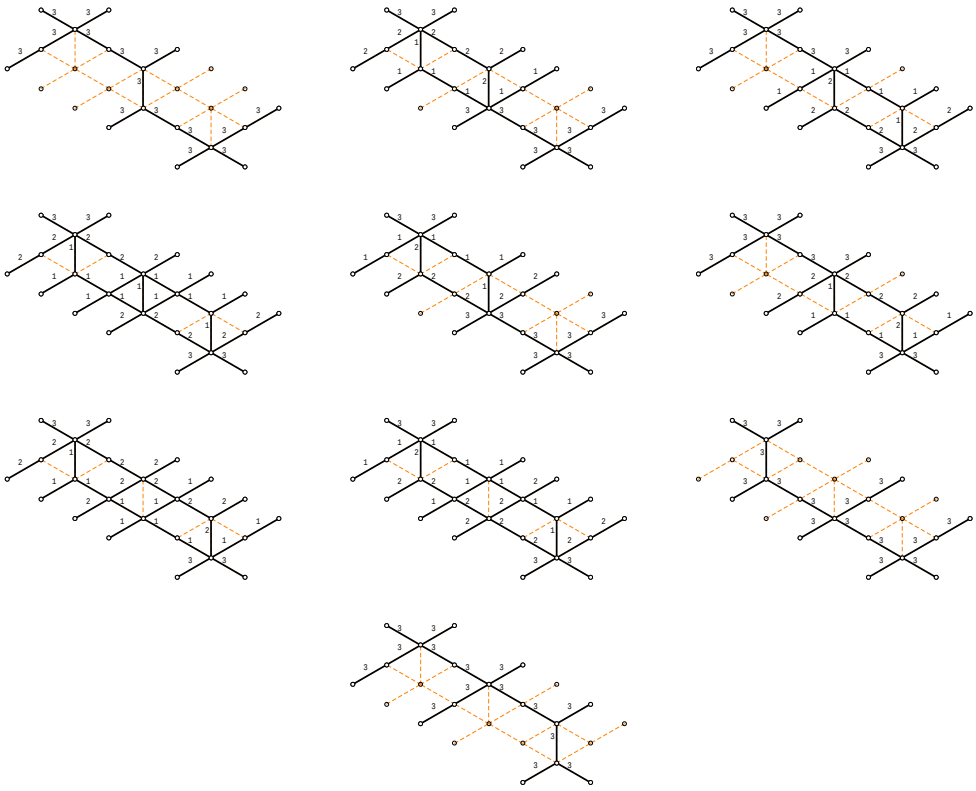

Figure H.3: The set of $L_{3,r}$. Values of the $\alpha_r(p)$ are displayed.

Appendix I

A technical equivalence relation

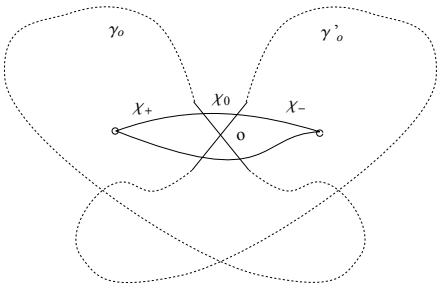

Figure I.1: The writhe as the origin of the quadratic refinement

First we would like to stress that the writhe implements a quadratic refinement function for the intersection pairing in the homology basis. Indeed the both quantities are of the same nature: they both can be interpreted as certain signed sums over intersections or self-intersections of actual paths.

Suppose we consider two paths γ_o and γ'_o intersecting in some point o and suppose we are able to concatenate them (somehow) then the writhe (a signed sum over all self-intersections of the concatenation) is expected to have the following three contributions:

1. The sum over self-intersections of γ_o
2. The sum over self-intersections of γ'_o
3. The sum over mutual intersections of γ_o and γ'_o

The problem is that according to our rules we are not able to concatenate two closed paths if they do not have a common tangent vector in the intersection point. Thus we add a small refinement: we

consider an auxiliary path χ intersecting both γ_o and γ'_o near the point o as it is depicted in fig.I.1. There are two possibilities to choose χ going above or below the point o.

First consider the choice of χ going above and consider paths γ_o and γ'_o as detours then the writhe of the resulting path reads

$$\mathrm{wr}(\chi_+\gamma_o\chi_0\gamma'_o\chi_-) = \mathrm{wr}(\chi_+\gamma_o\chi_0\chi_-) + \mathrm{wr}(\chi_+\chi_0\gamma'_o\chi_-) + \langle[\gamma_o],[\gamma'_o]\rangle \tag{I.1}$$

where $\langle\star,\star\rangle$ is the intersection pairing of homology classes $[\star]$ on Σ^*[1]. Then we *shrink* the auxiliary path to zero and rewrite this relation as

$$\mathrm{wr}(\gamma_o\gamma'_o) = \mathrm{wr}(\gamma_o) + \mathrm{wr}(\gamma'_o) + \langle[\gamma_o],[\gamma'_o]\rangle \tag{I.2}$$

In this form the writhe represents a *quadratic refinement* of the intersection pairing on cycles, and we imply a smooth gluing of the paths via an auxiliary path as in (I.1).

Notice that for the lower choice of χ we take a detour along γ'_o first and then along γ_o, this we describe as

$$\mathrm{wr}(\gamma'_o\gamma_o) = \mathrm{wr}(\gamma'_o) + \mathrm{wr}(\gamma_o) + \langle[\gamma'_o],[\gamma_o]\rangle \tag{I.3}$$

And the difference reads

$$\mathrm{wr}(\gamma_o\gamma'_o) - \mathrm{wr}(\gamma'_o\gamma_o) = 2\langle[\gamma_o],[\gamma'_o]\rangle \tag{I.4}$$

This relation can be continued to the ρ-projections of the algebraic variables

$$\begin{aligned}\rho\Big(\hat{\Upsilon}_{\gamma_o}\hat{\Upsilon}_{\gamma'_o}\Big) = \rho\Big(\hat{\Upsilon}_{\gamma_o\gamma'_o}\Big) &= y^{2\langle[\gamma_o],[\gamma'_o]\rangle}\rho\Big(\hat{\Upsilon}_{\gamma'_o\gamma_o}\Big)\\ &= y^{2\langle[\gamma_o],[\gamma'_o]\rangle}\rho\Big(\hat{\Upsilon}'_{\gamma_o}\hat{\Upsilon}_{\gamma_o}\Big)\end{aligned} \tag{I.5}$$

The punchline is that, formally, $\hat{\Upsilon}_{\gamma_o}\hat{\Upsilon}_{\gamma'_o}$ and $y^{2\langle[\gamma_o],[\gamma'_o]\rangle}\hat{\Upsilon}_{\gamma'_o}\hat{\Upsilon}_{\gamma_o}$ give the same contribution when projected under ρ. We must stress that this by no means implies something like an algebra rule for the $\hat{\Upsilon}$ (nor the $\hat{Y}$) variables!

To lighten computations in the main body of the paper (most notably section 4.4) we will sometimes employ the following *equivalence relation*

$$\hat{\Upsilon}_{\gamma_o}\hat{\Upsilon}_{\gamma'_o} \doteq y^{2\langle[\gamma_o],[\gamma'_o]\rangle}\hat{\Upsilon}_{\gamma'_o}\hat{\Upsilon}_{\gamma_o} \tag{I.6}$$

for the purpose of eventually projecting through the map ρ from $\hat{\Upsilon}$ variables to $\hat{Y}$ variables. The symbol $\doteq$ is meant to warn the reader that *this is not an identity* regarding the algebra of $\hat{\Upsilon}$ variables.

[1]Incidentally, since Σ^* differs from Σ only by punctures, the pairing coincides with the intersection pairing of homology classes on Σ.

Appendix J

Off-diagonal herds

In section 4.3.3 we encountered a particular type of wild critical network, which is actually part of a larger family of "off-diagonal" herds $\mathcal{H}_p^{(m,n)}$[1]. We call these networks p-(m,n) herds, in this section we describe schematically their structure.

The structure of off-diagonal herds is closely related to that of the usual "diagonal" herds: the general structure of the network consists of p blocks glued together, as shown in figure J.1

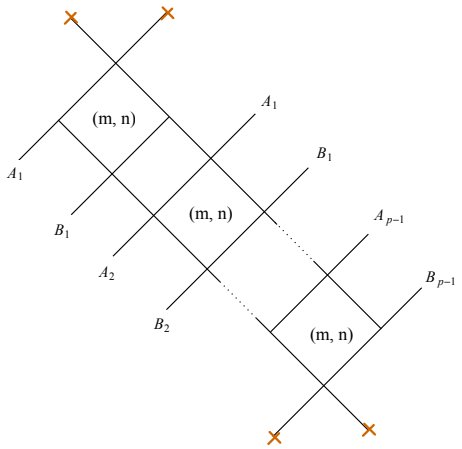

Figure J.1: A p-herd is a collection of "fat" horses glued together with appropriate boundary conditions.

The gluing conditions are similar to those implemented in diagonal herds: blocks are glued to each other in the natural way, throughout the herd which wraps the cylinder of $\mathcal{C}$. Terminal blocks are connected to branch points.

The novel feature of these types of networks in comparison to diagonal herds is that the single (m,n)-block is now an $m \times n$ array of elementary horses glued together. This is displayed in figure

[1] T. Mainiero has independently come to the picture of the off-diagonal herds and is currently studying them.

J.2, street types are analogous to those of section 4.4.1: ij, jk, ik-types are marked in blue, red and purple respectively.

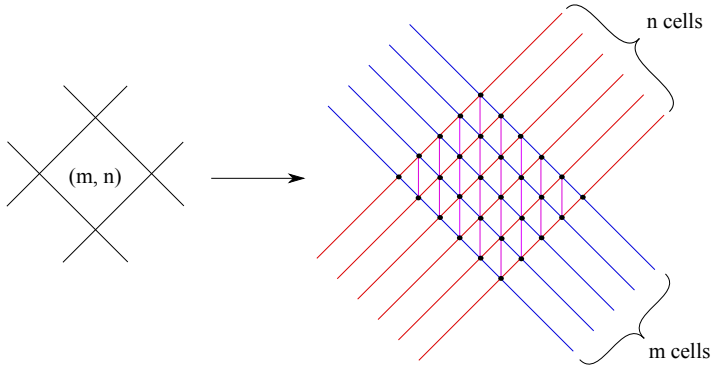

Figure J.2: A "fat" (m, n)-horse

Physically p-(m, n) - herds encode the protected spin characters of bound states of particles of charges γ and γ' with $\langle\gamma, \gamma'\rangle = p$, with the ratio of particles of the first and the second types being $m : n$.

Put differently, these networks can be associated to "slope-m/n" p-Kronecker quiver representations [73]

$$\mathcal{K}_p^{(m,n)}: \quad \mathbb{C}^{\alpha m} \xrightarrow{p} \mathbb{C}^{\alpha n}, \quad \alpha \in \mathbb{N}\,. \tag{J.1}$$

From this perspective, the Poincaré polynomial of the corresponding quiver variety is expected to coincide with the protected spin character calculated from the network. The computation of the PSC from the network can be carried out applying the techniques discussed above in section 4.3.3.

To give an example, consider the following generating function for the Euler characteristics of the moduli spaces

$$Q(\mathcal{K}_p^{(m,n)}) := \prod_{\alpha\in\mathbb{N}} (1 + (-1)^{\alpha mn} z^{\alpha})^{\alpha\, \chi(\mathcal{M}_p^{(\alpha n, \alpha m)})}\,. \tag{J.2}$$

From the network's side, we may associate soliton generating functions ν, τ (solitons going into/out of the joint respectively) to every joint of $\mathcal{H}_p^{(m,n)}$. We also introduce the notation $\nu_k^{(i,j)}[g]$, $\tau_k^{(i,j)}[g]$, where $k = 1, \ldots, p$ labels the fat horse within the herd, while $i = 0, \ldots, m$ and $j = 0, \ldots, n$ label the joint within the fat herd, and $g = 1, \ldots, 6$ labels the six streets connected to the joint. The enumeration of the streets at a generic 6-way joint goes clockwise starting from "noon". With this notation, we define the following generating function:

$$Q(\mathcal{H}_p^{(m,n)}) := \sqrt[n]{1 + \tau_p^{(m,n)}[3]\nu_p^{(m,n)}[3]} = \sqrt[m]{1 + \tau_p^{(m,n)}[5]\nu_p^{(m,n)}[5]} \tag{J.3}$$

Some examples of the network-quiver correspondence are

$$\begin{aligned} Q(\mathcal{K}_3^{(3,1)}) &= Q(\mathcal{H}_3^{(3,1)}) = 1 + z\,, \\ Q(\mathcal{K}_3^{(3,2)}) &= Q(\mathcal{H}_3^{(3,2)}) = 1 + 13z + 1034z^2 + 115395z^3 + O(z^4)\,, \\ Q(\mathcal{K}_3^{(4,3)}) &= Q(\mathcal{H}_3^{(4,3)}) = 1 + 68z + 66378z^2 + O(z^3)\,, \end{aligned} \tag{J.4}$$

in agreement with the general expectation

$$Q(\mathcal{K}_p^{(m,n)}) = Q(\mathcal{H}_p^{(m,n)})\,. \tag{J.5}$$

It appears to be a challenging problem to generalize equation (1.16) (or (4.111)) to the case of p-(m,n) herds, even in the classical case. One might expect a system of equations for a well-chosen set of generating functions, but finding a manageable such system is a problem we leave for the future.

Appendix K

Generic interfaces and the halo picture

This section is devoted to showing how the factorization property deriving from the halo picture fails to capture the $\mathcal{K}$-wall jump (4.88). More precisely, the $\mathcal{K}$-wall jump cannot be written as a conjugation by dilogarithms *unless* some extra techical assumptions are introduced (see immediately above 4.91) about the algebra of formal variables. It is sufficient to consider the truncated expression

$$\begin{aligned} F_{jj}(\wp, \vartheta_c^+; y) &= \hat{Y}_{\wp^{(j)}} + y^2\, \hat{Y}_{\wp^{(j)}+\tilde{\gamma}_1} + (y+y^5)\hat{Y}_{\wp^{(j)}+\tilde{\gamma}_1+\tilde{\gamma}_2} + 2y^4\hat{Y}_{\wp^{(j)}+2\tilde{\gamma}_1} + \cdots \\ &= \hat{Y}_{\wp^{(j)}}\Big(1 + y^3\, \hat{Y}_{\tilde{\gamma}_1} + (y^2+y^6)\hat{Y}_{\tilde{\gamma}_1+\tilde{\gamma}_2} + 2y^6\hat{Y}_{2\tilde{\gamma}_1} + \cdots\Big)\,. \end{aligned} \tag{K.1}$$

In order to assess whether it admits a factorization similar to (4.91), involving quantum dilogs, consider the following identity

$$\begin{aligned} \Phi((-y)^m\, \hat{Y}_{\tilde{\gamma}})^k\, \hat{Y}_{\wp^{(j)}}\, \Phi((-y)^m\, \hat{Y}_{\tilde{\gamma}})^{-k} &= \hat{Y}_{\wp^{(j)}}\, \Phi_{-\langle\wp^{(j)},\tilde{\gamma}\rangle}((-y)^m y^{-2\langle\wp^{(j)},\tilde{\gamma}\rangle}\, \hat{Y}_{\tilde{\gamma}})^{-k\,\mathrm{sgn}(\langle\wp^{(j)},\tilde{\gamma}\rangle)} \\ &= 1 + k\,\frac{1-y^{2\langle\wp^{(j)},\tilde{\gamma}\rangle}}{1-y^{-2}}\, y^{-1}\,(-y)^m y^{-2\langle\wp^{(j)},\tilde{\gamma}\rangle}\, \hat{Y}_{\tilde{\gamma}} + O(\hat{Y}_{2\tilde{\gamma}})\,, \end{aligned} \tag{K.2}$$

where in the last line we expanded in powers of $\hat{Y}_{\tilde{\gamma}}$ and used the fact cycles $\tilde{\gamma}$ appearing in the expression of interest all satisfy $\langle\wp^{(j)},\tilde{\gamma}\rangle < 0$. From this, taking $\tilde{\gamma} = \tilde{\gamma}_1$ and comparing with the above we find only one possibility compatible with a dilog factorization: $\Phi((-y)^2\, \hat{Y}_{\tilde{\gamma}_1})$. Note that this would contribute a factor of $\Phi_1((-y)^4\, \hat{Y}_{\tilde{\gamma}_1})$ when switching to finite-type dilogs, which is equal to $1 + y^3\, \hat{Y}_{\tilde{\gamma}_1}$. Therefore this dilog would not contribute to any other term in parentheses on the RHS of (K.1), hence we may use (K.2) directly on the other terms as well. Thus considering the term in $\hat{Y}_{2\tilde{\gamma}_1}$, if it were coming from a dilog expansion we would expect the following pre-factor

$$k\, y^3\,(-y)^m\,\frac{1-y^{-4}}{1-y^{-2}} = k\,(-y)^m(y+y^3) \tag{K.3}$$

which clearly cannot match $2y^6$. This establishes that (4.88) cannot be cast into the form of conjugation by quantum dilogarithms.

Bibliography

[1] URL: http://www.physics.rutgers.edu/het/wwc/strong-coupling-full-range.flv.

[2] URL: http://www.physics.rutgers.edu/het/wwc/charge-disposition-movie.flv.

[3] URL: http://www.physics.rutgers.edu/het/wwc/spectrum-charges.flv.

[4] URL: http://www.physics.rutgers.edu/het/wwc/focus-before-wall.flv.

[5] Mina Aganagic, Nathan Haouzi, and Shamil Shakirov. *A_n-Triality*. 2014. arXiv:1403.3657 [hep-th].

[6] Mina Aganagic and Masahito Yamazaki. "Open BPS Wall Crossing and M-theory". In: *Nucl.Phys.* B834 (2010), pp. 258–272. DOI: 10.1016/j.nuclphysb.2010.03.019. arXiv:0911.5342 [hep-th].

[7] Mina Aganagic et al. "Black holes, q-deformed 2d Yang-Mills, and non-perturbative topological strings". In: *Nucl.Phys.* B715 (2005), pp. 304–348. DOI: 10.1016/j.nuclphysb.2005.02.035. arXiv:hep-th/0411280 [hep-th].

[8] Mina Aganagic et al. "Wall Crossing and M-theory". In: *Publ.Res.Inst.Math.Sci.Kyoto* 47 (2011), p. 569. arXiv:0908.1194 [hep-th].

[9] Luis F. Alday et al. "Loop and surface operators in N=2 gauge theory and Liouville modular geometry". In: *JHEP* 1001 (2010), p. 113. eprint: 0909.0945.

[10] A.S. Alexandrov, A. Mironov, and A. Morozov. "Solving Virasoro constraints in matrix models". In: *Fortsch.Phys.* 53 (2005), pp. 512–521. DOI: 10.1002/prop.200410212. arXiv:hep-th/0412205 [hep-th].

[11] Murad Alim et al. "BPS Quivers and Spectra of Complete N=2 Quantum Field Theories". In: *Commun.Math.Phys.* 323 (2013), pp. 1185–1227. DOI: 10.1007/s00220-013-1789-8. arXiv:1109.4941 [hep-th].

[12] Murad Alim et al. "$\mathcal{N} = 2$ quantum field theories and their BPS quivers". In: *Adv.Theor.Math.Phys.* 18 (2014), pp. 27–127. DOI: 10.4310/ATMP.2014.v18.n1.a2. arXiv:1112.3984 [hep-th].

[13] Evgeny Andriyash et al. "Bound state transformation walls". In: *JHEP* 1203 (2012), p. 007. DOI: 10.1007/JHEP03(2012)007. arXiv:1008.3555 [hep-th].

[14] Evgeny Andriyash et al. "Wall-crossing from supersymmetric galaxies". In: *JHEP* 1201 (2012), p. 115. DOI: 10.1007/JHEP01(2012)115. arXiv:1008.0030 [hep-th].

[15] P. C. Argyres and M. R. Douglas. "New phenomena in SU(3) supersymmetric gauge theory". In: *Nuclear Physics B* 448 (Feb. 1995), pp. 93–126. DOI: 10.1016/0550-3213(95)00281-V. eprint: arXiv:hep-th/9505062.

[16] P. C. Argyres et al. "New N = 2 superconformal field theories in four dimensions". In: *Nuclear Physics B* 461 (Feb. 1996), pp. 71–84. DOI: 10.1016/0550-3213(95)00671-0. eprint: arXiv:hep-th/9511154.

[17] Philip C. Argyres and Nathan Seiberg. "S-duality in N=2 supersymmetric gauge theories". In: *JHEP* 0712 (2007), p. 088. eprint: 0711.0054.

[18] V. I. Arnold. "Plane curves, their invariants, perestroikas and classifications". In: *Singularities and Bifwrcations, Adv. in Soviet Math* 21 (1994), pp. 33–91.

[19] Dongsu Bak, Ki-Myeong Lee, and Piljin Yi. "Quantum 1/4 BPS dyons". In: *Phys.Rev.* D61 (2000), p. 045003. DOI: 10.1103/PhysRevD.61.045003. arXiv:hep-th/9907090 [hep-th].

[20] Dror Bar-Natan and Edward Witten. "Perturbative expansion of Chern-Simons theory with noncompact gauge group". In: *Commun.Math.Phys.* 141 (1991), pp. 423–440. DOI: 10.1007/BF02101513.

[21] A. Bilal and F. Ferrari. "The Strong-coupling Spectrum of the Seiberg-Witten Theory". In: *Nucl.Phys.B* 469 (1996), pp. 387–402. URL: http://arxiv.org/abs/hep-th/9602082.

[22] Adel Bilal and Frank Ferrari. "Curves of Marginal Stability and Weak and Strong-Coupling BPS Spectra in $N = 2$ Supersymmetric QCD". In: *Nucl.Phys.* B480 (1996), pp. 589–622. eprint: hep-th/9605101.

[23] J. de Boer et al. "A Farey Tail for Attractor Black Holes". In: *JHEP 0* 611 (2006), p. 24. URL: http://arxiv.org/abs/hep-th/0608059.

[24] Jan de Boer et al. "Quantizing N=2 Multicenter Solutions". In: *JHEP* 0905 (2009), p. 002. DOI: 10.1088/1126-6708/2009/05/002. arXiv:0807.4556 [hep-th].

[25] S. Cecotti and C. Vafa. "Ising model and N=2 supersymmetric theories". In: *Communications in Mathematical Physics* 157 (Oct. 1993), pp. 139–178. DOI: 10.1007/BF02098023. eprint: arXiv:hep-th/9209085.

[26] S. Cecotti and C. Vafa. "On classification of N=2 supersymmetric theories". In: *Communications in Mathematical Physics* 158 (Dec. 1993), pp. 569–644. DOI: 10.1007/BF02096804. eprint: arXiv:hep-th/9211097.

[27] S. Cecotti et al. "A new supersymmetric index". In: *Nuclear Physics B* 386 (Nov. 1992), pp. 405–452. DOI: 10.1016/0550-3213(92)90572-S. eprint: arXiv:hep-th/9204102.

[28] Sergio Cecotti. *The quiver approach to the BPS spectrum of a 4d N=2 gauge theory*. 2012. arXiv:1212.3431 [hep-th].

[29] Sergio Cecotti, Clay Cordova, and Cumrun Vafa. "Braids, Walls, and Mirrors". In: (2011). arXiv:1110.2115 [hep-th].

[30] Sergio Cecotti, Andrew Neitzke, and Cumrun Vafa. "R-Twisting and 4d/2d Correspondences". In: (2010). arXiv:1006.3435 [hep-th].

[31] Sergio Cecotti and Cumrun Vafa. "BPS Wall Crossing and Topological Strings". In: (2009). arXiv:0910.2615 [hep-th].

[32] O. Chacaltana, J. Distler, and Y. Tachikawa. "Nilpotent orbits and codimension-two defects of 6d N=(2,0) theories". In: *ArXiv e-prints* (Mar. 2012). arXiv:1203.2930 [hep-th].

[33] S. Cherkis and A. Kapustin. "Nahm Transform for Periodic Monopoles and N=2 Super Yang-Mills Theory". In: *Communications in Mathematical Physics* 218 (2001), pp. 333–371. DOI: 10.1007/PL00005558. eprint: arXiv:hep-th/0006050.

[34] S. A. Cherkis and A. Kapustin. "Singular monopoles and supersymmetric gauge theories in three dimensions". In: *Nuclear Physics B* 525 (Aug. 1998), pp. 215–234. DOI: 10.1016/S0550-3213(98)00341-1. eprint: arXiv:hep-th/9711145.

[35] Wu-yen Chuang et al. "Geometric engineering of (framed) BPS states". In: (2013). arXiv:1301.3065 [hep-th].

[36] Clay Cordova. "Regge Trajectories in $\mathcal{N} = 2$ Supersymmetric Yang-Mills Theory". In: (2015). arXiv:1502.02211 [hep-th].

[37] Clay Cordova and Daniel L. Jafferis. "Complex Chern-Simons from M5-branes on the Squashed Three-Sphere". In: (2013). arXiv:1305.2891 [hep-th].

[38] Clay Crdova and Andrew Neitzke. "Line Defects, Tropicalization, and Multi-Centered Quiver Quantum Mechanics". In: *JHEP* 1409 (2014), p. 099. DOI: 10.1007/JHEP09(2014)099. arXiv:1308.6829 [hep-th].

[39] Frederik Denef. "Quantum quivers and Hall / hole halos". In: *JHEP* 0210 (2002), p. 023. DOI: 10.1088/1126-6708/2002/10/023. arXiv:hep-th/0206072 [hep-th].

[40] Frederik Denef and Gregory W. Moore. "Split states, entropy enigmas, holes and halos". In: *JHEP* 1111 (2011), p. 129. DOI: 10.1007/JHEP11(2011)129. arXiv:hep-th/0702146 [HEP-TH].

[41] D. e. Diaconescu and G. W. Moore. "Crossing the Wall: Branes vs. Bundles". In: *Adv. Theor. Math. Phys.* 14 (2010), pp. 1621–1650. URL: http://arxiv.org/abs/0706.3193.

[42] T. Dimofte and S. Gukov. "Refined, Motivic, and Quantum". In: *Lett.Math.Phys.* 91 (2010), p. 1. URL: http://arxiv.org/abs/0904.1420.

[43] Tudor Dimofte, Sergei Gukov, and Yan Soibelman. "Quantum Wall Crossing in N=2 Gauge Theories". In: *Lett.Math.Phys.* 95 (2011), pp. 1–25. DOI: 10.1007/s11005-010-0437-x. arXiv:0912.1346 [hep-th].

[44] Tudor Dimofte et al. "Exact Results for Perturbative Chern-Simons Theory with Complex Gauge Group". In: *Commun.Num.Theor.Phys.* 3 (2009), pp. 363–443. DOI: 10.4310/CNTP.2009.v3.n2.a4. arXiv:0903.2472 [hep-th].

[45] Ron Donagi and Edward Witten. "Supersymmetric Yang-Mills Systems And Integrable Systems". In: *Nucl.Phys.B* 460 (1996), pp. 299–334. eprint: hep-th/9510101.

[46] Ron Donagi and Edward Witten. "Supersymmetric Yang-Mills theory and integrable systems". In: *Nucl.Phys.* B460 (1996), pp. 299–334. DOI: 10.1016/0550-3213(95)00609-5. arXiv:hep-th/9510101 [hep-th].

[47] Nadav Drukker, Davide Gaiotto, and Jaume Gomis. "The Virtue of Defects in 4D Gauge Theories and 2D CFTs". In: (Mar. 2010). eprint: 1003.1112.

[48] Nadav Drukker, David R. Morrison, and Takuya Okuda. "Loop operators and S-duality from curves on Riemann surfaces". In: *JHEP* 0909 (2009), p. 031. eprint: 0907.2593.

[49] Nadav Drukker et al. "Gauge Theory Loop Operators and Liouville Theory". In: *JHEP* 1002 (2010), p. 057. DOI: 10.1007/JHEP02(2010)057. arXiv:0909.1105 [hep-th].

[50] Gerald V. Dunne, R. Jackiw, and C.A. Trugenberger. "Chern-Simons Theory in the Schrodinger Representation". In: *Annals Phys.* 194 (1989), p. 197. DOI: 10.1016/0003-4916(89)90036-5.

[51] F. Ferrari. "The dyon spectra of finite gauge theories". In: *Nuclear Physics B* 501 (Feb. 1997), pp. 53–96. DOI: 10.1016/S0550-3213(97)00338-6. eprint: arXiv:hep-th/9702166.

[52] Frank Ferrari and Adel Bilal. "The Strong-Coupling Spectrum of the Seiberg-Witten Theory". In: *Nucl.Phys.* B469 (1996), pp. 387–402. eprint: hep-th/9602082.

[53] B. Fiol. "The BPS Spectrum of $\mathcal{N} = 2$ $SU(N)$ SYM". In: *JHEP 0* 602 (2006). URL: http://arxiv.org/abs/hep-th/0012079.

[54] V. V. Fock and A. B. Goncharov. "Moduli spaces of local systems and higher Teichmuller theory". In: *ArXiv Mathematics e-prints* (Nov. 2003). eprint: arXiv:math/0311149.

[55] C. Fraser and T. J. Hollowood. "On the weak coupling spectrum of N = 2 supersymmetric SU(n) gauge theory". In: *Nuclear Physics B* 490 (Feb. 1997), pp. 217–235. DOI: 10.1016/S0550-3213(97)00054-0. eprint: arXiv:hep-th/9610142.

[56] Abhijit Gadde et al. "Gauge Theories and Macdonald Polynomials". In: *Commun.Math.Phys.* 319 (2013), pp. 147–193. DOI: 10.1007/s00220-012-1607-8. arXiv:1110.3740 [hep-th].

[57] Abhijit Gadde et al. "S-duality and 2d Topological QFT". In: *JHEP* 1003 (2010), p. 032. DOI: 10.1007/JHEP03(2010)032. arXiv:0910.2225 [hep-th].

[58] Abhijit Gadde et al. "The 4d Superconformal Index from q-deformed 2d Yang-Mills". In: *Phys.Rev.Lett.* 106 (2011), p. 241602. DOI: 10.1103/PhysRevLett.106.241602. arXiv:1104.3850 [hep-th].

[59] D. Gaiotto. "N = 2 dualities". In: *Journal of High Energy Physics* 8 (Aug. 2012), p. 34. DOI: 10.1007/JHEP08(2012)034. arXiv:0904.2715 [hep-th].

[60] D. Gaiotto, G. W. Moore, and A. Neitzke. "Four-Dimensional Wall-Crossing via Three-Dimensional Field Theory". In: *Communications in Mathematical Physics* 299 (Oct. 2010), pp. 163–224. DOI: 10.1007/s00220-010-1071-2. arXiv:0807.4723 [hep-th].

[61] D. Gaiotto, G. W. Moore, and A. Neitzke. "Framed BPS States". In: *ArXiv e-prints* (June 2010). arXiv:1006.0146 [hep-th].

[62] D. Gaiotto, G. W. Moore, and A. Neitzke. "Private communication."

[63] D. Gaiotto, G. W. Moore, and A. Neitzke. "Spectral networks". In: *ArXiv e-prints* (Apr. 2012). arXiv:1204.4824 [hep-th].

[64] D. Gaiotto, G. W. Moore, and A. Neitzke. "Wall-crossing, Hitchin Systems, and the WKB Approximation". In: *ArXiv e-prints* (July 2009). arXiv:0907.3987 [hep-th].

[65] D. Gaiotto, G. W. Moore, and A. Neitzke. "Wall-Crossing in Coupled 2d-4d Systems". In: *ArXiv e-prints* (Mar. 2011). arXiv:1103.2598 [hep-th].

[66] Davide Gaiotto. "N=2 dualities". In: *JHEP* 1208 (2012), p. 034. DOI: 10.1007/JHEP08(2012)034. arXiv:0904.2715 [hep-th].

[67] Davide Gaiotto. "Open Verlinde line operators". In: (2014). arXiv:1404.0332 [hep-th].

[68] Davide Gaiotto. "Surface Operators in N = 2 4d Gauge Theories". In: *JHEP* 1211 (2012), p. 090. DOI: 10.1007/JHEP11(2012)090. arXiv:0911.1316 [hep-th].

[69] Davide Gaiotto, Sergei Gukov, and Nathan Seiberg. "Surface Defects and Resolvents". In: *JHEP* 1309 (2013), p. 070. DOI: 10.1007/JHEP09(2013)070. arXiv:1307.2578.

[70] Davide Gaiotto, Gregory W. Moore, and Andrew Neitzke. "Spectral Networks and Snakes". In: *Annales Henri Poincare* 15 (2014), pp. 61–141. DOI: 10.1007/s00023-013-0238-8. arXiv:1209.0866 [hep-th].

[71] D. Galakhov, A. Mironov, and A. Morozov. "S-Duality and Modular Transformation as a non-perturbative deformation of the ordinary pq-duality". In: *JHEP* 06 (2014), p. 050. DOI: 10.1007/JHEP06(2014)050. arXiv:1311.7069 [hep-th].

[72] Dmitry Galakhov, Pietro Longhi, and Gregory W. Moore. "Spectral Networks with Spin". In: (2014). arXiv:1408.0207 [hep-th].

[73] Dmitry Galakhov et al. "Wild Wall Crossing and BPS Giants". In: *JHEP* 1311 (2013), p. 046. DOI: 10.1007/JHEP11(2013)046. arXiv:1305.5454 [hep-th].

[74] A. Gorsky et al. "Integrability and Seiberg-Witten exact solution". In: *Phys.Lett.* B355 (1995), pp. 466–474. DOI: 10.1016/0370-2693(95)00723-X. arXiv:hep-th/9505035 [hep-th].

[75] M. Gross and R. Pandharipande. *Quivers, Curves, and the Tropical Vertex*. URL: http://arxiv.org/abs/0909.5153.

[76] S. Gukov. "Gauge theory and knot homologies". In: *Fortschritte der Physik* 55 (May 2007), pp. 473–490. DOI: 10.1002/prop.200610385. arXiv:0706.2369 [hep-th].

[77] Sergei Gukov. "Surface Operators". In: (2014). arXiv:1412.7127 [hep-th].

[78] Sergei Gukov and Edward Witten. "Gauge Theory, Ramification, And The Geometric Langlands Program". In: (). eprint: hep-th/0612073.

[79] Sergei Gukov and Edward Witten. "Rigid Surface Operators". In: (Apr. 2008). eprint: 0804.1561.

[80] Mans Henningson and Piljin Yi. "Four-dimensional BPS spectra via M theory". In: *Phys.Rev.* D57 (1998), pp. 1291–1298. DOI: 10.1103/PhysRevD.57.1291. arXiv:hep-th/9707251 [hep-th].

[81] Nigel Hitchin. "Stable bundles and integrable systems". In: *Duke Math. J.* 54 Number 1 (1987), pp. 91–114.

[82] A. Kapustin. "Wilson-'t Hooft operators in four-dimensional gauge theories and S-duality". In: *Phys. Rev. D* 74.2 (July 2006). DOI: Phys.Rev.D74. eprint: arXiv:hep-th/0501015.

[83] A. Klemm et al. "Self-Dual Strings and N=2 Supersymmetric Field Theory". In: *Nucl.Phys.* B477 (1996), pp. 746–766. eprint: hep-th/9604034.

[84] Barak Kol. "Thermal monopoles". In: *JHEP* 0007 (2000), p. 026. DOI: 10.1088/1126-6708/2000/07/026. arXiv:hep-th/9812021 [hep-th].

[85] Barak Kol and Michael Kroyter. "On the spatial structure of monopoles". In: (2000). arXiv:hep-th/0002118 [hep-th].

[86] M. Kontsevich. "Private communication".

[87] M. Kontsevich and Y. Soibelman. "Cohomological Hall Algebra, Exponential Hodge Structures and Motivic Donaldson-Thomas Invariants". In: (). URL: http://arxiv.org/abs/1006.2706.

[88] M. Kontsevich and Y. Soibelman. "Stability structures, motivic Donaldson-Thomas invariants and cluster transformations". In: *ArXiv e-prints* (Nov. 2008). arXiv:0811.2435 [math.AG].

[89] Maxim Kontsevich and Yan Soibelman. "Cohomological Hall algebra, exponential Hodge structures and motivic Donaldson-Thomas invariants". In: (2010). arXiv:1006.2706 [math.AG].

[90] Maxim Kontsevich and Yan Soibelman. "Motivic Donaldson-Thomas invariants: Summary of results". In: (2009). arXiv:0910.4315 [math.AG].

[91] Karl Landsteiner and Esperanza Lopez. "New curves from branes". In: *Nucl.Phys.* B516 (1998), pp. 273–296. DOI: 10.1016/S0550-3213(98)00022-4. arXiv:hep-th/9708118 [hep-th].

[92] Karl Landsteiner, Esperanza Lopez, and David A. Lowe. "N=2 supersymmetric gauge theories, branes and orientifolds". In: *Nucl.Phys.* B507 (1997), pp. 197–226. DOI: 10.1016/S0550-3213(97)00559-2. arXiv:hep-th/9705199 [hep-th].

[93] Ki-Myeong Lee and Piljin Yi. "Dyons in N=4 supersymmetric theories and three pronged strings". In: *Phys.Rev.* D58 (1998), p. 066005. DOI: 10.1103/PhysRevD.58.066005. arXiv:hep-th/9804174 [hep-th].

[94] Sungjay Lee and Masahito Yamazaki. "3d Chern-Simons Theory from M5-branes". In: *JHEP* 1312 (2013), p. 035. DOI: 10.1007/JHEP12(2013)035. arXiv:1305.2429 [hep-th].

[95] Pietro Longhi. "The BPS Spectrum Generator In 2d-4d Systems". In: *JHEP* 1211 (2012), p. 107. DOI: 10.1007/JHEP11(2012)107. arXiv:1205.2512 [hep-th].

[96] Pietro Longhi and Gregory Moore. "Notes on the BPS spectrum of N=2* theory; unpublished". 2012.

[97] Pietro Longhi, Gregory W. Moore, and Chan Y. Park. "Work in progress."

[98] J. Manschot, B. Pioline, and A. Sen. "Wall-Crossing from Boltzmann Black Hole Halos". In: *JHEP* 1107 (2011). URL: http://arxiv.org/abs/1011.1258.

[99] Jan Manschot, Boris Pioline, and Ashoke Sen. "A Fixed point formula for the index of multi-centered N=2 black holes". In: *JHEP* 1105 (2011), p. 057. DOI: 10.1007/JHEP05(2011)057. arXiv:1103.1887 [hep-th].

[100] A. Marshakov, A. Mironov, and A. Morozov. "On AGT Relations with Surface Operator Insertion and Stationary Limit of Beta-Ensembles". In: *J.Geom.Phys.* 61 (2011), pp. 1203–1222. DOI: 10.1016/j.geomphys.2011.01.012. arXiv:1011.4491 [hep-th].

[101] Emil J. Martinec and Nicholas P. Warner. "Integrable systems and supersymmetric gauge theory". In: *Nucl.Phys.* B459 (1996), pp. 97–112. DOI: 10.1016/0550-3213(95)00588-9. arXiv:hep-th/9509161 [hep-th].

[102] A. Mikhailov. "BPS states and minimal surfaces". In: *Nucl.Phys.* B533 (1998), pp. 243–274. DOI: 10.1016/S0550-3213(98)00524-0. arXiv:hep-th/9708068 [hep-th].

[103] Andrei Mikhailov, Nikita Nekrasov, and Savdeep Sethi. "Geometric realizations of BPS states in N=2 theories". In: *Nucl.Phys.* B531 (1998), pp. 345–362. DOI: 10.1016/S0550-3213(98)80001-1. arXiv:hep-th/9803142 [hep-th].

[104] G. W. Moore. "PiTP Lectures on Wall-Crossing, PiTP School at the Institute for Advanced Study". In: *July* (2010). URL: http://www.physics.rutgers.edu/$\sim$gmoore.

[105] Gregory W. Moore. "Four-dimensional N=2 Field Theory and Physical Mathematics". In: (2012). arXiv:1211.2331 [hep-th].

[106] Gregory W. Moore. "Lecture Notes for Felix Klein Lectures". In: *lecture notes* (). URL: http://www.physics.rutgers.edu/~gmoore.

[107] Gregory W. Moore, Andrew B. Royston, and Dieter Van den Bleeken. "Semiclassical framed BPS states". In: *to appear* ().

[108] Dimitri Nanopoulos and Dan Xie. "Hitchin Equation, Irregular Singularity, and $N = 2$ Asymptotical Free Theories". In: (May 2010). eprint: 1005.1350.

[109] Dimitri Nanopoulos and Dan Xie. "Hitchin Equation, Singularity, and N=2 Superconformal Field Theories". In: *JHEP* 1003 (2010), p. 043. eprint: 0911.1990.

[110] Andrew Neitzke. "Hitchin systems in N=2 field theory". In: (2014). arXiv:1412.7120 [hep-th].

[111] Andrew Neitzke. "Spectral networks in 2 and 3 dimensions". In: *talk at String-Math, June 2013* (). URL: http://www.ma.utexas.edu/users/neitzke.

[112] David I. Olive and Edward Witten. "Supersymmetry Algebras That Include Topological Charges". In: *Phys.Lett.* B78 (1978), p. 97. DOI: 10.1016/0370-2693(78)90357-X.

[113] H. Ooguri, A. Strominger, and C. Vafa. "Black Hole Attractors and the Topological String". In: *Phys.Rev.D* 70 (2004), p. 1060. URL: http://arxiv.org/abs/hep-th/0405146.

[114] Boris Pioline. "Four ways across the wall". In: *J.Phys.Conf.Ser.* 346 (2012), p. 012017. DOI: 10.1088/1742-6596/346/1/012017. arXiv:1103.0261 [hep-th].

[115] M. Reineke. *Cohomology of Quiver Moduli, Functional Equations, and Integrality of Donaldson-Thomas Type Invariants*. URL: http://arxiv.org/abs/0903.0261.

[116] M. Reineke. *Moduli of Representations of Quivers*. URL: http://arxiv.org/abs/0802.2147.

[117] M. Reineke. "The Harder-Narasimhan System in Quantum Groups and Cohomology of Quiver Moduli". In: *Invent. Math.* 152 (2003), p. 2. URL: http://arxiv.org/abs/math/0204059.

[118] M. Reineke. *The Use of Geometric and Quantum Group Techniques for Wild Quivers*. URL: http://arxiv.org/abs/math/0304193.

[119] Sylvain Ribault and Joerg Teschner. "$H+(3)$-WZNW correlators from Liouville theory". In: *JHEP* 0506 (2005), p. 014. DOI: 10.1088/1126-6708/2005/06/014. arXiv:hep-th/0502048 [hep-th].

[120] N. Seiberg and E. Witten. "Electric-magnetic duality, monopole condensation, and confinement in N=2 supersymmetric Yang-Mills theory". In: *Nuclear Physics B* 426 (Sept. 1994), pp. 19–52. DOI: 10.1016/0550-3213(94)90124-4. eprint: arXiv:hep-th/9407087.

[121] N. Seiberg and E. Witten. "Monopoles, duality and chiral symmetry breaking in N = 2 supersymmetric QCD". In: *Nuclear Physics B* 431 (Dec. 1994), pp. 484–550. DOI: 10.1016/0550-3213(94)90214-3. eprint: arXiv:hep-th/9408099.

[122] Nathan Seiberg and Edward Witten. "Gauge dynamics and compactification to three-dimensions". In: (1996). arXiv:hep-th/9607163 [hep-th].

[123] Alfred D. Shapere and Cumrun Vafa. "BPS Structure of Argyres-Douglas Superconformal Theories". In: (). eprint: hep-th/9910182.

[124] C. L. de Souza Batista and D. Li. "Analytic Calculations of Trial Wave Functions of the Fractional Quantum Hall Effect on the Sphere". In: *Phys.Rev.B* 55 (1997), p. 1582. URL: http://arxiv.org/abs/cond-mat/9607170.

[125] A. V. Stoyanovsky. "A relation between the Knizhnik-Zamolodchikov and Belavin-Polyakov-Zamolodchikov systems of partial differential equations". In: (2000). arXiv:math-ph/0012013 [math-th].

[126] David Tong and Kenny Wong. "Monopoles and Wilson Lines". In: *JHEP* 1406 (2014), p. 048. DOI: 10.1007/JHEP06(2014)048. arXiv:1401.6167 [hep-th].

[127] T. Weist. *Localization in Quiver Moduli Spaces*. URL: http://arxiv.org/abs/0903.5442.

[128] T. Weist. *On the Euler Characteristic of Kronecker Moduli Spaces*. URL: http://arxiv.org/abs/1203.2740.

[129] J. Wess and J. Bagger. *Supersymmetry and Supergravity*. Princeton University Press, 1992.

[130] Hassler Whitney. "On regular closed curves in the plane". In: *Compositio Mathematica* 4 (1937), pp. 276–284.

[131] Edward Witten. "Analytic Continuation Of Chern-Simons Theory". In: (2010), pp. 347–446. arXiv:1001.2933 [hep-th].

[132] Edward Witten. "Quantization of Chern-Simons Gauge Theory With Complex Gauge Group". In: *Commun.Math.Phys.* 137 (1991), pp. 29–66. DOI: 10.1007/BF02099116.

[133] Edward Witten. "Solutions of four-dimensional field theories via M theory". In: *Nucl.Phys.* B500 (1997), pp. 3–42. DOI: 10.1016/S0550-3213(97)00416-1. arXiv:hep-th/9703166 [hep-th].